Monitoring of boreal forests in Siberia Integrating ground and satellite (C- and L-band SAR) data

Dissertation

(kumulativ)

zur Erlangung des akademischen Grades doctor rerum naturalium
(Dr. rer. nat.)

vorgelegt dem Rat der Chemisch-Geowissenschaftlichen Fakultät der Friedrich-Schiller-Universität Jena

von Martyna Anna Stelmaszczuk-Górska, M.Sc.

Gutachter:
1. Prof. Dr. C. Schmullius, FSU Jena
2. apl. Prof. Dr. habil. C. Thiel, DLR Jena

Tag der Verteidigung: 02/12/2020

*Niczego w **ż**yciu nie nale**ż**y si**ę** bać,*
*nale**ż**y to tylko zrozumieć.*
(Nothing in life is to be feared,
it is only to be understood.)

Maria Skłodowska-Curie

Content

Appended papers

The following papers are the main scientific outcome of this cumulative dissertation.

Hüttich, C., **Stelmaszczuk-Górska, M.**, Eberle, J., Kotzerke, P., & Schmullius, C. C. (2014). Operational forest monitoring in Siberia using multi-source Earth Observation data. *Siberian Journal of Forest Science*, *5*, 38–52. Retrieved from http://sibjforsci.com/articles/h-ttich-c-stelmaszczuk-g-rska-m-a-eberle-j-kotzerke-p-schmullius-c-operational-forest-monitoring-in-/

Stelmaszczuk-Górska, M. A., Rodriguez-Veiga, P., Ackermann, N., Thiel, C., Balzter, H., & Schmullius, C. (2016). Non-Parametric Retrieval of Aboveground Biomass in Siberian Boreal Forests with ALOS PALSAR Interferometric Coherence and Backscatter Intensity. *Journal of Imaging*, *2*(1), 24. http://doi.org/10.3390/jimaging2010001

Stelmaszczuk-Górska, M. A., Thiel, C. J., & Schmullius, C. C. (2017). Remote Sensing for Aboveground Biomass Estimation in Boreal Forests. In H. Balzter (Ed.), *Earth Observation for Land and Emergency Monitoring* (1st ed., pp. 33–55). © 2017 John Wiley & Sons Ltd. http://doi.org/10.1002/9781118793787

Stelmaszczuk-Górska, M. A., Urbazaev, M., Schmullius, C., & Thiel, C. (2018). Estimation of Above-Ground Biomass over Boreal Forests in Siberia using updated in situ, ALOS-2 PALSAR-2, and RADARSAT-2 Data. *Remote Sensing*, *10*(10), 1550. http://doi.org/10.3390/rs10101550

Related publications

Apart from the appended papers, the author has contributed to other publications related to the scope of this thesis, including reports and conference contributions.

Balzter, H., Nicolas-Perea, V., Bochenek, Z., Brown, S., Chernetskiy, M., Comber, L., Dabrowska-Zielinska, K., Fisher, P., Fourie, C., Gatkowska, M., Kourkouli, P., Lamb, A. , Moser, L., Ofwono, M., Palmer, S., Papke, J., Rodríguez-Veiga, P., Schmullius, C., Schoepfer, E., Shrestha, S., Spies, B., **Stelmaszczuk-Górska, M.**, Stratoulias, D., Tansey, K., Tóth, V., Van Beijma, S., Veck, N., Voigt, S., Wegmüller, U, Wheeler, J., Wiesmann, A. & Zlinszky, A. (2012). Earth Observation Research for GMES Initial Operations. In Proceedings of the *RSPSoc Annual Conference of the Remote Sensing and Photogrammetry Society*, 12-14 September, University of Greenwich, London, UK.

Stelmaszczuk-Górska, M., Thiel, C., Schmullius, C. (2013). Optimization of coherence estimation window size aiming at growing stock volume retrieval in Siberian forest. In Proceedings of the *ESA Living Planet Symposium.* pp. 1–4. (Appendix A)

Chowdhury, T. A., Thiel, C., Schmullius, C., **Stelmaszczuk-Górska, M.** (2013). Polarimetric parameters for growing stock volume estimation using ALOS PALSAR L-Band data over siberian forests. *Remote Sens. 5*(11), 5725-5756.

Stelmaszczuk-Górska, M., Thiel, C. & Schmullius, C. (2014). Retrieval of growing stock volume using ALOS PALSAR L-band coherence and backscatter over boreal forest. *PhD Conference on Earth System Science*, 12-14 February, Jena, Germany. (oral presentation)

Rodriguez-Veiga, P., **Stelmaszczuk-Górska, M.**, Hüttich, C., Schmullius, C., Tansey, K., & Balzter, H. (2014). Aboveground Biomass Mapping in Krasnoyarsk Kray (Central Siberia) using Allometry, Landsat, and ALOS PALSAR. In Proceedings of the *RSPSoc Annual Conference of the Remote Sensing and Photogrammetry Society.* 2-5 September, Aberystwyth, Wales, UK.

Stelmaszczuk-Górska, M., Rodriguez-Veiga, P., Thiel, C., Balzter, H. & Schmullius, C. (2014). Estimation of aboveground biomass in Siberian boreal forest from optical and radar remote sensing data. *ForestSAT Conference.* 4-7 November, Riva del Garda, Italy. (oral presentation)

Stelmaszczuk-Górska, M., Thiel, C., & Schmullius, C. (2014). *Large-scale forest change monitoring scheme*. Deliverable of the project GIONET - GMES Initial Operations – Network for Earth Observation Research Training. Grant Agreement number PITN-GA-2010-264509.

Stelmaszczuk-Górska, M.A., Thiel, C. & Schmullius, C. (2014). Aboveground biomass monitoring over Siberian boreal forest using radar remote sensing data. *AGU Fall Meeting*, 15-19 December, San Francisco, USA. (oral presentation)

Balzter H., Rodriguez-Veiga P., Wheeler J., Tansey K.J., **Stelmaszczuk-Górska M.** & Schmullius C. (2015). Ground, stems and foliage: Forest above-ground biomass mapping from combined Synthetic Aperture Radar and Multispectral Imagery. *36th International Symposium on Remote Sensing of Environment*, 11-15 May, Berlin, Germany. (oral presentation)

Stelmaszczuk-Górska, M., Thiel, C. & Schmullius, C. (2016). Retrieval of Aboveground Biomass using Multi-frequency SAR. In Proceedings of the *ESA Living Planet Symposium*, 9-13 May, Prague, Czech Republic.

Figures

This section lists the figures from Chapters 1 and 2.

Tables

This section lists the tables from Chapters 1 and 2.

Abbreviations and symbols

AGB	Aboveground Biomass
AI	Artificial Intelligence
ALOS	Advanced Land Observing Satellite
ALS	Airborne Lidar Scanning
ASAR	Advanced Synthetic Aperture Radar
ASTER	Advanced Spaceborne Thermal Emission and Reflection Radiometer
ATLAS	Advanced Topographic Laser Altimeter System
AVHRR	Advanced Very High Resolution Radiometer
BFAST	Breaks for Additive Seasonal and Trends
BGB	Belowground Biomass
BOS	Basic Observation Scenario
BOREAS	Boreal Ecosystem Atmosphere Study
BRDF	Bidirectional Reflectance Distribution Function
CARABAS	Coherent All Radio Band Sensing
COP	Conference of the Parties
CP	Compact Polarimetry
CSA	Canadian Space Agency
DBH	Diameter at Breast Height
DSM	Digital Surface Model
DEM	Digital Elevation Model
DOI	Digital Object Identifier
DTM	Digital Terrain Model
EC	European Commission
ECV	Essential Climate Variables
EM	Electromagnetic
ENL	Equivalent Number of Looks
ENVISAT	ENVIronmental SATellite
EO	Earth Observation
EOM	Earth Observation Monitor
EORC	Earth Observation Research Center
ERS	European Remote Sensing

ESA	European Space Agency
EU	European Union
EVI	Enhanced Vegetation Index
FAO	Food and Agriculture Organization
FAPAR	Fraction of Absorbed Photosynthetically Active Radiation
FIP	Forest Inventory and Planning
FBD	Fine Beam Dual
FBS	Fine Beam Single
GCOS	Global Climate Observing System
GEDI	Global Ecosystem Dynamics Investigation
GEO	Group on Earth Observations
GFOI	Global Forest Observations Initiative
GHG	Greenhouse gas
GIS	Geographic Information System
GLAS	Geoscience Laser Altimeter System
GOFC-GOLD	Global Observation of Forest Cover and Land Dynamics
COSMO-SkyMed	Constellation of Small Satellites for Mediterranean basin Observation
GRD	Ground Range Detected
GSV	Growing Stock Volume
HH	Horizontal-Horizontal (polarization)
HRWS	High-Resolution Wide-Swath SAR
HUTSCAT	Helsinki University of Technology SCATterometer
HV	Horizontal-Vertical (polarization)
ICESat	Ice, Cloud, and Land Elevation Satellite
IIASA	International Institute for Applied Systems Analysis
InSAR	Interferometric Synthetic Aperture Radar
IPCC	Intergovernmental Panel on Climate Change
ISRO	Indian Space Research Organisation
ISS	International Space Station
IWCM	Interferometric Water Cloud Model
JAXA	Japan Aerospace Exploration Agency
JERS	Japanese Earth Resources Satellite
K&C	Kyoto and Carbon
KOMPSAT	KOrea Multi-Purpose SATellite
LAI	Leaf Area Index
LC	Land Cover
LCC	Land Cover Change
LiDAR	Light Detection And Ranging
LU	Land Use
LULCC	Land Use Land Cover Change
MaxEnt	Maximum Entropy
ML	Machine Learning
MLD	Multi-look Detected

MLI	Multi-looked Intensity
MODIS	Moderate Resolution Imaging Spectroradiometer
MOLI	Multi-footprint Observation Lidar and Imager
NASA	National Aeronautics and Space Administration
NDVI	Normalized Differenced Vegetation Index
NESZ	Noise-Equivalent Sigma Zero
NFI	National Forest Inventory
NIR	Near infrared
NiSAR	NASA-ISRO SAR Mission
NOAA	National Oceanic and Atmospheric Administration
NSIDC	National Snow and Ice Data Center
OBIA	Object-Based Image Analysis
PALSAR	Phased Array type L-band Synthetic Aperture Radar
PolInSAR	Polarimetric SAR Interferometry
PRF	Pulse Repetition Frequency
PRI	Precision Images
RADAR	Radio Detection and Ranging
RAR	Real Aperture Radar
RCS	Radar-Cross Section
REDD	Reducing Emissions from Deforestation and Forest Degradation
RF	Random Forests
RISAT	Radar Imaging Satellite
ROSE-L	Radar Observing System for Europe at L-band
RVoG	Random Volume over Ground
SAOCOM	Spanish for Argentine Microwaves Observation Satellite (In Spanish Satélite Argentino de Observación COn Microondas)
SAR	Synthetic Aperture Radar
SFA	Swedish Forest Agency
SI	Site Index
SIBERIA	SAR Imaging for Boreal Ecology and Radar Interferometry Applications
SIR	Shuttle Imaging Radar
SLA	Shuttle Laser Altimeter
SLC	Single Look Complex
SNR	Signal-to-Noise Ratio
SOAR	Sciences and Application Research
SPOT	Satellite for observation of Earth multispectral (In French: Satellite Pour l'Observation de la Terre)
SRTM	Shuttle Radar Topography Mission
TDX	Tandem-X
TDL	Tandem-L
TLS	Terrestrial Laser Scanning
TOPSAR	Terrain Observation with Progressive Scans

TSX	TerraSAR-X
UAV	Unmanned Aerial Vehicle
UN	United Nation
UNFCCC	United Nation Framework Convention on Climate Change
VCF	Vegetation Continuous Fields
VH	Vertical- Horizontal (polarization)
VHF	Very High Frequency
VV	Vertical-Vertical (polarization)
WCM	Water Cloud Model
WWF	World Wide Fund
3D	Three-dimensional
CH_4	Methane
CO_2	Carbon dioxide
dB	Decibel
ha	Hectare
N_2O	Nitrous oxide
r	Pearson's correlation coefficient
R^2	Coefficient of determination
RMSE	Root Mean Square Error
rRMSE	relative RMSE

Abstract

Forests cover more than 30% of the total land area and provide services covering a wide range of ecological, social (cultural and spiritual), economic and political aspects. They regulate water regimes, maintain soil quality and limit its erosion, modulate the climate by regulating carbon, water and energy cycles, and are rich in diversity of habitats and species. Forests are an important foundation for a whole range of economic sectors. They form the basis for energy supply with renewable raw materials, supply for the production of paper and pulp, provide materials for the chemical industry, are a source of natural rubber for rubber production, are important for the food industry and, last but not least, are also an important factor in the tourism sector and offer a generally accessible recreation area for the population. The management of forests is subject to local, national and international rules and regulations in order to reconcile economic and ecological needs and requirements (FAO, 2015).

Forests account for more than 70% of the terrestrial biomass and act as an important carbon sink (Bar-On, Phillips, & Milo, 2018). The forest is a dynamic environment that is constantly changing affecting the distribution of terrestrial carbon sources and sinks. The main causes of changes in forest cover are natural forest mortality, e.g., due to recently more frequent droughts that promote insect outbreaks leading to tree dieback and forest fires, such as forest wildfires in Siberia, bushfires in Australia and human-induced fires in the tropics (Allen et al., 2010; Le Quéré et al., 2015). Other causes of a change in forest cover are economic factors and developments in agriculture. The last two are responsible for reducing forest cover by over 40% (DeFries, 2013). Forests play an essential role in mitigating the effects of an anthropogenic climate change. Mitigation of anthropogenic climate change is possible by providing and continuously improving information on the distribution of terrestrial carbon sources and sinks through forest monitoring, together with more precise estimates of the biomass associated with it. This information can then be used by national and international decision-makers in defining climate-friendly forest policy for the protection, afforestation, and restoration of forest.

Forests in the Russian Federation are of particular importance for monitoring. It is the most forested country in the world. Forests cover 49% of its total area (FAO, 2012). At the same time, it is the country with the highest uncertainty when calculating global carbon stocks (Pan et al., 2011). Forests in Russia are subject to dramatic changes due to more frequent, catastrophic fires. Due to global warming and heat waves, a further increase in the frequency of forest fires is forecast (Shvidenko, Schepaschenko, Sukhinin, McCallum, & Maksyutov, 2011). This and release of large amounts of greenhouse gases (e.g., methane) through thawing permafrost could free more carbon than through deforestation in the tropics (FAO, 2012). In addition, some forest areas in Siberia have not been inventoried for more than two decades due to a lack of financial support (Shvidenko, Schepaschenko, Sukhinin, et al., 2011). Illegal logging is also a challenge in monitoring Russian forests (WWF Russia, World Bank).

Remote sensing is recommended as one of the tools to ensure systematic and operational forest monitoring. It can acquire data over large areas with a high repetition rate and at a relatively low cost. In particular, microwave sensors are recommended as they can provide weather and sun independent, systematic observations with high temporal frequency.

The main goal of this cumulative dissertation was to develop methods for estimating forest parameters from remote sensing data obtained with Synthetic Aperture Radar (SAR). Using the SAR data acquired by the sensor with the longest wavelength currently available in space, the L-band, methods for estimating the above-ground forest biomass were developed. For this purpose, algorithms for machine learning (ML) were applied and validated. These methods were chosen because they are recommended for large data sets and an incomplete theoretical understanding of processes, e.g., the interaction between the forest and the radar signal, and are relatively new in forest monitoring studies. In addition, efforts have been made to establish improved mapping of large-scale forest cover change.

Based on the comprehensive literature review, the following four research questions were formulated and analyzed:

1. How to improve large-scale mapping of boreal forest changes using SAR L-band products? (Paper 1, Chapter 4.1)
2. What are the research pathways of boreal forest aboveground biomass estimation using SAR data? (Paper 2, Chapter 4.2)
3. How to combine multi-temporal InSAR coherence and backscatter data to improve aboveground biomass estimation in boreal forests? (Paper 3, Chapter 4.3)

4. How can fusing of multi-temporal and multi-frequency SAR data improve aboveground biomass estimation in boreal forests? (Paper 4, Chapter 4.4)

In order to answer the above research questions, both the SAR amplitude and the phase were used to monitor boreal forests in Siberia. The research area was located in the Asian part of boreal forests, in southern Central Siberia in Russia. In total, the studies were carried out in three research areas. The forest change monitoring algorithm was developed in an area that covered approximately 620,000 km^2, while aboveground biomass models were trained and tested over 200 km^2 and 2,000 km^2. The reference data used in this study were collected as part of the Russian Forest Inventory and Planning (FIP) und updated using a new regional allometric model (Stelmaszczuk-Górska et al., 2016). Data from two new generation L-band sensors, namely from the Phased Array type L-band Synthetic Aperture Radar PALSAR and PALSAR-2 (33 images), and ALOS PALSAR backscatter mosaics (364 tiles) were analyzed. Additionally, SAR data in C-band were used as complementary information to the L-band data. In this study, data acquired by the satellite RADARSAT-2 (7 images) were analyzed as they played an important role in the Sentinel-1 preparatory phase.

To improve the large-scale forest/non-forest classification, an integrated GIS and pre-classification approach was tested. In total, 364 1-degree tiles of yearly mosaics of ALOS PALSAR were used. Only HV polarized data were used for annual forest cover change monitoring. Various temporal measures were implemented to assess the separation of classes of change from forest to non-forest or from non-forest to forest. A simple threshold approach based on a SAR mosaic ratio was used for the final automatic mapping of forest changes. The difference of 2 dB between the acquisitions has been implemented. The reported high potential for L-band sensors using HV cross-polarization data for large-scale forest mapping was consistent with previous studies (e.g., M. Santoro et al., 2012). Changes in the study area were identified with an accuracy of about 70%. The majority of forest loss was observed in 2008 and in 2010 in the north-eastern region of the study area. The same trend and pattern of changes showed global forest loss map by Hansen et al. (Hansen et al., 2013).

A literature review of aboveground biomass estimation using SAR has shown that most of the studies used the data acquired by C-band satellite missions followed by L-band, and X-band data, and focused on European sites. This was related to data availability. Only 12% applied data acquired over Siberian sites. Aboveground biomass estimation error ranged from 119% (Santoro, Askne, Smith, & Fransson, 2002) to 5.1%, when using the multi-temporal combination of ALOS

PALSAR backscattering coefficient data at a forest plot level in a machine-learning approach (Andersen, Strunk, Temesgen, Atwood, & Winterberger, 2011). Most of the methods presented used semi-empirical models. Although longer wavelengths are suggested when estimating forest aboveground biomass, recently the highest accuracy has recently been found using X-band data. The highest estimation accuracies are expected using a combination of data from multiple SAR sources (Santoro & Cartus, 2018; Santoro, Cartus, Fransson, & Wegmüller, 2019).

To combine multi-temporal InSAR coherence and backscatter data, two widely used machine-learning algorithms were implemented using thirteen variables. Maximum Entropy (MaxEnt) and Random Forests (RF) models showed good performance and promising estimations. The RMSEs were 35.8 tons/ha (38.8%) and 35 tons/ha (36.9%) for the MaxEnt and RF models, respectively. Coherence data were most important in the low and high aboveground biomass ranges, while the new backscatter/coherence ratio in the medium to high ranges. Thus, a strategy of using different data sets to estimate different levels of aboveground biomass could further increase the accuracy of biomass estimation. Furthermore, it was observed that the contribution of the radar backscatter in the model construction increased after filtering. The RF algorithm provided an average estimate of the biomass that almost corresponds to the reference value. On the other hand, MaxEnt provided a more realistic spatial distribution of the above-ground biomass values.

Multi-temporal SAR data of different wavelengths were combined using five ML models based on nine to forty-five SAR products. As expected, the longer wavelength L-band data in HH and HV polarizations performed better than C-band data in HH and HV polarizations. A comparison of the estimation errors showed that filtered L-band data co- and cross-polarized are sufficient to estimate AGB with good accuracy (approx. 30%). The inclusion of ratio and texture measure as well as C-band data did not improve the estimation. RADARSAT-2 data acquired in the Ultrafine mode showed greater sensitivity to roughness of objects, reducing the correlation between SAR and reference data, thus generating higher estimation errors. The lowest estimation error was calculated for L-band filtered data alone and was 29.1 tons/ha (30%). In general, all models provided the overestimated aboveground biomass values with a bias ranging from 3.9 tons/ha (C-band in Fine mode) to 10.6 tons/ha (C-band in Ultrafine mode). In previous studies in which single frequency L-band data were applied, relative estimation errors from 33.4% to 42.44% for Siberian boreal forests were reported (C. Hüttich et al., 2014; Wilhelm, Hüttich, Korets, & Schmullius, 2014).

The results of this work showed that a combination of multi-temporal, multi-frequency and interferometric SAR (InSAR) data should be used for future forest surveillance studies. In 2022, spaceborne missions collecting in X-, C-, and L-band will be complemented by the spaceborne P-band (BIOMASS) and new L-band (e.g., TanDEM-L) missions. The availability of single-pass InSAR L- and P-band data should improve the forest change mapping and biomass estimation. The ever-growing archive of time series of SAR data and the complexity of the interaction of SAR signals and forests imply the use of new methods, e.g., machine learning, for data evaluation. This is not possible without reliable and extensive reference data. Currently new ground data acquisition technologies such as Unmanned Aerial Vehicles (UAVs) are possible. In the future, these can replace existing standard techniques used for inventory of forest resources and eliminate currently unknown errors in human measurements.

Zusammenfassung

Wälder bedecken mehr als 30% der gesamten Landfläche der Erde und bieten Ökosystemdienstleistungen an, die ein breites Spektrum ökologischer, sozialer (kultureller und spiritueller), wirtschaftlicher und politischer Aspekte abdecken. Sie regulieren Wasserregime, erhalten die Bodenqualität und begrenzen ihre Erosion, beeinflussen das Klima durch Regulierung des Kohlenstoff-, Wasser- und Energiekreislaufs und sind reich an Lebensräumen und Arten. Wälder sind eine wichtige Grundlage für eine ganze Reihe von Wirtschaftszweigen. So bilden sie die Grundlage für die Energieversorgung mit nachwachsenden Rohstoffen, liefern das Ausgangsmaterial für die Herstellung von Papier und Zellstoff, stellen Stoffe für die chemische Industrie bereit, sind eine Quelle für Naturkautschuk zur Gummiherstellung, sind von Bedeutung für die Lebensmittelindustrie und sind nicht zuletzt auch ein wichtiger Faktor im Tourismussektor und bieten einen allgemein zugänglichen Erholungsraum für die Bevölkerung. Das Management der Wälder unterliegt lokalen, nationalen und internationalen Bestimmungen und Regulierungen, um wirtschaftliche und ökologische Bedürfnisse und Erfordernisse in Einklang zu bringen (FAO, 2015).

Wälder machen mehr als 70% der terrestrischen Biomasse aus und fungieren als wichtige Kohlenstoffsenke (Bar-On, Phillips, & Milo, 2018). Der Wald ist eine dynamische Umgebung, die sich ständig verändert und sich auf die Verteilung der terrestrischen Kohlenstoffquellen und -senken auswirkt. Die Hauptursachen für Veränderungen in der Waldbedeckung sind die natürliche Waldsterblichkeit, z. B. aufgrund der in letzter Zeit häufiger auftretenden Dürreperioden, die Insektenausbrüche fördern und die zum Absterben von Bäumen und zu Waldbränden führen, wie beispielsweise die Waldbrände in Sibirien, die Buschbrände in Australien und vom Menschen verursachte Brände in den Tropen. Weitere Ursachen für eine Veränderung der Waldbedeckung sind wirtschaftliche Faktoren und Entwicklungen in der Landwirtschaft (Allen et al., 2010; Le Quéré et al., 2015). Die letzten beiden sind für eine Reduzierung der weltweiten Waldbedeckung um über 40% verantwortlich (DeFries, 2013). Wälder spielen eine

wesentliche Rolle bei der Abschwächung der Auswirkungen des anthropogenen Klimawandels. Eine Minderung des anthropogenen Klimawandels ist möglich, indem Informationen über die Verteilung terrestrischer Kohlenstoffquellen und -senken durch ein Waldmonitoring zusammen mit genaueren Schätzungen der damit verbundenen Biomasse durchgeführt und ständig verbessert wird. Diese Informationen können dann nationalen und internationalen Entscheidungsträgern bei der Festlegung einer klimafreundlichen Forstpolitik für den Schutz, die Aufforstung und die Wiederherstellung von Wäldern dienen.

Wälder in der Russischen Föderation sind von besonderer Bedeutung für die Überwachung. Es ist das waldreichste Land der Welt. Wälder bedecken 49% seiner Gesamtfläche (FAO, 2012). Gleichzeitig ist es das Land mit der höchsten Unsicherheit bei der Berechnung des globalen Kohlenstoffbestands (Pan et al., 2011). Die Wälder in Russland unterliegen dramatischen Veränderungen aufgrund häufigerer, katastrophaler Waldbrände. Infolge der globalen Erwärmung und der dadurch zu erwartenden Hitzewellen wird eine weitere Zunahme der Häufigkeit von Waldbränden prognostiziert (Shvidenko, Schepaschenko, Sukhinin, McCallum, & Maksyutov, 2011). Dadurch und aufgrund der Freisetzung großer Mengen an Treibhausgasen (z.B. Methan) durch auftauenden Permafrost, könnte mehr Kohlenstoff freigesetzt werden als durch die Abholzung der Wälder in den Tropen (FAO, 2012). Darüber hinaus wurden einige Waldgebiete in Sibirien aufgrund mangelnder finanzieller Unterstützung seit mehr als zwei Jahrzehnten nicht mehr inventarisiert (Shvidenko, Schepaschenko, Sukhinin, et al., 2011). Die illegale Abholzung ist auch eine Herausforderung bei der Überwachung der russischen Wälder (WWF Russia, World Bank).

Fernerkundung ist eines der Instrumente, um eine systematische und operationelle Waldüberwachung sicherzustellen. Damit können Daten über große Gebiete mit einer hohen Wiederholungsrate und zu relativ geringen Kosten erfasst werden. Hierbei sind Mikrowellensensoren besonders gut geeignet, da sie wetter- und tageslichtunabhängige, systematische Beobachtungen mit hoher zeitlicher Frequenz liefern können.

Das Hauptziel dieser kumulativen Dissertation war es, Methoden zur Schätzung von Waldparametern aus Fernerkundungsdaten zu entwickeln, die mit Synthetic Aperture Radar (SAR) gewonnen werden. Unter Verwendung der vom Sensor erfassten weltraumgestützten SAR-Daten mit der längsten derzeit im Weltraum verfügbaren Wellenlänge, dem L-Band, wurden Methoden zur Abschätzung der oberirdischen Waldbiomasse entwickelt. Hierzu wurden Algorithmen für maschinelles Lernen (ML) angewendet und validiert. Diese Methoden wurden ausgewählt, weil sie für große Datenmengen (Big Data) und ein unvollständiges theoretisches Verständnis

von Prozessen, z. B. der Interaktion zwischen dem Wald und dem Radarsignal, empfohlen werden und in Waldüberwachungsstudien relativ neu sind. Darüber hinaus wurde eine verbesserte Kartierung der Waldänderung der Waldfläche in großem Maßstab durchgeführt.

Basierend auf einer umfassenden Literaturrecherche wurden die folgenden vier Forschungsfragen formuliert und analysiert:

1. Wie kann die großflächige Kartierung borealer Waldveränderungen mithilfe von SAR-L-Band-Produkten verbessert werden? (Papier 1, Kapitel 4.1)
2. Was sind die Forschungsrichtungen für die Schätzung der oberirdischen Biomasse borealer Wälder unter Verwendung von SAR-Daten? (Papier 2, Kapitel 4.2)
3. Wie können multi-temporale InSAR-Kohärenz- und Rückstreudaten kombiniert werden, um die Schätzung der oberirdischen Biomasse in borealen Wäldern zu verbessern? (Papier 3, Kapitel 4.3)
4. Wie kann die Fusion von multi-temporaler und Multifrequenz-SAR-Daten verbessert oberirdische Biomasse Schätzung in borealen Wäldern? (Papier 4, Kapitel 4.4)

Zur Beantwortung der obigen Forschungsfragen wurden sowohl die in SAR enthaltenen Amplituden- als auch die Phaseninformationen zur Überwachung der borealen Wälder in Sibirien verwendet. Das Forschungsgebiet befand sich im asiatischen Teil der borealen Wälder in Südmittelsibirien in Russland. Insgesamt wurden die Studien in drei Forschungsgebieten durchgeführt. Der Algorithmus zur Überwachung der Waldänderung der Waldfläche wurde in einem Gebiet mit einer Fläche von ca. 620.000 km^2 entwickelt, während oberirdische Biomassemodelle über 200 km^2 und 2.000 km^2 trainiert und getestet wurden. Die in dieser Studie verwendeten Referenzdaten wurden im Rahmen der Russischen Waldinventur und -planung gesammelt und unter Verwendung eines neuen regionalen allometrischen Modells aktualisiert (Stelmaszczuk-Górska et al., 2016). Daten von zwei L-Band-Sensoren der neuen Generation, nämlich vom Phased Array Type L-band Synthetic Aperture Radar PALSAR und PALSAR-2 (33 Datensätze) sowie von ALOS PALSAR-Rückstreumosaiken (364 Datensätze), wurden analysiert. Zusätzlich wurden SAR-Daten im C-Band als ergänzende Informationen zu den L-Band-Daten verwendet. In dieser Studie wurden die vom Satelliten RADARSAT-2 (7 Datensätze) erfassten Daten analysiert, da sie in der Sentinel-1-Vorbereitungsphase eine wichtige Rolle spielten.

Um die großflächige Wald-/Nichtwaldklassifizierung zu verbessern, wurde ein integrierter GIS- und Vorklassifizierungsansatz getestet. Insgesamt wurden 364 1-

Grad-Kacheln mit jährlichen Mosaiken von ALOS PALSAR verwendet. Für die Überwachung von Waldverlusten wurden nur HV-polarisierte Daten verwendet. Verschiedene zeitliche Maßnahmen wurden implementiert, um die Trennung von Klassen der Veränderung von Wald zu Nicht-Wald bzw. von Nicht-Wald zu Wald zu bewerten. Ein einfacher Schwellenwertansatz basierend auf einem SAR-Mosaikverhältnis wurde für die endgültige automatische Kartierung von Waldänderungen verwendet. Die Differenz zwischen den SAR-Aufnahmen von 2 dB wurde implementiert. Das gefundene hohe Potenzial für L-Band-Sensoren unter Verwendung von HV-Kreuzpolarisationsdaten für die großflächige Waldkartierung stimmte mit anderen früheren Studien überein (e.g., Santoro et al., 2012). Veränderungen im Untersuchungsgebiet wurden mit einer Genauigkeit von ca. 70% erfasst. Der größte Teil des Waldverlustes wurde 2008 und 2010 in der nordöstlichen Region des Untersuchungsgebiets beobachtet. Der gleiche Trend und das gleiche Muster von Veränderungen zeigten die globale Waldänderungstkarte von Hansen et al. (2013). (Hansen et al., 2013).

Eine Literaturrecherche zur Schätzung der oberirdischen Biomasse unter Verwendung von SAR hat gezeigt, dass die meisten Studien die Daten von C-Band-Satellitenmissionen gefolgt von L-Band- und X-Band-Daten verwendeten und sich auf europäische Standorte und Testgebiete konzentrierten. Dies hing mit der Datenverfügbarkeit zusammen. Nur 12% der verwendeten Daten wurden über Standorte in Sibirien erfasst. Der Schätzfehler der oberirdische Biomasse lag zwischen 119% (Santoro, Askne, Smith, & Fransson, 2002) und 5,1%, wenn die multi-temporale Kombination von ALOS PALSAR-Rückstreukoeffizientendaten auf Waldparzellenebene in einem maschinellen Lernansatz verwendet wurde (Andersen, Strunk, Temesgen, Atwood, & Winterberger, 2011). Die meisten der dargestellten Methoden verwendeten semi-empirische Modelle. Obwohl bei der Schätzung der oberirdischen Biomasse von Wäldern längere Wellenlängen vorgeschlagen werden, wurden in letzter Zeit die höchsten Genauigkeiten unter Verwendung von X-Band-Daten gefunden. Die höchsten Schätzgenauigkeiten werden unter Verwendung einer Kombination von Daten aus mehreren unterschiedlichen SAR Sensoren erwartet (Santoro & Cartus, 2018; Santoro, Cartus, Fransson, & Wegmüller, 2019).

Um multi-temporale InSAR-Kohärenz- und Rückstreudaten zu kombinieren, wurden zwei weit verbreitete Algorithmen für maschinelles Lernen unter Verwendung von dreizehn Variablen implementiert. Die Modelle Maximum Entropy (MaxEnt) und Random Forests (RF) zeigten eine gute Performance und vielversprechende Abschätzungen. Die RMSEs betrugen 35,8 t/ha (38,8%) und 35 t/ha (36,9%) für die Modelle MaxEnt bzw. RF. Kohärenzdaten waren für die

Abschätzungen im niedrigen und hohen oberirdischen Biomassebereich am wichtigsten, während die neue Rückstreu-Kohärenz-Ratio im mittleren bis hohen Bereich gute Ergebnisse lieferte. Demnach könnte eine Strategie zur Verwendung unterschiedlicher Datensätze zur Schätzung unterschiedlicher oberirdischer Biomassewerte die Genauigkeit der Biomasseschätzung weiter erhöhen. Des Weiteren wurde beobachtet, dass der Beitrag der Radarrückstreuung bei der Modellkonstruktion sich nach dem Filtern erhöht hat. Der RF-Algorithmus lieferte eine mittlere Schätzung der Biomasse, die nahezu dem Referenzwert entspricht. Andererseits lieferte MaxEnt eine realistischere räumliche Verteilung der oberirdischen Biomassewerte.

Multi-temporale SAR-Daten verschiedener Wellenlängen wurden unter Verwendung von fünf ML-Modellen kombiniert, die auf neun bis fünfundvierzig SAR-Produkten basierten. Wie erwartet zeigten die langwelligeren L-Band-Daten bei HH- und HV-Polarisationen eine bessere Eignung als die C-Band-Daten in HH- und HV-Polarisation. Ein Vergleich der Schätzfehler zeigte, dass gefilterte und kreuzpolarisierte gefilterte L-Band-Daten ausreichen, um die oberirdische Biomasse mit guter Genauigkeit (ca. 30%) zu schätzen. Die Einbeziehung von Verhältnis- und Texturmaßen sowie C-Band-Daten verbesserte die Schätzgenauigkeit nicht. RADARSAT-2-Daten, die im Ultrafine-Modus aufgenommen wurden, zeigten eine größere Empfindlichkeit gegenüber der Rauigkeit von Objekten, wodurch die Korrelation zwischen SAR- und Referenzdaten verringert und somit höhere Schätzfehler erzeugt wurden. Der niedrigste Schätzfehler wurde allein für gefilterte L-Band-Daten berechnet und betrug 29,1 t/ha (30%). Im Allgemeinen lieferten alle Modelle überschätzte oberirdische Biomassewerte mit einer Abweichung von 3,9 t/ha (C-Band im Feinmodus) bis 10,6 t/ha (C-Band im Ultrafeinmodus). In früheren Studien, in denen nur L-Band-Daten angewendet worden sind, wurden relative Schätzfehler von 33,4% bis 42,44% für sibirische boreale Wälder berichtet (C. Hüttich et al., 2014; Wilhelm, Hüttich, Korets, & Schmullius, 2014).

Die Ergebnisse dieser Arbeit zeigten, dass für zukünftige Waldüberwachungsstudien eine Kombination aus multi-temporalen, multi-frequenten und interferometrischen SAR (InSAR) Daten verwendet werden sollten. Im Jahr 2022 werden weltraumgestützte Missionen, die im X-, C- und L-Band aufnehmen werden, durch weltraumgestützte P-Band- (BIOMASS) und neue L-Band-Missionen (z. B. TanDEM-L) ergänzt. Die Verfügbarkeit von InSAR-L- und P-Band-Daten in eine gleichzeitige Aufnahme sollte die Kartierung von Waldveränderungen und die Schätzung der Biomasse verbessern. Das ständig wachsende Archiv von Zeitreihen von SAR-Daten und die Komplexität der

Interaktion von SAR-Signalen und Wäldern legen die Verwendung neuer Methoden, z. B. maschinelles Lernen, zur Datenauswertung nahe. Dies ist ohne zuverlässige und umfangreiche Referenzdaten nicht möglich. Derzeit sind neue Bodendatenerfassungstechnologien wie z.B. Unbemannte Luftfahrzeuge möglich. In Zukunft können diese bisherige Standardtechniken für die Bestandsaufnahme von Waldressourcen ersetzen und derzeit noch unbekannte Fehler bei menschlichen Messungen beseitigen.

Chapter 1

Introduction

Importance of forest monitoring

Remote sensing for forest monitoring

Scope and structure of this thesis

1.1 Importance of forest monitoring

Forest is defined as a "*land spanning more than 0.5 hectares with trees higher than 5 meters and a canopy cover of more than 10 percent, or trees able to reach these thresholds in situ"* (FRA, 2018). The importance of forest monitoring is manifold. It is of essential ecological, social, economic, and political value. Forests play an important role in the regulation of ecosystems, as they interact with water, energy, and carbon cycles, climate change, and biodiversity. They are vital for protection and regulation of water resources and quality. Forests provide important carbon storage as they bind significant amounts of atmospheric carbon. The forest conservation, afforestation, and restoration are key strategies for climate change mitigation (Bastin et al., 2019; Erb et al., 2018). They are rich in habitat and species diversity. Forests are places for recreation. They are essential to the economy as a source of renewable energy and valuable forest products such as wood, paper, and pulp. They are subject to local, national, and international policies aimed at balancing the economic and environmental needs. Moreover, since one third of the total global forest areas is used for production purposes (FAO, 2006), forest policies should rely on quantitative estimates of the current and future parameters of the forest condition and structure.

Climate change and carbon cycle

In 2019 and beginning 2020, forests and forest mortality were of particular concern not only for scientists but also for politicians and many citizens due to the increased number of large fires of the Amazon rainforest, series of uncontrolled Australian bushfires, and wildfires of the Siberian boreal forests and the related carbon dioxide (CO_2) and other greenhouse gases (GHG) emissions into the atmosphere. The main cause of this situation are the dry conditions due to global warming (IPCC, 2018b). Droughts in many regions of the world combined with human-induced fires in the tropics lead to more frequent and more severe large forest fires and promote insect outbreaks leading to tree dieback (Allen et al., 2010; Le Quéré et al., 2015). In addition to natural forest mortality, economic drivers and agriculture expansion have been the main causes of changes in forest cover through the years; together, these two forces are responsible for over 40% of the reduction of the world's forest cover (DeFries, 2013). It has been estimated that forests currently store ca. 50% of the carbon they potentially could retain globally (Erb et al., 2018). Moreover, global warming, especially in high latitudes, leads to shifts in boundaries of forests biomes

(Beck et al., 2011). Apart from changes in carbon storage, deforestation and forest mortality also interact with climate change through changes in albedo and evapotranspiration of the land surface (Bonan, 2008).

Climate change constitutes one of the main global crises in the 21st century. It manifests itself distinctly in global warming and its effects. Global warming has been caused by the anthropological pressure on the environment, mainly by the human-caused emissions of GHG, such as CO_2, methane (CH_4), and nitrous oxide (N_2O), into the atmosphere. From the beginning of the industrial era, since 1750, atmospheric CO_2 increased by 40%, CH_4 by 150%, and N_2O by 20% from which the concentration of CO_2 in the atmosphere is the highest (Ciais et al., 2013). Countries have committed to reduce the GHG emissions within the international conventions on climate change. The objective of the United Nations Framework Convention on Climate Change (UNFCCC) is "*stabilization of greenhouse gas concentrations in the atmosphere at a level that would prevent dangerous anthropogenic interference with the climate system*" (UN, 1992). In 1998, a follow-up document was agreed - the Kyoto Protocol. It is an implementation and commitment act of UNFCCC. Under Article 3.1 of the Kyoto Protocol, the industrialized countries have agreed to reduce overall emissions of GHG by at least 5 percent below 1990 levels in the commitment period 2008 to 2012 (UN, 1998). The document entered into force in 2005. In 2008, the United Nations Collaborative Programme on Reducing Emissions from Deforestation and Forest Degradation in Developing Countries (UN-REDD) was launched. The Programme supports climate change mitigation solution REDD+ - Reduce Emissions from Deforestation and forest Degradation, conservation of existing forest carbon stocks, sustainable forest management and enhancement of forest carbon stocks in developing countries a framework agreed by the UNFCCC in 2010 at the 16th session of the Conference of the Parties (COP-16). The current knowledge on climate change is summarized in the Intergovernmental Panel on Climate Change (IPCC) reports (IPCC, 2014, 2018a). The provided information is intended to be used to develop climate policies.

The quantification of the carbon cycle is key to improve our understanding of its response and feedback to climate change as CO_2 is one of the primary GHG. The global carbon cycle describes the exchange of carbon between the four major reservoirs (pools), i.e., atmosphere, oceans, land, and rocks and sediments (including fossil fuels). The distribution of terrestrial carbon sources and sinks is not yet well known (Herold et al., 2019). In order to mitigate the consequences of climate change it is important to improve our knowledge of the distribution of terrestrial carbon stocks and changes therein and the effects of forest mortality and land use (LU) and land cover change (LCC) on carbon stocks and the feedbacks of its changes on

climate. This can be provided through accurate and reliable LULCC monitoring, along with more precise estimates of the associated biomass gain and loss. Biomass is an Essential Climate Variable (ECV) (Bojinski et al., 2014; FAO, 2009). It is defined as the mass of all organic matter per unit area (e.g., tons/ha) and can be divided into aboveground biomass (AGB; biomass growing above the ground level) and belowground biomass (BGB; biomass growing below the ground level). Estimates of biomass change will give insight on the carbon balance (carbon sink or source) of the terrestrial vegetation and underlying drivers and hence can be used to improve carbon-cycle models (Carvalhais et al., 2014; Reichstein & Carvalhais, 2019).

Forest ecosystems as an important carbon stock

Forests cover 31% of the total land area (FAO, 2010). They account for more than 70% of the terrestrial biomass (Bar-On et al., 2018; Houghton, Hall, & Goetz, 2009) and currently acting as an important carbon sink at the global scale (Ciais et al., 2013; Pan et al., 2011). Trees hold much more carbon per unit area than other types of vegetation (Houghton, 2007). They assimilate carbon through the process of photosynthesis and accumulate it in the different tree compartments, i.e., stem, branch, root, and foliage. Forests are supposed to store approximately 45% of the carbon sequestered in land ecosystems (Bonan, 2008). Forests can constitute also a carbon source, in particular in case of LULCC. They account for 90%-95% of the net emission from LULCC (Houghton, 2013). Deforestation and forest degradation through intensive agricultural expansion, illegal logging, fires, etc., account for ca. 20% of global CO_2 emissions (IPCC, 2007).

Sustainable forest management

Since the middle of the 19th century the need for more quantitative information on forest parameters has been increasing worldwide (van Laar & Akca, 2007). Traditionally, the main interest to collect information on forest resources has been the optimization of the current and future volume and biomass of timber and by-products at local, regional, and national levels. However, in the last decades, with new technological developments and international and national commitments the forest monitoring systems have become more demanding, e.g., through National Forest Inventories (NFI) including GHG inventories, certification schemes and the Global Forest Resources Assessment (FAO, 2018).

Many countries have already developed operational methodologies for forest biomass inventories, e.g., in European countries, for example in Sweden by the Swedish Forest Agency. The inventories often differ in terms of definitions, details

and accuracy of information provided. The inventories are conducted typically every five to ten years based on field surveys, or a combination of remote sensing, airborne and spaceborne, and field measurements. However, there are still many countries, e.g., developing countries and/or countries where *in situ* monitoring is challenging, which provide biomass information associated with high uncertainties. In these cases, remote sensing-based information could be a useful data source.

All above-mentioned aspects make monitoring of forest biomass and its change necessary elements for sustainable forest management and for carbon accounting efforts. The scientific mission is to meet the users and policy needs and to provide robust, transparent, comparable, and plausible methodology for forest monitoring. Remote sensing is recommended as one of the tools that can provide systematic and operational forest monitoring, hence can contribute to better understanding of the carbon balance in forest ecosystems.

1.2 Remote sensing for forest monitoring

The Kyoto Protocol follow-up decisions, the Paris Agreement on Climate Change (UNFCCC, 2015) and the United Nations (UN) Sustainable Development Goals (UN, 2019), constitute guidance related to the GHG emission monitoring. To meet the policy needs, remote sensing is proposed as one of the methods for carbon measuring and monitoring techniques (IPCC, 2007). In the Report of the 15th session of the COP, held in Copenhagen from 7 to 19 December 2009 it is stated that (Decision 4/CP.15) national forest monitoring systems should be based on the usage of "*a combination of remote sensing and ground-based forest carbon inventory approaches for estimating, as appropriate, anthropogenic forest-related greenhouse gas emissions by sources and removals by sinks, forest carbon stocks and forest area changes*". Remote sensing is increasingly proposed as a mean of globally consistent monitoring tool (Cihlar et al., 2002).

In general, there are four methods of biomass estimation (FAO, 2008): (i) destructive *in situ* measurements, (ii) non-destructive *in situ* estimation, (iii) remote sensing-based estimation, and (iv) physical models (Figure 1.1).

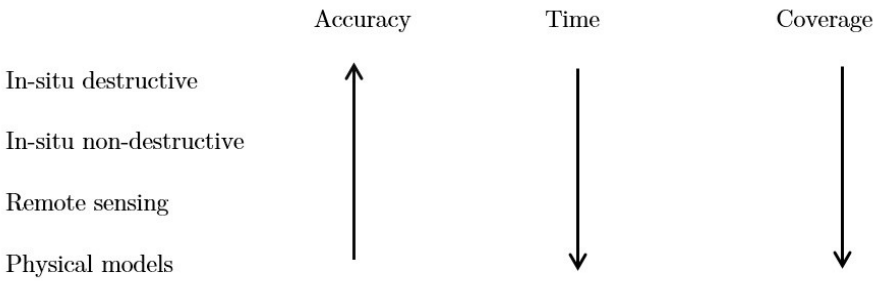

Figure 1.1: Methods of biomass estimation in terms of accuracy, time, and coverage.

Due to the high temporal dynamics and vast area of forests, remote sensing techniques are increasingly proposed as globally consistent environmental monitoring tools (Cihlar et al., 2002). Remote sensing can acquire data over large areas with a high repetition frequency and at a relatively low cost. Scientists have already demonstrated that remote sensing can contribute to monitoring of forested areas and estimating current carbon sources and sinks. There are extensive publications available on the topics of optical, LiDAR (Light Detection and Ranging), and radar remote sensing data in the context of forest monitoring. Several publications provide a comprehensive review, including sourcebooks of recommended methods and data sources (Fatoyinbo, 2012; GOFC-GOLD, 2009; Kellndorfer, Cartus, Bishop, Walker, & Holecz, 2011; Santoro & Cartus, 2018).

Remote sensing cannot measure forest biomass directly. However, when properly related to biophysical parameters, remote sensing data provide information from which AGB can be estimated. Moreover, in response to the need of forest monitoring, the number of new enhanced spaceborne missions for systematic mapping of forest ecosystems steadily increases (e.g., GEDI, NiSAR, Tandem-L, and BIOMASS).

A great effort has been done to provide global and regional, consistent, and systematic products for forestry. The most of them present forest cover and its changes over time. Other variables of forest are also possible to monitor using remote sensing data (e.g., forest height, tree cover and forest aboveground biomass). Recently, forest related vegetation maps have been published for global (Hansen et al., 2013; Hu et al., 2016; Lefsky, 2010; Santoro, 2018; Shimada, Takuya, et al., 2014; Simard, Pinto, Fisher, & Baccini, 2011), pan-tropical (Baccini, Laporte, Goetz, Sun, & Dong, 2008; Hansen et al., 2016; Saatchi et al., 2011), and northern hemisphere regions (Santoro et al., 2015) using fusion of optical, LiDAR, and/or SAR (Synthetic Aperture Radar) data. Furthermore, the global vegetation products and Pan-European high resolution layers of forested areas are available through the EC and ESA Program Copernicus (EU, 2014; Langanke, 2015). The above-

mentioned products have been or are created with a different time frequency, from annual or multi-annual to single date products. Some techniques require more investigations to move towards an operational stage (Avitabile, Herold, Henry, & Schmullius, 2011; Goetz & Dubayah, 2011; Santoro & Cartus, 2018; Tang, Bullock, Olofsson, Estel, & Woodcock, 2019).

Passive optical data

Historically, passive optical data have been the primary data source for forest monitoring. Optical images are the records of the sun radiance interactions with the objects.

Passive optical satellite sensors provide systematic observations of land cover at different levels from global to local, for instance, from, NOAA AVHRR observations, through MODIS, Landsat, ASTER, SPOT-5 to IKONOS like very high-resolution data. However, biomass estimates are limited because sensors are insensitive to biomass under closed canopies (Houghton et al., 2007). It is due the fact that the sunlight hardly penetrates into the forest. Nevertheless, the medium, high and very high resolution data in combination with other remote sensing and ground data using geostatistical or model-based approaches have been already successfully implemented for global biomass estimates (Baccini et al., 2008; Saatchi et al., 2011) and local forest inventory purposes, e.g., for forest stand density and volume estimation (Franco-Lopez et al., 2001; Muinonen et al., 2001; Tomppo et al. 2002; Pekkarinen, 2002; Muukkonen et al., 2005, 2007; Luther et al. 2006; Fuchs et al. 2009). Moreover, spectral information from optical Earth Observation (EO) data are of particular use in case of mapping different vegetation types and vegetation conditions, as well as detection of forest fires or other disturbances (Fassnacht et al., 2016, 2017; Souza, Firestone, Silva, & Roberts, 2003). Additionally, indirect estimates of biomass are feasible using vegetation indices, e.g., Normalized Difference Vegetation Index (NDVI), Leaf Area Index (LAI), and Fraction of Absorbed Photosynthetically Active Radiation (FAPAR), Bidirectional Reflectance Distribution Function (BRDF), and texture (Avitabile, Baccini, Friedl, & Schmullius, 2012; Boyd, Foody, & Curran, 1999; Dong et al., 2003; C. Joshi, Leeuw, Skidmore, Duren, & van Oosten, 2006; Sader, Waide, Lawrence, & Joyce, 1989; Wasseige & Defourny, 2002; Zheng et al., 2004). The main limitation of satellite optical data is cloud cover and haze that decreases data capability of forming basis for routine forest monitoring in near-real time.

LiDAR data

Unlike passive optical data, laser altimetry, known as LiDAR, has the potential to penetrate the forest canopy (Lefsky, Cohen, Parker, & Harding, 2002). The LiDAR system is an active remote sensing system. It measures distance between the sensor and the target by determining the time difference between the transmission of the laser light pulse (optical wavelength, usually near infrared, NIR) and the detection of light reflected from the target. The target can be the top of canopy, the lower layers of vegetation or the ground, or a mixture of them. The content of information returned to the sensor depends on the size of the illuminated area by a single laser beam, i.e., the laser footprint.

LiDAR measures the three-dimensional (3D) vegetation structure that can be used to estimate various forest parameters, such as canopy height, for example. The tree height can then be applied using models or allometric equations, i.e., relationships between the tree characteristics, to estimate AGB. LiDAR data have shown great potential for estimating AGB over a range of geographic scales without signal saturation (Babcock, Finley, Cook, Weiskittel, & Woodall, 2016; Bortolot & Wynne, 2005; Lefsky et al., 1999; Means et al., 1999; Næsset et al., 2011; Ross Nelson, Krabill, & Tonelli, 1988; Nilsson, 1996; Patenaude et al., 2004). In practical applications, mainly airborne laser scanning (ALS) has been used to monitor forest resources. Although the prices of ALS are constantly decreasing, for larger areas the measurements are still too expensive. The alternative to the ALS-based forest measurements are spaceborne sensors.

The first operating system in space was the Shuttle Laser Altimeter (SLA) (Garvin et al., 1998) followed by the Geoscience Laser Altimeter System (GLAS) on-board NASA's Ice, Cloud and Land Elevation Satellite (ICESat) (Schutz, Zwally, Shuman, Hancock, & DiMarzio, 2005). The first space LiDAR was used for the topographic measurements and flown aboard the Space Shuttle Endeavour in January of 1996. ICESat was in operation from 2003 to 2009. The sensor was developed primarily for the ice sheet measurements. The footprint was 70 m, too large for precise forest mensuration. The large footprint introduced disturbing topographic effects and bias due to averaging (Lefsky et al., 2005; Nelson et al., 2009; Simard et al., 2011). To avoid these limitations, a successor of ICESat satellite was launched in September 2018. The ICESat-2 satellite carries the Advanced Topographic Laser Altimeter System (ATLAS) that uses photon counting multi-beam approach (Harding et al., 2010), which should increase the ATLAS performance and its application for vegetation monitoring. The data from the sensor, with a nominal 17 m diameter footprint with an along-track sampling interval of

0.7 m (Markus et al., 2017), have been released in August 2019 (NSIDC, 2019). Another spaceborne sensor in operation is the Global Ecosystem Dynamics Investigation (GEDI) LiDAR (Dubayah et al., 2020). It is a system mounted on the International Space Station (ISS). It was successfully launched in December 2018 with a mission to produce high-resolution 3D observations of the tropical forests. The instrument provides measurements with 25 m footprint in diameter. The first products have been released in January 2020 (NASA & University of Maryland, 2020). Both data sources are freely available. New JAXA's LiDAR mission, the Multi-footprint Observation LIDAR and Imager (MOLI), is planned to be launched in 2021 (Herold et al., 2019). As in case of passive optical data, the cloud cover limits the spaceborne LiDAR measurements of vegetation (Simard et al., 2011).

SAR data

Sensors that can observe forested areas despite the cloud cover are the microwave systems. The studies on the use of the imaging SAR for forest monitoring has been carried out since more than 30 years.

The first radar applications were done simultaneously to the developments in radar systems. The earliest was done in 1967 in case of mapping tropical forest in Darien Province in Panama. It was carried out using airborne platform with mounted Ka-band (1.18–0.75 cm wavelength) radar antenna. The first spaceborne SAR SEASAT L-band was launched in 1978. Although designed for ocean monitoring, it showed considerable results for land applications (Henderson & Lewis, 1998). Starting from the end of 80's a boom in radar backscatter studies of forest can be observed (Kessler, 1987; Sader, 1987; Wu, 1987). Data acquired by new systems with longer and multi-wavelength and multi-polarization have been evaluated. It is already known that radar data are physically related to the vegetation characteristics allowing retrieving forest AGB and other correlated parameters (Dobson et al. 1992; Le Toan et al. 1992; Beaudoin et al. 1994). Many SAR properties can be exploited to estimate forest parameters; these properties are: backscattering intensity (e.g., Pulliainen *et al.* 1994, Fransson & Israelsson 1999, Ling *et al.* 2008), interferometric phase (e.g., Solberg *et al.* 2010, Askne *et al.* 2013), interferometric coherence (e.g., Koskinen *et al.* 2001, Santoro *et al.* 2002), polarimetric signatures (e.g., Papathanassiou & Cloude 2001, Neumann *et al.* 2012), SAR tomography, and radargrammetry (e.g., Tebaldini & Rocca 2012, Persson & Fransson 2014). SAR imagery can be efficiently applied for forest cover and disturbance mapping, but in terms of biomass estimation, the capability is limited due to the signal saturation, i.e., a loss of signal sensitivity to forest AGB above certain value (Imhoff, 1995; Le Toan, Beaudoin, Riom, & Guyon, 1992). The latter

can be overcome using longer radar wavelengths, e.g., P-Band on the future ESA BIOMASS mission, together with information on forest characteristics, e.g., forest structure (Joshi et al., 2017).

A major advantage of the radar remote sensing is that it can provide weather and sun independent, systematic observations with high temporal frequency over large areas. Hence, this technology is recommended for forest monitoring to inform international climate policy and related international programs (e.g., Global Forest Resources Assessment led FAO). It is part of initiatives such as Global Forest Observations Initiative (GFOI), i.e., a flagship program of the Group on Earth Observations (GEO), ALOS Kyoto & Carbon Initiative (ALOS K&C), and the Global Forest Watch established by the World Resources Institute. The main objective of all above mentioned programs and initiatives is to provide systematic and synoptic information on forest extent, its condition, and management practices. This can further support national, regional, and global efforts in sustainable, continuous, economically efficient and ecological forest use.

Currently, the use of satellite data for forest monitoring is moving from local studies using a limited number of satellite images to national, regional, and global big data monitoring scenarios. The first radar-based systematic, i.e., coverage within short time periods, observation strategy dates back to the L-band mission JERS-1 (Rosenqvist et al., 2000). This acquisition strategy was continued with a launch of ALOS and ALOS-2 satellite missions (Rosenqvist et al., 2014; Rosenqvist, Shimada, & Watanabe, 2004). With the launch of the Sentinel-1 C-band SAR mission (Torres et al., 2012), for the first time, dense time series of SAR data are freely available.

Comparison of different sensors

A comparison of different satellite remote sensing sensors indicates their advantages and disadvantages (Table 1.1).

The use of remote sensing data for forest monitoring is necessary and in many cases already operational, e.g., the system of annual global monitoring of forest loss and the early warning system for forest disturbances developed as part of the Global Forest Watch Initiative (Hansen et al., 2016, 2013).

From a review of available remote sensing techniques, the most promising approach to estimate forest AGB and forest cover change shall be the use of SAR data and/or SAR and LiDAR data fusion. The fusion method is highly recommended as a way to maximize the use of remote sensing techniques (Mitchell, Rosenqvist, & Mora, 2017; Genevieve Patenaude, Milne, & Dawson, 2005; Rosenqvist, Milne, Lucas, Imhoff, & Dobson, 2003; Sun et al., 2011)

Table 1.1: A comparison of remote sensing techniques for forest monitoring.

	Sensitivity to biomass	**Affected by saturation**	**Coverage**	**Main advantage**	**Main disadvantage**
LiDAR	yes	no	from local to global	direct measurement of a 3D vegetation structure	point measurement; limited number of spaceborne sensors; limited to cloud free weather conditions
Passive optical data	limited	yes	from local to global	intuitive data interpretation; many spectral information	limited to sun position and cloud free weather conditions
SAR	Yes	depends on the wavelength used	from local to global	provide data on regular basis; future missions	many parameters that influence the SAR signal (e.g., moisture content, topography); no long wavelength satellite sensor (e.g., P-band) currently available

Machine learning approaches in remote sensing

The amount of data currently generated from remote sensing sensors, e.g., from the Sentinel missions through Copernicus Program (European Union, 2014), is growing exponentially. Available large volumes of data, i.e., big data, cannot be any more effectively processed and analyzed without implementing the new developments in digital technologies (Bruzzone et al., 2016; Garrison et al., 2019). One of these developments is machine learning (ML) a branch of Artificial Intelligence (AI) that is based on the algorithms and statistical models that are capable of learning from data and human interactions, relying on patterns and inference (Bamler et al., 2018; Lary et al., 2018). The ML is a game changer in many areas from science and medicine to technology and business. The algorithms are commonly used for classification, predictions, and data mining purposes. Over the last decade, the ML has also been successfully implemented in many remote sensing applications. It is particularly recommended to use in case of incomplete theoretical understanding of the biophysical processes, for which a large number of observations are available (Lary, Alavi, Gandomi, & Walker, 2016).

A meta-analysis of 1651 articles summarized that the machine-learning methods for classification purposes performed better than other classifiers, e.g., maximum likelihood algorithm (Yu et al., 2014). Recent extensive review articles on using the

ML in remote sensing have confirmed generally better classification accuracies obtained using ML approaches (Belgiu & Drăgu, 2016; Maxwell, Warner, & Fang, 2018; Pal & Mather, 2005). These articles report mainly on the use of ML for classification in remote sensing. However, the applications of ML in remote sensing is very diverse and ranges from bias correction and cross calibration to land, ocean and atmosphere monitoring (Belgiu & Drăgu, 2016; Lary et al., 2018). One of the applications is forest monitoring and retrieval of its biophysical parameters. The forest parameters, e.g., AGB, tree height, forest cover, have been classified or retrieved with high accuracy at different spatial scales from global (Hansen et al., 2013; Simard et al., 2011), continental (Baccini et al., 2008; Saatchi et al., 2011), national (Avitabile et al., 2012; Urbazaev et al., 2018), regional (Tanase et al., 2014) to local (Stelmaszczuk-Górska, Sagischewski, & Chmara, 2017).

One of the main disadvantages of the ML algorithms is that, the methods are 'black boxes', i.e., methods that do not provide appropriate explanations on how the classification/regression results are derived (Lary et al., 2016; Maxwell et al., 2018). However, some methods provide additional statistical outputs, e.g., Random Forests (RF) relative importance of each predictor variables in the model (Breiman, 2001), that can be used to better understand the classification/regression models. Nevertheless, the algorithms need to be used with caution and the results obtained using the ML should be interpreted taking into account the physical principles together with other relevant scientific information. Additionally, as ML is an empirical approach, the algorithms need a comprehensive set of training data (to mitigate the Hughes phenomenon (Hughes, 1968)), which often is difficult to obtain. The need of the large number of representative reference data often limits model transferability. It is also often prone to overfitting (Belgiu & Drăgu, 2016).

The main advantages of the ML approaches, on the other hand, are that the methods do not make assumptions about the data distribution, i.e., are non-parametric, the algorithms are robust extracting information from data automatically, and outperform the classical approaches. Hence, it seems that in the era of big data the use of the ML algorithms together with additional information that allow the interpretation of the ML models performance will be a very effective approach.

1.3 Scope and structure of this thesis

Based on the above considerations, the main scope of this thesis is to develop methods for estimating forest parameters based on SAR, because at the time of writing this dissertation LiDAR data for regional purposes were not available. Using the spaceborne SAR data acquired by the sensor with the longest wavelength available from space, L-band, the method for forest AGB estimation has been developed. For this, ML algorithms have been applied and evaluated. Moreover, an effort to establish an improved operational large-scale mapping of forest change has been made.

This introductory part serves as background to this cumulative dissertation outlining the overall motivation to monitor forest biomass and forest change using ground- and space-based remote sensing data. It gives an overview of national and international forest monitoring needs, and presents the use of EO technology for forest monitoring.

The thesis is organized as follows:

- ✓ Chapter 2 presents the theoretical background of SAR and describes a state-of-the art in terms of forest monitoring by means of radar remote sensing. First, the characteristics of boreal forests and challenges associated with their monitoring are provided. Afterwards, a brief introduction to radar theory is given. Radar principles and radar scattering from different type of surfaces and volumes, with particular emphasis on scattering from forests, are described. The processing steps of radar data analyzed in this thesis are discussed. Afterwards, developments in the radar remote sensing for boreal forest monitoring are reported. The chapter ends with a description of research areas and the data used.

- ✓ Chapter 3 summarizes the state-of-the art described in Chapter 2 and on this basis presents the objectives and research questions.

- ✓ Chapter 4 is the main part of this thesis. It presents the research contributions in the context of operational boreal forest monitoring and the use of new AGB estimation methods using multi-frequency and multi-temporal SAR backscatter and interferometric coherence data.

- ✓ Chapter 5 summarizes the results and presents outlook for future research.

Chapter 2

Theoretical background & state-of-the-art

Boreal forests

Radar theory

Radar remote sensing of boreal forests

Biomass estimation

Forest change monitoring

Study area and data

2.1 Boreal forests

The boreal forest, also known as "taiga", is one of the largest terrestrial biome (Breckle, 2002; Gauthier, Bernier, Kuuluvainen, Shvidenko, & Schepaschenko, 2015), covering over 16 million km^2, about one third of the world's forest cover (FAO, 2015; Yale University, 2019). It extends around the circumpolar region, occupying an area in the northern hemisphere down to a latitude of approximately 45°N in Russia and 50°-60° N in northern Europe, Canada, and Alaska (Figure 2.1). It is located in the boreal or subarctic climate zone, which is defined by cold, long winters, occurring for six to eight months and a short growing season with temperatures higher than 10°C for up to 120 days. Precipitation is low and varies across the boreal forest zone, with an average value of 150 to 450 mm/year (Breckle, 2002).

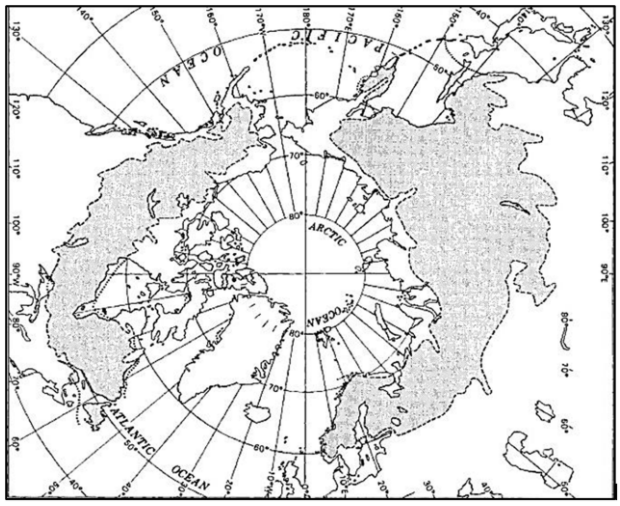

Figure 2.1: Global extent of boreal forest. Adapted from (Hare & Ritchie, 1972).

Boreal forests are characterized by a low diversity of tree species. Typically, the following four main coniferous tree species are present in the biome: spruce (*Picea*), pine (*Pinus*), fir (*Abies*) and larch (*Larix*). Deciduous species are also present, mainly: birch (*Betula*), aspen and poplar (*Populus*), willows (*Salix*), alders (*Alnus*), and mountain Ash (*Sorbus*), which are typical for early succession stages of the forest (Burton et al., 2010).

The boreal forest is a vast biome with unexploited resources and provides valuable benefits in terms of economy, culture and tourism, biodiversity, and climate change from local to global scales. As regards economy, about two-thirds of boreal forests are managed supporting over one million direct jobs (Burton et al., 2010). It

is a major source of forest products such as wood, paper and pulp, which are crucial for manufacturing, energy, and the construction industry, and a place of leisure and spiritual activities. In terms of biodiversity, boreal forests provide a habitat for over 100,000 species of plants and mushrooms, as well as many species of mammals, birds, insects, and other types of animals (Nilsson, 1997). In the regional and global context, the boreal forest supports climate regulation through exchange of energy, water, and carbon between the land surface and the atmosphere (Steffen et al., 2015). It constitutes one of the largest terrestrial carbon pools. Seventy five percent of the carbon in boreal forests is accumulated in the soil, characterizing this region as having one of the most carbon-rich soils in the world (Mukhortova, Schepaschenko, Shvidenko, McCallum, & Kraxner, 2015). One fifth of the carbon is stored in the vegetation, which plays a crucial role in regulating carbon as well as other GHG concentrations in the atmosphere (Pan et al., 2011). Based on the results conducted by Thurner et al. (Thurner et al., 2014) using remote sensing products, carbon stocks in boreal trees (stems, branches, roots, and foliage) for the year 2010 were estimated at 40.7 ± 15.7 Pg C, with the largest carbon stocks in the Asian part of the boreal forests with 22.1 ± 8.3 Pg C (54%) (Table 2.1). Thus, vegetation in boreal forests is the second largest carbon pool after the tropical forests. Neigh et al., 2013 reported the total aboveground carbon in boreal forests to amount to 38 ± 3.1 Pg C.

Table 2.1: Recent total forest carbon values for boreal, temperate, and tropical forests.

Total forest carbon [Pg C]	**North America**	**Europe**	**Asia**	**Sum**
Boreal forests*	8.9±3.7	9.8±3.6	22.1±8.3	40.7±15.7
Boreal forests**	14.0	12.1	27.9	53.9
Temperate**	19.4	10.5	8.3	38.2
	Americas	**Africa**	**South Asia**	
Tropical**	139.8	79.2	43.2	262.1

* From (Thurner et al., 2014)

** From (Pan et al., 2011) Supporting online material Table S3 - Total living biomass from 2007

Forest mortality in boreal forests is characterized by different types of disturbances (e.g., fire, pest outbreaks, windthrow) that play an essential role in the natural processes in the boreal zone (Burton et al., 2010). Forest fires are especially important in nutrient cycling but also constitute a carbon source (IPCC, 2013). Regions at high latitudes are particularly at risk of climate changes (IPCC, 2018b). Current climate model predictions indicate that the number of fire events in the boreal zone may double by the end of 2100 (Shvidenko, Schepaschenko, Sukhinin, et

al., 2011). More frequent fires are the most significant cause of boreal forest loss (Hansen et al., 2013). Fires are a major natural disturbance in the Russian boreal forest in particular, where coniferous stands dominate and most of the forest territory is unmanaged and unprotected (Shvidenko, Schepaschenko, Sukhinin, et al., 2011). Due to the vastness of the Russian territory, comprising different ecosystem types, Russia is expected to suffer the most significant transformation due to climate change (FAO, 2012). The average annual temperature has already increased substantially, by up to 2°C in the period from 1971 to 2010, whereas the global annual average increase is less than 1°C over the same period (IPCC, 2013). It is expected that the temperature in the boreal zone could increase from 4°C to 11°C by the end of the 21st century (World Bank Group, 2014 after Gauthier et al., 2015). The forest in Russia is of special interest not only because of the more frequent, catastrophic fires expected as a result of global warming and heat waves which occurred, for instance, in 2010 (Shvidenko, Schepaschenko, Sukhinin, et al., 2011) and 2019, but also because of thawing permafrost that could release much more carbon than tropical deforestation (FAO, 2012).

The Russian Federation is the most forested country in the world (with forest covering 49% of its total area), providing more than 90% of the carbon sink of the world's boreal forests in the 2000 to 2007 period (FAO, 2012; Pan et al., 2011). At the same time, it is associated with the highest uncertainty in global carbon stock calculations. Due to the lack of financial support, some forested regions in Siberia have not been inventoried for more than 20 years (Shvidenko, Schepaschenko, McCallum, & Nilsson, 2011). Additionally, illegal logging poses a huge problem for the monitoring of Russian forests. Different sources (WWF Russia, World Bank) estimate that illegal logging in Russia comprises approximately 25% of all logging activities. According to the most recent global forest change map, tree cover loss in the Russian Federation reached more than 5.5 million hectares last year (2018), the highest deforestation since 2001 (World Resources Institute, 2019).

All of the aforementioned aspects make Russian boreal forests particularly interesting in terms of monitoring by satellite remote sensing.

2.2 Imaging radar theory

At the beginning of the 20th century, along with the developments before and during World War II, there was a major technological progress in radar systems. Since then, radar has been widely used not only for military but also civil applications based on increasingly elaborated systems. Many textbooks are available to various aspects of radars, their design and applications (e.g., Henderson & Lewis, 1998; Ulaby, Moore, & Fung, 1982).

This section gives a brief introduction to imaging radar theory. The radar principles are outlined and radar scattering from different type of surfaces and volumes are described. A particular focus is made on scattering from forests. Furthermore, the processing steps for the SAR data analyzed in this thesis are discussed.

2.2.1 Radar principles

RADAR is an acronym for RAdio Detection And Raging. In this thesis data from an active, imaging radar were analyzed. An active radar system sends out pulses and records the echoes scattered back by the objects (scatterers) to the sensor. The systems use the two-way travel time of the radar pulse to determine the distance (range) to the illuminated object. Its backscatter intensity is determined by the radar system and object properties and depends on the quantity of energy coming back to the sensor. It carries information on the object physical characteristics (geometry, surface, water content) (Hanssen, 2001). The radar operates in the microwave portion of the electromagnetic (EM) spectrum with a wavelength generally from 1 millimeter to 1 meter. Imaging radars are independent of weather conditions and can operate day or night. EM-waves are polarized; the direction of the polarization corresponds to the direction of oscillation of the electromagnetic field. Normally only the horizontal (H) or vertical (V) linear polarizations are used. The radar system is characterized by combination of polarization of transmitted and received pulse: HH, HV, VH or VV. Based on the polarization sent and obtained the radar systems are divided in three polarization modes. Single polarization refers to the same polarization transmitted and received; dual polarization, one polarization is sent and another received; or quad polarization, when system is able to transmit and receive all four types of polarization. When making a contact with a scatterer, the polarization of the EM-wave can change, depending on the geometrical and dielectrical properties of the scatterer. In order to get all necessary information

about those changes, full polarimetric systems are required. The data can be acquired from both the ascending (northwards) and descending (southwards) satellite passes. Water clouds can interfere with the radars operating below 2 cm in wavelength. The effects of rain can be generally ignored at wavelengths above 4 cm (Henderson & Lewis, 1998). For longer wavelengths (above 20 cm), an effect called Faraday rotation caused by the ionosphere, i.e., free charges (electrons) and the Earth's magnetic field, can lead to a rotation of the polarization plane (Shaun Quegan & Lomas, 2015; Gustaf Sandberg, Eriksson, & Ulander, 2009). In the presence of Faraday rotation, the data, usually fully polarimetric, should be corrected (Freeman, 2004).

Imaging radar can be mounted on aircraft or satellite. It operates in a side-looking configuration, left or right with reference to the flight direction. Figure 2.2 A presents the acquisition geometry of a radar system. In the figure, the look angle, i.e., elevation angle, is the angle between the vertical of the antenna to the ground and the line-of-sight (slant range direction); incident angle is the angle between the radar line-of-sight and the local vertical with respect to the geoid; the local incidence angle (Figure 2.2 B) is the angle between the radar line-of-sight and the normal line to the surface (Henderson & Lewis, 1998). This acquisition geometry allows the distinct mapping of scatterers corresponding to their respective distance to the sensor. It causes also geometric distortions in the radar image, i.e., relief displacement (foreshortening and layover) and shadow. For the sake of homogeneity of the backscatter intensity independently of the terrain relief, those effects can be radiometrically corrected using a local digital elevation model (DEM). In terms of the azimuth resolution, i.e., the resolution in the flight direction, it is proportional to the distance to the object and inversely proportional to the length of the radar antenna. In case of the spacecrafts, it is impossible to mount very long antennas. The radar sensor operates therefor not in the real aperture, i.e., real spatial width, radar (RAR) mode but in the synthetic aperture radar (SAR) mode. Synthetic aperture is possible to set up through the forward motion of the spacecraft, which enables to "extend" the real size of the radar antenna (Rees, 2001). With a SAR, each object on the ground is sampled at several antenna positions along the flight path, i.e., as long as the antenna beam is illuminating it. Therefore, the SAR image generation is complex, because many echoes from one object have to be retrieved based on the time delay information and the Doppler history (Ulaby et al., 1982).

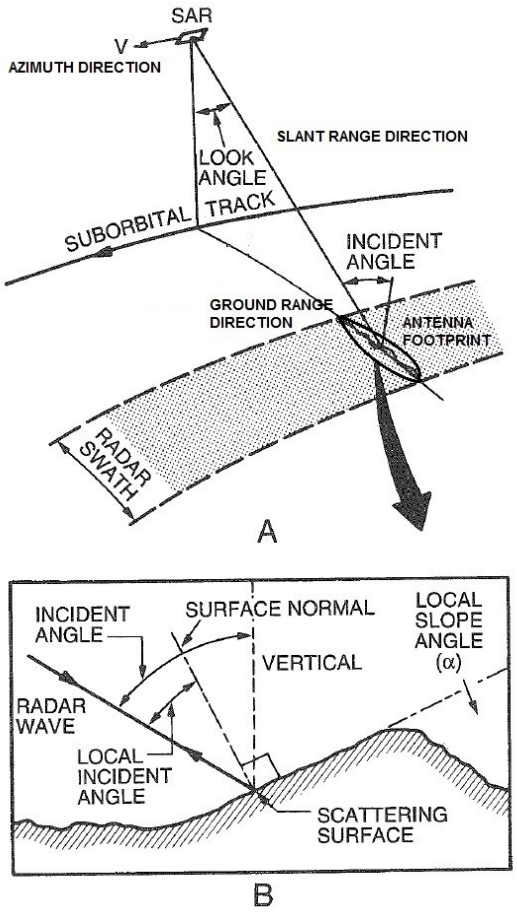

Figure 2.2: Acquisition geometry of SAR system (A) and representation of a local incident angle (B). Adapted from (Henderson & Lewis, 1998).

A SAR can operate in different modes, which differ depending on the sensor. Typical nomenclature is as follows: Stripmap SAR, when the antenna pointing direction is held constant as radar platform moves; ScanSAR, a variation of stripmap SAR, the antenna is shifted in range in several times at the different positions of the synthetic aperture, including a larger range of look angles; Spotlight, the illumination of an area is increased by steering the beam forwards and backwards as the sensor passes (Cumming & Wong, 2005).

The radar system consists of a transmitter that generates the electromagnetic waves, a transmitting and receiving antenna (often the same antenna), a receiver and a signal processor. To image an area, the sensor transmits pulses at a fixed rate at so-called pulse repetition frequency (PRF), and known wavelength (Woodhouse, 2006). The radar bands characteristics in terms of different frequency, wavelength, past, current, and future spaceborne missions are given in Table 2.2. The most common wavelengths for environmental applications are X-, C-, S-, L- and P-band. The selection of SAR system for acquiring data depends on their application. For

forestry, longer wavelengths starting from C- or S-band are preferred. The difference between the radar bands can be summarized as a different ability to penetrate into the target. A longer wavelength improves signal penetration into the forest canopy.

Table 2.2: Radar bands characteristics.

Band	**Frequency**	**Wavelength [cm]**	Spaceborne missions (*past*, in **operation**, future)
X	8-12.5 GHz	3.75-2.40	*SIR-C/X-SAR (1994)*, *SRTM (2000)*, **TSX (2007-)**, **TDX (2010-)**, **COSMO-SkyMed (2007-)**, **KOMPSAT-5 (2013-)**, **PAZ (2018-)**, HRWS (2022)
C	4-8 GHz	7.5-3.75	*SIR-C/X-SAR (1994)*, *ERS-1 (1991-2000)*, *SRTM (2000)*, *ERS-2 (1995-2011)*, *ENVISAT ASAR (2002-2012)*, *RISAT-1 (2012-2017)*, **RADARSAT-1 (1995-), RADARSART-2 (2007-)**, **Sentinel-1 A&B (2014-),** Senitnel-1 C&D (2023)
S	2-4 GHz	15-7.5	**NovaSAR-S (2018-)**, NISAR (2022)
L	1-2 GHz	30-15	*SEASAT (1978)*, *SIR-A (1981)*, *SIR-B (1984)*, *SIR-C/X-SAR (1994)*, *JERS-1 (1992-1998)*, *ALOS PALSAR (2007-2011)*, **ALOS-2 PALSAR-2 (2014-)**, **SAOCOM-1 (2018-)**, ALOS-4 PALSAR-3 (2021), TDL (2022), NISAR (2022), ROSE-L (Copernicus High Priority Candidate mission)
P	280-390 MHz	107-77	**only airborne**, BIOMASS (2022)
VHF	30-300 MHz	1000-100	**only airborne**

2.2.2 Radar scattering

In order to use fully the potential of SAR imagery for environmental monitoring, e.g., forest monitoring, it is important to understand the electromagnetic interactions and scattering mechanisms in the observed area.

The radar backscatter from the object is a result of both radar system parameters (frequency, polarization, acquisition geometry) and the object physical properties (dielectric constant, i.e., water content; geometrical properties, i.e., the roughness, shape and orientation of the scatterer) (Oliver & Quegan, 2004). The amount of the signal scattered back depends on the local incidence angle relatively to those parameters. If the surface is facing towards the antenna, a large portion of

the energy is reflected and received by the radar system. With a larger local incidence angle, the transmitted energy is being reflected away from the sensor (Henderson & Lewis, 1998).

In general, three main scattering mechanisms can be distinguished: surface scattering, volume scattering, and double bounce (Jensen, 2007). The surface scattering depends on the roughness of the illuminated area. The roughness determinates the amount of energy scattered back to the radar sensor (rough surface = diffuse reflection; smooth surface = no return, specular reflection). The volume scattering is related to the radar ability of the penetration into the object and takes place when the radar pulse is transmitted through the target. The third type of scattering mechanism gives the strongest re-radiated signal observed by the radar. It is the result of double specular reflection by two surfaces perpendicular to each other.

The scattering mechanism from the forest is a complex phenomenon due to its heterogeneity related to different forest types, density, tree morphology, moisture content, seasonality, topography, forest understory, etc. Depending on the wavelength used, the main tree elements that interact with the radar signal are leaves or needles, twigs, branches, and trunks (Beaudoin et al., 1994; Harrell, Bourgeau-Chavez, Kasischke, French, & Christensen Jr., 1995; Harrell, Kasischke, Bourgeau-Chavez, Haney, & Christensen, 1997; Kurvonen, Pulliainen, & Hallikainen, 1999; Luckman, 1998; Pulliainen, Mikkela, Hallikainen, & Ikonen, 1996; Rignot, Way, Williams, & Viereck, 1994). The scattering from a forested area consists of at least five mechanisms (Henderson & Lewis, 1998; Moghaddam & Saatchi, 1995; Richards, 1990):

1. Direct scattering from crown/branch layer
2. Direct scattering from the forest floor
3. Direct scattering from the trunk and big branches
4. Crown/branch layer-ground double-bounce backscattering
5. Trunk–ground double-bounce backscattering.

These five scattering mechanisms are illustrated in Figure 2.3.

The backscattering characteristics of forest are highly related to the used wavelength. For longer wavelengths (L- and P-band), the dominant type of backscatter mechanism is volume scattering from tree crown and is related to, in most cases, HV polarization, whereas double bounce is observed for HH and VV polarization and is related to trunk-ground and/or branch-ground returns (Beaudoin et al., 1994). Double bounce scattering is stronger at HH- polarization than at VV-polarization (Rignot et al., 1994). Cross-polarized backscatter was found less influenced by the surface condition (Ranson & Sun, 1994). In case of short

wavelengths (C- and X-band), the radar beam not fully penetrates inside the tree canopy. The volume that is penetrated is proportional to the area of the objects illuminated by the radar beam. The attenuation increases with increasing incident angle, is greater in the summer than in winter, and decreases with increasing radar wavelength (Henderson & Lewis, 1998; Hess, Melack, & Simonett, 1990; McDonald, Zimmermann, Way, & Chun, 1999; Rignot et al., 1994). The attenuation of the re-radiated signal is the smallest in case of P- and relatively small in case of L-band radar systems. It is due to the longer wavelength that interacts with the largest parts of the tree elements such as trunk and largest branches. Therefore, these radar bands are recommended for the forest monitoring applications (Henderson & Lewis, 1998). At S-, C- and X-band the density of the tree scatterers (e.g., leaves, twigs, small branches) is higher which result in higher attenuation.

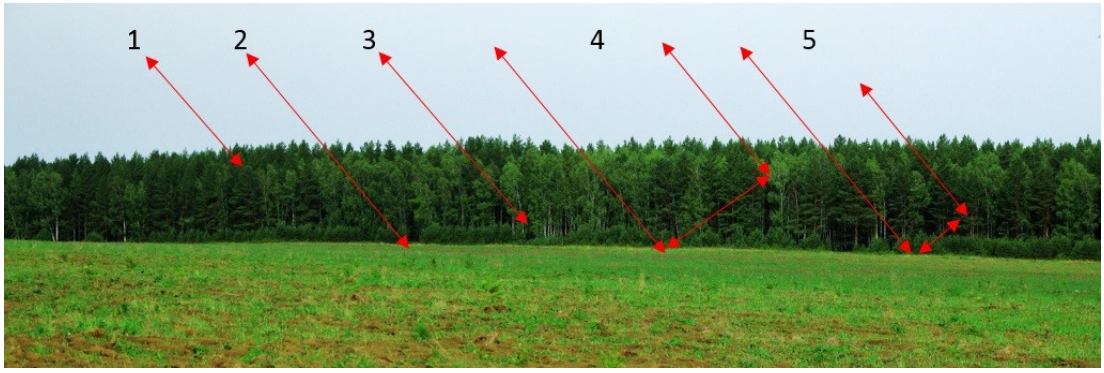

Figure 2.3: Scattering mechanisms from a forest and its floor.

The signal scattered back to the sensor is a complex quantity (g). It is characterized by amplitude (A) or intensity ($I=(A)^2$) and phase (φ), which represents the real and imaginary part of the signal. It can be expressed as (Henderson & Lewis, 1998):

$$g = A * e^{-j\varphi} \tag{2.2.1}$$

The amplitude represents the amount of the energy scattered back to the radar sensor. The phase is related to the two-way path length between the satellite and the target (2R) (Henderson & Lewis, 1998):

$$\varphi = -\frac{2\pi}{\lambda} 2R + \varphi_{scatter} \tag{2.2.2}$$

where λ is the wavelength, $\varphi_{scatter}$ is phase modulation by the scatterer. The phase has values from 0 to 2π. By neglecting any losses of radar signal due to e.g. thermal noise, the total power scattered back to the sensor, P_R [W], can be expressed by the following radar equation (Moore, 1966):

$$P_R = P_T \frac{G^2 \lambda^2}{(4\pi)^3 R^4} \sigma \tag{2.2.3}$$

where P_T is transmitted power, G is the gain of transmitting antenna, λ is the used wavelength, R the distance between radar and the target, and σ is the radar cross-section (RCS). RCS is a result of the multiplication of the object receiving area, the energy reflected by this area and object gain, which is related to its size and geometry. RCS is the most important scattering property of the object. In case of distributed targets, the average radar cross-section is defined as the radar scattering per unit area (A [m^2]), known as the backscattering coefficient σ^0, sigma nought (Jensen, 2007):

$$\sigma^0 = \frac{\sigma}{A} \tag{2.2.4}$$

where σ [m^2] is the radar cross-section. When the backscattering is normalized taking into account the local incident angle, i.e., an area projected into the plane perpendicular to the line of sight, we use a term gamma nought, γ^0 (Atwood, Andersen, Matthiss, & Holecz, 2014; Frey, Santoro, Werner, & Wegmüller, 2013; Small, 2011; Ulander, 1996). Typically, the backscattering coefficient is expressed in the decibel scale [dB], i.e., 10 times $\log_{10}$ of the SAR intensity.

The received echo consists not only of the backscatter from the target. It is corrupted by noise in the receiver. This noise is governed by the radar equation. So called Signal-To-Noise Ratio (SNR) is defined as the ratio between received and noise signal (Cumming & Wong, 2005). It is an important property of a radar system. Another characteristic of the system performance is a Noise-Equivalent Sigma-Zero (NESZ). It is a measure of the sensitivity of a given SAR and is defined as the minimum sigma nought. Smaller values of NESZ are better. Both radar system properties can be improved by increasing the power of the radar transmitter (Henderson & Lewis, 1998).

A typical "salt-and-pepper" noise-like physical phenomenon that is not a noise but a deterministic property of SAR imagery is the so-called speckle. It appears when a resolution cell of a SAR system contains more than one scatterer. In that case, the total scattering from the resolution cell is a coherent sum of the backscatter originating from the different scatterers. In order to reduce this effect, speckle reduction methods can be applied. These methods are briefly introduced in the next section.

2.2.3 SAR data processing

In this study, both the amplitude and the phase were utilized in the context of forest monitoring.

After the SAR image formation (Oliver & Quegan, 2004), the following SAR formats can be generated: (i) Single Look Complex (SLC), (ii) Multi-look Detected/Multi-looked Intensity (MLD/MLI), Ground Range Detected (GRD), (iii) Precision Images (PRI), (iv) Geocoded/Orthorectified product. The Single Look Complex SAR format is a single look product of the focused signal. It means that the azimuth compression has been carried out using the full azimuth bandwidth and therefore contains the highest azimuth spatial resolution and at the same time, it suffers from maximum speckle. The data are in the radar geometry, i.e., in slant range coordinates, not projected onto any reference surface. Each pixel of the SLC product is a complex number. It consists of one real and one imaginary component that represents the amplitude and phase of the wave corresponding to the resolution cell (Woodhouse, 2006). From the SLC product the MLD/MLI can be generated. It is produced by multi-looking, i.e., averaging, over range and/or azimuth resolution cells. Before performing multi-looking, the SLC slant-range geometry is projected onto ground. This kind of product, i.e., in ground range geometry, is known as a Ground Range Detected (GRD), e.g., product of the Sentinel-1 mission. The pixel spacing in ground range R_{GR} can be obtained from the ratio of the slant range (R_{SR}) and the sine of the incident angle in the mid-swath (Henderson & Lewis, 1998):

$$R_{GR} = \frac{R_{SR}}{\sin \theta_i} \tag{2.2.5}$$

In order to get square pixels, the resolution in ground range and azimuth should be similar. Whilst deteriorating the spatial resolution of the image, the multi-looking is a simple and robust method of reducing the speckle in SAR image. Commonly the image is averaged with multi-look factors between 3 and 6. These factors are reported to be a good trade-off between spatial resolution and radiometric variation due to speckle (Woodhouse, 2006). The speckle can be also reduced using different filtering methods (Cremer et al., 2018; Lee, Wen, Ainsworth, Chen, & Chen, 2009; Quegan & Yu, 2001). As a result, after speckle filtering, a not geocoded product is generated in which each pixel represents a real number (digital number DN), i.e., amplitude of the signal within the pixel. The gain in radiometric precision can be calculated using the Equivalent Number of Looks (ENL). In SAR intensity (I) data,

the speckle variance is proportional to the mean intensity squared (Oliver & Quegan, 2004):

$$ENL = \frac{(mean\ I)^2}{\mathrm{var}\ I} \tag{2.2.6}$$

The ENL can be estimated from the image statistics for a homogenous region, where the backscattering coefficient is assumed to be constant. If ENL is large, the speckle effect has been reduced and is small.

Precision Images (PRI) are the MLD/MLI images that have been resampled into square pixels, rotated to account for the view direction of the instrument and warped by some predefined operation that the projected image pixels are georeferenced onto a specified geographical coordinate system (Woodhouse, 2006). This product contains still topographic distortions.

In order to obtain a high precision corrected geocoded, i.e., orthorectified, SAR product, the radiometric and geometric corrections are required. The radiometric correction depends on sensor and data type. Absolute calibration is obtained by providing the calibration constant. Furthermore, the radiometric normalization is implemented for precise radiometric correction of terrain induced distortions (e.g., Ulander, 1996). The correction of these effects is very important for the quantitative image analysis such as biomass estimation. For this a high-resolution DEM is required. The higher the geometric resolution, the more accurate is the estimation of the scattering area and radiometric normalization (Loew & Mauser, 2007). This product is in map geometry.

In summary, the following steps of processing a single SAR image to produce backscattering coefficient corrected due to the local incident angle, i.e., gamma nougth, were implemented:

1. SLC data import and improvement of state vectors (position and velocity of a satellite)
2. Data calibration
3. Multi-looking
4. Filtering
5. Conversion to dB scale
6. Geocoding
7. Topographic normalization
8. Creation of output files.

2.2.4 SAR Interferometry

In this part of the chapter, the InSAR processing is briefly introduced.

The principle of the SAR interferometry relies on the observation of the target by the radar antenna from two slightly different positions and/or at different times (Bamler & Hartl, 1998) - Figure 2.4

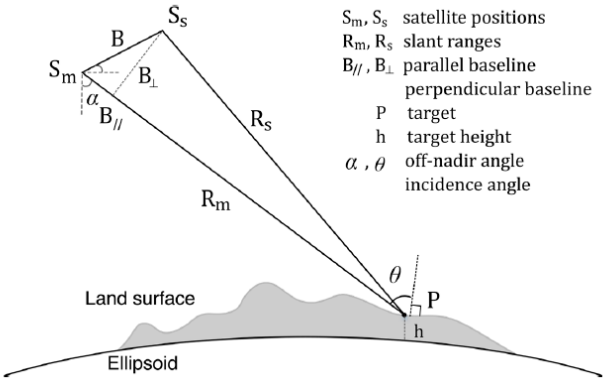

Figure 2.4: The geometry of SAR interferometry (Xiong, Muller, & Li, 2017).

The distance between the positions of the systems is called spatial baseline and can be split into two components: parallel baseline (parallel to the line of sight) and perpendicular baseline (perpendicular to the line of sight). The perpendicular baseline can vary from a few meters up to several kilometers. To calculate the critical value at which complete decorrelation occurs the following equation is used (Goldstein, Zebker, & Werner, 1988):

$$B_n \leq \frac{R\lambda}{2L_c cos\theta} \tag{2.2.7}$$

where L_c is the size of the resolution cell in slant range and θ is the incident angle.
In terms of time, the term temporal baseline is used. The InSAR acquisitions can be done simultaneously, and then the temporal baseline is equal to zero. In this case, one transmitting and two receiving antennas are mounted on the same platform (e.g., SRTM) or on two platforms flying next to each other (TerraSAR-X and TanDEM-X). In this case, it is called single-pass interferometry. The other case is the repeat-pass interferometry, where both necessary acquisitions are conducted by the same platform after a specific time interval, called revisit time. It is the elapsed time between two acquisitions of the same area with the same acquisition parameters (e.g., look angle).

The input data for the InSAR processing are the complex SAR images in the SLC format; the main output is the interferogram. It is formed by multiplication of

one SAR image with the complex conjugate of a second image (Hagberg, Ulander, & Askne, 1995). As a result, an intensity image and a phase image are created. The first one corresponds to the multiplication of both amplitude images, the second to the difference of both phase information. A co-product of the interferogram can be created by cross-correlation of both complex acquisitions - the coherence. We can express the pixel value (s_i) in the interferogram as follow:

$$s_i = g_{1,i}\, g^*_{2,i} = (A_{1,i}A_{2,i})e^{j[\frac{4\pi}{\lambda}(R_2-R_1)+\Delta\varphi_{scatter,i}+\Delta\varphi_{delay,i}]} \quad (2.2.8)$$

where $g_{1,i}$ is a pixel value in the first SAR image, $g^*_{2,i}$ is the complex conjugate of the corresponding pixel in the second SAR image, φ_{delay} is a phase delay due to the wave travel through the object. The InSAR processing consists of the following steps: (i) pre-processing (co-registration and common band filtering for range and azimuth spectra to compensate for differences in slightly different acquisition geometries of two SAR images), (ii) interferogram generation, (iii) post-processing (filtering and geocoding). It is necessary to perfectly co-register one image with the other, with an accuracy of less than 0.1 pixel (Balzter, 2001). Afterwards, the complex coherence is computed. The coherence was defined by Born & Wolf (Born & Wolf, 1999) as follows:

$$\gamma = |\gamma|e^{j\phi} = \frac{E\{g_1 g^*_2\}}{\sqrt{E\{|g_1|^2\}E\{|g_2|^2\}}} \quad (2.2.9)$$

where ϕ is the phase and E{} represents expected value. It measures the degree of correlation between two SAR images and takes values between 0 for total decorrelation and 1 for perfect correlation. In practice, the coherence is estimated using estimators by spatial averaging within two-dimensional window. As it is presented in Figure 2.5, the coherence estimate is biased towards higher values, in particular for low coherence values and small estimation windows (Touzi, Lopes, Bruniquel, & Vachon, 1999). The topic of finding the optimized window size for coherence estimation for forest monitoring purposes is discussed in the proceeding paper presented in the Appendix A.

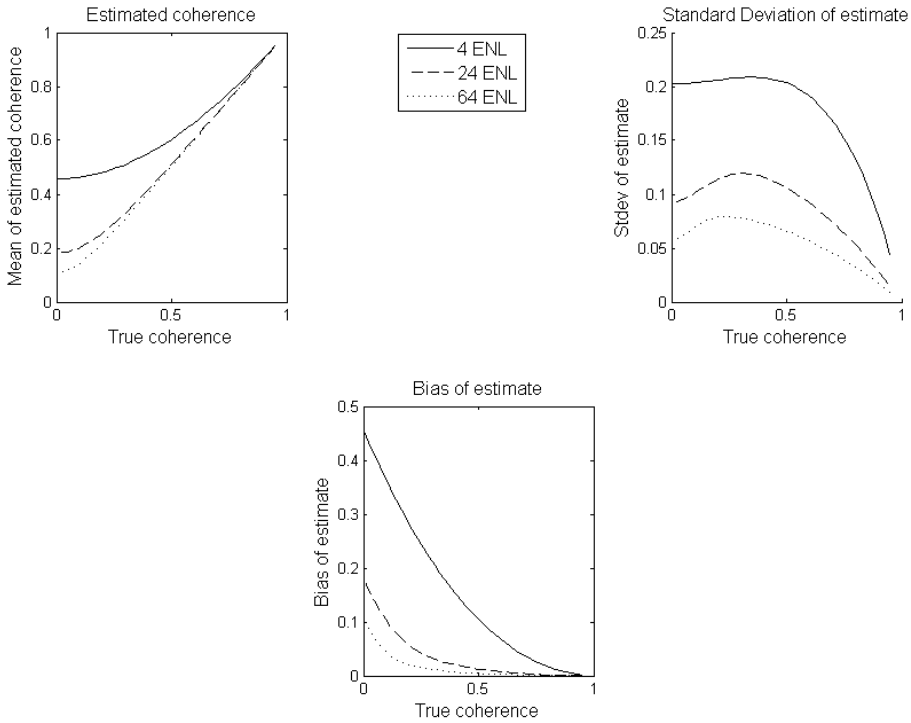

Figure 2.5: The coherence expectation value, standard deviation, and the bias as a function of the "true" coherence for various equivalent number of looks (ENL).

There are several sources of decorrelation that influence the InSAR processing: processor (e.g., misregistration), noise azimuth (misalignment of the azimuth spectra), noise (noise due to receiver state), spatial (decorrelation related to the acquisition from slightly different angles), temporal (decorrelation related to the time difference between acquisitions) (Hanssen, 2001). However, the perpendicular component of the baseline and the time difference between acquisitions are the main factors affecting the coherence (Smith, Dammert, & Askne, 1996; Zebker & Villasenor, 1992):

$$|\gamma| = \cancel{|\gamma|_{processor}} * \cancel{|\gamma|_{noise}} * \cancel{|\gamma|_{azimuth}} * |\gamma|_{spatial} * |\gamma|_{temporal} \tag{2.2.10}$$

Another important information from InSAR processing is the interferometric phase. The interferometric phase has values between 0 and 2π. It measures the phase difference of the target with respect to both sensor positions and can be expressed by its contributors:

$$\phi = \phi_{flat\,Earth} + \phi_{topo} + \phi_{disp} + \phi_{path} + \phi_{noise} + n * 2\pi \tag{2.2.11}$$

where the first element represents the phase for a curved Earth, the second represents the phase due to the elevation, the third phase component is due to

displacement between the two observations, the fourth component is due to the path delays caused by the atmosphere, the fifth phase component is noise and the last contributor corresponds to the ambiguity factor due to the fact that InSAR phase is between 0 and 2π.

The last processing step consists of the enhancement of the coherence image and geocoding. The first task is done using different filtering methods; the second is the transformation of the image from radar coordinates to map coordinates (Hanssen, 2001).

In summary, the following steps of processing two SAR images to produce coherence image were implemented:

1. SLC data import and improvement of state vectors (position and velocity of a satellite)
2. Data calibration
3. Multi-looking
4. Data co-registration
5. Interferogram computation and baseline estimation
6. Removal of flat Earth phase
7. Common band filtering and coherence estimation
8. Geocoding
9. Topographic normalization
10. Creation of output files.

The SAR data were processed using the GAMMA software (Werner, Wegmüller, Strozzi, & Wiesmann, 2000).

2.3 Radar remote sensing of boreal forests

Radar data has been demonstrated to be physically related to vegetation structure, allowing researchers to determine forest parameters and to generate forest cover maps. The data in horizontal polarization transmitted and horizontal and vertical received (HH and HV) and in longer wavelengths (e.g., L- and P-band) have been reported to be superior to shorter wavelengths (e.g., X- and C-band) for these purposes (Achard & Hansen, 2013; Beaudoin et al., 1994; Dobson, et al., 1992; Kellndorfer et al., 2011; Le Toan et al., 1992; Wegmuller & Werner, 1995). Many SAR properties can be exploited to quantify forest parameters; these properties are:

backscattering intensity (Fransson & Israelsson, 1999; Ling et al., 2008; Pulliainen et al., 1994), interferometric phase (Askne et al., 2013; Solberg et al., 2010), interferometric coherence (Koskinen et al., 2001; Santoro et al., 2002), polarimetric signature (Neumann et al., 2012; Papathanassiou & Cloude, 2001), SAR tomography, and radargrammetry (Persson & Fransson, 2014; Tebaldini & Rocca, 2012).

A recent overview of the methods and the research pathways of forest AGB estimation using SAR backscatter and InSAR were summarized by Santoro & Cartus (Santoro & Cartus, 2018). The study based on the 186 peer-reviewed papers concluded that the multi-temporal and multi-frequency approach that maximizes the information content on biomass of the individual data sources shall be pursued. This was at the focus of this research study.

According to the author's knowledge, until now, there is no operational system for forest change monitoring using SAR data. However, availability of new spaceborne multi-temporal very high-resolution SAR acquisition modes, and acquisition of polarimetric data at X- to P-bands, i.e., HRWS, NISAR, Tandem-L, BIOMASS, combined with the interferometric capability of SAR can support the efforts of establishing an operational SAR-based deforestation system at regional, national and global scales.

2.3.1 Estimation of aboveground biomass

This section summaries and complements review article on SAR-based biomass estimation: Stelmaszczuk-Górska, M. A., Thiel, C. J., & Schmullius, C. C. (2017). Remote Sensing for Aboveground Biomass Estimation in Boreal Forests. In H. Balzter (Ed.), Earth Observation for Land and Emergency Monitoring (1st ed., pp. 33–55). © 2017 John Wiley & Sons Ltd. http://doi.org/10.1002/9781118793787 (Chapter 4.2). Mentioned paper presents studies published by mid-2014. This section describes the latest research (until mid-2019). Parts of the article used in this section are written in italics and marked with quotation marks.

The list of research papers that the review paper and this section are based on is presented in the Appendix B. The Appendix gives an overview of seventy peer-reviewed papers on biomass retrieval of boreal forests using SAR data. The reported results are summarized in terms of sensor parameters (frequency, polarization, look angle), study area, range of estimated variable, number of images and input data applied for modelling the biomass, model used, as well as selected statistics on model performance. The results of the biomass retrieval are given in terms of model fit, i.e., the explained data variability of the response data, the coefficient of determination

(R^2) or coefficient of correlation (r), root mean square error (RMSE), and relative root mean square error (rRMSE) (Rawlings, Pantula, & Dickey, 1998). rRMSE is normalized to the mean of the observed estimated variable. The variables are growing stock volume (GSV) that is defined as a mean stem volume for all living species in a stand in m^3/ha (GSV) or aboveground biomass (AGB), i.e., the mass of all living matter above the soil including stem, stump, branches, bark, seeds, and foliage in a particular area in e.g., tons/ha (FAO, 2006). In this chapter, the term "biomass" is used interchangeably to refer to both GSV and AGB. In some cases the biomass estimation error RMSE was corrected by the systematic sampling errors in the reference data (Askne, Santoro, Smith, & Fransson, 2003; Chowdhury, Thiel, & Schmullius, 2014; Fransson, Smith, Askne, & Olsson, 2001; Fransson, Walter, & Ulander, 2000; Santoro et al., 2002; Santoro, Eriksson, Askne, & Schmullius, 2006; Stelmaszczuk-Górska et al., 2016; Stelmaszczuk-Górska, Urbazaev, Schmullius, & Thiel, 2018). In cases where the rRMSE was not given, it was calculated based on the provided mean biomass value.

The first studies in boreal forests were focused on the investigation of the correlation between the backscattering coefficient and biomass of the pine plantations and monoculture forests (Dobson, Ulaby, Beaudoin, Kasischke, & Christensen, 1992). It was shown that the radar backscatter increases with the increasing biomass until the signal saturates (Dobson, Ulaby, et al., 1992; Wu, 1987). The radar signal saturates at a certain biomass level depending on used SAR system parameters (wavelength, polarization, and incident angle), forest structure and environmental conditions. Saturation levels can be increased by integrating multiple SAR images obtained with the same polarization or/and by implementing data acquired with different polarizations and frequencies (Pulliainen, Kurvonen, & Hallikainen, 1999; Yrjo Rauste, 2005; Santoro et al., 2011). The HV and HH polarizations are most sensitive to biomass (Antropov, Rauste, Ahola, & Häme, 2013; Dobson, Ulaby, et al., 1992; Harrell et al., 1997; G. Sandberg, Ulander, Fransson, Holmgren, & Le Toan, 2011). The longer wavelength VHF (Fransson et al., 2000) and P- (Sandberg et al., 2011), only from airborne platforms, L-band (Andersen et al., 2011; Atwood et al., 2014; Cartus, Kellndorfer, Rombach, & Walker, 2012; Fransson & Israelsson, 1999; Kurvonen et al., 1999; Rauste, Häme, Pulliainen, Heiska, & Hallikainen, 1994; Santoro, Eriksson, & Fransson, 2015) due to the deeper penetration into canopy showed no saturation up to maximum biomass values and were recommended as the most suitable data for the estimation of forest parameters.

Complementary and new information to the backscattering intensity gives the SAR interferometry. "*Both interferometric height information and coherence were*

used for biomass retrieval." The interferometric coherence is inversely correlated to the biomass due to the volume decorrelation (Askne & Smith, 1996; Eriksson, Santoro, Wiesmann, & Schmullius, 2003; Santoro, 2003; Wagner et al., 2003). In case of temporal decorrelation, the environmental conditions should be stable between the data acquisitions. In boreal zone winter conditions were reported to be preferable (Koskinen et al., 2001; Pulliainen, Engdahl, & Hallikainen, 2003; Santoro et al., 2002). Freezing and thawing periods showed complete decorrelation (Eriksson et al., 2003). As it is in case of backscattering intensity, the interferometric coherence also saturates at the certain level of biomass. No saturation was reported up to the maximum biomass values with InSAR data acquired under stable conditions (Fransson et al., 2001; Santoro et al., 2002, 2015; Solberg, Astrup, Gobakken, Næsset, & Weydahl, 2010). Results shown that in optimal environmental conditions the saturation level is higher than in case of backscatter (Thiel & Schmullius, 2016). It was also observed that beside the environmental conditions, decrease in the coherence can be explained by the topography (>10°) and stand characteristics (stand size <3-4 ha and relative stocking <50%) (Santoro, Shvidenko, Mccallum, Askne, & Schmullius, 2007).

Biomass estimation has been modeled using different approaches. Most are based on empirical and semi-empirical models. "*The semi-empirical models employ radar data as a function of biomass. It is a combination of physical modelling and empirical observations. The scatterers can be described as a layer, water cloud model WCM (Ulaby et al., 1982) or layer with gaps (water cloud model with gaps), which are especially important in studies in the boreal forests (Askne, Dammert, Ulander, & Smith, 1997), or randomly distributed scatterers, Random Volume over Ground model (RVoG) (Papathanassiou & Cloude, 2001). The empirical models are based on regression analysis. (…) There are advantages and disadvantages of both approaches. The main drawback of the semi-empirical method is that the models can be either oversimplified, leading to great estimation errors, or too complex, resulting in inversion problems. The main disadvantage in the case of empirical approaches is that they strongly depend on the data set used for model selection and training, and therefore result in poor model transferability.*" Both types of models have already demonstrated very good biomass estimation accuracy (Askne et al., 2013; Solberg, Astrup, Breidenbach, Nilsen, & Weydahl, 2013). The biomass retrievals based on the empirical model provided equally good estimations compared to the semi-empirical approach (Fransson & Israelsson, 1999). Machine learning algorithms have been also successfully implemented for biomass estimation in boreal forests (Andersen et al., 2011; Antropov, Rauste, Häme, & Praks, 2017; Hüttich et al., 2014; Karila, Vastaranta, Karjalainen, & Kaasalainen, 2015; Karjalainen, Kankare,

Vastaranta, Holopainen, & Hyyppä, 2012; Rodríguez-Veiga et al., 2019; Stelmaszczuk-Górska et al., 2016, 2018; Wilhelm et al., 2014).

Backscatter and Polarimetric Parameters

One of the first models implemented in the boreal zone employing backscatter information to estimate stem volume were the semi-empirical models, the HUTSCAT model, based on the large number of measurements recorded using high-resolution ranging scatterometer (Pulliainen et al., 1994), and the WCM model with gaps (Askne et al., 1997). As a result of using these models, it was found that scattering from forested areas is a mixture of parameters related to surface topography, roughness, soil moisture and weather conditions, and that the estimation error depends on the characteristics of the forest stand, such as size. For the stands greater than 10 ha, the error become negligible (Pulliainen et al., 1994, 1996). "*In Pulliainen et al. (Pulliainen et al., 1999) it was demonstrated that for stands larger than 20 ha, a correlation coefficient between the estimates and the reference values of up to 0.85 and 25% relative error can be calculated using L-band and 0.65 with 27% relative error using C-band. The estimates were improved when the C- and L-band data were combined (rRMSE < 25%).*" The WCM model also provided a very good relative estimation error of 25% (36 m^3/ha), showing no saturation up to 350 m^3/ha (Santoro et al., 2006). The model was implemented as part of the BIOMASAR algorithm, which uses hyper-temporal SAR data acquired by the Envisat ASAR C-band sensor and the Vegetation Continuous Field (VCF) product for model training (Santoro et al., 2011). The results using this algorithm were below 20% at a 0.5° or 0.01° resolution, at global and regional scale (Santoro et al., 2015, 2013). At the forest stand level, using five ALOS PALSAR L-band images, Peregon and Yamagata (Peregon & Yamagata, 2013) reported estimation error in the range of 25 to 32%.

Different regressions were implemented to estimate the biomass, e.g., linear and multiple linear regression (Fransson & Israelsson, 1999; Ranson et al., 1997; Rauste, 2005; Rignot, Zimmermann, & Zyl, 1995; Soja, Sandberg, & Ulander, 2013; Ulander, Sandberg, & Soja, 2011), polynomial regression (E. Rignot et al., 1994), nonlinear regression (Thiel & Schmullius, 2016; Wagner et al., 2003). The estimation error was found to be approximately 20% when using L-band and P-band (Ranson, Sun, Kharuk, & Kovacs, 2001; Soja et al., 2013). Similar results were reported when using VHF data. "*In Folkesson et al. (Folkesson, Smith-Jonforsen, & Ulander, 2009), the best coefficient of determination between estimated biomass and reference measurements was reported to be 0.93, with an estimation error of 48 m^3/ha (rRMSE of approximately 25%).*"

The recent studies focuses on the use of multi-frequency data for biomass estimation (Cartus & Santoro, 2019; Santoro et al., 2019; Stelmaszczuk-Górska et al., 2018). Cartus et al. (Cartus & Santoro, 2019) reported 2% decrease of the estimation error at the plot level when the L- and P-band data are combined. The authors also reported the decrease in the estimation error when the biomass estimates were obtained by summing independent radar-derived stem and branch biomass or by introducing information on tree species in the model calibration. The combination of the C- and L-band data improved the results only in the limited extent (Cartus & Santoro, 2019; Stelmaszczuk-Górska et al., 2018). At the same time, the authors emphasized that the crucial requirement for decreasing the estimation error when combining the C- and L-band data is the use of multi-temporal observations. The combination of C- and L-bands allowed for retrieval accuracies similar to those estimated with P-band (Cartus, Santoro, Wegmüller, & Rommen, 2019). The retrieval errors were: 28% at 1 ha LiDAR-derived biomass map (Cartus et al., 2019), 31.3% (Santoro et al., 2019) and 40% (Cartus et al., 2019) at the forest plot level 0.5 ha and 0.03 ha, respectively, and 32% at pixel level (0.25 ha) (Stelmaszczuk-Górska et al., 2018).

Radargrammetry

Better results were reported when two backscatter images were combined using radargrammetry (Stelmaszczuk-Górska, Thiel, & Schmullius, 2017). This method is based on stereoscopic height measurements using SAR images. The errors were compared to that of much more expensive LiDAR measurements. At the forest stand level, an error of approximately 16% was calculated (Vastaranta et al., 2014). It was recommended to use the data with an intersection angle between 8° and 16°. The estimation errors increased with the topography, slopes above 4°(Persson & Fransson, 2014).

Interferometric SAR (InSAR)

One of the first studies that reported a high potential of the interferometric phase information and coherence in forestry applications was the study by Hagberg et al. (Hagberg et al., 1995). Using repeat-pass InSAR on ERS-1 C-band data, the authors obtained very good results based on winter acquisitions reporting a 10% estimation error for the tree height in a dense forest. "*One of the first results presenting the accuracy of stem volume estimation was published by Smith et al. (Smith et al., 1998). The study over Swedish test sites utilizing C-band tandem ERS-1/2 coherence data estimated the stem volume based on linear regression analysis. The results showed high correlation between the coherence and stem volume.*"

It was reported that coherence is seasonally dependent and very sensitive to differences in the acquisition times, showing for example a great potential for LCLCC mapping and clear-cut detection (Askne & Smith, 1996; Wegmuller & Werner, 1995). For the InSAR studies, it was recommended to use data acquired under low and stable temperatures without precipitation events (Dammert & Askne, 1998). *"Koskinen et al. (Koskinen et al., 2001) demonstrated that the highest coherence can be obtained under winter conditions in the presence of snow cover."*

The lowest estimation errors were reported using the multi-temporal data from the TanDEM-X mission. The errors in the range of 14 to 18% were calculated at the stand level (Askne et al., 2013; Askne & Persson, 2019; Askne & Santoro, 2015; Askne, Soja, & Ulander, 2017; Persson & Fransson, 2017; Soja, Persson, & Ulander, 2015, 2018) and of approximately 30-40% at the plot level (Persson & Fransson, 2017; Rahlf, Breidenbach, Solberg, Næsset, & Astrup, 2014). The results were comparable regardless of the estimation method used.

Estimations without in situ data

"One of the difficulties in estimating biomass over vast areas, e.g., Central Siberia is the lack of any and/or reliable in situ data. Therefore, approaches that do not make use of in situ data have been developed." It should be noted that such approaches require some basic knowledge about the distribution of biomass in the study area. The methods use backscattering statistics and coherence values for non-forest and dense forest based on other remote sensing products or based on the temporal consistency of radar data. This kind of approach was introduced in the BIOMASAR algorithm (Santoro et al., 2011). This method made use of the synergy between the optically sensed tree cover product and time series of C-band backscatter. Another method made use of a consistency plots between two coherence observations (Askne & Santoro, 2009; Santoro et al., 2008). Using four tandem pairs in the IWCM model, a relative error of 18% was calculated at forest stand level (Askne & Santoro, 2009). *"(…) it must be underlined that this method requires some manual adjustment to the ridges of the density plots (Askne, 2013 personal communication)."*

Estimations at fine scale

The above-mentioned biomass retrievals were predominantly (approximately 80%) done at the stand and/or plot level. The recent results provide estimates at the pixel level in the range of 15 m x 15 m to 50 m x 50 m (Hüttich et al., 2014; Neumann et al., 2012; Rodríguez-veiga et al., 2019; Stelmaszczuk-Górska et al., 2016, 2018; Sun et al., 2011; Wilhelm et al., 2014). The 50 m x 50 m (0.25 ha) resolution is the

current suggestion of the Global Climate Observing System (GCOS) for biomass estimation outside the tropics (GCOS, 2016). The authors trained the models using the forest stands or plots and afterwards predicted the biomass at the pixel level. As stated in Neumann et al (Neumann et al., 2012) this is a trade-off between reducing the estimation error and achieving a higher resolution, and thus better spatial distribution of biomass. The applied models performed well providing the estimation error rRMSE in the range of 23% to 43%. The results are comparable to the estimation errors at the stand level. The best retrievals are similar to the accuracies of the conventional stand-wise forest inventory and LiDAR biomass estimates. The biomass, in most cases, was estimated using non-parametric empirical models and the machine learning algorithms.

In this study, the biomass was estimated at the fine scale using both multi-temporal interferometric coherence and/or multi-frequency and multi-temporal backscatter data. The results are presented in chapters 4.3 and 4.4.

2.3.2 Monitoring of forest change

For the reasons stated in Chapter 1.1, it is not only important to have information on biomass but also on forest change. Changes in forest can be caused by different natural or human-induced events. The following processes can be distinguished: deforestation, i.e., a conversion from forest to a non-forest LC type, afforestation, i.e., is the conversion from other land uses into forest, reforestation, i.e., is the re-establishment of forest through planting on land classified as forest, and forest degradation, i.e., is the reduction of the capacity of forest to provide goods and services (FAO FRA, 2012). In this study, focus was on evaluating the potential of SAR data for large-scale operational mapping of forest aboveground biomass loss caused mainly by logging activities. Deforestation is particularly important, as it constitutes significant carbon source (FAO, 2016).

SAR systems have already been reported to be a useful tool for mapping deforestation (Achard & Hansen, 2013). When the woody vegetation is completely removed from the forest ground a significant change in the scattering mechanism can be observed, i.e., the change from volume and double-bounce scattering to surface scattering. At C-band the backscatter decreases up to 5 dB (Ranson, Kovacs, Sun, & Kharuk, 2003), at L-band up to 3 dB with respect to mature boreal forests (Fransson et al., 2007; Ranson et al., 2003; Santoro, Fransson, Eriksson, & Ulander, 2010). The interferometric coherence data has also been reported to show potential for forest monitoring (Kellndorfer et al., 2011). Environmental conditions at the time of image acquisition and to some extent the topography and acquisition

geometry can affect the radar signal. Thawing or melting of snow, shortages in precipitation resulted, for example, in decreasing SAR backscatter (Lucas et al., 2013; Santoro et al., 2009). Another factor that can influence the detection of deforestation is the presence of woody vegetation on the forest ground. The presence of horizontal structures on the ground can increase the backscatter at L-band HH polarization, at L-band HV the difference between the clear-cut area and the mature forest is smaller as reported for tropical forests (Rignot, Salas, & Skole, 1997).

A number of methods exist for forest change mapping (Coppin & Bauer, 1996; Coppin, Jonckheere, Nackaerts, Muys, & Lambin, 2004; Lu, Mausel, Brondizio, & Moran, 2004; Reiche, Hamunyela, Verbesselt, Hoekman, & Herold, 2018). In general, these methods can be grouped into post- and pre-classification techniques. The first group of methods compares classification products generated for at least two-time intervals at the pixel or segment level. The advantage of this approach is that not only change or no-change areas are detected, but also the type and direction of changes. However, the drawback is that the quality of the final change detection product depends on the accuracy of individual classifications. Unlike the post-classification method, the pre-classification technique employs unclassified images. Methods that are used to identify change areas include image differencing or rationing, bi-temporal linear data transformation (principal component analysis; PCA; multivariate alteration detection; MAD), image regression, and Change Vector Analysis; CVA (Coppin et al., 2004). No matter the method used, because of the nature of the SAR images, the classifications are often error prone (Lucas et al., 2013). Recently, the time-series methods for deforestation mapping have been introduced (Reiche et al., 2018; Reiche, Verbesselt, Hoekman, & Herold, 2015). The advantage of these time series-based methods is the higher spatial and temporal accuracy of the multi-data approach compared to the single data results, and the timely detection of deforestation activities.

The classification of clear-cuts has been mostly reported within general forest cover mapping. The first attempt of boreal forests mapping at a large-scale was done within the SAR Imaging for Boreal Ecology and Radar Interferometry Applications SIBERIA project (Schmullius et al., 2001). In this project, the data from two SAR missions, the C-band European Remote Sensing Satellites (ERS-1/2), and the L-band Japanese Earth Resources Satellite JERS-1 were used to map an area of approximately one million km^2. Statistics of ERS coherence and JERS intensity images for 1997 to 1998 were applied to classify forest cover. The final forest map was generated using a maximum likelihood algorithm based on class statistics and was reported to have an accuracy of more than 80% (Balzter et al., 2002). Comparing ALOS PALSAR L-band data from 2007 to the forest map produced by

the SIBERIA project from 1997, Le Toan et al. observed a high forest biomass loss (approximately total loss of 10%) over this 10-year period (Le Toan et al., 2009).

Another study on the Siberian forest was conducted by Thiel et al. (Thiel, Thiel, & Schmullius, 2009), who used a combination of ALOS PALSAR L-band coherence acquired during winter stable conditions and summer backscattered intensities to classify an area of approximately 100,000 km^2. The authors reported classification accuracy above 90%. The final product was generated using object-based classification and nearest-neighbor algorithm. Seven forest-related classes were distinguished: old clear cut, recent clear cut, fire scar, undisturbed coniferous forest, undisturbed deciduous forest, undisturbed mixed forest, re-growing/low biomass forest. In the previous study, using the JERS images, the authors (Thiel, Drezet, Weise, Quegan, & Schmullius, 2006) reported also the accuracy above 90%.

In 2018, latest global forest/non-forest map was published by the Japan Aerospace Exploration Agency Earth Observation Research Center (JAXA EORC), through the ALOS K&C initiative (JAXA Earth Observation Research Center, 2018). This product was generated using a simple thresholding approach with values − 7.5 and − 14.0 dB for HH and HV polarization respectively at a global level to ALOS PALSAR backscattering coefficient data. The data were produced using 25 m resolution PALSAR and PALSAR-2 mosaic. The high backscatter values were classified as "forest" and the low values as "non-forest" (Shimada, Takuya, et al., 2014). The forest, was defined, same as by FAO, as the area covered by trees that is larger than 0.5 ha and has canopy cover over 10%. This product is freely available for scientific users. It has been not fully validated. However, the validation of the first release of the product showed the overall agreement with forest/non-forest assessments using the Degree Confluence Project, the Forest Resource Assessment, and Google Earth images of 85%, 91%, and 95%, respectively (Shimada, Takuya, et al., 2014). In 2019, the TanDEM-X Forest/Non-Forest Map products were made available for download (Microwaves and Radar Institute, 2019). They are provided as raster data with a ground resolution of 50 m x 50 m. The global forest/non-forest map are the result of a forest classification using bistatic interferometric TanDEM-X radar data acquired between 2011 and 2015 in Stripmap Single Polarization (HH) mode. The resulting products were validated using external reference information as well as with other existing classification maps. An overall agreement of 90% was reported (Martone et al., 2018).

Using the differencing approach, the ALOS PALSAR HH and HV-backscatter change was reported to be between 2 and 3 dB (Fransson et al., 2007; Santoro et al., 2010). Using a simple thresholding algorithm with three different values (2.0, 2.5, and 3.0 dB) Santoro et al. (Santoro et al., 2010) reported the increased classification

accuracy of the clear-cut areas from 57.4% to 78.2% for decreasing value of the threshold. More than 90% of the clear-cuts recorded in the available database of the harvested areas were identified. The ALOS PALSAR in HV polarization performed better than in HH polarization when using thresholding approach combined with data fusion based multi-channel change detection (Moser & Serpico, 2009; Pantze, Fransson, & Santoro, 2010). In another study, similar approach and the ALOS PALSAR HV data were implemented to create a map of clear-cut areas for all of Sweden's forested areas (Santoro et al., 2012). The authors analyzed the potential of the SAR L-band data as the current system of the Swedish Forest Agency (SFA) for monitoring of the clear-cuts is based on the use of the optical data. On average 59.9% of the pixels within validated clear-cuts were correctly classified. The authors reported increase of accuracy to 88.9% when 50 m edge-eroded version of the reference data was used for validation. Small-scale changes (< 2 ha) could not be detected. The researchers concluded that the 50 m spatial resolution of the data was a limiting factor in accurately delineating forest changes at the county and national level. This could be overcome using the full-resolution data (20 m resolution).

The first approach to providing comprehensive forest information (e.g., LC, biomass, and forest change) for a part of Siberian boreal forests was done within the Assessment and Monitoring of Forest Resources in the Framework of the EU-Russia Space Dialogue ZAPÁS project: http://zapas.uni-jena.de/ (Hüttich et al., 2012). In this research project, multi-temporal L-band ALOS PALSAR backscatter mosaics in HH and HV polarization were applied for large-scale biomass (GSV) and forest cover change monitoring. An object-based image analyses (OBIA) was developed for an automated wall-to-wall mapping of forest change. Afterwards, a multi-stage threshold-based classification process tree was developed. Three classes were generated: forest, non-forest, and forest regrowth. The result was a segment-based forest cover and disturbance product for the years 2007 and 2010. The products have not been fully validated. The ALOS PALSAR data were reported to have a great potential for forest mapping purposes (Hüttich et al., 2014).

In this study, an integrated GIS and pre-classification approach was implemented. The details are given in Chapter 4.1.

2.4 Study area and data

The following sections describe the characteristics of the location of study areas. In addition, a brief description of the *in situ* and SAR missions that acquired the data analyzed in this study is presented.

2.4.1 Location of study areas

The study area is located in the Asian part of the boreal forests, in the southern Central Siberia in Russia. In total, the analyses were conducted on three research areas. The algorithm for the forest change monitoring was developed on the area that covered approximately 620,000 km^2 whereas the models for the AGB retrieval were trained and tested on the area of over 200 km^2 and 2,000 km^2 (Figure 2.6). The extent of the research areas corresponds to the size of the available SAR data. The detailed description of the research areas is given in the Chapters 4.1, 4.3 and 4.4, respectively.

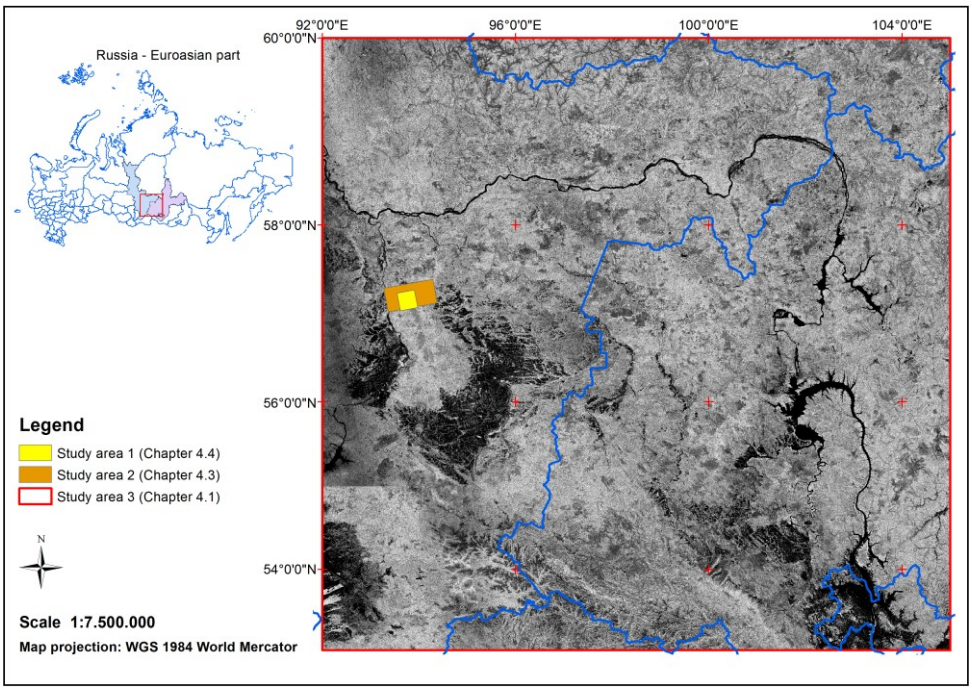

Figure 2.6: Location of the study areas. In background mosaic of 91 tiles of ALOS PALSAR HV-intensity for 2010. Data source: ALOS K&C © JAXA/METI. Adapted from (Hüttich, Stelmaszczuk-Górska, Eberle, Kotzerke, & Schmullius, 2014).

2.4.2 Processing of *in situ* data

This section is based on the *in situ* data description given in the Chapters 4.3 and 4.4.

The reference data used in this study were gathered in the framework of the Russian Forest Inventory and Planning (FIP) and are available in GIS vector format. All information is given for a forest stand, i.e., a group of trees occupying a specific area uniform in species composition, size, age, and management strategy.

Attributes such as GSV, age of the dominant tree species in a stand, an average tree height of each species in the stand, diameter at breast height (DBH) measured at 1.3 meters above ground, and species composition were provided. In total, the forest and trees parameters of more than 1,600 stands were available. The field data were acquired within the SIBERIA project (Schmullius et al., 2001).

The inventory dates back to 1998. Because of the time difference between inventory data and the SAR data acquisitions (8-14 years) the *in situ* data were updated. It was done using semi-empirical phytomass models (Shvidenko, Schepaschenko, Nilsson, & Bouloui, 2007) and growth (yield) tables. The latter were developed in the International Institute for Applied Systems Analyses (IIASA) in collaboration with V.N. Sukachev Institute of Forest, Siberian Branch, Russian Academy of Sciences, and Moscow State Forest University. Those models and tables are recommended for use in forestry and forest management of Russia (Protocol of the Council of Federal Agency of Forest Management No 2 dated by 8 June 2006) (Shvidenko, Schepaschenko, Nilsson, & Boului, 2008).

The reference data were updated to the year 2010 and 2014. The data improvement consisted of four stages. First, the forest stands that changed from forest to non-forest were excluded by using very high and high resolution optical (KOMPSAT-2 and SPOT-5) and SAR (ALOS-2 PALSAR-2 and RADARSAT-2) data. Then, from the resulted stands only those were selected in which at least 60% of the trees belong to a single species. The reason for the selection is that the growth tables were generated for dominant tree species. In the second step, the stands were used in the semi-empirical phytomass models. The basis for the improvement of the outdated inventory data is a site index (SI). SI is defined as edaphic and climatic characteristics of a site which has an impact on growth and yield of a given tree species (van Laar & Akca, 2007). SI classes are usually determined by the relationship between the mean tree height and the mean age of a stand. As the SI was not available in the original forest inventory data it was calculated using the following equations (IIASA, 2007):

$$H_t = 22.47\left(1 - e^{-0.0234A\left(1-e^{-0.0057A}\right)}\right)^{0.548} + (3 - SI)\Delta \quad (2.4.1)$$

$$\Delta = 4.35\left(1 - e^{-0.0205A}\right)^{0.957} \quad (2.4.2)$$

where H_t represents a tree height, A denotes a forest stand age and the Δ is an interval between the site indexes. In the case of Russian forests, the SI from Ib, Ia, I –V, Va, Vb are denoted, where the class with the lowest SI indicates the best site conditions for forest trees to grow.

After calculating the SI, the growth rate was derived by implementing the Richards-Chapman growth function in polynomial quadratic form (Shvidenko et al., 2008):

$$GSV_{growth\ rate} = c_1 c_2 c_3 (1 - e^{-c_2 A})^{c_3 - 1} e^{-c_2 A} \quad (2.4.3)$$

where A denotes age, c_i are the parameters, which have an ecological interpretation and depend on SI (Shvidenko et al., 2008):

$$c_i = c_{i3} SI^2 + c_{i2} SI + c_{i1} \quad (2.4.4)$$

After obtaining the GSV growth rate, the correction coefficient GSV_{cc} was introduced (Stelmaszczuk-Górska et al., 2016):

$$GSV_{cc} = \frac{GSV_{in\ situ}}{GSV_{model}} \quad (2.4.5)$$

where $GSV_{in\ situ}$ represents GSV measured in the field, whereas GSV_{model} is GSV calculated using the growth models for a particular site index and forest stand age (Eq. 3 and 4). An updated GSV was then derived by calculating GSV_{new} (Stelmaszczuk-Górska et al., 2016):

$$GSV_{new} = GSV_{in-situ} + A_{diff} GSV_{growth\ rate} GSV_{cc} \quad (2.4.6)$$

where A_{diff} is an age difference between the old inventory and reference year 2010 and equals 12.

In the third step, GSV was converted to AGB. The following regional allometric model was applied (Stelmaszczuk-Górska et al., 2016):

$$AGB = 0.94 * GSV^{0.9} \quad (2.4.7)$$

The model (Eq. 6) was constructed relating freely available measurements of forest live biomass (phytomass) (IIASA, 2007).

In the final step, the updated *in situ* data were rasterized to the spatial resolution of SAR data. In order to avoid border effects, the stands were eroded by 2 pixels. Afterwards, the forest inventories were converted into points using the center of gravity (centroid) of the stand.

The update between years 2010 and 2014 was limited to the first step of the reference data processing.

2.4.3 SAR L-band data: PALSAR & PALSAR-2

The long wavelength sensors (L- and P-band or longer) are of particular use for the retrieval of biophysical forest parameters such as biomass and forest/non-forest mapping. In this study, data from the L-band satellite SAR were used, as no P-band data are available. The first P-band data from satellite SAR system will be acquired

starting from year 2022 within the ESA Earth Explorer Biomass Mission ESA, 2019).

Data from two new generation L-band sensors were investigated, namely from the Phased Array type L-band Synthetic Aperture Radar PALSAR and PALSAR-2. Both systems are active microwave sensors using L-Band frequency onboard the Advanced Land Observing System (ALOS nicknamed "Daichi" meaning land) and the follow-on satellite mission ALOS-2. ALOS and ALOS-2 are Japanese Earth Observation satellites, developed by the Japan Aerospace Exploration Agency (JAXA) and manufactured by the NEC, Toshiba, and Mitsubishi Electric Corporation.

The data were available within the ALOS Kyoto & Carbon Initiative Phase 3 and 4 (Thiel, Chowdhury, Stelmaszczuk-Górska, Hüttich, & Schmullius, 2014). It is an international collaborative project led by JAXA EORC. It was initiated in 2001 with a main objective "*to support information needs raised by the UNFCCC Kyoto Protocol and by the international global carbon cycle science community, by provision of systematic, consistent, repetitive and regional scale data of the global forest cover"* (Rosenqvist, Ogawa, Shimada, & Igarashi, 2001). Furthermore, the PALSAR and PALSAR-2 aims are monitoring of deformations, wetlands and its inundation patterns at local and regional scales. The data are acquired based on the radar-based systematic observation strategy so-called Basic Observation Scenario BOS (Rosenqvist et al., 2014; Rosenqvist et al., 2004).

The system characteristics of ALOS PALSAR and ALOS-2 PALSAR-2 are given in Table 2.3, Table 2.4, and Table 2.5 and are limited to the main instrument characteristics and information on operational observation modes (Kankaku, Suzuki, & Osawa, 2013; Kramer, 2002; Okada et al., 2013; Rosenqvist et al., 2004; Suzuki, Kankaku, & Shimada, 2013). The ALOS is an inactive mission retired after 4.5 years of operations on May 12, 2011.

Table 2.3: ALOS PALSAR and ALOS-2 PALSAR-2 system characteristics.

	ALOS PALSAR	**ALOS-2 PALSAR-2**
Launch Date	January 24, 2006	May 24, 2014
Status (Retired on)	Inactive (May 12, 2011)	Active
Orbit	Sun-synchronous	Sun-synchronous
Altitude	691.65 km	628 km
Descending node	~10:30 a.mm	~12:00 a.m.
Ascending node	~10:30 p.m.	~12:00 p.m.
Repeat cycle	46 days	14 Days
Active antenna	L-band	L-band

Centre frequency (Wavelength)	1.27 GHz (23.6 cm)	1.24, 1.26 or 1.28 GHz (24.2, 23.8 or 23.4 cm)
Bandwidth	14 or 28 MHz	14, 28, 42 or 84 MHz
Aperture length	8.9 m	10 m
Aperture width	3.1 m	3 m
Look direction	Right looking	Left- and right (nominal) looking
Polarization	Single, Dual or Quad	Single, Dual or Quad
NESZ	from -32dB to -23dB (@41.5° Fine mode, ScanSAR 5-beam, @21.5° Polarimetry)	from -28dB to -23dB (@37°)

For PALSAR, six acquisition modes were chosen, four operational: two high resolution Stripmap modes (Fine Beam Single FBS and Fine Beam Dual FBD), fully polarimetric mode and ScanSAR mode in 5-beam HH mode, and two semi-operational modes. PALSAR-2 operates additionally in Spotlight mode and the two Stripmap modes (24 beams for Ultrafine and High Sensitive modes). Furthermore, a new polarization mode was introduced - compact polarimetry (CP), i.e., the transmitted polarization can be either circular or linear. Operations of both PALSAR and PALSAR-2 are planned foremost for ascending passes, as the descending node is used for the optical sensors mounted on the ALOS and ALOS-2 satellites.

The L-band PALSAR and PALSAR-2 data were obtained in the Single Look Complex (SLC) format (level 1.1) and as ALOS PALSAR backscatter mosaic. The global mosaics were produced by JAXA using the ALOS PALSAR data in HH and HV polarization (FBD) acquired between June and October during 2007, 2008, 2009 and 2010.

Table 2.4: PALSAR observation modes.

Beam mode	**Nominal swath width [km]**	**Maximal spatial resolution [m]**	**Incidence angle [°]**	**Polarization**
Fine Beam Single	70	7	7.9-60.0	HH or VV
Fine Beam Dual	70	14	7.9-60.0	HH+HV or VV+VH
Fine Beam Quad-Pol	30	24	7.9-30.1	HH+VV+HV+VH
ScanSAR 5 beam	350	100 (multi-look)	18.0-43.3	HH or VV

Table 2.5: PALSAR-2 observation modes.

Beam mode	Nominal swath width [km]	Maximal spatial resolution [m]	Incidence angle [°]	Polarization
Spotlight	25	1	8-70	HH, VV or HV
Ultra Fine	50	3	8-70	HH, HV, VV or VH HH+HV or VV+VH
High Sensitive	50	6	8-70	HH, VV or HV HH+HV or VV+VH CP
High Sensitive Quad-Pol	50	6	17-40	HH+VV+HV+VH
Fine Beam Single	70	10	8-70	HH, VV or HV CP
Fine Beam Dual	70	10	8-70	HH+HV or VV+VH CP
Fine Beam Quad-Pol	30	10	22-26	HH+VV+HV+VH
ScanSAR Normal	350	100 (multi-look)	8-70	HH, VV or HV HH+HV or VV+VH
ScanSAR Wide	490	60 (multi-look)	8-70	HH, VV or HV HH+HV or VV+VH

The data were resampled to 25 m spatial resolution. The mosaics were obtained in 1-degree tiles as level 1.5 data, i.e., radiometrically- and slope-corrected, orthorectified data (Shimada, 2010). The description of mosaic generation can be found in Shimada et al. (Shimada et al., 2014). A summary of used data is given in Table 2.6. The detailed description of available data and obtained results is given in Chapter 4.1-4.4.

Table 2.6: L-band data analyzed in this study.

Data	Acquisition time Year or Date (DD.MM.YYYY)	Number of Images/Tiles	Application	Details given in Chapter
ALOS PALSAR mosaic	2007-2010	364	Forest change monitoring	4.1
ALOS PALSAR	28.12.2006-23.02.2011	29*	Biomass estimation	4.3
ALOS-2 PALSAR-2	26.09.-01.10.2014	4**	Biomass estimation	4.4

*9 FBS and 10 FBD scenes

**2 FBD scenes

2.4.4 SAR C-band data: RADARSAT-2

The complementary information to the L-band data provides a C-band SAR. As described in Chapter 2.2, the C-band satellite system operates at the wavelength of approximately 6 cm. The L-band radar provides information related to branches and eventually tree trunks. The radiation from the C-band sensor, on the other hand, penetrates only small objects, such as tree leaves on top of the tree canopy.

In this study, a data acquired by the satellite RADARSAT-2 were analyzed. The data were available within the Second Sciences and Application Research for Europe (SOAR-EU) call for proposals announced by the ESA jointly with the Canadian Space Agency (CSA). The deadline for the proposal submission was 31 October 2013.

After the loss of ENVISAT satellite in 2012 and before the start of the Sentinel -1 mission in 2014, ESA did not provide any new C-band SAR acquisitions. The RADARSAT mission filled this gap and supported the ESA in maintaining the long-standing tradition of providing the C-band data. The RADARSAT-2 played an important role in the Sentinel-1 preparatory phase. The special projects were carried out in order to support the Copernicus satellite mission. For example, the Sentinel-1 Terrain Observation by Progressive Scans SAR (TOPSAR) technique was implemented on RADARSAT-2. In this acquisition mode, the data is acquired in bursts by cyclically switching the antenna beam between multiple adjacent sub-swaths. In this way, large swath widths are provided and the radiometric performance is enhanced. TOPSAR is used in Sentinel-1's Interferometric Wide swath and Extra Wide swath modes. (De Zan & Guarnieri, 2006; Geudtner, 2014).

The RADARSAT-2 is a follow-on satellite of RADARSAT-1 with the objective to continue the RADARSAT program and to ensure the data continuity in particular focusing on environmental monitoring, managing natural resources, and performing costal surveillance. It is an active SAR system operated and owned by the MacDonald, Dettwiler and Associates Ltd. (MDA). The CSA co-founded the construction and launch of the satellite. The SAR instrument may be operated in one of the three main imaging sensor modes for terrestrial and maritime applications: Single Beam (15 Stripmap modes), ScanSAR (4 modes) or Spotlight (CSA, 2017; Maxar Technologies Ltd., 2018). The selected characteristics of the system and the information on RADARSAT-2 acquisition modes are given in Table 2.7 and Table 2.8.

Table 2.7: RADARSAT-2 system characteristics.

Launch Date	**December 14, 2007**
Status	**Active**
Orbit	**Sun-synchronous**
Altitude	798 km
Descending node	6 a.m.
Ascending node	6 p.m.
Repeat cycle	24 days
Active antenna	C-band
Centre frequency (Wavelength)	5.405 GHz (5.6 cm)
Bandwidth	11.6, 17.3, 30, 50, or 100 MHz
Aperture length	15 m
Aperture width	1.37 m
Look direction	Left- and right looking
Polarization	Single, Dual or Quad
NESZ	from -34dB to -24dB

In this study, seven RADARSAT-2 images were analyzed. In order to compare the C- and L-band data performance for biomass estimation, it was important to acquire data under similar weather conditions. The data were acquired in summer-autumn 2014 between June 25th and October 10th in Ultra-Fine 3 images in single polarization and Fine modes 2 scenes in dual polarization (4 images). The Ultra-Fine and Fine modes were chosen to investigate the data with similar characteristics as, at that time, future Sentinel-1 data as well as to analyze potential of new RADARSAT-2 acquisition modes for biomass estimation. The detailed description of available data and obtained results is given in Chapter 4.4.
The C-band data were obtained in the Single Look Complex (SLC) format.

Table 2.8: RADARSAT-2 observation modes.

Beam mode	**Nominal swath width [km]**	**Maximal spatial resolution [m]**	**Incidence angle [°]**	**Polarization**
Spotlight	18	1	20-50	HH, HV, VH, or VV
Ultra-Fine	20	3	20-50	HH, HV, VH, or VV
Wide Ultra-Fine	50	3	30-50	HH, HV, VH, or VV
Extra-Fine	125	5	22-49	HH, HV, VH, or VV
Multi-Look Fine	50	8	30-50	HH, HV, VH, or VV
Wide Multi-Look Fine	90	8	30-50	HH, HV, VH, or VV

Fine	50	8	30-50	HH, HV, VH, or VV HH+HV or VV+VH
Wide-Fine	150	8	20-45	HH, HV, VH, or VV HH+HV or VV+VH
Fine Quad-Pol	25	12	18-49	HH+VV+HV+VH
Wide Fine Quad-Pol	50	12	18-42	HH+VV+HV+VH
Standard Quad-Pol	25	25	18-49	HH+VV+HV+VH
Wide Standard Quad-Pol	50	25	18-42	HH+VV+HV+VH
Standard	100	25	20-52	HH, HV, VH, or VV HH+HV or VV+VH
Extended Low	170	60	10-23	HH
Wide	150	25	20-45	HH, HV, VH, or VV HH+HV or VV+VH
Extended High	75	25	49-60	HH
Ship Detection	450	Variable	35-56	HH, HV, VH, or VV
ScanSAR Narrow	300	50	20-47	HH, HV, VH, or VV HH+HV or VV+VH
Ocean Surveillance	530	Variable	20-50	HH, HV, VH, or VV HH+HV or VV+VH
ScanSAR Wide	500	100	20-49	HH, HV, VH, or VV HH+HV or VV+VH

Chapter 3

Research rationale

Research needs

Research questions

3.1 Research needs

Based on the previously reported results described in the Chapter 2.3, the following recommendations and findings for boreal forests monitoring using SAR data can be summarized as follows:

1. Use of data acquired by low frequency SAR systems (Cartus & Santoro, 2019). The SAR with longer wavelengths reduces the attenuation of the radar signal and thus strengthens the response from the forested areas.
2. Use of data in HV or HH polarizations. The data in horizontal polarization transmitted and horizontal or vertical received (HH or HV) are superior to vertical transmitted and vertical or horizontal received (VV or VH). HV polarization has been reported to provide slightly better results for forest volume estimation (Thiel & Schmullius, 2016). However, the sensitivity of co- and cross-polarized backscatter to vegetation parameters may vary across regions and forest structures. In case of forest change monitoring, the HV-backscatter of L-band data have been reported to provide better results (Santoro et al., 2010).
3. The thresholds for separating forest and non-forest using SAR data have been reported to vary regionally (Shimada, Itoh, et al., 2014).
4. Use of data acquired with a higher incident angle/shallow look angle (Santoro et al., 2015). Higher incident angles decrease the penetration depth and thus increase the difference between the forested and non-forested areas eliminating impacts of the underlying soil moisture variations.
5. Use of data from areas with flat to moderate topography (Ranson et al., 2001). The AGB retrieval accuracies in flat areas are higher than in areas with steep slopes. In the areas with high topography, it has been recommended to use a local DEM with high spatial resolution to successfully overcome SAR geometric distortions.
6. Use of both phase information and backscattering intensity. InSAR coherence (Thiel & Schmullius, 2016) and InSAR height (Askne et al., 2017) have been reported to provide better results for AGB estimation.
7. For the interferometric analysis, use of data from stable winter frozen conditions with possible shortest temporal baseline in case of interferometric coherence (Eriksson et al., 2003).

8. Use of backscattering intensity data acquired during the vegetation season as at this time the crown volume backscattering dominants (Ranson & Sun, 1994).
9. Use of radargrammetry (Rahlf et al., 2014) or tomography (Tebaldini & Rocca, 2012) techniques have been also reported to be powerful tools for forest monitoring. However, the latter method is available only from airborne platforms.
10. Use of multi-temporal approach (Santoro et al., 2011). The integration of many SAR images can increase the point at which saturation of the radar signal occurs. The multi-temporal approach reduces the impact of environmental conditions in SAR data.
11. Implementation of multi-temporal polarimetric coherence (PolInSAR) increased the AGB retrieval accuracies (Antropov et al., 2017).
12. Use of multi-frequency data (Santoro & Cartus, 2018). The sensitivity of radar signal to the forest AGB increases with the use of multi-frequency SAR data as the different frequencies reflect different scattering mechanisms, i.e., reflect from different parts of a tree.
13. Both parametric and non-parametric models are feasible to retrieve forest parameters (Santoro & Cartus, 2018). There are only few examples of non-parametric models (Stelmaszczuk-Górska, Thiel, et al., 2017). However, a combination of both can provide better results (Tanase et al., 2014).
14. Include forest structure information to the mapping approaches, if possible (Joshi et al., 2017). This can also improve sensitivity of SAR signal to forest AGB.
15. The target spatial scale should be considered (Herold et al., 2019). The horizontal resolution of 0.25 ha has been recommended (GCOS, 2016).

In the context of the future developments, the following research needs have been recognized:

- Evaluate and improve SAR L-band products for large-scale forest change mapping;
- Define a threshold for Siberian boreal forest/non-forest mapping;
- Investigate the use of SAR backscatter and coherence synergistically for AGB estimations;
- Investigate the use of multi-frequency, multi-polarization, and multi-temporal SAR observation for AGB estimations;
- Examine the merit of additional measures from the SAR backscatter for AGB retrieval;

- Evaluate the machine-learning algorithms for AGB retrieval with a target spatial resolution of 0.25 ha.

3.2 Research questions

Although many SAR properties have been already successfully implemented for forest monitoring, there is still a need to further exploit the SAR properties and improve the estimation accuracies. Based on the identified research needs, the specific research questions are defined as follows:

1. **How to improve large-scale mapping of boreal forest changes using SAR L-band products?**

To address this research question, data from multi-source EO observations were analyzed. Annual ALOS PALSAR backscatter mosaics in HV polarization were used together with time series of the Enhanced Vegetation Index (EVI) with a temporal resolution of 16 days from the Moderate Resolution Imaging Spectral Radiometer (MODIS). Using the Earth Observation Monitor (EOM) (Eberle, Clausnitzer, Hüttich, & Schmullius, 2013) the capabilities of the SAR and optical data for an operational detection of forest aboveground biomass loss in the forest ecosystem of Central Siberia were assessed.

The author of this thesis was responsible for SAR data processing and SAR data classification. The results of operational forest monitoring in Siberia are given in Chapter 4.1.

2. **What are the research pathways of boreal forest aboveground biomass estimation using SAR data?**

In order to identify research pathways of biomass estimation for boreal forests, a survey of 70 peer-reviewed papers were analyzed. Reported results were summarized in terms of sensor parameters (frequency, polarization, look angle), study area, range of estimated variable, number of images and input data applied for modelling the GSV/AGB, model used, as well as selected statistics on model performance. GSV/AGB estimation results were analyzed in terms of model fit, the coefficient of determination (R^2) or coefficient of correlation (r), root mean square error (RMSE), and relative root mean square error (rRMSE).

A review of available research papers on the forest GSV/AGB estimations is given in Chapter 4.2 and Appendix B.

3. **How to combine multi-temporal InSAR coherence and backscatter data to improve aboveground biomass estimation in boreal forests?**

For this research question, the multi-temporal ALOS PALSAR L-band data were applied. The SAR backscatter intensity and InSAR coherence were used synergistically; a new ratio of backscatter and coherence was introduced. Nineteen ALOS PALSAR scenes acquired in FBD and FBS modes along with the same number of coherence images were used as explanatory variables in two recently popular machine-learning approaches. The predictive contribution of individual datasets to the seven defined AGB classes was examined. AGB was estimated using RF and MaxEnt algorithms with a target spatial resolution of 0.25 ha. The resulting AGB maps were validated using an independent set of reference data. These data were generated using a new regional allometric equation.

This research question is discussed in Chapter 4.3.

4. **How can fusing of multi-temporal and multi-frequency SAR data improve aboveground biomass estimation?**

For this research question, the combination of multi-frequency, multi-polarization, and multi-temporal SAR data for AGB estimation was explored. Data from ALOS-2 PALSAR-2 L-band SAR were used together with C-band RADARSAT-2 data. Backscattering coefficients from both SAR systems were used independently and in combination using a non-parametric model for AGB estimation with a target spatial resolution of 0.25 ha. In addition, polarimetric ratios and texture measures were used for AGB modelling. In total, five models were developed using from nine to forty-five predictor variables. The predictive performance of all generated models was assessed.

This research question is discussed in Chapter 4.4.

Chapter 4

Research contributions

Operational forest monitoring in Siberia

Remote sensing for aboveground biomass estimation in boreal forests

Non-parametric retrieval of aboveground biomass

Multi-frequency SAR for estimation of aboveground biomass

4.1 Operational forest monitoring in Siberia

This section presents the manuscript entitled
"Operational forest monitoring in Siberia using multi-source Earth Observation data" prepared and written by Hüttich, C., Stelmaszczuk-Górska, M., Eberle, J., Kotzerke, P. & Schmullius, C.

The manuscript was peer-reviewed and published in
Siberian Journal of Forest Science, 5, 38-52.

СИБИРСКИЙ ЛЕСНОЙ ЖУРНАЛ. 2014. № 5. С. 38–52

УДК 629.78; 630.52: 587/588

OPERATIONAL FOREST MONITORING IN SIBERIA USING MULTI-SOURCE EARTH OBSERVATION DATA

© 2014 C. Hüttich[1], M. A. Stelmaszczuk-Górska[1], J. Eberle[1], P. Kotzerke[2], C. Schmullius[1]

[1] *Friedrich-Schiller University, Department of Earth Observation*
Löbdergraben, 32, Jena, 07743 Germany

[2] *GAF AG*
Arnulfstrasse, 199, Munich, D-80634 Germany

E-mail: christian.huettich@uni-jena.de, m.stelmas@uni-jena.de, jonas.eberle@uni-jena.de, paul.kotzerke@gaf.de, c.schmullius@uni-jena.de

Received 04.09.2014

Forest cover disturbance rates are increasing in the forests of Siberia due to intensification of human activities and climate change. In this paper two satellite data sources were used for automated forest cover change detection. Annual ALOS PALSAR backscatter mosaics (2007–2010) were used for yearly forest loss monitoring. Time series of the Enhanced Vegetation Index (EVI, 2000–2014) from the Moderate Resolution Imaging Spectroradiometer (MODIS) were integrated in a web-based data middleware system to assess the capabilities of a near-real time detection of forest disturbances using the break point detection by additive season and trends (Bfast) method. The SAR-based average accuracy of the forest loss detection was 70%, whereas the MODIS-based change assessment using breakpoint detection achieved average accuracies of 50% for trend-based breakpoints and 43.4% for season-based breakpoints. It was demonstrated that SAR remote sensing is a highly accurate tool for up-to-date forest monitoring. Web-based data middleware systems like the Earth Observation Monitor, linked with MODIS time series, provide access and easy-to-use tools for on demand change monitoring in remote Siberian forests.

Keywords: *remote sensing, SAR, MODIS, time series, forest change monitoring, near-real time.*

INTRODUCTION

In order to mitigate the consequences of climate change caused by land use change, it is important to improve information on the terrestrial distribution of carbon sources and sinks. This can be provided through accurate and reliable vegetation cover change monitoring. Due rapid rates of change and vast area of land cover, remote sensing techniques are increasingly proposed as globally consistent environmental monitoring tools (Cihlar et al., 2002). Remote sensing acquires data over large areas with high repetition frequency, and at a relatively low cost. These techniques are recommended for forest monitoring to inform international climate policy and related international programs (e.g., REDD; Reduced Emissions from Deforestation and Forest Degradation), and initiatives (e.g., ALOS K&C; ALOS Kyoto & Carbon Initiative and GFOI; Global Forest Observations Initiative). Remote sensing has already been demonstrated to be capable of contributing to the current and future measurement and monitoring of carbon sources and sinks, through its ability to provide systematic, globally consistent estimates of land cover (LC), land cover change (LCC), forest disturbances, and aboveground biomass (AGB). Multiple publications are available on optical, radar, as well as LiDAR (Light Detection and Ranging) EO (earth observation) data for LCC and biomass estimation.

The Russian Federation is of special monitoring concern. It is the most forested country in the world, with forest covering 49% of its total area (FAO, 2012). The forests of the Russian Federation represented 90% of the carbon sink

of the world's boreal forests from 2000 to 2007 (Pan et al., 2011). At the same time, they also provide the largest source of uncertainty in global carbon stock calculations (Pan et al., 2011). Moreover, tree cover loss in the Russian Federation from 2000 to 2012 was the highest in the world, totaling more than 5 million hectares in the year 2012 alone (Hansen et al., 2013). This tree cover loss is mainly due to fires, which are the biggest overall cause of forest loss in boreal ecosystems. Fires are a particularly damaging form of disturbance in the Russian boreal forest. This is because conifers dominate and most of the forest is unmanaged and unprotected (Shvidenko et al., 2011). Current model predictions indicate that the number of fire events in the boreal zone may double by the end of 2100 (Shvidenko et al., 2011). Illegal logging also poses a huge problem for the monitoring of Russian forests. According to established sources like World Wide Fund for Nature (WWF) Russia and the World Bank, illegal clear-cutting in Russia is estimated to account for approximately 25% of all logging activity in this country (WWF, 2014). Moreover, due to the lack of funding for monitoring efforts, some forested regions in Siberia have not been inventoried for more than 25 years (Hüttich et al., 2014*a*).

The number and availability of Earth Observation (EO) resources is continuously increasing. Interactive and interoperable access to satellite time series data is increasing, as demonstrated by various EO data infrastructure projects, such as the Siberian Earth System Science Cluster (SIBESSC, Eberle et al., 2013*a*), NASA Giovanni (Acker & Leptoukh, 2007), and the Earth Observation Monitor (EOM, Eberle et al., 2013*b*). The application of data middleware systems enables operational monitoring of remote forest territories in a near real-time mode, as shown for Central Siberia (Hüttich et al., 2014*b*). User-friendly clients for accessing and analyzing operational frequently updated EO time series provide opportunities for the monitoring of forest disturbances and dynamics. In order to quantify the accuracy of both spatial and temporal high resolution forest disturbance monitoring techniques further research has to be focused on the integration of multi-source change detection techniques.

The objective of this paper is to analyze multi-source optical and Synthetic Aperture Radar (SAR) EO data for forest disturbance monitoring for a test site in Central Siberia. In order to evaluate the capabilities of selected operational satellite data products for forest change monitoring, two operational satellite data sources were analyzed with a focus on forest loss. Forest loss is defined as a disturbance, or a change from forest to a non-forest stage without tree cover.

ALOS PALASAR data with the high spatial resolution of 25 m were used for the application and assessment of pre-classification change detection techniques for assessing the yearly extent of forest loss. Further, time series of the Enhanced Vegetation Index (EVI) with a temporal resolution of 16 days (2000–2014) from the Moderate Resolution Imaging Spectral Radiometer (MODIS) were integrated in a web-based data middleware system. Using the Earth Observation Monitor (EOM, www.earth-observation-monitor.net) an operational monitoring system was used for assessing for the capabilities of a near-real time detection of biomass loss in the forest ecosystem of Central Siberia, and to analyze temporal patterns of forest cover loss related to logging activities, fire events or other disturbances.

STUDY AREA

The study area is located in the Asian part of the boreal forest, in southern Central Siberia (Fig. 1). The area covers approximately 620 000 km^2 (longitude: 92–105° E; latitude: 53–60° N) and belongs to two Siberian Federal districts: Krasnoyarsk territory and Irkutsk region.

The test site is characterized by a continental climate, with long, severe winters and short (from mid-June to mid-September), warm, and relatively wet (as high as approximately 70 mm in a month of rainfall) summers. The coldest months are December and January, with temperatures of around –20 °C during the day, and the warmest months are June and July, with temperatures above +20 °C. Annual precipitation is approximately 400 mm with the most rainy season from July to October (based on weather data from the SIB-ESS-C portal, data

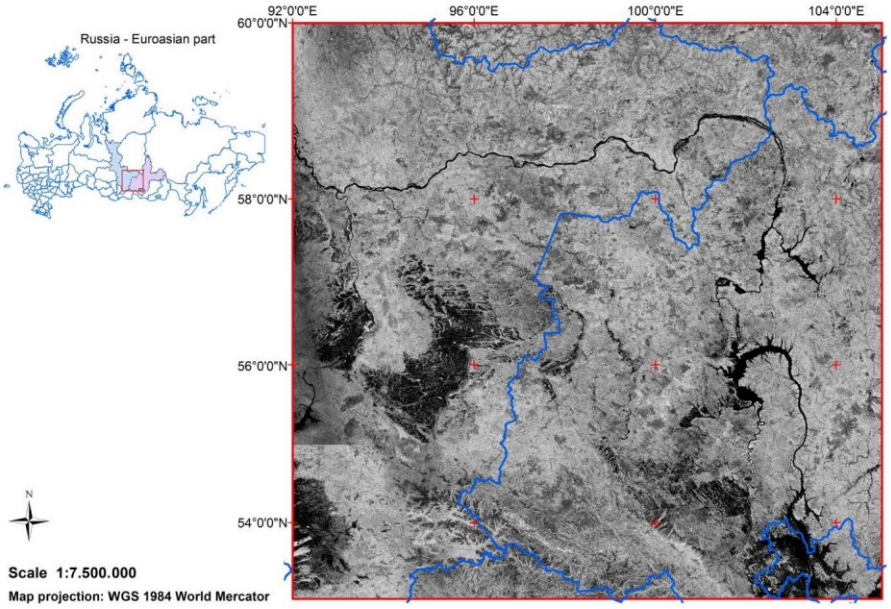

Fig. 1. The study area is located in two Siberian Federal districts: Krasnoyarsk territory and Irkutsk region, within Angara river basin. In background mosaic of 91 tiles of ALOS PALSAR HV-intensity data for 2010; amplitude data source: ALOS K&C © JAXA/METI.

source: World Meteorological Organization). The study area is covered mainly by forest; for-est cover is approximately 70% (based on Land Cover Map for Central Siberia (2010) © IKI, ZAPÁS project). The main dominant species in the study area are spruce (*Picea*), pine (*Pinus*), fir (*Abies*), and larch (*Larix*). Deciduous species are also present, mainly birch (*Betula*), aspen, and poplar (*Populus*), which are typical for early succession stages of such forests. These forests are hardly managed or protected, leading it to suffer disturbances such as wild fires, logging, and insect outbreaks (Schmullius et al., 2001; Shvidenko et al., 2011).

DATA

ALOS PALSAR backscatter mosaic data. For the forest loss detection ALOS PALSAR yearly backscatter mosaics with a 25 m spatial resolu-tion were used. The data were acquired using L-band frequency in the Fine Beam Double (FBD) mode in two polarizations, horizontal transmitted and received (HH) and horizontal transmitted and vertical received (HV), with a 34.3° incidence angle, from May to October for the years from 2007 to 2010. The data were available through the ALOS K&C Initiative led by the Japan Aerospace Exploration Agency (JAXA). An example of an RGB composite of PALSAR mosaic for the selected area with clearly visible clear-cuts is shown in Fig. 2.

For Siberian test sites, a total of 364 of 1 degree tiles were delivered as level 1.5 data, which means radiometrically, slope-corrected, and orthorectified SAR amplitude data (Shimada et al., 2009; Shimada, 2010). According to Shimada et al. (2009) visible artifacts and unusual backscatter values were set to no data (< –34 dB HV / < –32 dB HH). The upper limit of the backscattering coefficient was +8 dB for both polarizations. The obtained data were converted from digital number (DN) into normalized radar cross section (NRCS) on the dB scale, according to the equation:

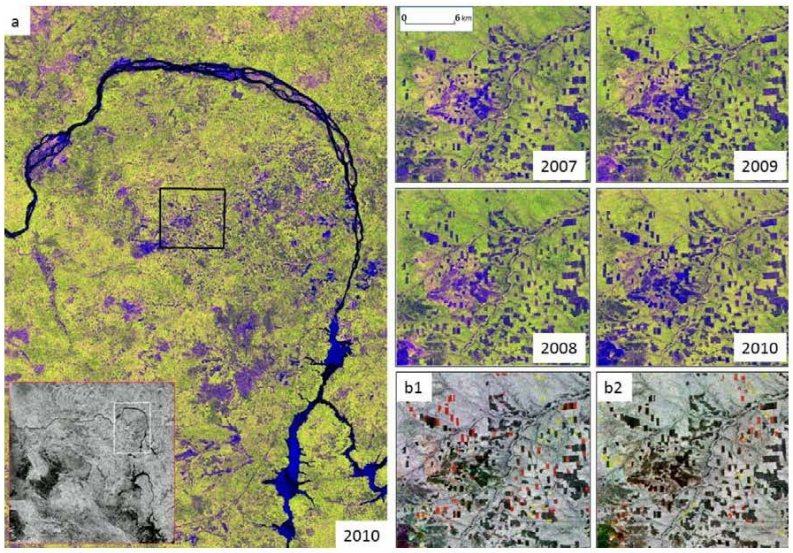

Fig. 2. RGB composite of PALSAR 25-m mosaic: a. red: HH-intensity, green: HV-intensity, blue: ratio HH/HV; HV-intensity b1. red: 2007, green: 2008, blue: 2009, b2. red: 2008, green: 2009, blue: 2010.

$$\gamma^0\,[\mathrm{dB}] = 10 \times \log_{10}(\mathrm{DN}^2) + \mathrm{CF}, \qquad (1)$$

where γ^0 is the backscattering coefficient (gamma nought) in the logarithmic scale, DN represents amplitude value, and CF is a calibration constant, which in this case is equal to –83 dB.

Optical satellite data. In addition to the SAR products, data acquired by optical sensors were also used. Landsat-5/-7 data with less than 10 % cloud cover for 2007–2010 were available via the United States Geological Survey (USGS) Earth Explorer portal. The MODIS Vegetation Continuous Fields (VCF; Collection 5) were downloaded from the Global Land Cover Facil-ity portal (GLCF). In addition, very high resolu-tion KOMPSAT-2 data were available through the European Space Agency CAT1 project (ID 13300). The data were used as reference LC in-formation for validation.

MODIS time series were retrieved from USGS and integrated in the Earth Observation Monitor. The NASA MODIS MOD13 standard vegetation indices (VI) products include the normalize difference vegetation index (NDVI) and the enhanced vegetation index (EVI) to effectively characterize biophysical/biochemical states and processes from vegetated surfaces. There exists a complete, global time series record of VI products from each of the Terra and Aqua MODIS sensors, at varying spatial (250 m, 1 km, 0.05°) and temporal (16-day, monthly) resolutions to meet the needs of the research and application communities. For this study, the MODIS EVI product with 250 m spatial resolution was used.

METHODS

Forest loss monitoring using ALOS PALSAR data. A number of methods exist for forest mapping and change monitoring. In general, these methods can be grouped into post- and pre-classification techniques (Coppin et al., 2004). The first group of methods compare classification products either on the pixel, or segment level, with changes detected based on statistical analyses. The advantage of this approach is that not only change or no-change areas are detected, but also the type and direction of changes. However, the drawback is that the quality of the final change detection product depends on the accuracy of individual classifica-

tions. Unlike the post-classification method, the pre-classification technique employs unclassified images. Methods used to identify change areas include image differencing or rationing, bi-temporal linear data transformation (principal component analysis; PCA; multivariate alteration detection; MAD), image regression, and Change Vector Analysis; CVA (Coppin et al., 2004). Using the differencing approach, the ALOS PALSAR HH and HV-backscatter change was reported to be between 2 and 3 decibels; dB (e. g., Fransson et al., 2007; Santoro et al., 2010). Implementing HH, HV, HH/HV ratio, and HH-HH images difference maps, Dong et al. (2012) developed a decision tree algorithm to produce ALOS PALSAR-based forest maps for southeast Asia, with a high reported overall accuracy of 86%.

In order to identify optimal classification threshold, different multi-temporal metrics were used. In this study, forest/non-forest class separability was investigated using a decision-tree classifier. Due to the small time difference between the datasets, only changes from forest to non-forest were considered. First the PALSAR mosaics were filtered by applying temporal and spatial filters. A multi-temporal filter averaging intensity values in a local window around each pixel and in each image was used (Quegan & Yu, 2001). The window size for the filtering was calculated using the equivalent number of looks (*ENL*):

$$ENL = \frac{(mean)^2}{variance}. \quad (2)$$

The higher *ENL*, the smaller is the scattering caused by speckle or image noise and the better is reduction of speckle effect (Quegan et al., 2000; Yu et al., 2008). As a trade of between resolution and information loss a 7×7 filter window size was selected. All available mosaics in HH and HV polarization were used for the filtering process.

After filtering, the multi-temporal metrics were employed (Bruzzone et al., 2004). They compare the single pixel values over all annual mosaics. In total eight multi-temporal metrics were calculated: minimum backscatter, maximum difference, maximum-minimum ratio (MMR), standard deviation, saturation, normalized standard deviation, mean average variability (MVA), and logarithmic measure based on normalized standard deviation (LMNSTDEV) (Fig. 3).

The largest class separability was calculated for HV-polarization. This observation is in agreement with the previous results (Santoro et al., 2009, 2012; Morel et al., 2011) that the ALOS PALSAR data in HV polarization are more sensitive to detect forest change comparing with HH polarization. The forest to non-forest change thresholds were detected using non-parametric support vector machines (SVM). This approach employs the statistical distribution of the data values to create hyperplane, which is aplane that separates the dataset into defined number of classes. Samples of forest and non-forest areas were collected using Landsat-TM images. The thresholds were derived by visual interpretation of the hyperplanes in the multi-temporal scatter plots. From the analysis of the plots it was concluded that the values of the mean backscatter and minimum backscatter were not suitable for forest change detection.

A clear threshold was observed using MMR, saturation, LMNSTDEV, and MVA. Maximum difference was also found to be a useful variable. For the final automatic yearly forest disturbances monitoring the pre-classification approach based on a ratio was used according to the equation:

$$10 \times \log_{10}\left(\frac{\gamma_1}{\gamma_2}\right), \quad (3)$$

where γ_1 and γ_2 represent backscatter values of the year 1 and year 2, respectively.

Only HV-polarized mosaic data were used for the yearly forest loss monitoring. The processing steps are presented in Fig. 4. Forest change areas were classified using a simple threshold approach – a threshold of –2 dB was finally implemented. Using a reference map and LC information, other changes in non-forest areas were then masked. Further improvement of the classification results was done by removing small patches (2 ha) and by employing a shape compactness using following equation (Bogaert et al., 2000):

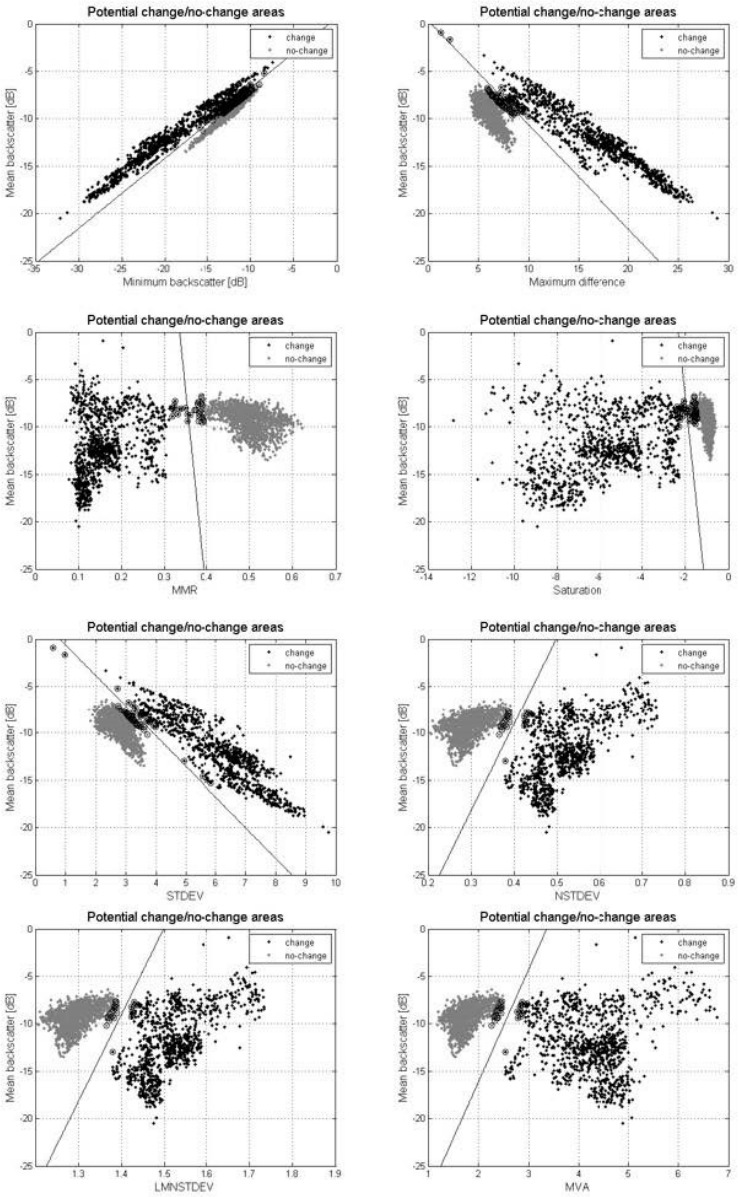

Fig. 3. Multi-temporal metrics to identify thresholds for forest change/no-change areas classification using ALOS PALSAR data.

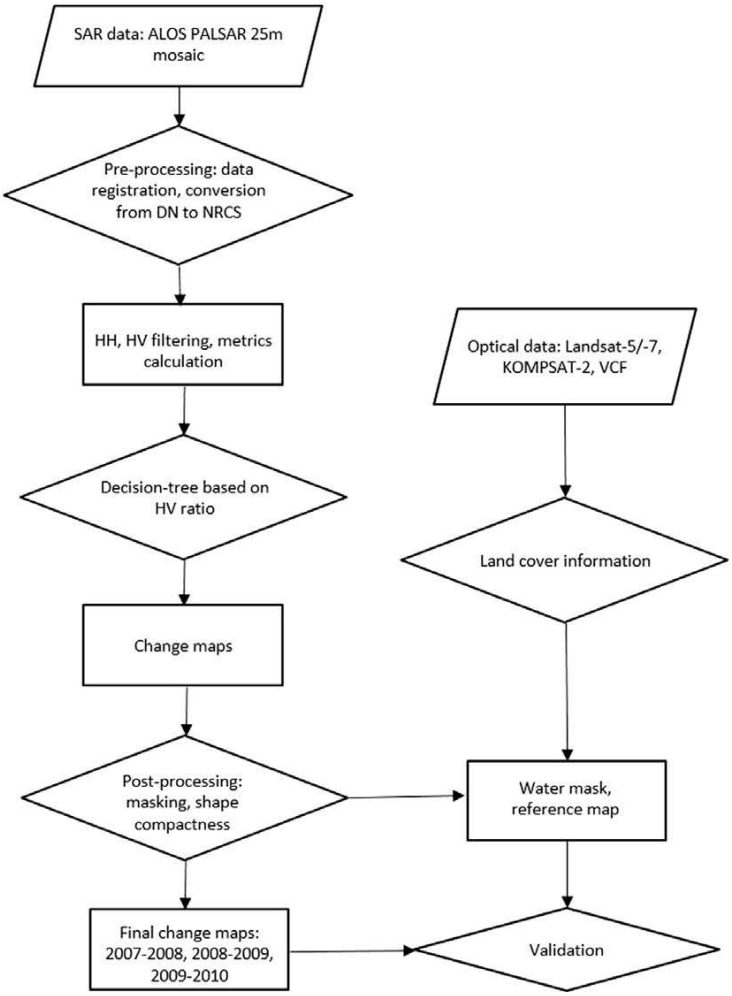

Fig. 4. Workflow for large-scale forest disturbances monitoring.

$$\frac{4\sqrt{A}}{P}, \tag{4}$$

where A represents area, and P perimeter.

The accuracy of change classifications was assessed by comparing the change results with reference maps. Data from two consecutive years were used to check whether the change from forest to non-forest was correctly classified. The overall accuracy was calculated as a ratio of total number of correctly classified pixels over the total number of pixels using 50 randomly distributed points.

Operational forest monitoring using the Earth Observation Monitor (EOM). The Earth Observation Monitor (Eberle et al., 2013*b*) is a web-based data middleware system for land observations. The geoportal functions as a web-

based visualization and analyses platform for selected EO time series form the MODIS data product line. The geoportal provides standard-compliant Web Services based on a Data Processing Middleware (Eberle et al., 2013*a*) and statistical analysis and processing functions. Analyses tools comprise seasonal time series decomposition by moving averages, break point detection by additive season and trends (BFAST, Verbesselt et. al., 2010) and greenbrown, analyzing trends and trend changes in gridded time series like from satellite observations or climate model simulations (Forkel et al., 2013). BFAST integrates the decomposition of time series into trend, season, and remainder components with methods for detecting and characterizing change within time series. BFAST detects multiple abrupt changes in seasonal and trend components of the EVI time series. In this study BFAST was applied on MODIS EVI time series from 2000 to 2014 to detect change events (break points) in the VI time series. The analyses were conducted using the EOM date middleware by selecting a part of the study area for the high-resolution SAR-based forest loss detection. The BFAST output, a spatially explicit temporal information of change events (break points), was compared with local scale reference data on forest logging activities and the ALOS PALSAR forest loss mapping results. Areas were integrated in the cross-validation only where in both time series components (season and trend) a breakpoint occurred.

RESULTS AND DISCUSSION

ALOS PALSAR based forest loss detection. Resulting change map is given in Fig. 5. Changes were identified and validated using the ALOS PALSAR L-band data with 25 m spatial resolution and LC information extracted from the optical-based products. Analyzing the generated maps, most of the forest loss can be observed in 2007–2008 and 2009–2010. This is reflected in the forest loss statistics presented in

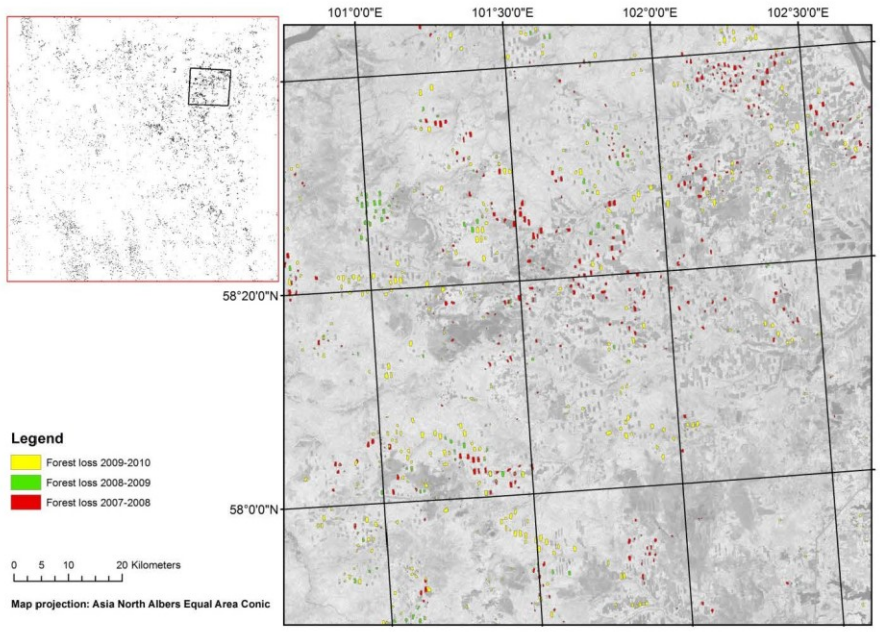

Fig. 5. Example of forest loss detection. Zoom on the region with the most changes classified in 2007–2010. In background HV-intensity 2010 with applied transparency.

Table 1. Forest loss statistics based on ALOS-PALSAR and Landsat data

Years	Overall accuracy of forest loss detection, %	Forest loss, km^2	Forest loss vs. forest cover, %	Forest loss by Hansen et al., 2013, km^2	Forest loss by Hansen et al., 2013 vs. forest cover, %
2007–2008	66	669	0.1	2.666	0.5
2008–2009	76	212	0.04	1.706	0.3
2009–2010	70	631	0.1	2.055	0.4
2007–2010	–	1.512	0.24	6.427	1.2

Table 1. The forest loss area was compared with the freely available results of global forest loss obtained by Hansen et al. for the study area (Hansen et al., 2013). Hansen et al. defined the forest loss similarly as in this study as «a stand-replacement disturbance, or a change from a forest to non-forest state». The global maps were created using Landsat data.

Hansen's results showed the same trend as the present study, with the most forest loss taking place in 2008 and 2010. However, the size of mapped areas of forest depletion differ by 1.997 km^2 in 2008, 1.494 km^2 in 2009, and 1.424 km^2 in 2010, with larger areas identified in Hansen's products. In particular the highest discrepancy, eight times difference, was observed in year 2009. The reason for the extreme difference may result from the Hansen's annual product generation. The «Forest Loss Year» product is a disaggregation of total «Forest Loss» to annual time scales (Hansen et al., 2013), which may overestimate forest loss in case of years with less forest disturbances occurred. Most of the forest loss change for both studies was observed in the northeastern area of the Siberian study region.

The average accuracy for the present study was over 70 %. The highest validation result was obtained for the forest change analysis between 2008 and 2009. This can be explained by

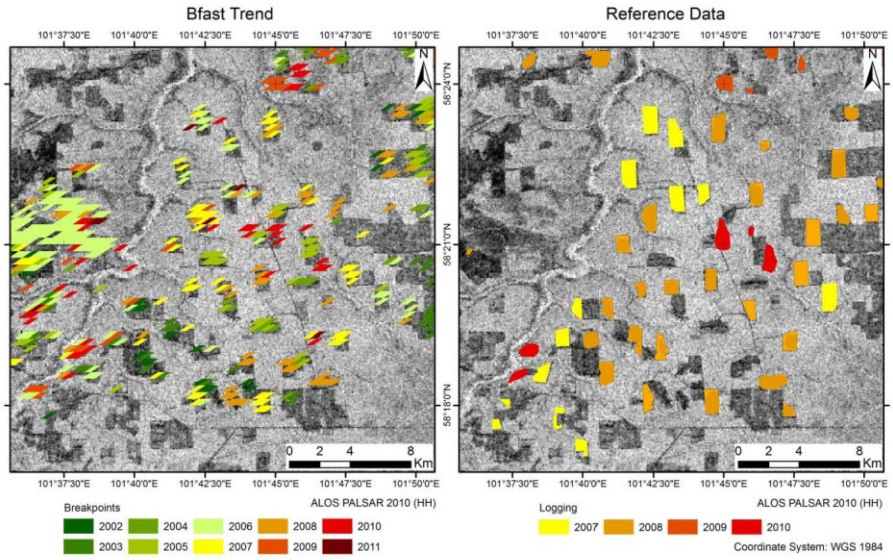

Fig. 6. Comparison of forest disturbance dates (breakpoints) based on BFAST (left) with local scale ALOS PALSAR and forest inventory based forest disturbance event information (right), overlain ALOS PALSAR HH-backscatter image from 2010.

the fact that the difference image between those years resulted in the least number of misclassifications, meaning that the mosaics that were created used data acquired under similar weather conditions.

Operational MODIS-EVI-based breakpoint detection. Phenologically-driven land cover changes were mapped using the BFAST tool implemented into EOM data middleware. Hereby, only areas were selected as change patterns where in both time series components (trend and season) a minimum of one breakpoint occurred. The result was a map of change dates (breakpoint) indicating inter-annual dynamics of forest disturbances. Fig. 6 shows the change areas detected between 2000 and 2014, compared to the ALOS PALSAR-based change areas and local scale forest inventory data.

The example from Abanskii region demonstrates that most of the forest disturbances were captured using the operational change monitoring method within EOM, e.g. a fire event was detected for 2006 and numerous clear cutting areas were detected between 2004 and 2011.

The breakpoints detected by EOM were cross-compared with the ALOS PALSAR based change areas and local forest inventory data. Fig. 6 shows a good agreement of MODIS and reference local scale forest disturbances. Most of the clear cuts were detected with the fully automatic approach. A general agreement is visible by comparing the change event dates. A validation was conducted by selecting 100 reference points within the local scale test sites. The breakpoints were cross-validated for the trend and the seasonal component.

Fig. 7 visualizes the temporal match and scattering of the breakpoint detection for trend and season.

It is obvious that breakpoints derived with the trend component have a better temporal match rate than the season-based break points. Depending on the number of reference points per year the trend-based breakpoints show a high temporal variation (e.g. 2006, 2008, 2010), whereas the medial shows a good temporal match. Breakpoints detected by the seasonal component show a general shift towards the actual date. This is particularly visible for the early disturbances in 2006 and 2007.

Despite the temporal mismatch, the seasonal breakpoints show a less distinct temporal variability. The accuracy metrics prove this observation (Table 2). The trend-based breakpoint detection achieved an overall accuracy of 50%, while the season-based change detection shows an accuracy of 43.4%.

The accuracies varied between the years. The best producer's accuracy was detected for 2010. Due to a smaller number of reference points a

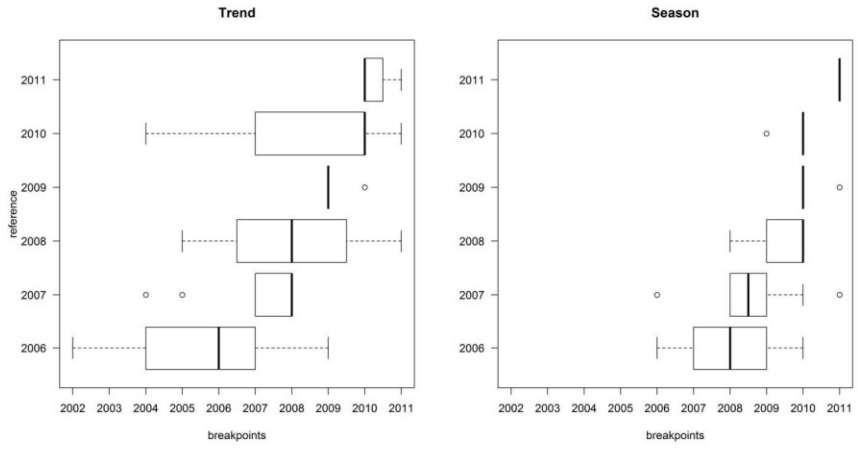

Fig. 7. Cross-comparisons of BFAST breakpoint derived from MODIS EVI time series analyses for the trend and the seasonal component of the time series.

Table 2. Accuracy assessment for BFAST break point detection

Trend	Reference								
Breakpoints	Years	2006	2007	2008	2009	2010	2011	Total	Producer's accuracy
	2002	1	0	0	0	0	0	1	0.00
	2003	3	0	0	0	0	0	3	0.00
	2004	1	1	0	0	2	0	4	0.00
	2005	1	1	2	0	5	0	9	0.00
	2006	**5**	0	1	0	5	0	11	0.00
	2007	3	**4**	2	0	0	0	9	44.44
	2008	2	7	**1**	0	6	0	16	6.25
	2009	2	0	2	**4**	1	0	9	44.44
	2010	0	0	2	1	**31**	3	37	83.78
	2011	0	0	1	0	1	**1**	3	33.33
	Total	18	13	11	5	51	4	102	Overall
	User's accuracy	27.78	30.77	9.09	80.00	60.78	25.00	–	**50.00**
Season	Reference								
Breakpoints	Years	2006	2007	2008	2009	2010	2011	Total	Producer's accuracy
	2006	**1**	1	0	0	0	0	2	0.00
	2007	5	**0**	0	0	0	0	5	0.00
	2008	6	4	**1**	0	0	0	11	9.09
	2009	0	3	1	**0**	0	0	4	0.00
	2010	4	1	3	4	**20**	0	32	62.50
	2011	0	1	0	1	1	**1**	4	25.00
	Total	16	10	5	5	21	1	58	Overall
	User's accuracy	6.25	0.00	20.00	0.00	95.24	100.00	–	**43.40**

good user's accuracy was also reached for 2009.

Better matches of the trend-based breakpoints can be explained by the distinct detection of a phenology-driven decline of the EVI value within the EVI time series trend. The breakpoint will be assigned to the date where the land cover change occurred.

A different situation is apparent in the seasonal breakpoint detection. Due to a delayed temporal response on a seasonal level, the breakpoints were detected in one of the following seasons after the disturbance event which leads to a general delay of the change date detection towards the following years. The final result was based on a synergy of both breakpoint detection methods. The most reliable result achieved the combination of the seasonal and the trend-based change date detection, as shown in Fig. 6.

CONCLUSIONS

Monitoring Russia's forests is of a special interest due to the vast size of these forests. Since traditional, ground-based methods cannot efficiently monitor changes over entire forest cover, remote sensing appears to be a suitable tool for operational forest monitoring.

This paper demonstrated the application of a SAR-based and an optical operational satellite data source for operational forest cover change monitoring. These datasets are operational and freely accessible through USGS (MODIS) or being released on annual basis by JAXA (ALOS PALSAR annual mosaics) and being integrated in geoportals focussing on multi-source forest monitoring (Hüttich et al., 2014*b*).

Firstly, it was demonstrated that SAR remote sensing data have a great potential for automated large-scale forest change monitoring in the boreal zone in a high spatial resolution. Only SAR images can provide sufficiently regular data, due to the ability to operate and collect data under all weather and sunlight conditions. The results demonstrated great potential for L-band sensors using HV cross-polarization data for large-scale forest mapping, as was reported in previous studies (e.g. Santoro et al., 2012).

Using ALOS PALSAR mosaics with 25 m spatial resolution, forest cover loss was mapped with reasonable accuracy. The data were provided by the ALOS K&C Initiative as level 1.5, co-registered tiles. The changes in the study area were identified with approximately 70% accuracy. However, higher accuracy would be expected if the data were corrected due to fur-ther time series variations (e.g., Motohka et al., 2014). The coherence of the large-scale product should hopefully further decrease the number of misclassifications and other data-related errors for the boreal zone. The 46-day revisit time of the sensor is not a limitation in this part of the world due to the stable environmental condi-tions during winter. This is of particular impor-tance in order to fully use the potential of ALOS PALSAR data within an operational large-scale forest-monitoring system.

Secondly, in addition to SAR data, frequently available time series data tracking the phonological activity, such as the MODIS EVI prod-uct with a 16-day temporal resolution provide another important data source for regional scale forest disturbance tracking. Combining opera-tional satellite time series with the BFAST change detection method implemented in the EOM data middleware system enables a fast and easy to use forest monitoring tool. The integra-tion of data acquisition, time series quality en-hancement, data integration and analyses in a web-based environment enables a broad appli-cability of EO data for local and regional stake-holders, environmental scientists, and land man-agers. The MODIS-based BFAST change detec-tion produced an overall accuracy of 50% for an observation period of 14 years. Within this period, two years (2009, 2010) showed a user's accuracy of 80.0 and 60.8% which proved the applicability of the method. For local scale analyses we demonstrated a good matching to reference data but the application and integra-tion in forest management processes required a sound understanding of the SAR data process-ing and analyses. User friendly data access and analyses can be improved by using data mid-dleware systems such as the EOM platform. Up to now, a fully operational system can be used based on the NASA MODIS vegetation indices product line. Further developments will focus on the implementation of SAR-based time series products and newly available satellite time series.

The authors thank Dr. Mikhail Korets (V. N. Sukachev Institute of Forest, Russian Academy of Sciences, Siberian Branch) for providing reference data of forest disturbances for Central Siberian test sites. This work was partly undertaken within the framework of the GMES Initial Operations – Network for Earth Observation Research Training GIONET project, grant agreement PITN-GA-2010-264509. This paper was also realized in the framework of the FP 7 EU-Russia ZAPÁS project on the assessment and monitoring of forest resources in Central Siberia. ZAPÁS was funded by the European Commission, Space, Cross-cutting Activities, International Cooperation, Grant no. SPA.2010.3.2-01 EU-Russia Cooperation in GMES (SICA). This work has partly been undertaken within the framework of the JAXA Kyoto & Carbon Initiative. Helpful comments and suggestions from the reviewers are highly appreciated.

REFERENCES

Acker J. G., Leptoukh G. Online analysis enhances use of NASA earth science data // Eos Transact. Amer. Geophys. Union. 2007. V. 88.

Bogaert J., Rousseau R., Van Hecke P., Impens I. Alternative area perimeter ratios for measurement of 2D shape compactness of habitats // Appl. Mathem. Comput. 2000. V. 111. N. 1. P. 71–85.

Bruzzone L., Marconcini M., Wegmüller U., Wiesmann A. An advanced system for the automatic classification of multitemporal SAR images // IEEE Transact. Geosci. Remote Sens. 2004. V. 42. N. 6. P. 1321–1334.

Cihlar J., Denning S., Ahem F., Arino O., Belward A., Bretherton F., Cramer W., Dedieu G., Field C., Francey R., Gommes R., Gosz J., Hibbard K., Igarashi T., Kabat P., Olson D., Plummer S., Rasool I., Raupach M., Scholes R., Townshend J., Valentini R., Wickland D. Initiative to quantify terrestrial carbon sources and sinks // Eos,

Transact. Amer. Geophys. Union. 2002. V. 83. N. 1. P. 6–7.

Coppin P., Jonckheere I., Nackaerts K., Muys B., Lambin E. Digital change detection methods in ecosystem monitoring: a review // Int. J. Remote Sens. 2004. V. 25. N. 9. P. 1565–1596.

Dong J., Xiao X., Sheldon S., Biradar C., Duong N. D., Hazarika M. A comparison of forest cover maps in Mainland Southeast Asia from multiple sources: PALSAR, MERIS, MODIS and FRA // Remote Sens. Environ. 2012. V. 127. P. 60–73.

Eberle J., Clausnitzer S., Hüttich C., Schmullius C. Multi-source data processing middleware for land monitoring within a web-based spatial data infrastructure for Siberia // ISPRS Int. J. Geo-Inform. 2013*a*. V. 2. P. 553–576.

Eberle J., Hüttich C., Schmullius C. Web-based multi-source data processing middleware for land observations and monitoring // ESA Living Planet Symp. Edinburgh, Scotland, 2013*b*.

FAO. The Russian Federation forest sector outlook study to 2030. Rome, 2012.

Forkel M., Carvalhais N., Verbesselt J., Mahecha M., Neigh C., Reichstein M. Trend change detection in NDVI time series: Effects of inter-annual variability and methodology // Remote Sens. 2013. V. 5. P. 2113–2144.

Fransson J. E. S., Magnusson M., Eriksson L. E. B., Sandberg G., Smith G., Ulander L. M. H. Detection of forest changes using ALOS PALSAR satellite images // Geosci. Remote Sens. Symp. IGARSS, 2007. P. 2330–2333.

Hansen M. C., Potapov P. V., Moore R., Hancher M., Turubanova S., Tyukavina A., Thau D., Stehman S. V., Goetz S. J., Loveland T. R., Kommareddy A., Egorov A., Chini L., Justice C. O., Townshend J. R. G. High-resolution global maps of 21st century forest cover change // Science. 2013. V. 342. N. 6160. P. 850–853.

Hüttich C., Korets M., Bartalev S., Zharko V., Schepaschenko D., Shvidenko A., Schmullius C. Exploiting growing sock volume maps for large scale forest resource assessment: cross-comparisons of ASAR- and PALSAR-based GSV estimates with forest inventory in Central Siberia // Forests. 2014*a*. V. 5. P. 1753–1776.

Hüttich C., Eberle J., Schmullius C., Bartalev S., Emelyanov K., Korets M. Supporting a forest observation system for Siberia: Earth observation for monitoring, assessing and providing forest resource information // Earthzine. 2014*b*. P. 1. http://www.earthzine.org/2014/07/16/supporting-a-forest-observation-system-for-siberia-earth-observation-for-monitoring-assessing-and-providing-forest-resource-information/

Morel A. C., Saatchi S. S., Malhi Y., Berry N. J., Banin L., Burslem D., Nilus R., Ong R. C. Estimating aboveground biomass in forest and oil palm plantation in Sabah, Malaysian Borneo using ALOS PALSAR data // For. Ecol. Manage. 2011. V. 262. N. 9. P. 1786–1798.

Motohka T., Shimada M., Uryu Y., Setiabudi B. Using time series PALSAR gamma nought mosaics for automatic detection of tropical deforestation: A test study in Riau, Indonesia // Remote Sens. Environ. 2014 (*in press*).

Pan Y., Birdsey R. A., Fang J., Houghton R., Kauppi P. E., Kurz W. A., Phillips O. L., Shvidenko A., Lewis S. L., Canadell J. G., Ciais P., Jackson R. B., Pacala S. W., McGuire A. D., Piao S., Rautiainen A., Sitch S., Hayes D. A large persistent carbon sink in the world's forests // Science. 2011. V. 333. N. 6045. P. 988–993.

Quegan S., Le Toan T., Yu J. J., Ribbes F., Floury N. Multitemporal ERS SAR analysis applied to forest mapping // IEEE Transact. Geosci. Remote Sens. 2000. V. 38. N. 2. P. 741–753.

Quegan S., Yu J. J. Filtering of multichannel SAR images // IEEE Transact. Geosci. Remote Sens. 2001. V. 39. N. 11. P. 2373–2379.

Santoro M., Fransson J. E. S., Eriksson L. E. B., Magnusson M., Ulander L. M. H., Olsson H. Signatures of ALOS PALSAR L-band backscatter in Swedish forest // IEEE Transact. Geosci. Remote Sens. 2009. V. 47. N. 12. P. 4001–4019.

Santoro M., Fransson J. E. S., Eriksson L. E. B., Ulander L. M. H. Clear-cut detection in Swedish boreal forest using multi-temporal ALOS PALSAR backscatter data // IEEE J. Select. Topics in Appl. Earth Observ. Remote Sens. 2010. V. 3. N. 4. P. 618–631.

Santoro M., Pantze A., Fransson J. E. S., Dahlgren J., Persson A. Nation-wide clear-cut mapping in Sweden using ALOS PALSAR strip images // Remote Sens. 2012. V. 4. N. 12. P. 1693–1715.

Schmullius C., Baker J., Balzter H., Davidson M., Eriksson L., Gaveau D., Gluck M., Holz A., Le Toan T., Luckman A., Marschalk U., McCallum I., Nilsson S., Oeskog A., Quegan S., Rauste Y., Roth A., Rozhkov V., Sokolov V., Shvidenko A., Skudin V., Strozzi T., Tansey K., Vietmeier J., Voloshuk L., Wagner W., Wegmuller U. SAR imaging for boreal ecology and radar interferometry. A publ. SIBERIA project (Contract No. ENV4-CT97-0743-SIBERIA) – Final Report. 2001.

Shimada M. Ortho-rectification and slope correction of SAR data using DEM and its accuracy evaluation // IEEE Transactions on Geoscience and Remote Sensing. 2010. V. 3. N. 4. P. 657–671.

Shimada M., Isoguchi O., Tadono T., Isono K. PALSAR radiometric and geometric calibration // IEEE Transact. Geosci. Remote Sens. 2009. V. 47. N. 12. P. 3915–3932.

Shvidenko A., Schepaschenko D., Sukhinin A., McCallum I., Maksyutov S. Carbon emissions from forest fires in Boreal Eurasia between 1998–2010 // 5th Int. Wildland Fire Conf. Sun City, South Africa, 2011.

Verbesselt J., Hyndman R., Zeileis A., Culvenor D. Phenological change detection while accounting for abrupt and gradual trends in satellite image time series // Remote Sens. Environ. 2010. V. 114. N. 12. P. 2970–2980.

WWF. http://wwf.panda.org/about_our_earth/about_forests/deforestation/forest_illegal_logging/ (visited November, 2014).

Yu H., Qing X., Shuai X. A Method for SAR speckle reduction based on partial differential equation // Int. Arch. Photogram. Remote Sens. Spat. Inform. Sci. 2008. V. XXXVII. P. 617–620.

4.2 Remote sensing for aboveground biomass estimation in boreal forests

This section presents the second publication, which is the book chapter entitled "Remote sensing for aboveground biomass estimation in boreal forests" prepared and written by Stelmaszczuk-Górska, M. A., Thiel, C. J. & Schmullius, C. C.

The manuscript was peer-reviewed and published in the book edited by H. Balzter
Earth Observation for Land and Emergency Monitoring
(1st ed., pp. 33–55). © 2017 John Wiley & Sons Ltd.
doi: 10.1002/9781118793787

3

Remote Sensing for Aboveground Biomass Estimation in Boreal Forests

M.A. Stelmaszczuk-Górska, C.J. Thiel and C.C. Schmullius

Friedrich-Schiller-University Jena, Department of Earth Observation, Jena, Germany

3.1 Introduction

In order to understand the state and dynamics of ecosystems, their roles within global cycles and their responses to climate change, it is important to quantify and monitor different biophysical parameters. Of these, it is particularly essential to measure forest aboveground biomass (*AGB*) [1]. *AGB* is the mass of all living matter above the soil including stem, stump, branches, bark, seeds and foliage in a particular area [2]. Another important variable is growing stock volume (GSV), which is directly related to *AGB*. GSV is defined as the stem volume of all living species per unit area, including bark and excluding branches and stumps. For the sake of simplicity, the term "biomass" will be used throughout the text to refer collectively to both variables.

When properly related to biophysical tree parameters, remote sensing data can provide information on forest biomass from local to global scales. This information is of special interest in global carbon budget studies since forest biomass estimates still introduce significant source of uncertainty [3–5]. Moreover, accurate estimates of biomass are important in terms of commitments to the reduction of greenhouse gas emissions within international conventions on climate change. An understanding of biomass changes in the boreal forest ecosystem is important for studies of climate change since the boreal forest system covers the largest land area and constitutes a substantial carbon sink. Successful monitoring and modelling of forest biomass depends on the availability of frequent, local to global scale measurements. These can only be provided by means of remotely acquired data e.g., from satellite or airborne sensors. There are different remote sensing sensors: optical, light detection and ranging (LiDAR) and radio detection and ranging (radar). In this chapter the emphasis has been put on radar remote sensing in particular due to the all-weather, global coverage capacity and new, upcoming radar missions. At least seven new radar missions are planned before the end of the 2020s. In April 2016, the Sentinel-1B has been successfully put into orbit, already fourth of the Sentinel satellites. The satellites are designed to increase European Earth Observation capability as a part of the European Copernicus program. The Sentinel data are available without charge [6].

Earth Observation for Land and Emergency Monitoring, First Edition. Edited by Heiko Balzter.

Despite more than 30 years of research and algorithm development using radar data, there is still no operational method for global biomass estimation. The main objective of this book chapter is to summarize and synthesize existing estimates of boreal forest biomass obtained using radar sensors. In order to analyse the potential of radar remote sensing, an extensive body of literature has been gathered and reviewed by authors. We systematically compared the methods, taking into account different radar sensor parameters as well as the accuracy of the estimates achieved.

This book chapter is organized in three parts. First, the characteristics of the boreal forest and future challenges with regards to climate change are described. Second, a general overview is given of the remote sensing techniques for biomass estimation from optical, LiDAR and radar sensors. Third, quantified data of the performance of radar biomass estimation in boreal forests are presented and summarized.

3.2 The Boreal Forest Ecosystem

The boreal forest, also known as "taiga", is the world's largest terrestrial biome, covering more than 1.5 billion hectares [7] – just under 11% of the total land surface and 37.5% of the world's forested area [8]. It spreads around the circumpolar region, occupying an area in the northern hemisphere down to a latitude of approximately 45°N in Russia and 50–60°N in northern Europe, Canada and Alaska.

The boreal forest is of great importance in economic, biodiversity and climate change terms alike. It is a major source of forest products such as wood, paper and pulp, which are crucial for manufacturing, energy and the construction industry. It provided circa 23% of forest and other wooded land growing stock in 2010 [8]. Moreover, it creates employment directly in the forestry sector for approximately 1.5 million people [9]. In terms of biodiversity, boreal forests have a low level of species variability. They are characterized by the presence of four main coniferous tree species: spruce (*Picea*), pine (*Pinus*), fir (*Abies*) and larch (*Larix*). Deciduous species are also present: mainly birch (*Betula*), aspen and poplar (*Populus*), which are typical for early succession stages of the forest. Boreal forest is also a habitat for many other plants and fungi, as well as many species of mammals, birds, insects and other types of animals. In terms of climate change, it is important due to (i) global greenhouse gas modelling and remaining uncertainties in the spatial distribution of the terrestrial carbon sink [10,11]; (ii) the sensitivity of the boreal ecosystem to climate warming and (iii) monitoring and reporting obligations within international legislation. Based on the recent results [10], the boreal carbon stock is estimated to be 272 ± 23 Pg C (32%). That makes the boreal biome the second most important terrestrial carbon pool after the tropical forest.

The majority of the carbon (60%) in boreal forests is accumulated in the soil, characterizing this region as having one of the most carbon-rich soils in the world. 20% of the carbon is stored in biomass, which plays a crucial role in regulating carbon as well as other greenhouse gas concentrations in the atmosphere [10]. Forest fires are especially important in nutrient cycling and the release of carbon to the atmosphere [12]. Moreover, fires are the most significant cause of boreal forest loss [13]. Current model predictions indicate that the number of fire events in the boreal zone may double by the end of 2100 [14]. Fires are a major natural disturbance in the Russian boreal forest in particular, where coniferous stands dominate and most of the forest territory is

unmanaged and unprotected [15]. Due to the vastness of the Russian territory, comprising different ecosystem types, Russia is expected to suffer the most significant transformation due to climate change [16]. The average annual temperature has already increased substantially, by up to 2 °C in the period from 1971 to 2010, whereas the global annual average increase is less than 1 °C over this same period [12].

The forest in Russia is of special interest because of the more frequent, catastrophic fires expected as a result of climate warming and heat waves such as that which occurred in 2010 [15]. It is also the most forest-rich country in the world (809 million ha [8]), providing more than 90% of the carbon sink of the world's boreal forests in the 2000 to 2007 period [10]. At the same time, it provides the highest uncertainty in global carbon stock calculations. Asian part of Russia provided uncertainty of ± 66 Tg C yr^{-1} and European part of Russia provided ± 50 Tg C yr^{-1} of annual change in carbon stock calculated for 2000–2007 [10]. For this time period the uncertainty for the boreal biome was calculated to be ±83 Tg C yr^{-1} [10]. Additionally, illegal logging poses a huge problem for the monitoring of Russian forests. According to different sources (WWF Russia, World Bank), illegal clear-cutting in Russia is estimated to comprise approximately 25% of all logging activity. Between 2000 and 2013 Russia has lost more than 37 million hectares of forest [13], more forest than any other country in the world. Moreover, due to the lack of financial support, some forested regions in Siberia have not inventoried for more than 20 years [17]. All of the aforementioned aspects combined make the Russian boreal forest of special monitoring interest.

3.3 Remote Sensing for Biomass Estimation

The ground-based methods for biomass estimation are expensive and labour extensive. Hence, remotely sensed data, especially in combination with *in situ* data when possible, can offer a solution for forest mapping over large areas. Scientists have already demonstrated that remote sensing can contribute to measuring and monitoring current carbon sources and sinks through its ability to provide systematic, globally consistent observations of land cover (LC), land cover change (LCC), forest disturbance and biomass. There are extensive publications available on the topics of optical, LiDAR and radar earth observation (EO) data for LCC and biomass estimation. Several publications provide a comprehensive review of use of remote sensing techniques for biomass estimation including sourcebooks of recommended methods and data sources [18–28]. However, since now no detailed review on accuracy of radar-based biomass estimates for boreal forests has been published.

Optical images record the interaction of solar radiance with Earth surface. The optical satellite sensors provide systematic observations of LC at scales, from global to local. However, direct biomass measurements are unfeasible [29]. This is due to the fact that the sunlight hardly penetrates vertically into the forest cover. Nevertheless, it must be underlined that very high and high resolution data in combination with geostatistical or modelling-based approaches have already been implemented for forest inventory purposes (e.g., for forest stand density, and volume estimation) [30–37]. Furthermore, spectral information from optical EO data are of particular use in the mapping of different vegetation types and vegetation conditions, as well as in the detection of forest fires or other disturbances [38,39]. Indirect estimates of biomass from optical data are

feasible at low biomass levels using vegetation indices, bidirectional reflectance distribution function (BRDF) and texture [40–47]. The latest results of biomass estimation based on Landsat data revealed that accuracy of ±36% can be measured in boreal zone [48].

The most accurate, but most financially demanding estimates of biomass are based on airborne LiDAR. Because of the system properties, LiDAR can directly measure the three-dimensional vegetation structure, unlike conventional radar and optical sensors. Airborne small footprint (approximately 20 cm in diameter) [21,49–54] and satellite large footprint LiDAR systems (approximately 70 m in diameter) [55–58] have been already successfully used for biomass estimation. Hyyppä *et al.* [59] demonstrated that Airborne Laser Scanning (ALS) can provide accurate information on the stem volume in boreal zones, comparable with field survey measurements. However, in the case of the ALS system, measurements are too expensive for larger areas. For global applications, archive datasets from only one satellite sensor are available, namely the Ice, Cloud, and land Elevation (ICESat) Geoscience Laser Altimeter System (GLAS). In contrast to the airborne systems, the GLAS LiDAR had some limitations related to the large footprint, sparse coverage and sensitivity to terrain variability. Due to the large footprint, the interference of topographic impacts can hardly be corrected [57,60–63]. The assessment of global vegetation biomass was a secondary mission priority. To reduce these limitations, the ICESat-2 satellite, which is planned for launch in 2017, will use a micro-pulse, multi-beam photon counting approach to provide footprint of 10 m in diameter [64]. Another planned LiDAR mission is the Global Ecosystem Dynamics Investigation (GEDI). The GEDI LiDAR will be mounted on the International Space Station (ISS) with its main objective to create detailed 3D maps and measure the biomass of forests. The mission is scheduled for deployment on the ISS in 2019 [65].

Since no LiDAR mission is in operation, radar sensors are expected to provide the most accurate biomass estimates [20]. Similar to the LiDAR sensors, radar systems are sensitive to the geometrical properties of the observed objects. In addition, the signals are also affected by the dielectric properties of the targets. Moreover, radar systems are weather independent and relatively cost-efficient, which makes the Synthetic Aperture Radar (SAR) sensors suitable for forest biomass estimation; they can provide data on regular basis. Furthermore, new radar satellite missions are planned to be launched (see Figure 3.1). The basic SAR terminology is given in the previous chapter.

It has been already demonstrated that radar data can be physically related to vegetation structure until the saturation point, allowing the retrieval of forest parameters, and that longer wavelengths are superior to shorter ones for this purpose [66–73]. Many SAR properties can be exploited to quantify biomass: backscattering intensity (e.g., [74,75]), interferometric phase (e.g., [76,77]), interferometric correlation (e.g., [78,79]), polarimetric signature (e.g., [80,81]), SAR tomography and radargrammetry (e.g., [82,83]).

Description of global forest monitoring can be found in the chapter titled: Methodology for regional to global mapping of aboveground forest biomass: Integrating forest allometry, ground plots, and satellite observations, whereas the aspects of tropical forest monitoring, case study of the central African forests, are given in Chapter 4: Forest Mapping of the Congo Basin using Synthetic Aperture Radar (SAR).

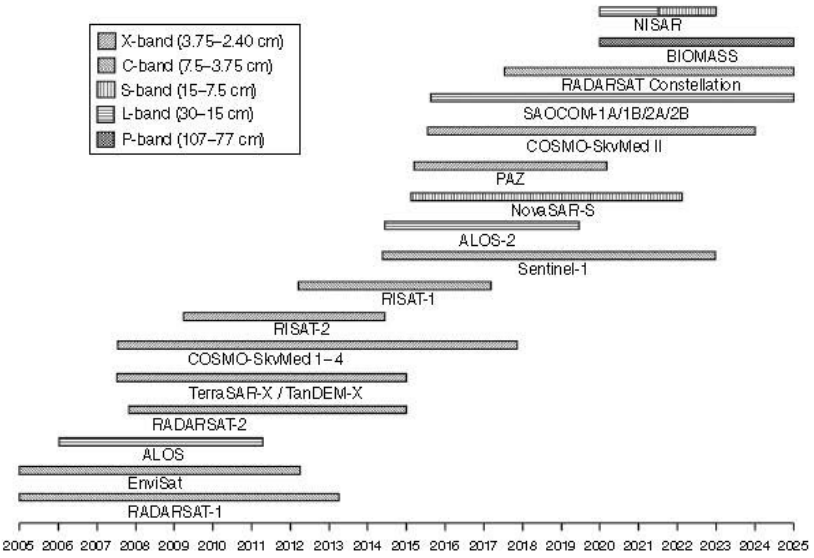

Figure 3.1 SAR missions up to year 2025.

3.4 Radar Remote Sensing for Biomass Estimation in Boreal Forests

3.4.1 Estimation Methods

A variety of approaches have already been developed to estimate biomass in boreal forests using radar remote sensing. Most of the methods that have been implemented are based on empirical and semi-empirical models. The semi-empirical models employ radar data as a function of biomass. It is a combination of physical modelling and empirical observations. The scatterers can be described as a layer, water cloud model [84] or layer with gaps (water cloud model with gaps), which are especially important in studies in the boreal forests [85], or randomly distributed scatterers, Random Volume over Ground model (RVoG) [80]. The empirical models are based on regression analysis. Using linear, multiple-linear or non-linear functions, the biomass is related to the SAR remote sensing data. There are advantages and disadvantages of both approaches. The main drawback of the semi-empirical method is that the models can be either over-simplified, leading to great estimation errors, or too complex, resulting in inversion problems. The main disadvantage in the case of empirical approaches is that they strongly depend on the data set used for model selection and training, and therefore result in poor model transferability. However, both methods have already demonstrated very good biomass estimation accuracy (e.g., [77,86]). It was found that the biomass retrievals based on the empirical model provide equally good estimations compared to the semi-empirical approach [75]. Currently, machine learning algorithms have been also successfully implemented for biomass estimation in boreal forests [87–90].

In order to synthetize the biomass estimation errors reported in the literature using the semi-empirical and empirical approaches, selected statistics from almost 50 peer-reviewed journal articles have been analysed. The papers up to mid-2014 were reviewed. In Table 3.1, a summary of recently reported biomass retrieval results is presented. The accuracy is represented by the coefficient of determination (R^2) or coefficient of correlation (r), root mean square error (RMSE), and relative root mean square error (rRMSE). rRMSE is normalized to the mean of the observed values. In some cases the biomass estimation error RMSE was corrected by the systematic, sampling errors (e.g., for Sweden) [91]. In cases where the rRMSE was not given, it was calculated based on the provided biomass value.

In general, it is difficult to compare all implemented methods due to the differences between the test sites and stand characteristics, stand size, weather conditions during the acquisitions, validation procedures (training, testing), and the model used. However, authors have made efforts to describe the results according to the radar data used, the method implemented and the test site characteristics so that general conclusions can be drawn in order to summarize the retrieval procedures.

3.4.2 Results Using Backscatter, Polarimetric Parameters and Radargrammetry

One of the first models implemented in the boreal zone employing backscatter information for stem volume estimation was a semi-empirical model developed based on the large number of measurements recorded with a high-resolution ranging scatterometer (HUTSCAT). The scatterometer operated at C-band and X-band frequencies. This model presumes that the signal scattered back from the forest canopy is a function of stem volume, soil moisture, and vegetation water content. The results from the HUTSCAT airborne measurements at C-band VV polarization showed high correlation ($r = 0.75$) between the backscattering coefficient and stem volume for a forest test site in southern Finland [74]. The same region was later studied using the satellite multi-temporal C-band ERS–1 data [97]. Employing the satellite data, a Pearson's coefficient of 0.64 between estimated biomass and *in situ* measurements was calculated. The RMSE was reported to be $90\,m^3ha^{-1}$ (rRMSE = 58%). Both experiments showed that scattering from forested areas is a mixture of parameters related to surface topography and roughness as well as soil moisture and weather conditions. It was concluded that the retrieval error depends on the forest stand size. For the stands greater than 10 ha, the error become negligible. The model was also used for L-band JERS-1 data [98]. The L-band data showed more sensitivity to stem volume and less to environmental conditions, and resulted in a correlation coefficient of 0.65 between the estimated stem volume and the ground truth and a relative error approximately 35% for data acquired in the month of March. It was also emphasized that in the case of the multi-temporal approach, the accuracy can be improved (rRMSE = 25% and $r = 0.73$ for forest blocks >10 ha). In [99] it was demonstrated that for stands larger than 20 ha, a correlation coefficient between the estimates and the reference values of up to 0.85 and 25% relative error can be achieved using L-band and 0.65 with 27% relative error using C-band. The estimates were improved when the C- and L-band data were used together (rRMSE <25%).

A similar semi-empirical model was introduced by Askne *et al.* [85]. The model is based on the water cloud model including gaps in the layer and expresses the total forest

Table 3.1 Summary of recently published biomass estimation results in boreal forests using SAR data.

Reference	Sensor	Wavelength Polarization	Location/site/No. of stands (No. of plots)	No. of images	Estimated variable	Range of estimated variable (mean)/ range of stand size (mean) [ha]	Radar data used	Method to estimate variable	R^2 (r)	RMSE [unit as estimated variable] (rRMSE [%])**
[81]	E-SAR*	L-band P-band	Sweden/Krycklan/27	Multiple acquisitions	*AGB* [t ha^{-1}]	23–183 (94.3)/2.4–26.3	PolInSAR	Multiple linear regression	(0.86) (0.84)	21.3–36.2 (17–27) 22.7–40.7 (5–43)
[92]	E-SAR*	P-band HH, HV, VV	Sweden/ Remningstorp/50(10) Sweden/ Krycklan/29(97)	9 7	*AGB* [t ha^{-1}]	52–267 (181)/0.5–9.4 8–257 (95)/1.5–22	Backscattering coefficient	Multiple linear regression	0.22–0.64 0.31–0.64	40–59 (22–33) 27–40 (28–42)
[93]	ALOS PLASAR	L-band HH, HV	Finland/Kuortane/123 Finland/Heinävesi/103	3 3	Stem volume [m^3 ha^{-1}]	0–314 (95)/(3) 0–425 (110)/(4.8)	Backscattering coefficient	Semi-empirical model	0.65 0.71	41.2 (43.4) 47.0 (42.8)
[94]	ENVISAT ASAR	C-band HH, VV	Sweden/country/11425 Russian Fed./Central Siberia/46487 Canada/Québec/731	Hyper-temporal dataset	Stem volume [m^3 ha^{-1}]	(125) (180)/(26) (63)	Backscattering coefficient	Semi-empirical model (BIOMASAR algorithm)	(0.73) (0.86) (0.93)	(22) (15) (27)
[77]	TanDEM-X	X-band HH	Sweden/ Remningstorp/201	18 pairs	*AGB* [t ha^{-1}]	6–267 (150)/>0.25	InSAR height	Semi-empirical models: Interferometric Water Cloud Model (IWCM) Random Volume over Ground (RVoG) Penetration depth (PD)	– – –	(16.7–33) (16.7–39.7) (17.9–33.1)
[95]	TerraSAR-X Stereo	X-band	Finland/Espoo-Kirkkonummi/94 (207)	2	*AGB* [t ha^{-1}]	3.9–347.1 (116.5)/ 0.5–12.2(4.1)	Backscattering coefficient (radargrammetry)	Multiple linear regression	–	15.6–16.7 (16.1–17.3)

*Airborne sensor;

**Relative error of less than 25% is considered to be satisfactory in terms of biomass estimation [96].

backscatter as the sum of direct scattering from the ground through canopy gaps, ground scattering attenuated by the tree canopy and direct scattering from the vegetation. Based on this semi-empirical model, Santoro *et al.* [100] reported a very good relative estimation error of 25% ($36\,m^3\,ha^{-1}$) using the JERS-1 L-band data over a Swedish test site located northwest of Stockholm. Additionally, no saturation was observed up to $350\,m^3\,ha^{-1}$. The relationship was almost linear. The data were acquired under unfrozen conditions. In the case of frozen conditions and L-band HH ALOS PALSAR single image an estimation error of 30% was reported (south-eastern Sweden) [101]. The model used in aforementioned studies was implemented by Santoro *et al.* [102] as part of the BIOMASAR algorithm. The algorithm employs hyper-temporal SAR data acquired by the Envisat ASAR C-band sensor and the Vegetation Continuous Field (VCF) product for model training. The retrieved biomass values showed results reaching 34.2% estimation error for Central Siberia. The authors stated that "the key to such results was the optimal weighting of the GSV from individual observations based on the forest/non-forest backscatter sensitivity". The weight is calculated as the difference between the two model parameters, namely the backscatter from vegetation and from the ground [98]. The methodology proved to be robust and consistently resulted in an estimation error in the range of 20 to 30% at a 0.5° resolution. Using five ALOS PALSAR L-band images, Peregon and Yamagata [103] reported estimation error in the range of 25 to 32% for a test site in Western Siberia. Using the same model inversion but multi-temporal filtering of ALOS PALSAR L-band, Antropov *et al.* [93] reported 43% estimation error for a Finnish test site.

Research by Fransson and Israelsson [75] showed that backscatter can be modelled by a semi-empirical water cloud model as well as through linear regression, providing equally good results. Correlation coefficient of 0.78 was calculated between SAR L-band estimated stem volume and ground measurements. Rauste [104] confirmed that multiple linear regression performs satisfactorily using the L-band data showing no saturation up to $150\,m^3\,ha^{-1}$.

Based on a first regression analysis for biomass estimation, second order polynomial regression was implemented by Rignot *et al.* [105]. The model was developed using data acquired by the NASA/JPL radar system (airborne AIRSAR) that operated in three frequencies and polarizations. An estimation error of approximately 20% using P-band HH, HV, VV and L-band HH, HV, VV was achieved. Moreover, the authors demonstrated that the radar acquisition geometry influences biomass retrieval. Similar regression results were found for a temperate forest (Landes, a forest plantation in France), obtaining 11% relative error using P-band, and 13% using L-band HV polarization. These results already showed the potential of implementing the same empirical approach across different ecosystems and large area biomass mapping at an early stage of investigations using backscattering coefficient data. In the case of [106], an empirical model based on multiple linear regression analysis was used. The model resulted in very good agreement between estimated biomass from an airborne P-band acquisition and *in situ* measurements. 99% of the variability in radar estimated biomass was explained by *in situ* biomass measurements. This result was obtained for a summer acquisition. Ranson *et al.* [107] also reported very good model performance ($R^2 = 0.91$, 90 m spatial resolution) for hemi-boreal forest. The estimation was made using multiple linear regression analysis for L- and C-band data acquired by shuttle mission SIR-C/X-SAR. The L- and P-band data from the airborne Experimental-SAR (E-SAR) system were studied in [108]. Results obtained for southern Sweden indicated that P-band in HH polarization can be successfully used for biomass

estimation at the same level of accuracy as the *in situ* measurements (rRMSE of less than 20%). Even better results were found by [109] from the same sensor implementing polarimetric parameters, forest height and ground-to-volume ratio. The estimation error was found to be between 25 to 30% using L-band and 18 to 39% using P-band for northern Sweden. Ulander *et al.* [110] evaluated six different regression models for southern and northern Sweden employing E-SAR airborne data acquired at the P-band. The best biomass estimation, with 20 to 30% RMSE of the mean biomass was achieved by implementing a multiple linear regression including HV backscatter, the VV/HH backscatter ratio, and the ground slope. Further results using E-SAR P-band data and a similar model were obtained by Soja *et al.* [92]. The estimation error was reported to be in the range of 22 to 33% for a test site in south-western Sweden, which is similar to the upper error limit for *in situ* and LiDAR biomass estimates in Sweden (up to 21%).

The applications above describe the use of X- to P-band SAR data. However, even better biomass estimation is expected from a SAR system operating in longer wavelengths (e.g., Very High Frequency (VHF, 30–300 MHz, metric waves)). This is due to the fact that the long waves penetrate deeper to the foliage and thus the radar signal scatters back mainly from the stem, where the majority of the biomass is accumulated [111]. No saturation for stem volumes up to 900 $m^3 ha^{-1}$ has been reported for a temperate forest in France [112], acquired by the airborne system CARABAS-II, owned by the Swedish Defence Research Agency. However, the long wavelength also faces some limitations related to the change in wave properties when going through the ionosphere. In [113], where a Swedish forest is studied, the best coefficient of determination between estimated biomass and reference measurements was reported to be 0.93, with an estimation error of 48 $m^3 ha^{-1}$ (rRMSE of approximately 25%).

Promising results of biomass estimation based on height information were also obtained by employing radargrammetry. This method is based on stereoscopic height measurements using SAR images. For the plot-level estimation based on the TerraSAR-X data, Karjalainen *et al.* [114] reported a 34% relative estimation error for a Finnish test site using the regression trees method. Additionally, no saturation up to 400 $m^3 ha^{-1}$ was observed. Even better results employing the same source of data for a Swedish test site were reported by Persson *et al.* [83]. Based on the multiple linear regression, the biomass was calculated with a 22.9% estimation error, which is comparable to that of much more expensive LiDAR measurements. The latest results over a Finnish test site reported an estimation error as low as 16.1% with −9.5% bias [95].

3.4.3 Results Using SAR Interferometry (InSAR) and Polarimetric Interferometry SAR (PolInSAR)

Complementary information on forested areas can be obtained through the analysis of interferometric SAR data. One of the first studies using repeat-pass InSAR on ERS-1 C-band data from over boreal forest [115] demonstrated the high potential of the interferometric phase information and coherence for forestry applications. The authors obtained very good results based on winter acquisitions over northern Sweden. The tree height for dense forest was estimated with a 10% estimation error using the phase information. In later studies, [116] and [117], authors used interferometric correlation information, which showed very good potential for land-use and forest type mapping, due to high coherence values for non-forest and low values for forested areas. The authors concluded that coherence is seasonally dependant and very sensitive to

differences in the acquisition times, showing for example a great potential for clear-cut detection. In [118], the authors indicated that low and stable temperatures without precipitation events are more favourable in InSAR studies. Koskinen *et al.* [78] demonstrated that the highest coherence can be obtained under winter conditions in the presence of snow cover. The authors calculated a correlation coefficient of –0.76 between stem volume and observed coherence for a test site in southern Finland, using a tandem ERS-1/2 image pair acquired under frozen conditions. Moreover, the authors developed an empirical model that expresses coherence information using backscatter information described through a semi-empirical model.

One of the first results presenting the accuracy of stem volume estimation was published by Smith *et al.* [119]. The study over Swedish test sites utilizing C-band tandem ERS-1/2 coherence data estimated the stem volume based on linear regression analysis. The results show high correlation between the coherence and stem volume. In the best case, the coefficient of determination was 0.86 (data from March) with the accuracy of stem volume retrieval of 31 $m^3 ha^{-1}$ (relative error = 23%, assuming 135 $m^3 ha^{-1}$ mean stem volume from [79]). Additionally, no saturation was observed up to 400 $m^3 ha^{-1}$. For the same test site, Santoro *et al.* [79] and [120] showed that the retrieval accuracy can be improved through the implementation of a multi-temporal combination of interferometric data. Using the coherence and backscatter values from ERS-1/2 C-band data and the semi-empirical interferometric water cloud model (IWCM), 21 $m^3 ha^{-1}$ (15.5% error, assuming 135 $m^3 ha^{-1}$ mean stem volume from [79]) and 10.0 $m^3 ha^{-1}$ (7.4% error, $R^2 = 0.94$) accuracy was achieved based on four coherence pairs (March, April). The model was introduced by Askne *et al.* [85]. The model describes coherence as a function of stem volume, perpendicular baseline and tree height, which can be expressed as a function of stem volume. In addition to the study of C-band data, Askne *et al.* [121] investigated four JERS-1 L-band coherence images over the same Swedish test site using the same semi-empirical model. The authors achieved an accuracy in the range of 30 to 35 $m^3 ha^{-1}$ (21.4 to 25%). The achieved accuracy was in agreement with the previous studies by Santoro *et al.* [120] over the same test site, but using a different number of stands for model training. In the study by Pulliainen *et al.* [122], tandem ERS-1/2 data were used over a Finnish test site. 14 image pairs were employed to estimate stem volume based on a simplified formulation of the semi-empirical water cloud model. The authors confirmed that images acquired under frozen (winter) conditions are superior to those obtained under unfrozen conditions. The authors measured an rRMSE of 48%. Over the same Finnish test site semi-empirical, IWCM was also implemented using tandem ERS-1/2 data [123]. The best achieved accuracy of 22% was obtained when only large, homogenous stands were considered. It was shown at Finnish and Swedish test sites in the next study [124] that using large homogenous forest stands and data acquired under frozen conditions, a relative RMSE on the order of 20% can be achieved. Moreover, no saturation of C-band ERS-1/2 was observed for stem volume. The authors demonstrated that small stands cause larger uncertainties than very steep slopes. The accuracy was improved to 17% when only large, homogenous stands were included in the retrieval accuracy analysis [125]. When all stands were included, the retrieval accuracy was 63%. The authors concluded that for selected forest stands and based on multi-temporal filtering, an accuracy in the range of 20 to 30% can be measured.

Based on coherence information, a classification of the Central Siberia was performed [69,126]. Four stem volume classes (0–20, 20–50, 50–80, >80 $m^3 ha^{-1}$) were delineated

by employing C-band ERS-1/2 and backscatter information from L-band JERS-1with high resulting accuracy (>81% for user's and producers's accuracy).

Santoro *et al.* [127] used 10 tandem ERS-1/2 pairs to retrieve stem volume in Central Siberia using a semi-empirical water cloud model. The best estimation accuracy achieved was in the range of 20 to 25%. However, such RMSE was obtained only for stands larger than 3 ha and a relative stocking of at least 50%.

In the study of Solberg *et al.* [128] the usability of interferometric X-band SAR for the inventory of boreal forest over southern Norway was investigated. The authors employed Digital Surface Model (DSM) data from the 11 day repeat-pass Shuttle Radar Topography Mission (SRTM) in conjunction with detailed Digital Terrain Models (DTM). The relationship between biomass and InSAR height was reported to be linear with coefficient of determination in the range of 0.45 to 0.81 showing no saturation. The estimation error was between 18 to 36%, indicating promising results of a new, at that time, TanDEM-X mission. The best result was obtained for homogeneous stands (>90% species composition) larger than 2 ha. In the next study, Solberg *et al.* [86] investigated two interferometric pairs acquired by TanDEM-X for a site in southeast Norway. At the stand level, the accuracy for stem volume estimation was reported to be 19–20%. At the plot level (circular plots of 250 m^2), the error doubled, resulting in 43–44% relative RMSE. In the most recent study [77], 18 bistatic image pairs acquired by the TanDEM-X mission were utilized to estimate biomass over a southern Sweden test site. The results are in agreement with the previous studies, namely error in the range of 17 to 33% was reported. When all 18 pairs were used and weighed inversely proportional to the square of the height of ambiguity (HOA), RMSE was 16% and the coefficient of determination was 0.93 using IWCM retrieval (stands larger than 1 ha). The authors also used other models: RVoG and a simple model based on penetration depth (PD). However, the results were comparable to those obtained using IWCM or resulted in a slightly higher estimation error.

In the study by Neumann *et al.* [81], the performance of L-band and P-band PolInSAR data in estimating boreal forest biomass was assessed. The data were acquired by an airborne E-SAR system over a test site located in southern Sweden. From multiple linear regression, an accuracy in the range of 17 to 25% at L-band and 5 to 27% at P-band was achieved when combining polarimetric information and estimated structure information (forest height and ground–volume ratio). In addition, non-parametric methods (support vector machines and random forests algorithms) were implemented and showed no improvement in estimation accuracy, although a more realistic distribution of biomass values was reported.

3.4.4 Biomass Estimation Without *in situ* Data

One of the difficulties in estimating biomass over vast areas e.g., Central Siberia is the lack of any and/or reliable *in situ* data. Therefore, approaches that do not make use of *in situ* data have been developed. It is important to note that such approaches require some basic knowledge of the biomass distribution in the investigated area. The methods exploit statistics of backscatter and coherence values for non-forest and dense forest based on other remote sensing products or based on the temporal consistency of radar data. The BIOMASAR algorithm introduced by Santoro *et al.* [102] made use of synergy between the optically sensed tree cover product (Moderate Resolution Imaging Spectroradiometer Vegetation Continuous Field) and Envisat ASAR coherence.

The other approach introduced by Santoro [129] and Askne [130] makes use of a consistency plot between two coherence observations. In the latter study, tandem ERS-1/2 data acquired in March and April over a Swedish test site were used. Implementing four tandem pairs in IWCM model, a relative error of 18% and a coefficient of determination of 0.9 was measured. However, it must be underlined that this method requires some manual adjustment to the ridges of the density plots.

3.5 Summary

Biomass estimation using radar remote sensing is a complex task. It includes radar data acquisition, processing and analysis. Furthermore, each step requires an in depth understanding of radar data properties and interpretation. In this review chapter, mainly the last step of the SAR data analysis has been discussed. By means of the retrieved accuracies of biomass: RMSE and R^2, the research findings have been reported and compared.

Historically, the first studies focused on airborne data, backscattering coefficient correlated with biomass over pine plantations and monoculture forests (e.g., [67,131]). Thereafter, more complex, heterogeneous forests were chosen as test sites (e.g., [105,132]). It has already been demonstrated that the radar backscatter increases with increasing biomass until it saturation (e.g., [133]). The relationship has already been successfully modelled by means of empirical and semi-empirical models (e.g., [97–100]). It was also found that the radar signal saturates at a certain biomass level depending on the wavelength used, polarisation, forest structure and environmental conditions. The L- and P-bands are considered to be the most suitable for the estimation of forest parameters due to the deeper penetration into canopy (e.g., [66,67]). It was also shown that the integration of many SAR images can increase the point at which saturation of the radar signal occurs to higher biomass levels up to no saturation (e.g., [102]). The saturation point also increases with the usage of different polarisations and radar frequencies (e.g., [132]). The HV and HH polarizations were proven to be the most sensitive to biomass (e.g., [108]).

InSAR provides new information, complementary to the backscatter intensity. Both interferometric height information and coherence were used for biomass retrieval. The first studies found that the SAR interferometry can be used to derive height information and for classification purposes (e.g., [116]). It has already been demonstrated that the interferometric coherence is inversely correlated to the biomass due to the volume decorrelation. The relationship between biomass and coherence has been described using empirical and semi-empirical models (e.g., [69,121]). It has been shown that the interferometric information provides better biomass estimation results than does backscattering coefficient (e.g., [86,130]). It was stated that environmental conditions need to be stable between data acquisitions to keep the temporal decorrelation at a low level. Nevertheless, the magnitude of temporal decorrelation is related to biomass-increasing biomass typically results in increased temporal decorrelation. It could be shown by means of ALOS PALSAR data that this relationship is most significant during frozen conditions. Therefore, frozen conditions are preferable for biomass estimation based on PALSAR InSAR coherence [79, 134, 135]. Thawing periods or the usage of images from dissimilar seasons showed complete decorrelation (e.g., [135]). Like backscatter intensity, the interferometric coherence also saturates at a certain level of biomass and the multi-temporal approach increases the biomass level at which saturation occurs and the

accuracy of the retrieval (e.g., [79]). In many research results, it has been shown that under optimal environmental conditions, the saturation level of interferometric correlation is higher than it would be using backscatter (e.g., [78]). It was also found that in addition to the environmental conditions, SAR data are affected by radar system acquisition geometry, topography and stand characteristics (e.g., [127]).

Most of the studies (53%) employed data acquired by C-band satellite missions and were focused on European sites, 35% using L-band, and 12% using X-band data (Figure 3.2). Only 12% used data acquired over Siberian sites (Figure 3.3).

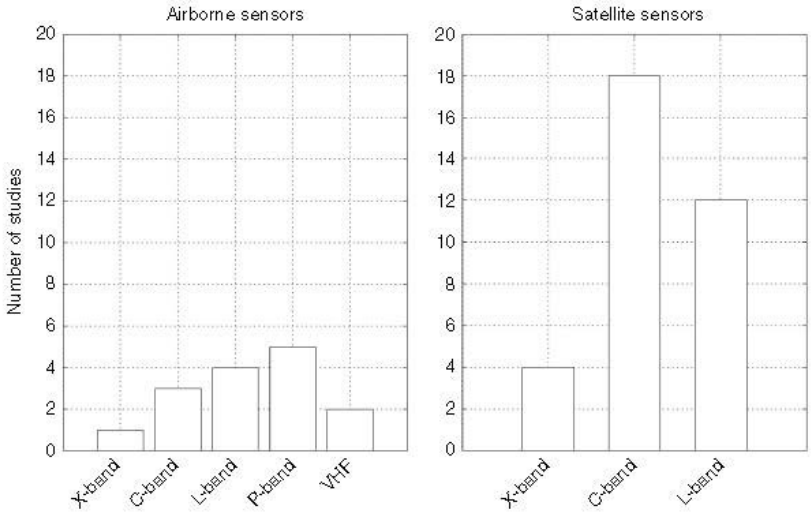

Figure 3.2 Type of radar remote sensing sensors for biomass estimation in boreal forests.

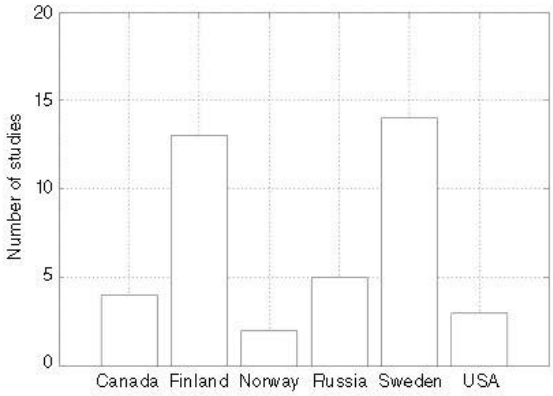

Figure 3.3 Summary of studies per test site in boreal forests.

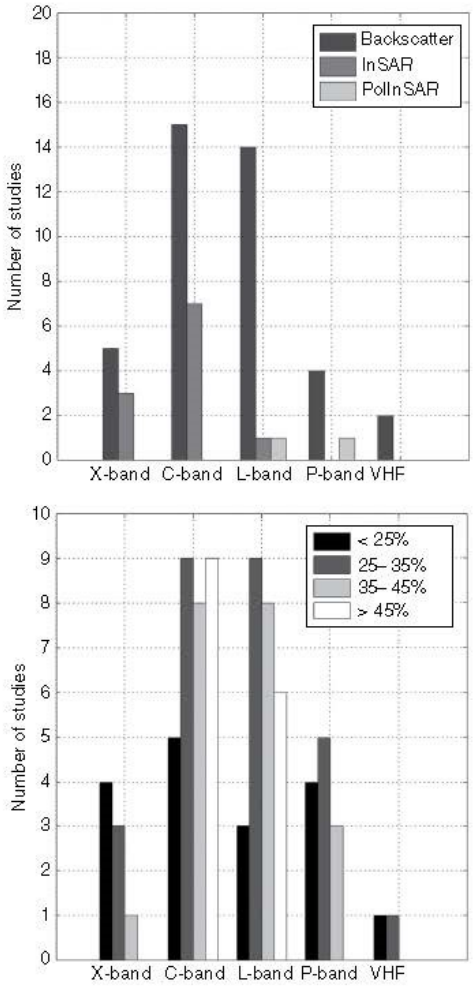

Figure 3.4 Type of data used for biomass estimation (top plot); biomass estimation errors reported depending on the SAR frequency used (bottom plot).

Biomass estimation error varied from more than 100% to 7.4%, when multi-temporal combination was used [79]. Most of the reported models used semi-empirical models (54%). However, Fransson and Israelsson [75] showed that backscatter can be modelled by a semi-empirical model as well as through linear regression, providing equally good results. Most of the reported models employed ground reference data for biomass estimation. Thus, these methods cannot be used when no reliable *in situ* data are available, which is an issue especially for vast territories such as Russia or Canada. Hence,

researchers have implemented other strategies for model training. Two studies proposed the use of complementary optical remote sensing tree cover products [102,136]. Another study implemented a consistency plots approach [130]. In this study an estimation error of 18% was calculated.

Although greater wavelengths are preferable for biomass estimation in general, the most useful results have been achieved using C- and X-band data. Figure 3.4 presents a summary of reported estimation errors using aforementioned SAR products: backscatter intensity, interferometric coherence (InSAR), and polarimetric interferometric coherence (PolInSAR).

The lowest estimation errors were reported employing semi-empirical models based on multi-temporal C-band coherence and backscatter (7.4% [79]) and X-band data using InSAR height (16% [77]) and radargrammetry method (16% [95]) for European forest sites. For Siberian forests an estimation error of 25% was achieved [127]. Nevertheless, expedient results can be expected from the forthcoming missions, e.g. P-band BIOMASS mission, which are highly anticipated within the forest biomass remote sensing community.

Acknowledgments

We would like to thank Stephanie Palmer for English proofreading of the first version of the manuscript.

References

1 R.A. Houghton, F. Hall, and S.J. Goetz, Importance of biomass in the global carbon cycle, *Journal of Geophysical Research: Biogeosciences*, **114**(G2), 1–13 (2009).
2 FAO, *Global Forest Resources Assessment 2005: Progress towards sustainable forest management*, Rome, 2006.
3 P.A. Harrell, L.L. Bourgeau-Chavez, E.S. Kasischke, N.H.F. French, and N.L. Christensen Jr., Sensitivity of ERS-1 and JERS-1 radar data to biomass and stand structure in Alaskan boreal forest, *Remote Sensing of Environment*, **54**, 247–260 (1995).
4 FAO, Terrestrial Essential Climate Variables. For Climate Change Assessment, Mitigation and Adaptation – BIOMASS, FAO, Rome, 2009.
5 S. Nilsson, A. Shvidenko, M. Jonas, I. McCallum, A. Thomson, and H. Balzter, Uncertainties of a regional terrestrial biota full carbon account: A systems analysis, *Water, Air Soil Pollution, Focus*, **7**, 425–441 (2007).
6 EU, *Regulation (EU) No 377/2014 of the European Parliament and of the Council of 3 April 2014 establishing the Copernicus Programme and repealing Regulation (EU) No 911/2010 (Text with EEA relevance)*, 44–66, 2014.
7 WHRC, *The boreal forest ecosystem, 2014*. Online. Available: www.whrc.org/ecosystem/highlatitude/.
8 FAO, *Global Forest Resources. Assesment 2010*. Main report, FAO, Rome, 2010.
9 FAO, *State of the World's Forests: Enhancing the socioeconomic benefits from forests*, FAO, Rome, 2014.
10 Y. Pan, R.A. Birdsey, J. Fang, R. Houghton *et al.*, A large and persistent carbon sink in the world's forests., *Science*, **333**, 988–93 (2011).

11 R.A. Houghton, Aboveground forest biomass and the global carbon balance, *Global Change Biology*, **11**, 945–958 (2005).

12 IPCC, Climate Change 2013: *The physical science basis*. Working Group I contribution to the fifth assessment report of the Intergovermental Panel on Climate Change, 2013.

13 M.C. Hansen, P.V Potapov, R. Moore, M. Hancher, S.A. Turubanova, A. Tyukavina, D. Thau, S.V Stehman, S.J. Goetz, T.R. Loveland, A. Kommareddy, A. Egorov, L. Chini, C.O. Justice, and J.R.G. Townshend, High-resolution global maps of 21st-century forest cover change, *Science*, **342**, 850–3 (2013).

14 A.Z. Shvidenko, D.G. Shchepashchenko, E.A. Vaganov, A.I. Sukhinin, S.S. Maksyutov, I. McCallum, and I.P. Lakyda, Impact of wildfire in Russia between 1998–2010 on ecosystems and the global carbon budget, *Doklady Earth Sciences*, **441**, 1678–1682 (2011).

15 A. Shvidenko, D. Schepaschenko, A. Sukhinin, I. McCallum, and S. Maksyutov, Carbon emissions from forest fires in boreal Eurasia between 1998–2010, *in Proceedings of the 5th International Wildland Fire Conference*, 2011.

16 FAO, *The Russian Federation forest sector outlook study to 2030*, FAO, Rome, 2012.

17 A. Shvidenko, D. Schepaschenko, I. McCallum, and S. Nilsson, Can the uncertainty of full carbon accounting of forest ecosystems be made acceptable to policymakers?, *in Greenhouse Gas Inventories*, Springer., Dordrecht, 137–157, 2011.

18 E.S. Kasischke, J. M. Melack, and M.C. Dobson, The use of imaging radars for ecological applications - A review, *Remote Sensing of Environment*, **59**, 141–156 (1997).

19 Å. Rosenqvist, A. Milne, R. Lucas, M. Imhoff, and C. Dobson, A review of remote sensing technology in support of the Kyoto Protocol, *Environmental Science and Policy*, **6**, 441–455 (2003).

20 G. Patenaude, R. Milne, and T.P. Dawson, Synthesis of remote sensing approaches for forest carbon estimation: reporting to the Kyoto Protocol, *Environmental Science and Policy*, **8**, 161–178 (2005).

21 I. McCallum, W. Wagner, C. Schmullius, A. Shvidenko, M. Obersteiner, S. Fritz, and S. Nilsson, Satellite-based terrestrial production efficiency modeling, *Carbon Balance and Management*, **4**, 8 (2009).

22 S.J. Goetz, A. Baccini, N.T. Laporte, T. Johns, W. Walker, J. Kellndorfer, R.A. Houghton, and M. Sun, Mapping and monitoring carbon stocks with satellite observations: a comparison of methods., *Carbon Balance and Management*, **4**, 2 (2009).

23 S. Frolking, M.W. Palace, D.B. Clark, J.Q. Chambers, H.H. Shugart, and G.C. Hurtt, Forest disturbance and recovery: A general review in the context of spaceborne remote sensing of impacts on aboveground biomass and canopy structure, *Journal of Geophysical Research: Biogeosciences*, **114**, G00E02.

24 C. Thiel, M. Santoro, O. Cartus, C. Thiel, T. Riedel, and C. Schmullius, Perspectives of SAR based forest cover, forest cover change and biomass mapping, *in The Kyoto Protocol: Economic Assessments, Implementation Mechanisms, and Policy implications*, C.P. Vasser (Ed.), New York: Nova Science Publishers, Inc., 13–56, 2009.

25 S. Goetz and R. Dubayah, Advances in remote sensing technology and implications for measuring and monitoring forest carbon stocks and change, *Carbon Management*, **2**, 231–244 (2011).

26 S.G. Zolkos, S.J. Goetz, and R. Dubayah, A meta-analysis of terrestrial aboveground biomass estimation using lidar remote sensing, *Remote Sensing of Environment*, **128**, 289–298 (2013).

27 GOFC-GOLD, *A sourcebook of methods and procedures for monitoring and reporting anthropogenic greenhouse gas emissions and removals caused by deforestation, gains and losses of carbon stocks in forests remaining forests, and forestation*, 2009.

28 T. Fatoyinbo (Ed), *Remote sensing of biomass – Principles and applications*. InTech, 2012.

29 R.A. Houghton, D. Butman, A.G. Bunn, O.N. Krankina, P. Schlesinger, and T.A. Stone, Mapping Russian forest biomass with data from satellites and forest inventories, *Environmental Research Letters*, **2** (2007).

30 H. Franco-Lopez, A.R. Ek, and M.E. Bauer, Estimation and mapping of forest stand density, volume, and cover type using the k-nearest neighbors method, *Remote Sensing of Environment*, **77**, 251–274 (2001).

31 E. Muinonen, M. Maltamo, and H. Hyppa, Forest stand characteristics estimation using a most similar neighbor approach and image spatial structure information, *Remote Sensing of Environment*, **78**, 223–228 (2001).

32 E. Tomppo, M. Nilsson, M. Rosengren, P. Aalto, and P. Kennedy, Simultaneous use of Landsat-TM and IRS–1C WiFS data in estimating large area tree stem volume and aboveground biomass, *Remote Sensing of Environment*, **82**, 156–171 (2002).

33 A. Pekkarinen, Image segment-based spectral features in the estimation of timber volume, *Remote Sensing of Environment*, **82**, 349–359 (2002).

34 P. Muukkonen and J. Heiskanen, Estimating biomass for boreal forests using ASTER satellite data combined with standwise forest inventory data, *Remote Sensing of Environment*, **99**, 434–447 (2005).

35 P. Muukkonen and J. Heiskanen, Biomass estimation over a large area based on standwise forest inventory data and ASTER and MODIS satellite data: A possibility to verify carbon inventories, *Remote Sensing of Environment*, **107**, 617–624 (2007).

36 J.E. Luther, R.A. Fournier, D.E. Piercey, L. Guindon, and R.J. Hall, Biomass mapping using forest type and structure derived from Landsat TM imagery, *International Journal of Applied Earth Observation and Geoinformation*, **8**, 173–187 (2006).

37 H. Fuchs, P. Magdon, C. Kleinn, and H. Flessa, Estimating aboveground carbon in a catchment of the Siberian forest tundra: Combining satellite imagery and field inventory, *Remote Sensing of Environment*, **113**, 518–531 (2009).

38 R. Fraser and Z. Li, Estimating fire-related parameters in boreal forest using SPOT VEGETATION, *Remote Sensing of Environment*, **82**, 95–110 (2002).

39 C. Souza, L. Firestone, L.M. Silva, and D. Roberts, Mapping forest degradation in the Eastern Amazon from SPOT 4 through spectral mixture models, *Remote Sensing of Environment*, **87**, 494–506 (2003).

40 S.A. Sader, R.B. Waide, W.T. Lawrence, and A.T. Joyce, Tropical Forest Biomass and Successional Age Class Relationships to a Vegetation Index Derived from Landsat TM Data, *Remote Sensing of Environment*, **28**, 143–156 (1989).

41 D.S. Boyd, G.M. Foody, and P.J. Curran, The relationship between the biomass of Cameroonian tropical forests and radiation reflected in middle infrared wavelengths (3.0–5.0 μm), *International Journal of Remote Sensing*, **20**, 1017–1023 (1999).

42 C. De Wasseige and P. Defourny, Retrieval of tropical forest structure characteristics from bi-directional reflectance of SPOT images, *Remote Sensing of Environment*, **83**, 362–375 (2002).

43 J. Dong, R.K. Kaufmann, R.B. Myneni, C.J. Tucker, P.E. Kauppi, J. Liski, W. Buermann, V. Alexeyev, and M.K. Hughes, Remote sensing estimates of boreal and temperate forest woody biomass: carbon pools, sources, and sinks, *Remote Sensing of Environment*, **84**, 393–410 (2003).

44 G. Zheng, J. M. Chen, Q.J. Tian, W.M. Ju, and X.Q. Xia, Combining remote sensing imagery and forest age inventory for biomass mapping, *Journal of Environmental Management*, **85**, 616–23 (2007).

45 C. Joshi, J. De Leeuw, A.K. Skidmore, I.C. Van Duren, and H. van Oosten, Remotely sensed estimation of forest canopy density: A comparison of the performance of four methods, *International Journal of Applied Earth Observation and Geoinformation*, **8**, 84–95 (2006).

46 V. Avitabile, M. Herold, M. Henry, and C. Schmullius, Mapping biomass with remote sensing: a comparison of methods for the case study of Uganda, *Carbon Balance and Management*, **6**, 7 (2011).

47 V. Avitabile, A. Baccini, M. A. Friedl, and C. Schmullius, Capabilities and limitations of Landsat and land cover data for aboveground woody biomass estimation of Uganda, *Remote Sensing of Environment*, **117**, 366–380 (2012).

48 L. Ji, B.K. Wylie, D.R. Nossov, B. Peterson, M.P. Waldrop, J.W. McFarland, J. Rover, and T.N. Hollingsworth, Estimating aboveground biomass in interior Alaska with Landsat data and field measurements, *International Journal of Applied Earth Observation and Geoinformation*, **18**, 451–461 (2012).

49 R. Nelson, W. Krabill, and J. Tonelli, Estimating forest biomass and volume using airborne laser data, *Remote Sensing of Environment*, **24**, 247–267 (1988).

50 M. Nilsson, Estimation of tree heights and stand volume using an airborne Lidar system, *Remote Sensing of Environment*, **56**, 1–7 (1996).

51 E. Næsset, Estimating timber volume of forest stands using airborne laser scanner data, *Remote Sensing of Environment*, **61**, 246–253 (1997).

52 E. Næsset and K.-O. Bjerknes, Estimating tree heights and number of stems in young forest stands using airborne laser scanner data, *Remote Sensing of Environment*, **78**, 328–340 (2001).

53 G. Patenaude, R. Hill, R. Milne, D.L.A. Gaveau, B.B.J. Briggs, and T.P. Dawson, Quantifying forest above ground carbon content using LiDAR remote sensing, *Remote Sensing of Environment*, **93**, 368–380 (2004).

54 Z.J. Bortolot and R.H. Wynne, Estimating forest biomass using small footprint LiDAR data: An individual tree-based approach that incorporates training data, *ISPRS Journal of Photogrammetry and Remote Sensing*, **59**, 342–360 (2005).

55 M.A. Lefsky, W.B. Cohen, S.A. Acker, G.G. Parker, T.A. Spies, and D. Harding, Lidar remote sensing of the canopy structure and biophysical properties of Douglas-Fir Western Hemlock forests, *Remote Sensing of Environment*, **70**, 339–361 (1999).

56 M.A. Lefsky, W.B. Cohen, S.W.J. Way, D.J. Harding, G.G. Parker, S.A. Acker, F. Avenue, and S.T. Gower, LiDAR remote sensing of aboveground biomass in three biomes, *International Archives of Photogrammetry and Remote Sensing*, **XXXIV–3/W4**, 22–24 (2001).

57 M.A. Lefsky, D.J. Harding, M. Keller, W.B. Cohen, C.C. Carabajal, F. Del Bom Espirito-Santo, M.O. Hunter, and R. de Oliveira, Estimates of forest canopy height and aboveground biomass using ICESat, *Geophysical Research Letters*, **32**, 22–25 (2005).

58 J.B. Drake, R.O. Dubayah, R.G. Knox, D.B. Clark, J.B. Blair, and C. Rica, Sensitivity of large-footprint lidar to canopy structure and biomass in a neotropical rainforest, *Remote Sensing of Environment*, **81**, 378–392 (2002).

59 J. Hyyppä, H. Hyyppä, D. Leckie, F. Gougeon, X. Yu, and M. Maltamo, Review of methods of small footprint airborne laser scanning for extracting forest inventory data in boreal forests, *International Journal of Remote Sensing*, **29**, 1339–1366 (2008).

60 R. Nelson, K.J. Ranson, G. Sun, D.S. Kimes, V. Kharuk, and P. Montesano, Estimating Siberian timber volume using MODIS and ICESat/GLAS, *Remote Sensing of Environment*, **113**, 691–701 (2009).

61 L.I. Duncanson, K.O. Niemann, and M.A. Wulder, Estimating forest canopy height and terrain relief from GLAS waveform metrics, *Remote Sensing of Environment*, **114**, 138–154 (2010).

62 M. Simard, N. Pinto, J.B. Fisher, and A. Baccini, Mapping forest canopy height globally with spaceborne lidar, *Journal of Geophysical Research: Biogeosciences*, **116**, G04021, (2011).

63 E. Khalefa, I.P.J. Smit, A. Nickless, S. Archibald, A. Comber, and H. Balzter, Retrieval of savanna vegetation canopy height from ICESat-GLAS spaceborne LiDAR with terrain correction, *IEEE Geoscience and Remote Sensing Letters*, **10**, 1439–1443 (2013).

64 D. Harding, P. Dabney, J. Abshire, T. Huss, G. Jodor, R. Machan, J. Marzouk, K. Rush, A. Seas, C. Shuman, X. Sun, S. Valett, A. Vasilyev, A. Yu, and Y. Zheng, The slope imaging multi-polarisation photon-counting LiDAR: an advanced technology airborne laser altimeter, *in Proceedings of the NASA Earth Science Technology Forum*, 2010.

65 GEDI Mission, 2014. Online. Available: http://geog.umd.edu/feature/gedi-lidar-piralph-dubayah-selected-earth-ventures-instrument-program.

66 M.C. Dobson, F.T. Ulaby, A. Beaudoin, E.S. Kasischke, and N. Christensen, Dependence of radar backscatter on coniferous forest biomass, *IEEE Transactions on Geoscience and Remote Sensing*, **30**, 412–415 (1992).

67 T. Le Toan, A. Beaudoin, J. Riom, and D. Guyon, Relating forest biomass to SAR data, *IEEE Transactions on Geoscience and Remote Sensing*, **30**, 403–411 (1992).

68 A. Beaudoin, T. Le Toan, S. Goze, E. Nezry, A. Lopes, E. Mougin, C.C. Hsu, H.C. Han, J.A. Kong, and R. T. Shin, Retrieval of forest biomass from SAR data, *International Journal of Remote Sensing*, **15**, 2777–2796 (1994).

69 W. Wagner, A. Luckman, J. Vietmeier, K. Tansey, H. Balzter, C. Schmullius, M. Davidson, D. Gaveau, M. Gluck, T. Le, S. Quegan, A. Shvidenko, A. Wiesmann, and J. Jiong, Large-scale mapping of boreal forest in SIBERIA using ERS tandem coherence and JERS backscatter data, *Remote Sensing*, **85**, 125–144 (2003).

70 K.J. Tansey, A.J. Luckman, L. Skinner, H. Balzter, T. Strozzi, and W. Wagner, Classification of forest volume resources using ERS tandem coherence and JERS backscatter data, *Forestry* (2004).

71 H. Balzter, Forest mapping and monitoring with interferometric synthetic aperture radar (InSAR), *Progress in Physical Geography*, **25**, 159–177 (2001).

72 H. Balzter, C.S. Rowland, and P. Saich, Forest canopy height and carbon estimation at Monks Wood National Nature Reserve, UK, using dual-wavelength SAR interferometry, *Remote Sensing of Environment*, **108**, 224–239 (2007).

73 A. Luckmann, J. Baker, and U. Wegmüller, Repeat-Pass Interferometric Coherence Measurements of Disturbed Tropical Forest from JERS and ERS Satellites, *Remote Sensing of Environment*, **73**, 350–360 (2000).

74 J.T. Pulliainen, K. Heiska, J. Hyyppa, and M.T. Hallikainen, Backscattering properties of boreal forests at the C- and X-bands, *IEEE Transactions on Geoscience and Remote Sensing*, **32**, 1041–1050 (1994).

75 J.E.S. Fransson and H. Israelsson, Estimation of stem volume in boreal forests using ERS–1 C- and JERS-1 L-band SAR data, *International Journal of Remote Sensing*, **20**, 123–137 (1999).

76 S. Solberg, R. Astrup, T. Gobakken, E. Næsset, and D.J. Weydahl, Remote sensing of environment estimating spruce and pine biomass with interferometric X-band SAR, *Remote Sensing of Environment*, **114**, 2353–2360 (2010).

77 J. Askne, J. Fransson, M. Santoro, M. Soja, and L. Ulander, Model-based biomass estimation of a hemi-boreal forest from multitemporal TanDEM-X acquisitions, *Remote Sensing*, **5**, 5574–5597 (2013).

78 J.T. Koskinen, J.T. Pulliainen, J. M. Hyyppä, M.E. Engdahl, and M.T. Hallikainen, The seasonal behavior of interferometric coherence in boreal forest, *IEEE Transactions on Geoscience and Remote Sensing*, **39**, 820–829 (2001).

79 M. Santoro, J. Askne, G. Smith, and J.E.S. Fransson, Stem volume retrieval in boreal forests from ERS-1/2 interferometry, *Remote Sensing of Environment*, **81**, 19–35 (2002).

80 K.P. Papathanassiou and S.R. Cloude, Single-baseline polarimetric SAR interferometry, *IEEE Transactions on Geoscience and Remote Sensing*, **39**, 2352–2363 (2001).

81 M. Neumann, S.S. Saatchi, L.M.H. Ulander, and J.E.S. Fransson, Assessing performance of L- and P-Band polarimetric interferometric SAR data in estimating boreal forest above-ground biomass, *IEEE Transactions on Geoscience and Remote Sensing*, **50**, 714–726 (2012).

82 S. Tebaldini and F. Rocca, Multibaseline polarimetric SAR tomography of a boreal forest at P- and L-bands, *IEEE Transactions on Geoscience and Remote Sensing*, **50**, 232–246 (2012).

83 H. Persson and J. Fransson, Forest variable estimation using radargrammetric processing of TerraSAR-X images in boreal forests, *Remote Sensing*, **6**, 2084–2107 (2014).

84 F.T. Ulaby, R.K. Moore, and A.K. Fung, *Microwave Remote Sensing Active and Passive. Volume II. Radar Remote Sensing and Surface Scattering and Emission Theory*. Norwood, MA, USA: Artech House, Inc., 1982.

85 J.I.H. Askne, P.B.G. Dammert, L.M.H. Ulander, and G. Smith, C-band repeat-pass interferometric SAR observations of the forest, *IEEE Transactions on Geoscience and Remote Sensing*, **35**, 25–35 (1997).

86 S. Solberg, R. Astrup, J. Breidenbach, B. Nilsen, and D. Weydahl, Monitoring spruce volume and biomass with InSAR data from TanDEM-X, *Remote Sensing of Environment*, **139**, 60–67 (2013).

87 P. Rodriguez-Veiga, M. Stelmaszczuk-Górska, C. Hüttich, C. Schmullius, K. Tansey, and H. Balzter, Aboveground Biomass Mapping in Krasnoyarsk Kray (Central Siberia) using Allometry, Landsat, and ALOS PALSAR, *in Proceedings of the RSPSoc Annual Conference*, 2014.

88 S. Wilhelm, C. Hüttich, M. Korets, and C. Schmullius, Large area mapping of boreal Growing Stock Volume on an annual and multi-temporal level using PALSAR L-band backscatter mosaics, *Forests*, **5**, 1999–2015 (2014).

89 C. Hüttich, M. Korets, S. Bartalev, V. Zharko, D. Schepaschenko, A. Shvidenko, and C. Schmullius, Exploiting Growing Stock Volume Maps for Large Scale Forest Resource Assessment: Cross-Comparisons of ASAR- and PALSAR-Based GSV Estimates with Forest Inventory in Central Siberia, *Forests*, **5**, 1753–1776 (2014).

90 M.A. Stelmaszczuk-Górska, P. Rodriguez-Veiga, N. Ackermann, C. Thiel, H. Balzter, and C. Schmullius, Non-Parametric Retrieval of Aboveground Biomass in Siberian Boreal Forests with ALOS PALSAR Interferometric Coherence and Backscatter Intensity, *Journal of Imaging*, **2**, 1 (2015).

91 J.E.S. Fransson, F. WaLter, and L.M.H. Ulander, Estimation of forest parameters using CARABAS-II VHF SAR data, *IEEE Transactions on Geoscience and Remote Sensing*, **38**, 720–727 (2000).

92 M.J. Soja, G. Sandberg, L.M.H. Ulander, and S. Member, Regression-based retrieval of boreal forest biomass in sloping terrain using P-band SAR backscatter intensity data, *IEEE Transactions on Geoscience and Remote Sensing*, **51**, 2646–2665 (2013).

93 O. Antropov, Y. Rauste, H. Ahola, and T. Häme, Stand-level stem volume of boreal forests from spaceborne SAR imagery at L-band, *IEEE Transactions on Geoscience and Remote Sensing*, **6**, 4776–4779 (2013).

94 M. Santoro, O. Cartus, J. Fransson, A. Shvidenko, I. McCallum, R. Hall, A. Beaudoin, C. Beer, and C. Schmullius, Estimates of Forest Growing Stock Volume for Sweden, Central Siberia, and Québec Using Envisat Advanced Synthetic Aperture Radar Backscatter Data, *Remote Sensing*, **5**, 4503–4532 (2013).

95 M. Vastaranta, M. Niemi, M. Karjalainen, J. Peuhkurinen, V. Kankare, J. Hyyppä, and M. Holopainen, Prediction of forest stand attributes using TerraSAR-X stereo imagery, *Remote Sensing*, **6**, 3227–3246 (2014).

96 H. Balzter, E. Talmon, W. Wagner, D. Gaveau, S. Plummer, J.J. Yu, S. Quegan, M. Davidson, T. Le Toan, M. Gluck, A. Shvidenko, S. Nilsson, K. Tansey, A. Luckman, and C. Schmullius, Accuracy assessment of a large-scale forest cover map of central Siberia from synthetic aperture radar, *Canadian Journal of Remote Sensing*, **28**, 719–737 (2002).

97 J.T. Pulliainen, P.J. Mikkela, M.T. Hallikainen, and J. Ikonen, Seasonal dynamics of C-band backscatter of boreal forests with applications to biomass and soil moisture estimation, *IEEE Transactions on Geoscience and Remote Sensing*, **34**, 758–770 (1996).

98 L. Kurvonen, J. Pulliainen, and M. Hallikainen, Retrieval of biomass in boreal forests from multitemporal ERS-1 and JERS-1 SAR images, *IEEE Transactions on Geoscience and Remote Sensing*, **37**, 198–205 (1999).

99 J.T. Pulliainen, L. Kurvonen, and M.T. Hallikainen, Multitemporal behavior of L- and C-band SAR observations of boreal forests, *IEEE Transactions on Geoscience and Remote Sensing*, **37**, 927–937 (1999).

100 M. Santoro, L. Eriksson, J. Askne, and C. Schmullius, Assessment of stand-wise stem volume retrieval in boreal forest from JERS-1 L-band SAR backscatter, *International Journal of Remote Sensing*, **27**, 3425–3454 (2006).

101 L.E.B. Eriksson, M. Magnusson, J.E.S. Fransson, G. Sandberg, and L.M.H. Ulander, Stem volume estimation for boreal forest using ALOS PALSAR, *in Proceedings of the the International Symposium on Retrieval of Bio- and Geophysical Parameters from SAR Data for Land Applications, Bari, Italy, September 25–28, 2007, ESA*, 2007.

102 M. Santoro, C. Beer, O. Cartus, C. Schmullius, A. Shvidenko, I. Mccallum, U. Wegmüller, and A. Wiesmann, Retrieval of growing stock volume in boreal forest using hyper-temporal series of Envisat ASAR ScanSAR backscatter measurements, *Remote Sensing of Environment*, **115**, 490–507 (2011).

103 A. Peregon and Y. Yamagata, The use of ALOS/PALSAR backscatter to estimate above-ground forest biomass: A case study in Western Siberia, *Remote Sensing of Environment*, **137**, 139–146 (2013).

104 Y. Rauste, Multi-temporal JERS SAR data in boreal forest biomass mapping, *Remote Sensing of Environment*, **97**, 263–275 (2005).

105 E. Rignot, J. Way, C. Williams, and L. Viereck, Radar estimates of aboveground biomass in boreal forests of interior Alaska, *IEEE Transactions on Geoscience and Remote Sensing*, **32**, 1117–1124 (1994).

106 E.J. Rignot, R. Zimmermann, and J.J. Van Zyl, Spaceborne applications of P-band imaging radars for measuring forest biomass, *IEEE Transactions on Geoscience and Remote Sensing*, **33**, 1162–1169 (1995).

107 K.J. Ranson, G. Sun, R.H. Lang, N.S. Chauhan, R.J. Cacciola, and O. Kilic, Mapping of boreal forest biomass from spaceborne synthetic aperture radar, *Remote Sensing of Environment*, **102**, 29599–29610 (1997).

108 G. Sandberg, L.M.H. Ulander, J.E.S. Fransson, J. Holmgren, and T. Le Toan, L- and P-band backscatter intensity for biomass retrieval in hemiboreal forest, *Remote Sensing of Environment*, **115**, 2874–2886 (2011).

109 M. Neumann, S.S. Saatchi, L.M.H. Ulander, and J.E.S. Fransson, Boreal forest biomass estimation Using PolInSAR Vertical and morphological structure indicators, *in Proceedings of the PolInSAR 5th Int. Workshop on Science and Applications of SAR Polarimetry and Polarimetric Interferometry*, 2011.

110 L.M.H. Ulander, G. Sandberg, and M.J. Soja, Biomass retrieval algorithm based on P-band biosar experiments of boreal forest, *in Proceedings of the 2011 IEEE International Geoscience and Remote Sensing Symposium*, 4245–4248, 2011.

111 A.Z. Shvidenko, E. Gustafson, A.D. Mcguire, V.I. Kharuk *et al.*, Terrestrial Ecosystems and Their Change, *in Regional Environmental Changes in Siberia and Their Global Consequences*, P. Y. Groisman and G. Gutman (Eds), Dordrecht: Springer Netherlands, 171–249, 2013.

112 P. Melon, J.M. Martinez, T. Le Toan, L.M.H. Ulander, and A. Beaudoin, On the retrieving of forest stem volume from VHF SAR data: observation and modeling, *IEEE Transactions on Geoscience and Remote Sensing*, **39**, 2364–2372 (2001).

113 K. Folkesson, G. Smith-jonforsen, and L.M.H. Ulander, Model-based compensation of topographic effects for improved stem-volume retrieval from CARABAS-II VHF-band SAR images, *IEEE Transactions on Geoscience and Remote Sensing*, **47**, 1045–1055 (2009).

114 M. Karjalainen, V. Kankare, M. Vastaranta, M. Holopainen, and J. Hyyppä, Prediction of plot-level forest variables using TerraSAR-X stereo SAR data, *Remote Sensing of Environment*, **117**, 338–347 (2012).

115 J. Hagberg, S. Member, L.M.H. Ulander, and J. Askne, Repeat-pass SAR interferometry over forested terrain, *IEEE Transactions on Geoscience and Remote Sensing*, **33**, 331–340 (1995).

116 U. Wegmuller and C.L. Werner, SAR interferometric signatures of forest, *IEEE Transactions on Geoscience and Remote Sensing*, **33**, 1153–1161 (1995).

117 J. Askne and G. Smith, Forest InSAR decorrelation and classification properties, *in Proceedings of the FRINGE 96 Workshop on ERS SAR Interferometry*, 1996.

118 B.G. Dammert and J. Askne, Interferometric tree height observations in boreal forests with SAR interferometry, *in Proceedings of the IEEE International Geoscience and Remote Sensing Symposium 1998*, 1363–1366, 1998.

119 G. Smith, P.B.G. Dammert, M. Santoro, J.E.S. Fransson, U. Wegmüller, J. Askne, and N. Federico, Biomass retrieval in boreal forest using ERS and JERS SAR, *in Proceedings of the Retrieval of Bio- and Geophysical Parameters from SAR Data for Land Applications*, 293–300, 1998.

120 M. Santoro, J. Askne, P.B.G. Dammert, J.E.S. Fransson, and G. Smith, Retrieval of biomass in boreal forest from multi-temporal ERS-1/2 interferometry, *in Proceedings of the FRINGE '99 Advancing ERS SAR Interferometry from Applications towards Operations*, 1999.

121 J. Askne, M. Santoro, G. Smith, and J.E.S. Fransson, Multitemporal repeat-rass SAR interferometry of boreal forests, *IEEE Transactions on Geoscience and Remote Sensing*, **41**, 1540–1550 (2003).

122 J. Pulliainen, M. Engdahl, and M. Hallikainen, Feasibility of multi-temporal interferometric SAR data for stand-level estimation of boreal forest stem volume, *Remote Sensing of Environment*, **85**, 397–409 (2003).

123 J. Askne and M. Santoro, Multitemporal repeat pass SAR interferometry of boreal forests, *IEEE Transactions on Geoscience and Remote Sensing*, **43**, 1219–1228 (2005).

124 J. Askne and M. Santoro, Boreal forest stem volume estimation from multitemporal C-band InSAR observations, *in Proceedings of the Envisat Symposium 2007*, 2007.

125 J. Askne and M. Santoro, Selection of forest stands for stem volume retrieval from stable ERS tandem InSAR observations, *IEEE Geoscience and Remote Sensing Letters*, **4**, 46–50 (2007).

126 W. Wagner, J. Vietmeier, C. Schmullius, M. Davidson, T. Le Toan, S. Quegan, J.J. Yu, A. Luckman, K. Tansey, H. Balzter, and D. Gaveau, The use of coherence information from ERS Tandem Pairs for determining forest stock volume in Siberia, *in Proceedings of the IGARSS 2000 Geoscience and Remote Sensing Symposium*, 1396–1398, 2000.

127 M. Santoro, A. Shvidenko, I. Mccallum, J. Askne, and C. Schmullius, Properties of ERS-1/2 coherence in the Siberian boreal forest and implications for stem volume retrieval, *Remote Sensing of Environment*, **106**, 154–172 (2007).

128 S. Solberg, R. Astrup, T. Gobakken, E. Næsset, and D.J. Weydahl, Estimating spruce and pine biomass with interferometric X-band SAR, *Remote Sensing of Environment*, **114**, 2353–2360 (2010).

129 M. Santoro, J. Askne, C. Beer, O. Cartus, C. Schmullius, U. Wegmüller, and A. Wiesmann, Automatic model inversion of multi-temporal C-band coherence and backscatter measurements for forest stem volume retrieval, *in Proceedings of the Geoscience and Remote Sensing Symposium, 2008. IGARSS 2008*, 124–127, 2008.

130 J.I.H. Askne and M. Santoro, Automatic model-based estimation of boreal forest stem volume from repeat pass C-band InSAR coherence, *IEEE Transactions on Geoscience and Remote Sensing*, **47**, 513–516 (2009).

131 M.C. Dobson, S. Member, F.T. Ulaby, A. Beaudoin, E.S. Kasischke, and N. Christensen, Dependence of radar backscatter on coniferous forest biomass, *IEEE Transactions on Geoscience and Remote Sensing*, **30**, 412–415 (1992).

132 M.L. Imhoff, Radar backscatter and biomass saturation: ramifications for global biomass inventory, *IEEE Transactions on Geoscience and Remote Sensing*, **33**, 511–518 (1995).

133 K.J. Ranson and G. Sun, Mapping biomass of a northern forest using multifrequency SAR data, *IEEE Transactions on Geoscience and Remote Sensing*, **32**, 388–396 (1994).

134 C. Thiel and C. Schmullius, Investigating ALOS PALSAR interferometric coherence in central Siberia at unfrozen and frozen conditions: implications for forest growing stock volume estimation, *Canadian Journal of Remote Sensing*, **39**, 232–250 (2013).

135 L.E.B. Eriksson, M. Santoro, A. Wiesmann, and C.C. Schmullius, Multitemporal JERS repeat-pass coherence for growing-stock volume estimation of Siberian forest, *IEEE Transactions on Geoscience and Remote Sensing*, **41**, 1561–1570 (2003).

136 O. Cartus, M. Santoro, C. Schmullius, P. Yong, C. Erxue, and L. Zengyuan, Creation of large area forest biomass maps for Northeast China using ERS-1/2 tandem coherence, *in Proceedings of the Dragon 1 Programme Final Results 2004–2007*, 2008.

4.3 Non-parametric retrieval of aboveground biomass

This section presents the manuscript entitled
"Non-parametric retrieval of aboveground biomass in Siberian boreal forests with ALOS PALSAR interferometric coherence and backscatter intensity" prepared and written by Stelmaszczuk-Górska, M. A., Rodriguez-Veiga, P., Ackermann, N., Thiel, C., Baltzer, H. & Schmullius, C.

The manuscript was peer-reviewed and published in
Journal of Imaging 2: 95-118; Special Issue: *Image Processing in Agriculture and Forestry*
doi: 10.3390/jimaging2010001

Journal of *Imaging*

MDPI

Article

Non-Parametric Retrieval of Aboveground Biomass in Siberian Boreal Forests with ALOS PALSAR Interferometric Coherence and Backscatter Intensity

Martyna A. Stelmaszczuk-Górska [1,*], Pedro Rodriguez-Veiga [2,3], Nicolas Ackermann [4], Christian Thiel [1], Heiko Balzter [2,3] and Christiane Schmullius [1]

1 Department of Earth Observation, Friedrich-Schiller-University Jena, Loebdergraben 32, Jena D-07743, Germany; christian.thiel@uni-jena.de (C.T.); c.schmullius@uni-jena.de (C.S.)
2 Centre for Landscape and Climate Research, University of Leicester, Bennett Building, University Road, Leicester LE1 7RH, UK; prv4@leicester.ac.uk (P.R.-V.); hb91@leicester.ac.uk (H.B.)
3 National Centre for Earth Observation, University of Leicester, Bennett Building, University Road, Leicester LE1 7RH, UK
4 Gamaya AG, Bâtiment C, EPFL Innovation Park, Lausanne 1015, Switzerland; nicolas.ackermann@gamaya.com
* Correspondence: m.stelmas@uni-jena.de; Tel.: +49-364-1948-978; Fax: +49-364-1948-882

Academic Editors: Francisco Rovira-Más and Gonzalo Pajares Martinsanz
Received: 30 October 2015; Accepted: 15 December 2015; Published: 25 December 2015

Abstract: The main objective of this paper is to investigate the effectiveness of two recently popular non-parametric models for aboveground biomass (AGB) retrieval from Synthetic Aperture Radar (SAR) L-band backscatter intensity and coherence images. An area in Siberian boreal forests was selected for this study. The results demonstrated that relatively high estimation accuracy can be obtained at a spatial resolution of 50 m using the MaxEnt and the Random Forests machine learning algorithms. Overall, the AGB estimation errors were similar for both tested models (approximately 35 t·ha^{-1}). The retrieval accuracy slightly increased, by approximately 1%, when the filtered backscatter intensity was used. Random Forests underestimated the AGB values, whereas MaxEnt overestimated the AGB values.

Keywords: SAR; MaxEnt; random forests; estimation error; forest; biomass; carbon

1. Introduction

Aboveground biomass (AGB) is an important variable in carbon accounting and climate science. In particular, forest AGB is relevant because forests constitute approximately 70%–90% of the Earth's aboveground biomass [1].

The AGB is defined as the mass of living organic matter growing above ground level per unit area at a particular time. The difference in AGB over time allows for measurement of carbon sequestration (excluding root growth) and carbon emission from deforestation, forest degradation, and forest fires. The estimation of AGB in the boreal forest is of special concern as it constitutes the largest biome in the world and has substantial carbon accumulation capability. Russia, as the country with the largest forested area in the world (809 million ha [2]), provided more than 90% of the carbon sink of the world's boreal forests between the years 2000 and 2007 [3]. Despite this importance, Russia's boreal forest has the highest uncertainty in carbon stock calculations [4,5]. This is mostly due to poor measurements of biomass stocks, forest degradation, deforestation, and forest growth. Additionally, due to the lack of financial support, some forested regions in Siberia have not been inventoried for more than 20 years [6]. Therefore, there is a strong need for earth observation-based methods to reduce costs and improve biomass estimations.

J. Imaging **2016**, *2*, 1

The most common method of measuring AGB is estimation from field measurements, such as stem diameter and tree height, using allometric models. However, due to the sampling nature of the field measurements and their high acquisition costs, they can only be collected over small areas. Satellite technology together with reliable *in situ* measurements allows for accurate and relatively cost-efficient wall-to-wall AGB estimates.

There are different remote sensing techniques for AGB retrieval. Several publications provide a comprehensive review of use of remote sensing techniques for biomass estimation including sourcebooks of recommended methods and data sources [7–16]. The estimates using optical sensors are feasible at low biomass levels using vegetation indices, bidirectional reflectance distribution function (BRDF), and texture [17–22]. The latest results of biomass estimation using Landsat data showed that an accuracy of $\pm 36\%$ can be measured in the boreal zones [23]. The most accurate estimates are gathered from airborne light detection and ranging (LiDAR) systems. The only archive data from the satellite profiling LiDAR for measuring and monitoring vegetation are from the Ice, Cloud, and land Elevation (ICESat) Geoscience Laser Altimeter System (GLAS). However, the data have some limitations related to the large footprint, sparse coverage, and sensitivity to terrain variability [24–28]. Another technique that has a potential for forest AGB estimation is synthetic aperture radar (SAR). Similar to LiDAR sensors, radar systems are sensitive to the geometrical properties of observed objects; on the contrary, SAR platforms are imaging sensors. SAR is an active system that transmits microwave energy at wavelengths ranging from 3.1 cm (the X band) to 23.6 cm (the L band). Longer wavelengths, *i.e.*, L-band, are preferable due to its deeper penetration into the forest canopy and due to saturation of radar signal at higher biomass levels [29–31]. Especially, SAR data with long wavelength, horizontal and vertical polarizations, interferometric capabilities, and global acquisition strategy are of great value for biomass retrieval. Data from those sensors are already available as archive data from L-band Japanese Earth Resources Satellite 1 (JERS-1) and Advanced Land Observing Satellite (ALOS) Phased Array L-band Synthetic Aperture Radar (PALSAR), or as new acquisitions from ALOS-2 PALSAR-2. Moreover, new SAR missions are planned that will ensure data continuity, e.g., the European Space Agency's P-band (68.9 cm) BIOMASS mission [32] and the UK NovaSAR S-band mission [33].

SAR data have been investigated for more than 30 years and were proved to be physically related to forest parameters until the saturation point showing correlation coefficients of up to approximately 0.9 [29,34–36]. Many SAR properties have been successfully exploited to quantify biomass: backscattering intensity [37,38], interferometric phase [39,40], interferometric correlation [41–43], polarimetric signature [44,45], SAR tomography, and radargrammetry [46–48]. In particular, satellite SAR data at the L-band have provided low AGB or growing stock volume (GSV) estimation error down to approximately 20% when forest stands greater than 10 ha were used and/or a multi-temporal approach was implemented [31,49–52]. Until now, only few retrieval results using interferometric coherence synergistically with backscatter over Russian boreal forests have been published [50,53,54].

Table 1 [50–52,55–60] presents a summary of the SAR retrieval statistics reported in the literature over Russian boreal forests, the same type of forest that was used in this study. The estimation error is represented as the root mean square error (RMSE) and the relative RMSE, *i.e.*, the RMSE divided by the mean GSV or AGB.

Table 1. Summary of previous studies of growing stock volume (GSV) or aboveground biomass (AGB) estimation over Siberian boreal forests using SAR data. The estimation error is given as the root mean square error (RMSE) and the relative RMSE, *i.e.*, the RMSE divided by the mean GSV or AGB.

Reference	SAR Sensor Wavelength	Estimated Variable	Model	Predictors	Spatial Resolution	Estimation Error RMSE (Units As Estimated Variable)/ Relative RMSE (%)
[55]	JERS-1 L-band	GSV ($m^3 \cdot ha^{-1}$)	Semi-empirical Water-Cloud type model	Backscatter in σ^0_{HH}, 9 images	Stand-wise > 8 ha	57–87/33–51
[50]	ERS-1/2 C-band	GSV ($m^3 \cdot ha^{-1}$)	Semi-empirical model Interferometric Water Cloud Model	Interferometric coherence adjusted by environmental conditions (relative stocking, stand size, topography)	Stand-wise > 3 ha	45–75/25–41
[56]	Envisat ASAR C-band	GSV ($m^3 \cdot ha^{-1}$)	BIOMASAR—semi-empirical Water-Cloud type model	Backscatter in γ^0_{HH} and γ^0_{VV} polarization, tens of images	1 km	-/34.2
[57]	Envisat ASAR C-band	GSV ($m^3 \cdot ha^{-1}$)	BIOMASAR—semi-empirical Water-Cloud type model	Backscatter in γ^0_{HH} and γ^0_{VV}, mean 93 observations	0.5°	-/15
[51]	ALOS PALSAR L-band	AGB ($t \cdot ha^{-1}$)	Single and multivariate regression, semi-empirical Water-Cloud type model	Backscatter in σ^0_{HH} and σ^0_{VV}, 1-5 images	Stand-wise > 10 ha	46–55/25–32
[58,59]	ALOS PALSAR L-band	GSV ($m^3 \cdot ha^{-1}$)	Machine learning approach—Random Forest	4 ALOS PALSAR mosaics, backscatter in γ^0_{HH} and γ^0_{HV}	25 m	54.4/39.4
[52]	ALOS PALSAR L-band	GSV ($m^3 \cdot ha^{-1}$)	Empirical exponential model	Polarimetric coherence, HHVV-coherence	Stand-wise > 2 ha	33–51/-
[60]	ALOS PALSAR L-band	AGB ($t \cdot ha^{-1}$)	Machine learning approach—MaxEnt	ALOS PALSAR mosaic, backscatter in γ^0_{HH} and γ^0_{HV}, Landsat bands, and categorical data	50 m	36.4/-

J. Imaging **2016**, *2*, 1

The study presented in this paper is based on multi-temporal ALOS PALSAR L-band backscatter intensity and coherence data. Both types of data were used as explanatory variables for AGB retrieval at a local scale of 0.25 ha. The AGB was estimated using two non-parametric machine learning algorithms: maximum entropy (MaxEnt) and Random Forests. Both models are popular in applied research. The MaxEnt approach [61] is particularly popular in species distribution modeling [62,63]. However, the method was also successfully implemented for AGB estimation at regional and global scale [60,64]. The Random Forests [65] are widely used for classification in ecology [66–68] as well as for AGB estimation [27,58,69–74]. The Random Forests were found to be superior to other methods such as support vector machine (SVM), k-nearest neighbour (KNN), Gaussian processes (GP), and stepwise linear models [75]. So far Random Forests have not been compared with the MaxEnt approach.

In summary, the aim of this paper is to:

1. use SAR L-band backscatter and coherence data synergistically to improve AGB estimation at a local scale;
2. compare AGB retrieval results using two recently popular machine learning algorithms.

2. Test Site and Available Data

2.1. Study Site

The study site is located in Krasnoyarskiy Kray in the Southern part of Central Siberia, Russia, approximately 120 km northeast of the city Krasnoyarsk—part of the Bolshe Murtinsky forest enterprise (center coordinates: 57°12′N and 93°49′E, Figure 1). The area is characterized by a continental climate with long, severe winters and short, warm, and wet summers. From mid-October until the beginning of April, the mean temperature is approximately −15 °C; in summer the mean temperature is approximately +15 °C. The annual precipitation is below 450 millimeters.

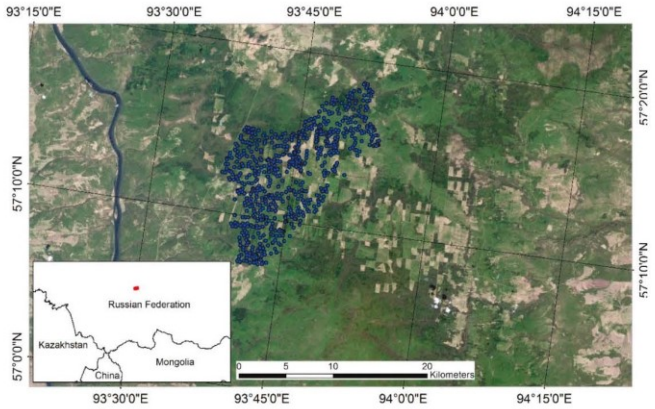

Figure 1. Extent of the study area and the spatial distribution of the reference points. Background image acquired by the Landsat 5 TM satellite (data available from the U.S. Geological Survey Earth Explorer).

The research area covers almost 2000 km^2. The area is mainly characterized by needleleaf, coniferous forests. The dominant trees are pine, spruce, fir, and larch. The main disturbances are logging activities and fire events. The study site is characterized by gentle topography with heights from 90 m to 572 m above sea level (a.s.l.) with an average height of 243 m a.s.l. The slopes range from 0° to 54° (riverside), with a mean value of 6°.

2.2. Available Data

The ALOS PALSAR L-band data were used for the explanatory variables. The data were delivered in Single Look Complex (SLC) Level 1.1 format. The data were provided by the Japan Aerospace Exploration Agency (JAXA) within the third phase of the Kyoto and Carbon Initiative [76,77]. In total, 19 scenes were available for this study area (Table 2). The weather data were downloaded from http://www.sibessc.uni-jena.de/ [78].

Ten scenes were acquired between 2006 and 2011 in fine beam single (FBS) mode and nine scenes were obtained in fine beam dual (FBD) mode. In the case of the FBS mode, the data were collected in horizontally transmitted and horizontally received polarization (HH), and in the case of the FBD mode, the data were given in HH and horizontally transmitted and vertically received (HV) polarizations.

The spatial resolution of the single-look image is 9.37 m in range and 3.14 m in azimuth for data acquired in the FBD mode and 4.68 m in range and 3.14 m in azimuth for data acquired in the FBS mode. The acquisition angle is 34.3°.

The forest inventory data were used as the dependent variable. The field data were provided by the Russian State Forest Inventory within the SIBERIA project [79]. The inventory dates back to 1998. Because of the time difference between inventory data and the SAR data acquisitions (>10 years) the field data were updated using semi-empirical phytomass models [80] and growth (yield) tables [81]. The latter were developed by the International Institute for Applied Systems Analyses (IIASA) in collaboration with the V.N. Sukachev Institute of Forest, Siberian Branch, Russian Academy of Sciences, and Moscow State Forest University. Those models and tables are recommended for use in forestry and forest management in Russia (Protocol of the Council of Federal Agency of Forest Management No. 2, dated 8 June 2006) [81].

The original data were gathered in the framework of the Russian forest inventory and planning (FIP) and are available in GIS vector format. Attributes such as GSV, age, tree height, diameter at breast height, and species composition were provided. All information is given for a forest stand, *i.e.* a group of trees occupying a specific area uniform in species composition, size, age, and management strategy. In total, information about 1604 stands was available.

Table 2. Summary of SAR data available for the test site. The data acquisition time was approximately 16 GMT—10 PM local time in summer or 11 PM local time in winter. The weather parameters are given as a mean from eight daily measurements [78]. The weather station is located approximately 50 km southwest from the center of the test site.

Image Name	Acquisition Date	Acquisition Mode	Weather Conditions: Mean Temperature (°C)/Wind Speed (m/s)/Precipitation (mm)/Snow Depth (mm)
ALPSRP049391140	28 December 2006	FBS	dry frozen conditions, −17.8/0.5/0/238.8
ALPSRP056101140	12 February 2007	FBS	dry frozen conditions, −18.9/1.7/0/340.4
ALPSRP082941140	15 August 2007	FBD	wet unfrozen conditions, 13.6/1.2/0/0 (2 days before heavy rain)
ALPSRP089651140	30 September 2007	FBD	wet unfrozen conditions, 13.1/3.9/-/0 (3 days before heavy rain)
ALPSRP103071140	31 December 2007	FBS	dry frozen conditions, −5.9/4.4/0/279.4
ALPSRP109781140	15 February 2008	FBD	dry frozen conditions, −17.2/0.4/0/381
ALPSRP129911140	2 July 2008	FBD	wet unfrozen conditions, 19.7/1.7/0.3/0
ALPSRP136621140	17 August 2008	FBD	wet unfrozen conditions, 16.8/1.6/0.8/0
ALPSRP156751140	2 January 2009	FBS	dry frozen conditions, −12.7/1.1/0/299.7
ALPSRP163461140	17 February 2009	FBS	dry frozen conditions, -31.3/0.6/0/459.7
ALPSRP190301140	20 August 2009	FBD	wet unfrozen conditions,14.7/0.8/1/0 (6 days before heavy rain)
ALPSRP197011140	5 October 2009	FBD	dry unfrozen conditions,11.5/1.6/0/0
ALPSRP210431140	5 January 2010	FBS	dry frozen conditions, −33.7/1.5/0/589.3
ALPSRP217141140	20 February 2010	FBS	dry frozen conditions, −22.9/1.2/0/599.4
ALPSRP243981140	23 August 2010	FBD	dry unfrozen conditions, 22.6/2.3/0/0
ALPSRP250691140	8 October 2010	FBD	wet unfrozen conditions, 1.4/1.7/0.5/10.2
ALPSRP257401140	23 November 2010	FBD	dry frozen conditions, −12.9/1.7/0/119.4
ALPSRP264111140	8 January 2011	FBS	dry frozen conditions, −23.3/1.5/0/360.7
ALPSRP270821140	23 February 2011	FBS	dry frozen conditions, −27.6/0.5/0/429.3

J. Imaging **2016**, *2*, 1

3. Processing Methods

3.1. Forest Inventory Data

The available forest inventory data are for 1998. Therefore, the first step of AGB retrieval was an update of the reference data. The data were improved to the year 2010. The data update consisted of four stages. First, the forest stands that changed from forest to non-forest were excluded by visual interpretation using very high and high resolution optical data. Cloud-free images were selected from KOMPSAT-2 and RapidEye. The data were acquired from spring to autumn in 2010, 2011, and 2012. Then, from the resulting stands only those were selected in which at least 60% of the trees belong to a single species. The reason for the selection is that the growth (yield) tables were done for dominant tree species. In the second step, the stands were used in the semi-empirical phytomass models. The basis for the improvement of the old inventory data is a site index (SI). SI is defined as the edaphic and climatic characteristics of a site that have an impact on the growth and yield of a given tree species [82]. Usually SI classes are determined by the relationship between the mean tree height and the mean age of a stand. As the SI was not available in the original forest inventory data it was calculated from the following equation [83]:

$$H_t = 22.47\left(1 - e^{-0.0234\mathrm{A}\left(1-e^{-0.0057A}\right)}\right)^{0.548} + (3 - SI)\,\Delta \quad (1)$$

$$\Delta = 4.35\left(1 - e^{-0.0205\mathrm{A}}\right)^{0.957} \quad (2)$$

where H_t represents tree height, A denotes forest stand age, and Δ is the interval between site indexes.

In the case of Russian forests, the SI from Ib, Ia, I–V, Va, and Vb are denoted as where the class with the lowest SI indicates the best site conditions for forest trees to grow. The site indexes II and III are dominant in the study area with fir, birch, and aspen as the dominant species (Figure 2).

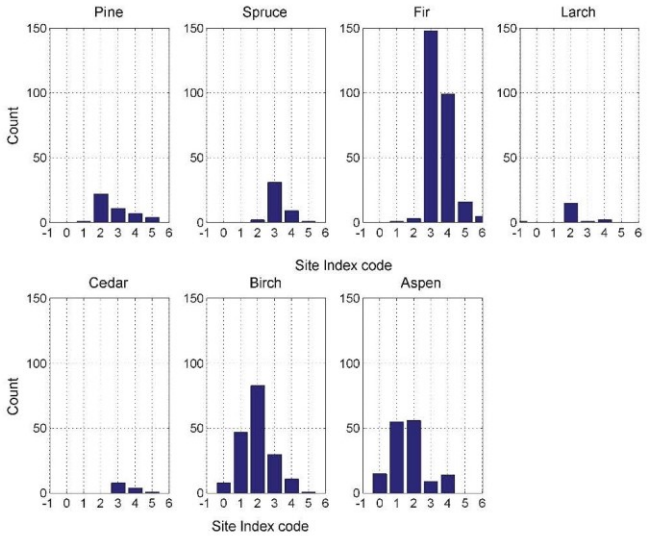

Figure 2. The number of stands with more than 60% of tree species per site index; site index code: −1-Ib, 0–Ia, 1–I, 2-II, 3-III, 4-IV, 5-V, 6-Va.

After calculating the SI, the growth rate was derived by implementing the Richards–Chapman growth function in polynomial quadratic form [81]:

$$GSV_{growth\ rate} = c_1 c_2 c_3 \left(1 - e^{-c_2 A}\right)^{c_3 - 1} e^{-c_2 A}, \quad (3)$$

where A denotes age and c_i are the parameters that have an ecological interpretation and depend on site index (SI) [81]:

$$c_i = c_{i3} SI^2 + c_{i2} SI + c_{i1}. \quad (4)$$

After obtaining the GSV growth rate, the correction coefficient GSV_{cc} was calculated:

$$GSV_{cc} = \frac{GSV_{in-situ}}{GSV_{model}} \quad (5)$$

where $GSV_{in-situ}$ represents the GSV measured in the field, whereas GSV_{model} is the GSV calculated according to the models [81] for a particular site index and forest stand age. A new GSV was then derived:

$$GSV_{new} = GSV_{in-situ} + A_{diff} GSV_{growth\ rate} GSV_{cc} \quad (6)$$

where A_{diff} is the age difference between the old inventory and reference year 2010 and equals 12.

Thirdly, GSV were converted to AGB. Based on freely available *in situ* measurements of forest live biomass (phytomass) [83], a regional allometric model relating GSV to AGB was developed (Figure 3).

The final step of the reference data processing was to rasterize the inventory data to 50 m spatial resolution, and then to erode the stands. An erosion of two pixels was used (100 m) to avoid border effects in the SAR products. Then, the stands were converted into points using the center of gravity (centroid) of the stand. The final updated AGB values ranged from 0 to 224 t· ha^{-1}, with a mean value of 98 t· ha^{-1}. The stand size with erosion varied from 0.5 to 130 ha, with a mean value of 16 ha that corresponds to 64 pixels. The stand age varied from 20 to 290 years. Six hundred forty-one stands remained for the investigations.

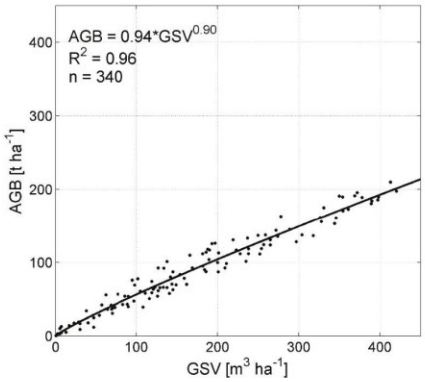

Figure 3. Allometric model relating AGB to GSV using *in situ* measurements of forest phytomass.

3.2. SAR Data Processing and Data Selection

The first pre-processing steps of SAR data included data calibration and multi-looking. In order to obtain data with squared pixels of approximately 50 m spatial resolution, the following multi-looking factors (range x azimuth) were used: FBS mode 6 × 15, FBD mode 3 × 15. Thereafter, the SAR

backscattering coefficient was calculated as γ°, which includes a correction of the backscatter for the local incidence angle θ_i [84]:

$$\gamma^0 = \sigma^0 \frac{A_{flat}}{A_{slope}} \left(\frac{\cos(\theta)}{cos(\theta_i)} \right)^n \quad (7)$$

where σ^0 is the backscattering coefficient and θ the incidence angle measured at mid-swathe (34.3°). A_{flat} and A_{slope} represent the local and the true pixel area, respectively. The cosine of the local incidence angle θ_i corrects the radiometry of backscatter for local slopes and converts the data from σ° to γ^0. This correction is known as a topographic normalization based on the local incidence angle and pixel area. In total eight backscatter images acquired in FBD mode were generated. The data selection was based on the recommendations from previous studies, in which it was reported that the backscatter data acquired during summer and autumn were superior to the winter acquisitions with regards to the AGB/GSV retrieval [31,85,86].

To reduce the speckle effect in the backscatter data, a filtering approach was implemented. The method was based on a multi-temporal speckle filtering calculated according to [87]:

$$J_k(x,y) = \frac{\langle I_k \rangle}{N} \sum_{i\ 1}^{N} \frac{I_i(x,y)}{I_i} \quad (8)$$

where I is the local mean value of pixels in a window with a center at (x, y) in image I, $k = 1,..,N$ and N represents the number of multi-temporal images, with intensity at position (x, y) in the k image—$I_i(x,y)$. J_k filters uncorrelated speckle between the images. In this study, N was equal to 8 for filtering of intensity images and window size was 5 × 5. No larger filtering window size was used because already large multi-looking factors were implemented.

The coherence images were calculated according to [88]:

$$\gamma = |\gamma| e^{j\Phi} = \frac{E\{g_1 g^*_2\}}{\sqrt{E\{|g_1|^2\} E\{|g_2|^2\}}} \quad (9)$$

where ϕ is the phase and E{} represents expected value.

Coherence measures the degree of correlation between two SAR images and takes values between 0 for total decorrelation and 1 for perfect correlation. Data processing consisted of co-registration at sub-pixel level (less than 0.05 pixel), common range and azimuth band filtering, and interferogram calculation and flattening. Coherence was estimated by spatial averaging within a two-dimensional window. In this study an adaptive estimation window was used with a window size between 3 × 3 and 5 × 5. A larger window size was used in the areas of low coherence in order to reduce the coherence bias. The resulting coherence was computed using the same number of looks as in the case of backscatter data (FBS mode 6 × 15, FBD mode 3 × 15 in range, and azimuth). This number of looks significantly reduced the coherence overestimation for low coherence values, as described in [89]. Therefore, the coherence bias was calculated to be close to zero (for coherence equal to 0 the values were ~0.002). The coherence was generated for 19 SLC pairs (Table 3). As a master image the image acquired in 2010 was used, additionally coherence for data acquired in 2011 was calculated. The perpendicular baselines B_n were between 224 and 3829 m and thus shorter than the critical baselines: 14.7 and 7.3 km for the FBS and FBD modes, respectively. Five coherence images were considered for the AGB retrieval. The latter were selected according to the stable weather and environmental conditions during the data acquisition [50] and a simple visual interpretation. To avoid coherence variability due to topography, slopes greater than 5° were masked out (mainly riverside areas). The mask was implemented to all SAR products used for AGB estimation. The SAR images were geocoded and normalized using the Shuttle Radar Topography Mission (SRTM) 90 m digital elevation model version 4.1 [90,91]. The SAR pre-processing was performed with the GAMMA Interferometric SAR Processor [92]. The backscatter data were geocoded using the bicubic-log spline resampling method while the coherence data were

processed with the bicubic spline interpolation approach. The final spatial resolution of the SAR products was 50 m.

Table 3. Summary of coherence images generated for the test site.

PALSAR Data	Perpendicular Baseline $\lvert B_n \rvert$ (m)	Temporal Baseline B_t (days)
5 January 2010 & 20 February 2010	789	46
23 August 2010 & 8 October 2010	461	46
8 October 2010 & 23 November 2010	224	46
28 December 2006 & 5 January 2010	2390	1104
12 February 2007 & 5 January 2010	1111	1058
12 February 2007 & 20 February 2010	1899	1104
31 December 2007 & 5 January 2010	1086	736
31 December 2007 & 20 February 2010	297	782
15 February 2008 & 5 January 2010	2190	690
15 February 2008 & 20 February 2010	1401	736
2 January 2009 & 5 January 2010	3041	368
2 January 2009 & 20 February 2010	3829	414
17 February 2009 & 5 January 2010	2339	322
17 February 2009 & 20 February 2010	3126	368
5 January 2010 & 8 January 2011	2978	368
20 February 2010 & 8 January 2011	2190	322
5 January 2010 & 23 February 2011	3780	414
20 February 2010 & 23 February 2011	2992	368
8 January 2011 & 23 February 2011	803	46

In addition to the backscatter and coherence data, the normalized ratio of the backscatter in linear scale and coherence, R_n, was calculated:

$$R_n = \frac{\gamma^0/\gamma - min\left(\gamma^0/\gamma\right)}{max\left(\gamma^0/\gamma\right) - min\left(\gamma^0/\gamma\right)}. \quad (10)$$

The rationale behind the ratio calculation is purely statistical. The ratio was introduced to enhance the backscatter relation to AGB and to reduce the number of potential outliers influencing the AGB retrieval error. In this approach, coherence γ values are considered as weighting factors for the backscatter γ° (linear scale) and strengthen the response over forested areas. The ratio calculation was performed using a reference coherence image with a temporal baseline of 46 days. The SLC data for the coherence calculation were acquired in winter 2010, namely on 5 January 2010 and 20 February 2010. This coherence was selected due to the highest dynamic range of coherence values resulted from optimal and similar environmental conditions during the data acquisition, as well as the short perpendicular baseline B_n. The resulting ratio values over forested areas are relatively high compared to the values over non-forested and sparsely forested areas. For example, a value of 0.16 of backscatter on a linear scale with a corresponding coherence value of 0.2 (dense forest) is approximately 0.8, whereas a backscatter value of 0.07 with a coherence value of 0.6 (non-forest) is approximately 0.1. In order to adjust the ratio values to a single scale, the values were normalized and ranged from 0 to 1. A normalized ratio between available backscatter data (in linear scale) acquired on 23 August 2010 and 8 October 2010 in both polarizations and the coherence between acquisitions taken in 2010 (5 January and 20 February) were calculated. The resulting range of calculated values is illustrated by box plots (Figure 4, plot A).

On each box the central mark is the median, the edges of the box are the 25th and 75th percentiles, and the whiskers extend to the extreme values. Most of the values varied from 0 to approximately 0.2 show an almost linear relationship up to approximately 60 t·ha^{-1} and a non-linear relationship for higher AGB values (Figure 4B,C). The values close to the upper boundary represented small heterogeneous stands in the forest inventory data (<8 ha).

J. Imaging **2016**, 2, 1

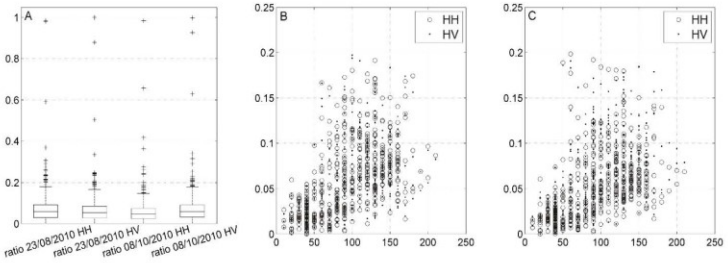

Figure 4. (**A**) presents box plots for four calculated ratios between backscatter images (acquired on 23 August 2010 and 8 October 2010) and coherence acquired in winter 2010 (5 January and 20 February); (**B**) and (**C**) present the ratio as a function of aboveground biomass (AGB).

In total, 13 SAR products were selected for AGB retrieval. The examples of the generated SAR products are presented in Figure 5.

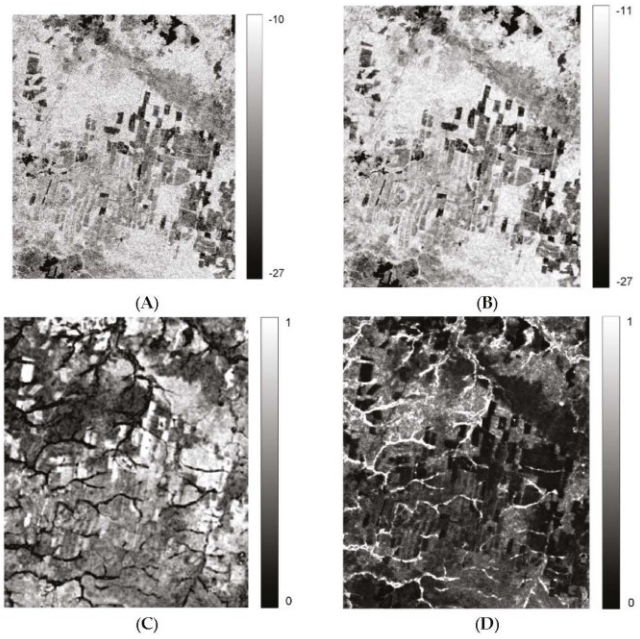

Figure 5. Subset of SAR products used for AGB retrieval. (**A**): backscatter data acquired on 23 August 2010 in HV polarization in dB; (**B**): filtered backscatter image in dB; (**C**): coherence between 5 January 2010 and 20 February 2010; (**D**): normalized ratio between acquired on 23 August 2010 in HV polarization and coherence (5 January & 20 February 2010).

3.3. AGB Retrieval Models

In this study, two non-parametric data fusion machine learning algorithms were considered: maximum entropy (MaxEnt) and Random Forests. In both cases the updated forest inventory was used as the response data. The model's training was done on 90% of the sample size (577 samples), whereas 10% was used for independent validation (64 samples). For the selection of training and validation data, a stratified sampling was implemented. Only 10% of the response data was used for the independent validation as the mentioned algorithms calculate unbiased model error using 25% in the case of MaxEnt and approximately 1/3 in the case of Random Forests of the data randomly excluded from the training data.

The first approach was a model based on the MaxEnt algorithm. The model was run using the MaxEnt program for maximum entropy modeling version 3.3.3 k (under Java Runtime Environment). The MaxEnt is an exponential model that can be compared with the generalized linear (GLM) and generalized additive (GAM) models. The concept of the method is to estimate the probability distribution of maximum entropy constrained by a set of remote sensing variables. Through numerous iterations, the weights of these variables are adjusted to maximize the average sample likelihood (training gain). The weights are then used to estimate the distribution over the whole space for each of the AGB classes. In this study, AGB reference data were divided into seven AGB classes, in t· ha^{-1}: 0–40, 40–60, 60–80, 80–100, 100–120, 120–140, and >140. The values were grouped such that each class could be represented equally in terms of occurrences. The classes' representation is illustrated as a histogram (Figure 6).

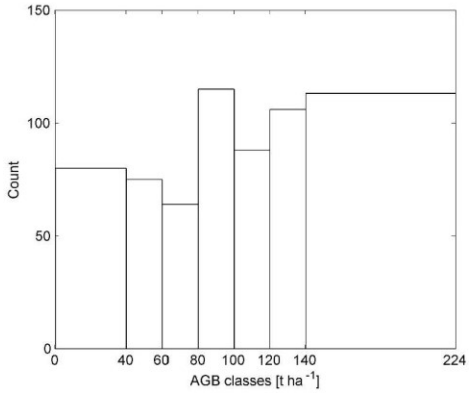

Figure 6. Number of measurements in selected AGB class.

Then, the AGB value was calculated for each pixel using the maximum probability weighted average [64]:

$$\widehat{AGB} = \frac{\sum_{i=1}^{N} \mathrm{P}_i^n AGB_i}{\sum_{i=1}^{N} P_i^n} \tag{11}$$

where i refers to the class number, P_i is the MaxEnt probability, AGB_i is the estimated average biomass range, and $\widehat{AGB}$ is the predicted value of AGB for each pixel.

As an input for the MaxEnt algorithm, all available variables were used and two groups of data were distinguished. The first one contained unfiltered data, whereas the second one was with backscatter data filtered according to Equation (8).

In the MaxEnt program the resampling of the data for each replication is done by bootstrapping, whereas the jackknife tests are used for calculation of variable contribution. The jackknife tests are generated using regularized gain and AUC. The jackknife test is used in two cases: withhold one predictor and refit model and withhold all predictors but one and refit the model. To determine the variable percent contribution, in each iteration of the training algorithm the increase in regularized gain was added to the contribution of the corresponding variable, or subtracted from it if the resulted value was negative. At the end the values were converted to percentages.

The second approach was based on a supervised Random Forests® regression approach, available as the randomForest package in the R software [93]. It is an ensemble learning method that operates by constructing a large number of trees by randomly selecting the predictors and then calculating a mean prediction from all individual regression trees. Each tree is constructed using a different randomly permuted sample from the input dataset. One-third of the data are left out of the bootstrap sample and not used in the construction of the tree. This sample is called out-off-bag (OOB) and is used to obtain an unbiased estimate for the retrieval error, OOB error.

The randomForest package also provides measures for evaluating the importance of the different predictors in the model development. In this study, we used the measure that is computed from permuting OOB data and permuting each predictor variable for each tree. The difference between the OOB MSE and predictor MSE are then averaged over all trees, and normalized by the standard deviation of the differences.

In order to evaluate the accuracy and performance of the implemented models, the following quantitative measures were considered for the independent validation:

a. root mean square error (RMSE) is defined as:

$$RMSE = \sqrt{\frac{\sum_{i}^{n}{}_{1}\left(AGB_{ref(i)} - \widehat{AGB}_i\right)^2}{n}} \quad (12)$$

where $AGB_{ref(i)}$ represents AGB reference value for stand i, $\widehat{AGB}_i$ predicted AGB and n a number of AGB observations.

b. corrected root-mean-square error ($rRMSE_{cor}$) is defined as:

$$rRMSE_{cor} = \sqrt{RMSE_{Sat}^2 - RMSE_{Ref}^2} \quad (13)$$

where $RMSE_{Sat}$ represents the root mean square error in a satellite-derived estimation of AGB and $RMSE_{Ref}$ is the root mean square error in the forest inventory data. According to the manual on forest inventory and planning in Russian forests, the maximum error of GSV is expected to be 15% [94]. This value was also considered in the AGB estimation because GSV is the main component of AGB. According to [95], GSV constitutes in our test site 73% of AGB.

Additionally, relative RMSEs were calculated by dividing the RMSEs by the mean AGB and multiplying by 100%.

c. bias is defined as the mean of estimation error:

$$bias = \frac{\sum_{i}^{n}{}_{1}\left(\widehat{AGB}_i - AGB_{ref(i)}\right)}{n} \quad (14)$$

where positive values of bias expresses overestimation, and negative values underestimation.

The models' predictive performance was evaluated using pseudo *R*-squared (1-MSE/variance) [93] in the case of the Random Forests and an area under receiver operating characteristic curves (AUC) [96] in the case of the MaxEnt. The parameters were generated using the models' testing samples.

J. Imaging **2016**, *2*, 1

4. Retrieval Results

4.1. MaxEnt Performance

As an output of MaxEnt seven continuous probability distribution maps with pixel values from 0 to 1 were obtained, where 1 is a high predicted probability of being classified to a specified AGB class. The probability values were then used to calculate the final AGB map according to Equation (11).

To assess the MaxEnt algorithm performance, AUC was calculated by bootstrapping 25% of the training data. The AUC was computed for each AGB class (Figure 7).

The AUC values are higher than 0.7, which shows that the model performed well. Only in the case of filtered data or the 60–80 t·ha^{-1} AGB class was the AUC was lower than 0.6. The highest predictive power of the model was observed for the high and the low AGB ranges. The mean AUC for all AGB classes was calculated to be 0.76 and 0.77 for unfiltered and filtered datasets, respectively.

To assess the importance of the predictors, the variable percent of contribution was calculated. A high value indicates that the model depends more on that variable (Figure 8A,B).

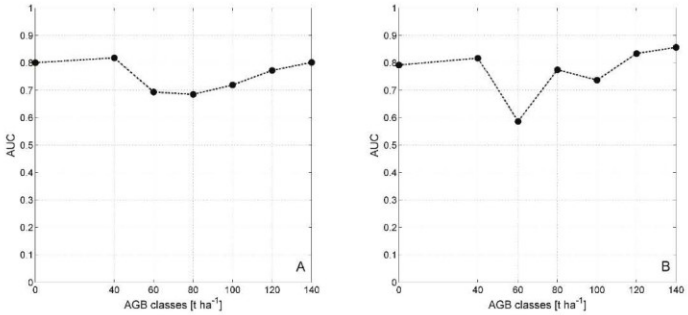

Figure 7. Evaluation of MaxEnt model performance using Area Under the Receiver Operator Curve (AUC) for testing dataset (**A**) with unfiltered and (**B**) with filtered backscatter data; aboveground biomass (AGB) classes 0: 0–40, 40: 40–60, 60: 60–80, 80: 80–100, 100: 100–120, 120: 120–140, 140: >140 t·ha^{-1}.

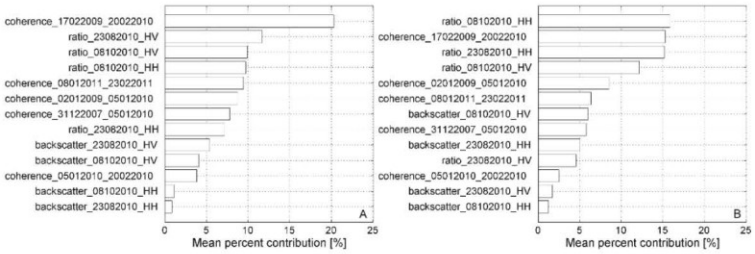

Figure 8. Predictor importance presented as percent contribution (**A**) dataset with unfiltered and (**B**) with filtered backscatter data.

In the case of the dataset with the unfiltered backscatter, the variable that mostly decreased model performance when it was omitted was coherence between data acquired on 17 February 2009 and 20 February 2010. For the filtered dataset, it was the ratio of backscatter in HH polarization acquired on 8

October 2010. Therefore, the coherence and normalized ratio appear to contain the most information that is not present in the other variables. The backscatter acquired on 23 August 2010 in HH and on 8 October 2010 in HH polarization seem to be of less importance for AGB prediction.

The variable importance was also analyzed per AGB class. To better illustrate how the variable contribution changes among the seven AGB classes, the data were distinguished between coherence, backscatter, and normalized ratio (Figure 9).

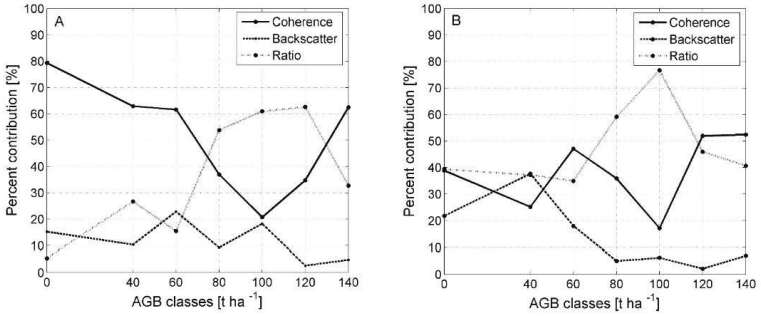

Figure 9. Coherence, backscatter, and normalized ratio contributions *versus* AGB classes. (**A**) Dataset with unfiltered or (**B**) filtered backscatter data. Class 0 represents AGB values from 0 to 40, 40: 40–60, 60: 60–80, 80: 80–100, 100: 100–120, 120: 120–140, 140: >140 t·ha^{-1}.

Figure 9 confirms with a mean percent contribution value of 51.2% that in the case of unfiltered data the most important variables were coherence data. The data were the most important in four AGB classes: 0–40, 40–60, 60–80, and >140 t·ha^{-1}. The mean percent contribution for the ratio products was 36.8% and for the backscatter products was 12%. Therefore, the backscatter seems to provide the least information for MaxEnt. When the filtered data were used, the most important group of data was the ratio layers, with a mean percent contribution of 47.7%. The data were the most important in two classes, *i.e.*, AGB classes 80–100 and 100–120 t·ha^{-1}. The second most important type of data was the coherence products, with a mean percent contribution of 38.3%. The data contributed most to the AGB retrieval for three AGB classes 60–80, 120–140, and >140 t·ha^{-1}. The backscatter data provided the least information for the retrieval. The mean percent contribution was 13.9%. In both plots the rise of the ratio importance is related to the decrease of the influence of the backscatter and coherence.

4.2. Random Forests Performance

The higher percent of variance explained was calculated for the dataset with filtered backscatter, the value of the pseudo R-squared was 38.4%. In the case of the unfiltered dataset the pseudo R-squared was 36.4%. The values were calculated based on the testing sample (OOB sample). Overall, the Random Forests predictor importance ranking (Figure 10) revealed only small differences between the datasets with unfiltered and filtered backscatter data. The ranking showed that of the 13 predictors the normalized ratio between the backscatter in HV polarization acquired on 8 October 2010 and coherence (5 January & 20 February 2010) was the most important for the retrieval of AGB with values of 26% and 28.7% for the unfiltered and filtered datasets, respectively. The mean value of the increase in MSE in the case of all ratio products was 22.2% and 24.9%.

The second most important data group in the case of the both datasets was backscatter products. The mean value of the increase in MSE was 17.4% and 17.9%. Random Forests suggested that coherence products had the smallest influence on AGB retrieval with a mean value of 16.4% and 15.4% for unfiltered and filtered datasets, respectively.

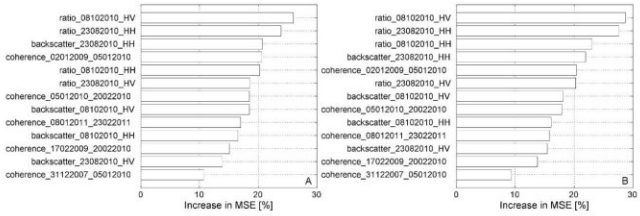

Figure 10. Predictor importance presented as increase in MSE for (**A**) unfiltered dataset and (**B**) dataset with filtered backscatter data.

4.3. AGB Mapping Results

Figures 11–14 show SAR-derived AGB maps with a spatial resolution of 50 m. Each map presents AGB retrieval results expressed in t· ha^{-1}. The first two maps show AGB values derived by the MaxEnt algorithm; the other two are by the Random Forests. Examining the results with a simple visual interpretation, it can be noticed that the maps differ taking into account the spatial variability of AGB values. In the case of the AGB maps generated by MaxEnt, the values seem to be more heterogonous both in high and low biomass ranges.

The range and the mean value of the retrieved AGB for each map are given in Table 4.

Table 4. Range of derived AGB.

Method	MaxEnt Unfiltered Dataset	Random Forests Unfiltered Dataset	Maxent Filtered Dataset	Random Forests Filtered Dataset
Range t· ha^{-1}	0–140	0–160	0–150	0–170
Mean AGB t ha^{-1}	87	95	89	97

In the case of the MaxEnt algorithm, the AGB ranged from 0 to 140 (150 t· ha^{-1}), whereas the values computed by the Random Forests were higher by 10 t· ha^{-1}. The mean values derived by MaxEnt were lower than 90 t· ha^{-1} and in the case of Random Forests greater than 95 t· ha^{-1}.

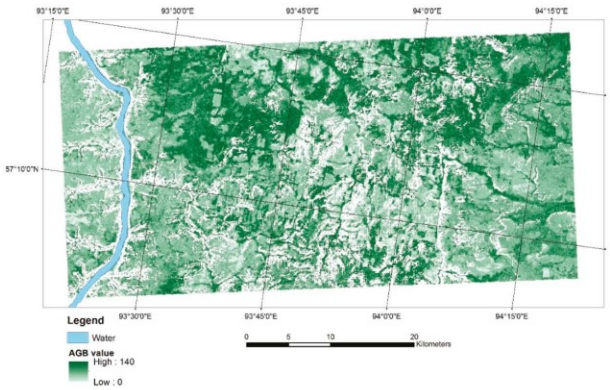

Figure 11. AGB map generated using the MaxEnt algorithm and a dataset with unfiltered backscatter data.

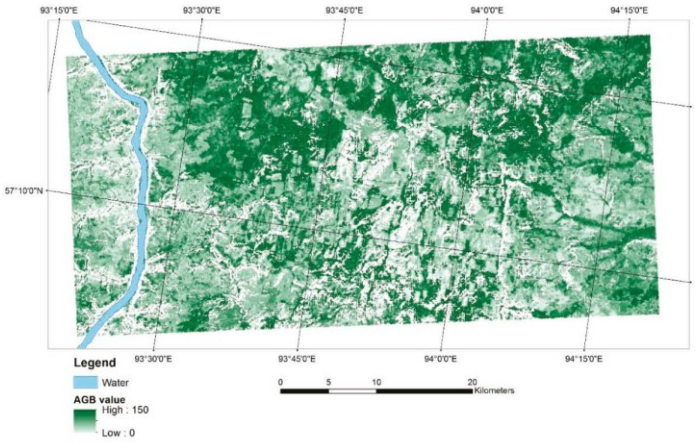

Figure 12. AGB map generated using the MaxEnt algorithm and a dataset with filtered backscatter data.

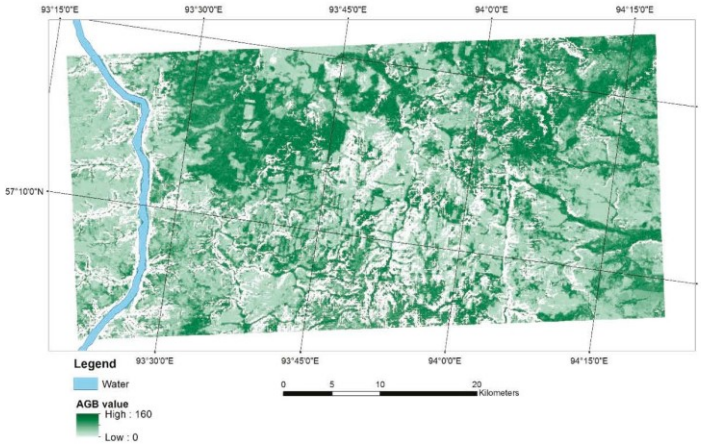

Figure 13. AGB map generated using the Random Forests algorithm and a dataset with unfiltered backscatter data.

To better observe the differences in spatial distribution, the difference maps between updated forest inventory (*in situ* data) and SAR-derived AGB were calculated (Figure 15). Green represents overestimation, whereas red is underestimation. In yellow are the AGB values estimated correctly.

In general, there are almost no differences between maps generated using unfiltered and filtered datasets. In the case of MaxEnt, the retrieved AGB values are displayed in green, which means overestimation. The Random Forests tends to underestimate. The AGB values are displayed in red and orange. In both cases, the overestimation can be seen on the borders of the stands. The underestimation is observed for stands with high AGB values.

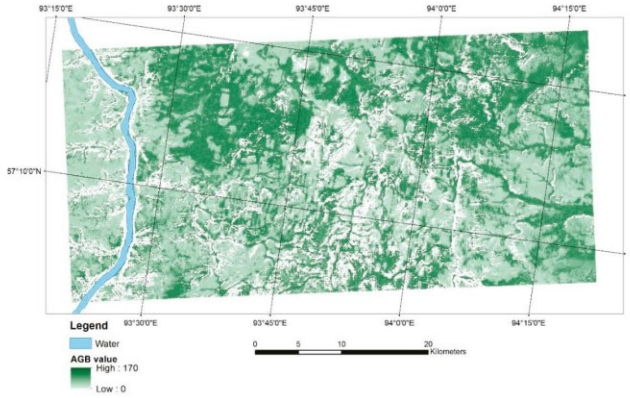

Figure 14. AGB map generated using the Random Forests algorithm and a dataset with filtered backscatter data.

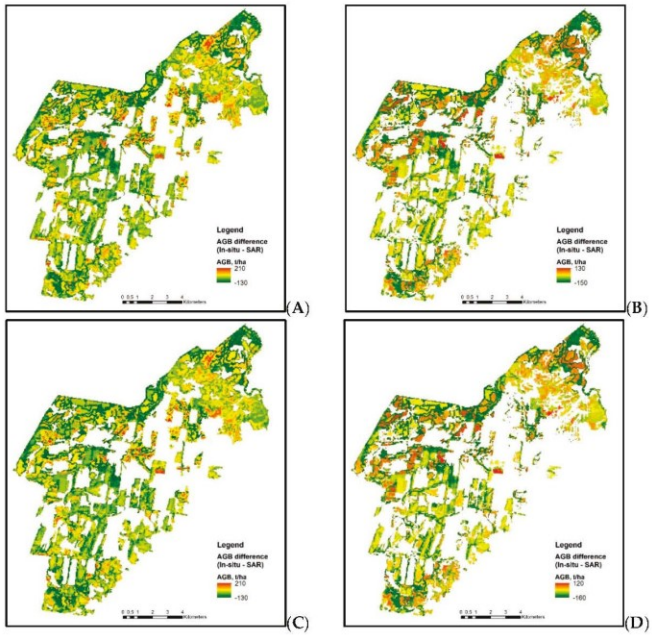

Figure 15. AGB difference maps between updated forest inventory (*in situ*) and SAR-derived AGB. (**A**) MaxEnt model—unfiltered data; (**B**) Random Forests—unfiltered data; (**C**) MaxEnt model with filtered backscatter; (**D**) Random Forests with filtered backscatter.

4.4. Validation

Table 5 summarizes the accuracies of the MaxEnt and the Random Forests AGB retrieval when using backscatter data (filtered and unfiltered), coherence images, and normalized ratio products. The corrected RMSE and relative corrected RMSE were calculated for a training sample and an independent sample.

Table 5. Validation of AGB retrieval results. RMSE values are given for training and validation samples (training/validation).

Model	Dataset	$RMSE_{cor}$ (t·ha ^{1})	$rRMSE_{cor}$ (%)	Bias (t·ha ^{1})
MaxEnt	Unfiltered	33.3/36.4	34.3/39.5	12.0/5.2
	Filtered	28.7/35.8	29.6/38.8	6.9/4.3
Random Forests	Unfiltered	21.6/35.4	22.3/38.4	3.2/ 4.4
	Filtered	21.3/35.0	22.0/36.9	0.9/ 4.5

In the case of MaxEnt, the corrected RMSE was 36.4 t·ha^{-1} (33.3 t·ha^{-1} for the training sample) and 28.7 t·ha^{-1} (35.8 t·ha^{-1} for the training sample) for unfiltered and filtered datasets, respectively. Overall, the estimation error of 39.5% (34.3% for training sample) was calculated for an unfiltered dataset and 38.8% (29.6% for the training sample) for a dataset with filtered backscatter data. The bias of 5.2 t·ha^{-1} (12 t·ha^{-1} for the training sample) was calculated in the case of unfiltered data and of 4.3 t·ha^{-1} (6.9 t·ha^{-1} for the training sample) in the case of the dataset with filtered backscatter data.

The Random Forests results show similar estimation error. The corrected RMSE was 35.4 t·ha^{-1} (21.6 t·ha^{-1} for training sample) and 35.0 t·ha^{-1} (21.3 t·ha^{-1} for training sample) for unfiltered and filtered datasets, respectively. The relative corrected RMSEs of 38.4% (22.3% for the training sample) in the case of unfiltered datasets and of 36.9% (22.0% for the training sample) were calculated. The bias of −4.4 t·ha^{-1} (3.2 t·ha^{-1} for the training sample) and of −4.5 t·ha^{-1} (0.9 t·ha^{-1} for the training sample) was calculated in the case of unfiltered and filtered data, respectively.

It should be noted that a difference of more than 10 t·ha^{-1} in the case of the Random Forests between corrected RMSE calculated using training and validation datasets could result from the small size of validation sample.

5. Discussion

In general, the MaxEnt machine learning algorithm as well as the Random Forests regression approach provided good AGB retrieval results compared to previous studies [51,52,55,58,60]. The reported analyses also used ALOS PALSAR L-band data for AGB/GSV retrieval over Siberian boreal forests. The researchers reported RMSEs between 33 and 87 m^3·ha^{-1} and 55 t·ha^{-1} at the coarser scales, and 36.4 t·ha^{-1} at 0.25 ha scale. Those results are similar to or worse than those derived in this study. The results presented in this paper showed that a relatively high estimation accuracy (down to 30%) can be obtained at a local scale. The AGB estimation showed only slightly better results when a dataset with filtered backscatter intensity was used.

When the model performance is taken into account, the MaxEnt performed better than the Random Forests. The area under the receiver operator curve (AUC) was higher than 0.7, except the AGB range from 60 to 80 t·ha^{-1}, whereas Random Forests reached an R^2 of 38.4%. MaxEnt generated AGB maps with dominantly overestimated AGB values, whereas Random Forests provided slightly underestimated values. The range of derived AGB values was underestimated but similar and differs by 10 t·ha^{-1} between the applied models. The mean AGB provided by Random Forests was comparable to the reference AGB mean. MaxEnt showed an underestimation of approximately 10 t·ha^{-1}. The estimation bias was lower in the case of Random Forests.

MaxEnt and Random Forests provided measures for evaluating the importance of the predictors used in the model construction. The algorithms showed no agreement between derived variable

rankings. In the case of MaxEnt, the coherence together with the ratio products were the most important for model construction, whereas ratio and backscatter products provided the most information in the case of modeling with Random Forests. In both cases, the ratio products seem to provide important information for AGB retrieval. Within the data groups, in the case of the MaxEnt the most important variables were the coherence between images acquired on 17 February 2009 and 20 February 2010, the normalized ratio between the backscatter from 23 August 2010 in HV and coherence, the backscatter from 23 August 2010 in HV polarization for unfiltered dataset. For filtered dataset, the most important variables within the data groups were the normalized ratio between the backscatter from 8 October 2010 in HH polarization and coherence, the coherence between images acquired on 17 February 2009 and 20 February 2010, and the backscatter image acquired on 23 August 2010 in HV polarization. In the case of Random Forests, the most important variables were the normalized ratio between the backscatter acquired on 8 October 2010 in HV polarization and coherence, the backscatter acquired on 23 August 2010 in HH polarization, and the coherence between images from 2 January 2009 and 5 January 2010 for both unfiltered and filtered datasets. The coherence images generated with the temporal baseline (B_t) greater than 46 days were superior to those derived with shorter B_t.

6. Conclusions

In this study we have demonstrated the feasibility of synergistic usage of backscatter and coherence for aboveground biomass (AGB) retrieval for boreal forests in Siberia at a local scale of 0.25 ha. This research was focused on the further exploitation of SAR data. The ALOS PALSAR L-band backscatter was combined with coherence, introducing the backscatter–coherence normalized ratio. The latter was developed based on the statistical data analysis. In total 13 variables were used for the AGB estimation. For the AGB retrieval two popular machine learning algorithms were implemented. The MaxEnt and the Random Forests performed well, showing promising AGB estimations and demonstrating the model's robustness. The corrected RMSEs were between 35.8 and 36.4 $t \cdot ha^{-1}$ and between 35.8 and 35.0 $t \cdot ha^{-1}$ for MaxEnt and Random Forests, respectively. The estimation error slightly decreased, by approximately 1%, when the filtered backscatter intensity was used. In this study, the retrieval of AGB using the SAR products was demonstrated only for Siberian unmanaged forests. It is expected that the estimation error over well-managed forests could be further reduced. Estimation improvement is also foreseen at the stand level due to the reduction of the spatial variability in the SAR data. Another issue that could have an influence on the retrieval accuracy is the reference data. Using optical remote sensing data and recommended yield tables and semi-empirical phytomass models in Russian forestry and forest management, the authors updated the old inventory data. Unfortunately, it was not possible to fully validate the obtained values in the field, hence the error in the reference data was only partially known.

The models provided different variable importance rankings. However, in both cases the normalized ratio products seem to contain important information for the model development. The coherence data were the most important in the low and high AGB ranges, whereas the ratio was most important for middle to high AGB ranges. Thus, a strategy of using different datasets for estimation of low, medium, and high AGB values could further increase biomass retrieval accuracy. It was observed that the backscatter data increased their contribution in the model construction after filtering. In terms of the retrieved AGB values, the Random Forests algorithm provided AGB mean estimation almost the same as the reference value. MaxEnt provided slightly overestimated AGB values, whereas Random Forests tended to underestimate the AGB values.

The MaxEnt and Random Forests machine learning algorithms demonstrated their potential use for forestry applications, especially for estimations in remote areas. Often no information about AGB is available in those regions. The models could be used to provide AGB estimations with relatively low estimation errors. Moreover, the results generated for different time spans could easily be applied for AGB change monitoring, which is very important from the carbon account calculations perspective.

Acknowledgments: Acknowledgments: This work was undertaken within the framework of the GMES Initial Operations—Network for Earth Observation Research Training GIONET project, grant agreement PITN-GA-2010-264509. This work was partly undertaken within the framework of the JAXA Kyoto & Carbon Initiative. H. Balzter was supported by the Royal Society Wolfson Research Merit Award, 2011/R3 and the NERC National Centre for Earth Observation. Pedro Rodriguez-Veiga was also supported by the NERC National Centre for Earth Observation. KOMPSAT-2 data were provided by the European Space Agency (project id: 13300).

The authors would like to acknowledge the support of Dmitry Schepaschenko and Anatoly Shvidenko from the International Institute for Applied Systems Analysis in updating the reference data. The authors would like to acknowledge the comments and suggestions of the reviewers.

Author Contributions: Author Contributions: Martyna A. Stelmaszczuk-Górska processed and analyzed in-situ and SAR data, modeled with the Random Forests approach, wrote the manuscript, and coordinated manuscript revisions. Pedro Rodriguez-Veiga assisted with the allometry and modelled using the MaxEnt algorithm. Nicolas Ackermann provided input for the backscatter–coherence ratio. Christian Thiel, Heiko Balzter, and Christiane Schmullius provided feedback for the study design and contributed to the manuscript.

Conflicts of Interest: Conflicts of Interest: The authors declare no conflict of interest.

References

1. Houghton, R.A.; Hall, F.; Goetz, S.J. Importance of biomass in the global carbon cycle. *J. Geophys. Res.* **2009**, *114*, 1–13. [CrossRef]
2. FAO. *Global Forest Resources. Assesment 2010. Main report*; FAO: Rome, Italy, 2010.
3. FAO. *State of the World 's Forests*; FAO: Rome, Italy, 2012.
4. Pan, Y.; Birdsey, R.A.; Fang, J.; Houghton, R.; Kauppi, P.E.; Kurz, W.A.; Phillips, O.L.; Shvidenko, A.; Lewis, S.L.; Canadell, J.G.; *et al.* A large and persistent carbon sink in the world's forests. *Science* **2011**, *333*, 988–993. [CrossRef] [PubMed]
5. Nilsson, S.; Shvidenko, A.; Jonas, M.; McCallum, I.; Thomson, A.; Balzter, H. Uncertainties of a regional terrestrial biota full carbon account: A systems analysis. *Water Air Soil Pollut. Focus* **2007**, *7*, 425–441. [CrossRef]
6. Shvidenko, A.Z.; Schepaschenko, D.G.; Vaganov, E.A.; Sukhinin, A.I.; Maksyutov, S.S.; McCallum, I.; Lakyda, I.P. Impact of wildfire in Russia between 1998–2010 on ecosystems and the global carbon budget. *Dokl. Earth Sci.* **2011**, *441*, 1678–1682. [CrossRef]
7. Kasischke, E.S.; Melack, J.M.; Dobson, M.C. The use of imaging radars for ecological applications—A review. *Remote Sens. Environ.* **1997**, *59*, 141–156. [CrossRef]
8. Rosenqvist, Å.; Milne, A.; Lucas, R.; Imhoff, M.; Dobson, C. A review of remote sensing technology in support of the Kyoto Protocol. *Environ. Sci. Policy* **2003**, *6*, 441–455. [CrossRef]
9. Patenaude, G.; Milne, R.; Dawson, T.P. Synthesis of remote sensing approaches for forest carbon estimation: Reporting to the Kyoto Protocol. *Environ. Sci. Policy* **2005**, *8*, 161–178. [CrossRef]
10. McCallum, I.; Wagner, W.; Schmullius, C.; Shvidenko, A.; Obersteiner, M.; Fritz, S.; Nilsson, S. Satellite-based terrestrial production efficiency modeling. *Carbon Balance Manag.* **2009**, *4*. [CrossRef] [PubMed]
11. Goetz, S.; Baccini, A.; Laporte, N.; Johns, T.; Walker, W.; Kellndorfer, J.; Houghton, R.; Sun, M. Mapping and monitoring carbon stocks with satellite observations: A comparison of methods. *Carbon Balance Manag.* **2009**, *4*, 1–7. [CrossRef] [PubMed]
12. Frolking, S.; Palace, M.W.; Clark, D.B.; Chambers, J.Q.; Shugart, H.H.; Hurtt, G.C. Forest disturbance and recovery: A general review in the context of spaceborne remote sensing of impacts on aboveground biomass and canopy structure. *J. Geophys. Res.* **2009**, *114*. [CrossRef]
13. Thiel, C.; Santoro, M.; Cartus, O.; Thiel, C.; Riedel, T.; Schmullius, C. Perspectives of SAR based forest cover, forest cover change and biomass mapping. In *The Kyoto Protocol: Economic Assessments, Implementation Mechanisms, and Policy implications*; Vasser, C.P., Ed.; Nova Science Publishers, Inc.: New York, 2009; pp. 13–56.
14. Goetz, S.; Dubayah, R. Advances in remote sensing technology and implications for measuring and monitoring forest carbon stocks and change. *Carbon Manag.* **2011**, *2*, 231–244. [CrossRef]
15. Zolkos, S.G.; Goetz, S.J.; Dubayah, R. A meta-analysis of terrestrial aboveground biomass estimation using lidar remote sensing. *Remote Sens. Environ.* **2013**, *128*, 289–298. [CrossRef]
16. GOFC-GOLD. *A Sourcebook of Methods and Procedures for Monitoring and Reporting Anthropogenic Greenhouse Gas Emissions and Removals Associated with Deforestation, Gains and Losses of Carbon Stocks in Forests Remaining Forests, and Forestation. GOFC-GOLD Report Versio*; GOFC-GOLD: Wageningen, The Netherlands, 2014.

17. Sader, S.A.; Waide, R.B.; Lawrence, W.T.; Joyce, A.T. Tropical Forest Biomass and Successional Age Class Relationships to a Vegetation Index Derived from Landsat TM Data. *Remote Sens. Environ.* **1989**, *28*, 143–156. [CrossRef]
18. Wasseige, C.; de Defourny, P. Retrieval of tropical forest structure characteristics from bi-directional reflectance of SPOT images. *Remote Sens. Environ.* **2002**, *83*, 362–375. [CrossRef]
19. Dong, J.; Kaufmann, R.K.; Myneni, R.B.; Tucker, C.J.; Kauppi, P.E.; Liski, J.; Buermann, W.; Alexeyev, V.; Hughes, M.K. Remote sensing estimates of boreal and temperate forest woody biomass: Carbon pools, sources, and sinks. *Remote Sens. Environ.* **2003**, *84*, 393–410. [CrossRef]
20. Joshi, C.; Leeuw, J.; de Skidmore, A.K.; Duren, I.C.; van Oosten, H. Remotely sensed estimation of forest canopy density: A comparison of the performance of four methods. *Int. J. Appl. Earth Obs. Geoinf.* **2006**, *8*, 84–95. [CrossRef]
21. Avitabile, V.; Herold, M.; Henry, M.; Schmullius, C. Mapping biomass with remote sensing: a comparison of methods for the case study of Uganda. *Carbon Balance Manag.* **2011**, *6*. [CrossRef] [PubMed]
22. Houghton, R.A. Balancing the Global Carbon Budget. *Annu. Rev. Earth Planet. Sci.* **2007**, *35*, 313–347. [CrossRef]
23. Ji, L.; Wylie, B.K.; Nossov, D.R.; Peterson, B.; Waldrop, M.P.; McFarland, J.W.; Rover, J.; Hollingsworth, T.N. Estimating aboveground biomass in interior Alaska with Landsat data and field measurements. *Int. J. Appl. Earth Obs. Geoinf.* **2012**, *18*, 451–461. [CrossRef]
24. Lefsky, M.A.; Harding, D.J.; Keller, M.; Cohen, W.B.; Carabajal, C.C.; Del Bom Espirito-Santo, F.; Hunter, M.O.; de Oliveira, R. Estimates of forest canopy height and aboveground biomass using ICESat. *Geophys. Res. Lett.* **2005**, *32*, 22–25. [CrossRef]
25. Nelson, R.; Ranson, K.J.; Sun, G.; Kimes, D.S.; Kharuk, V.; Montesano, P. Estimating Siberian timber volume using MODIS and ICESat/GLAS. *Remote Sens. Environ.* **2009**, *113*, 691–701. [CrossRef]
26. Duncanson, L.I.; Niemann, K.O.; Wulder, M.A. Estimating forest canopy height and terrain relief from GLAS waveform metrics. *Remote Sens. Environ.* **2010**, *114*, 138–154. [CrossRef]
27. Simard, M.; Pinto, N.; Fisher, J.B.; Baccini, A. Mapping forest canopy height globally with spaceborne lidar. *J. Geophys. Res.* **2011**, *116*. [CrossRef]
28. Khalefa, E.; Smit, I.P.J.; Nickless, A.; Archibald, S.; Comber, A.; Balzter, H. Retrieval of savanna vegetation canopy height from ICESat-GLAS spaceborne LiDAR with terrain correction. *IEEE Geosci. Remote Sens. Lett.* **2013**, *10*, 1439–1443. [CrossRef]
29. Le Toan, T.; Beaudoin, A.; Riom, J.; Guyon, D. Relating forest biomass to SAR data. *IEEE Trans. Geosci. Remote Sens.* **1992**, *30*, 403–411. [CrossRef]
30. Kurvonen, L.; Pulliainen, J.; Hallikainen, M. Retrieval of biomass in boreal forests from multitemporal ERS-1 and JERS-1 SAR images. *IEEE Trans. Geosci. Remote Sens.* **1999**, *37*, 198–205. [CrossRef]
31. Rignot, E.; Way, J.; Williams, C.; Viereck, L. Radar estimates of aboveground biomass in boreal forests of interior Alaska. *IEEE Trans. Geosci. Remote Sens.* **1994**, *32*, 1117–1124. [CrossRef]
32. Le Toan, T.; Quegan, S.; Davidson, M.W.J.; Balzter, H.; Paillou, P.; Papathanassiou, K.; Plummer, S.; Rocca, F.; Saatchi, S.; Shugart, H.; *et al.* The BIOMASS mission: Mapping global forest biomass to better understand the terrestrial carbon cycle. *Remote Sens. Environ.* **2011**, *115*, 2850–2860. [CrossRef]
33. Natale, A.; Guida, R.; Bird, R.; Whittaker, P.; Cohen, M.; Hall, D. Demonstration and analysis of the applications of S-band SAR. In Proceedings of the APSAR (The Asia-Pacific Conference on Synthetic Aperture Radar), Seoul, Korea, 26–30 September 2011.
34. Beaudoin, A.; Le Toan, T.; Goze, S.; Nezry, E.; Lopes, A.; Mougin, E.; Hsu, C.C.; Han, H.C.; Kong, J.A.; Shin, R.T. Retrieval of forest biomass from SAR data. *Int. J. Remote Sens.* **1994**, *15*, 2777–2796. [CrossRef]
35. Dobson, M.C.; Ulaby, F.T.; Pierce, L.E.; Sharik, T.L.; Bergen, K.M.; Kellndorfer, J.; Kendra, J.R.; Li, E.; Lin, Y.C.; Nashashibi, A.; *et al.* Estimation of forest biophysical characteristics in Northern Michigan with SIR-C/X-SAR. *IEEE Trans. Geosci. Remote Sens.* **1995**, *33*, 877–895. [CrossRef]
36. Ranson, K.J.; Sun, G. Mapping biomass of a northern forest using multifrequency SAR data. *IEEE Trans. Geosci. Remote Sens.* **1994**, *32*, 388–396. [CrossRef]
37. Pulliainen, J.T.; Heiska, K.; Hyyppa, J.; Hallikainen, M.T. Backscattering properties of boreal forests at the C- and X-bands. *IEEE Trans. Geosci. Remote Sens.* **1994**, *32*, 1041–1050. [CrossRef]
38. Fransson, J.E.S.; Israelsson, H. Estimation of stem volume in boreal forests using ERS-1 C- and JERS-1 L-band SAR data. *Int. J. Remote Sens.* **1999**, *20*, 123–137. [CrossRef]

39. Solberg, S.; Astrup, R.; Gobakken, T.; Næsset, E.; Weydahl, D.J. Estimating spruce and pine biomass with interferometric X-band SAR. *Remote Sens. Environ.* **2010**, *114*, 2353–2360. [CrossRef]
40. Askne, J.; Fransson, J.; Santoro, M.; Soja, M.; Ulander, L. Model-based biomass estimation of a hemi-boreal forest from multitemporal TanDEM-X acquisitions. *Remote Sens.* **2013**, *5*, 5574–5597. [CrossRef]
41. Koskinen, J.T.; Pulliainen, J.T.; Hyyppä, J.M.; Engdahl, M.E.; Hallikainen, M.T. The seasonal behavior of interferometric coherence in boreal forest. *IEEE Trans. Geosci. Remote Sens.* **2001**, *39*, 820–829. [CrossRef]
42. Santoro, M.; Askne, J.; Smith, G.; Fransson, J.E.S. Stem volume retrieval in boreal forests from ERS-1/2 interferometry. *Remote Sens. Environ.* **2002**, *81*, 19–35. [CrossRef]
43. Næsset, E.; Bollandsås, O.M.; Gobakken, T.; Solberg, S.; McRoberts, R.E. The effects of field plot size on model-assisted estimation of aboveground biomass change using multitemporal interferometric SAR and airborne laser scanning data. *Remote Sens. Environ.* **2015**, *168*, 252–264. [CrossRef]
44. Papathanassiou, K.P.; Cloude, S.R. Single-baseline polarimetric SAR interferometry. *IEEE Trans. Geosci. Remote Sens.* **2001**, *39*, 2352–2363. [CrossRef]
45. Neumann, M.; Saatchi, S.S.; Ulander, L.M.H.; Fransson, J.E.S. Assessing performance of L- and P-Band polarimetric interferometric SAR data in estimating boreal forest above-ground biomass. *IEEE Trans. Geosci. Remote Sens.* **2012**, *50*, 714–726. [CrossRef]
46. Tebaldini, S.; Rocca, F. Multibaseline polarimetric SAR tomography of a boreal forest at P- and L-bands. *IEEE Trans. Geosci. Remote Sens.* **2012**, *50*, 232–246. [CrossRef]
47. Persson, H.; Fransson, J. Forest variable estimation using radargrammetric processing of TerraSAR-X images in boreal forests. *Remote Sens.* **2014**, *6*, 2084–2107. [CrossRef]
48. Vastaranta, M.; Niemi, M.; Karjalainen, M.; Peuhkurinen, J.; Kankare, V.; Hyyppä, J.; Holopainen, M. Prediction of forest stand attributes using TerraSAR-X stereo imagery. *Remote Sens.* **2014**, *6*, 3227–3246. [CrossRef]
49. Askne, J.; Santoro, M.; Smith, G.; Fransson, J.E. S. Multitemporal repeat-rass SAR interferometry of boreal forests. *IEEE Trans. Geosci. Remote Sens.* **2003**, *41*, 1540–1550. [CrossRef]
50. Santoro, M.; Shvidenko, A.; Mccallum, I.; Askne, J.; Schmullius, C. Properties of ERS-1/2 coherence in the Siberian boreal forest and implications for stem volume retrieval. *Remote Sens. Environ.* **2007**, *106*, 154–172. [CrossRef]
51. Peregon, A.; Yamagata, Y. The use of ALOS/PALSAR backscatter to estimate above-ground forest biomass: A case study in Western Siberia. *Remote Sens. Environ.* **2013**, *137*, 139–146. [CrossRef]
52. Chowdhury, T.A.; Thiel, C.; Schmullius, C. Growing stock volume estimation from L-band ALOS PALSAR polarimetric coherence in Siberian forest. *Remote Sens. Environ.* **2014**, *155*, 129–144. [CrossRef]
53. Balzter, H.; Talmon, E.; Wagner, W.; Gaveau, D.; Plummer, S.; Yu, J.J.; Quegan, S.; Davidson, M.; Le Toan, T.; Gluck, M.; Shvidenko, A.; Nilsson, S.; Tansey, K.; Luckman, A.; Schmullius, C. Accuracy assessment of a large-scale forest cover map of central Siberia from synthetic aperture radar. *Can. J. Remote Sens.* **2002**, *28*, 719–737. [CrossRef]
54. Wagner, W.; Luckman, A.; Vietmeier, J.; Tansey, K.; Balzter, H.; Schmullius, C.; Davidson, M.; Gaveau, D.; Gluck, M.; Le, T.; *et al.* Large-scale mapping of boreal forest in SIBERIA using ERS tandem coherence and JERS backscatter data. *Remote Sens.* **2003**, *85*, 125–144. [CrossRef]
55. Santoro, M.; Eriksson, L.; Askne, J.; Schmullius, C. Assessment of stand-wise stem volume retrieval in boreal forest from JERS-1 L-band SAR backscatter. *Int. J. Remote Sens.* **2006**, *27*, 3425–3454. [CrossRef]
56. Santoro, M.; Beer, C.; Cartus, O.; Schmullius, C.; Shvidenko, A.; Mccallum, I.; Wegmüller, U.; Wiesmann, A. Retrieval of growing stock volume in boreal forest using hyper-temporal series of Envisat ASAR ScanSAR backscatter measurements. *Remote Sens. Environ.* **2011**, *115*, 490–507. [CrossRef]
57. Santoro, M.; Cartus, O.; Fransson, J.; Shvidenko, A.; McCallum, I.; Hall, R.; Beaudoin, A.; Beer, C.; Schmullius, C. Estimates of Forest Growing Stock Volume for Sweden, Central Siberia, and Québec Using Envisat Advanced Synthetic Aperture Radar Backscatter Data. *Remote Sens.* **2013**, *5*, 4503–4532. [CrossRef]
58. Wilhelm, S.; Hüttich, C.; Korets, M.; Schmullius, C. Large area mapping of boreal Growing Stock Volume on an annual and multi-temporal level using PALSAR L-band backscatter mosaics. *Forests* **2014**, *5*, 1999–2015. [CrossRef]

59. Hüttich, C.; Korets, M.; Bartalev, S.; Zharko, V.; Schepaschenko, D.; Shvidenko, A.; Schmullius, C. Exploiting Growing Stock Volume Maps for Large Scale Forest Resource Assessment: Cross-Comparisons of ASAR- and PALSAR-Based GSV Estimates with Forest Inventory in Central Siberia. *Forests* **2014**, *5*, 1753–1776. [CrossRef]
60. Rodriguez-Veiga, P.; Stelmaszczuk-Górska, M.; Hüttich, C.; Schmullius, C.; Tansey, K.; Balzter, H. Aboveground Biomass Mapping in Krasnoyarsk Kray (Central Siberia) using Allometry, Landsat, and ALOS PALSAR. In Proceedings of the RSPSoc Annual Conference; Remote Sensing and Photogrammetry Society, Aberystwyth, Wales, 2–5 September 2014.
61. Phillips, S.J.; Anderson, R.P.; Schapire, R.E. Maximum entropy modeling of species geographic distributions. *Ecol. Model.* **2006**, *190*, 231–259. [CrossRef]
62. Elith, J.; Kearney, M.; Phillips, S. The art of modelling range-shifting species. *Methods Ecol. Evol.* **2010**, *1*, 330–342. [CrossRef]
63. Elith, J.; Phillips, S.J.; Hastie, T.; Dudík, M.; Chee, Y.E.; Yates, C.J. A statistical explanation of MaxEnt for ecologists. *Divers. Distrib.* **2011**, *17*, 43–57. [CrossRef]
64. Saatchi, S.S.; Harris, N.L.; Brown, S.; Lefsky, M.; Mitchard, E.T.A; Salas, W.; Zutta, B.R.; Buermann, W.; Lewis, S.L.; Hagen, S.; *et al.* Benchmark map of forest carbon stocks in tropical regions across three continents. *Proc. Natl. Acad. Sci. USA* **2011**, *108*, 9899–9904. [CrossRef] [PubMed]
65. Breiman, L. Random Forests. *Mach. Learn.* **2001**, *45*, 5–32. [CrossRef]
66. Cutler, D.R.; Edwards, T.C.; Beard, K.H.; Cutler, A.; Hess, K.T.; Gibson, J.; Lawler, J.J. Random forests for classification in ecology. *Ecology* **2007**, *88*, 2783–2792. [CrossRef] [PubMed]
67. Hüttich, C.; Herold, M.; Strohbach, B.J.; Dech, S. Integrating in-situ, Landsat, and MODIS data for mapping in Southern African savannas: Experiences of LCCS-based land-cover mapping in the Kalahari in Namibia. *Environ. Monit. Assess.* **2011**, *176*, 531–547. [CrossRef] [PubMed]
68. Prasad, A.M.; Iverson, L.R.; Liaw, A. Newer classification and regression tree techniques: Bagging and random forests for ecological prediction. *Ecosystems* **2006**, *9*, 181–199. [CrossRef]
69. Walker, W.S.; Kellndorfer, J.M.; Lapoint, E.; Hoppus, M.; Westfall, J. An empirical InSAR-optical fusion approach to mapping vegetation canopy height. *Remote Sens. Environ.* **2007**, *109*, 482–466. [CrossRef]
70. Houghton, R.A.; Butman, D.; Bunn, A.G.; Krankina, O.N.; Schlesinger, P.; Stone, T.A. Mapping Russian forest biomass with data from satellites and forest inventories. *Environ. Res. Lett.* **2007**, *2*. [CrossRef]
71. Avitabile, V.; Baccini, A.; Friedl, M.A.; Schmullius, C. Capabilities and limitations of Landsat and land cover data for aboveground woody biomass estimation of Uganda. *Remote Sens. Environ.* **2012**, *117*, 366–380. [CrossRef]
72. Cartus, O.; Kellndorfer, J.; Rombach, M.; Walker, W. Mapping Canopy Height and Growing Stock Volume Using Airborne Lidar, ALOS PALSAR and Landsat ETM+. *Remote Sens.* **2012**, *4*, 3320–3345. [CrossRef]
73. Cartus, O.; Kellndorfer, J.; Walker, W.; Franco, C.; Bishop, J.; Santos, L.; Fuentes, J. A National, Detailed Map of Forest Aboveground Carbon Stocks in Mexico. *Remote Sens.* **2014**, *6*, 5559–5588. [CrossRef]
74. Baccini, A.; Laporte, N.; Goetz, S.J.; Sun, M.; Dong, H. A first map of tropical Africa's above-ground biomass derived from satellite imagery. *Environ. Res. Lett.* **2008**, *3*. [CrossRef]
75. Fassnacht, F.E.; Hartig, F.; Latifi, H.; Berger, C.; Hernández, J.; Corvalán, P.; Koch, B. Importance of sample size, data type and prediction method for remote sensing-based estimations of aboveground forest biomass. *Remote Sens. Environ.* **2014**, *154*, 102–114. [CrossRef]
76. JAXA Earth Observation Research Center (EORC) ALOS Kyoto & Carbon Initiative. Available online: http://www.eorc.jaxa.jp/ALOS/en/kyoto/kyoto_index.htm (accessed on 13 April 2015).
77. Schmullius, P.C.; (Friedrich-Schiller-University Jena, Germany); Thiel, C.; (Friedrich-Schiller-University Jena, Germany). *Proposal to JAXA for K & C Phase 3 PALSAR Intensities and Coherence for Forest Cover and Forest Cover Change Mapping and Biomass Retrieval*; Unpublished, 2011.
78. Friedrich-Schiller-University Siberian Earth System Science Cluster. Available online: http://www.sibessc.uni-jena.de/ (accessed on 20 June 2012).
79. Schmullius, C.; Baker, J.; Balzter, H.; Davidson, M.; Eriksson, L.; Gaveau, D.; Gluck, M.; Holz, A.; Le Toan, T.; Luckman, A.; *et al.* *SAR Imaging for Boreal Ecology and Radar Interferometry Applications SIBERIA project (Contract No. ENV4-CT97-0743-SIBERIA) – Final Report*; Friedrich-Schiller-University: Jena, Germany, 2001. Available online: http://www.siberia1.uni-jena.de/pdf_files/final_report.pdf (accessed on 11 January 2012).

80. Shvidenko, A.; Schepaschenko, D.; Nilsson, S.; Bouloui, Y. Semi-empirical models for assessing biological productivity of Northern Eurasian forests. *Ecol. Modell.* **2007**, *204*, 163–179. [CrossRef]
81. Shvidenko, A.; Schepaschenko, D.; Nilsson, S.; Boului, Y. *Tables and Models of Growth and Productivity of Forests of Major Forming Species of Northern Eurasia (standard and reference materials)*; Federal Agency of Forest Management: Moscow, Russia, 2008.
82. Van Laar, A.; Akca, A. *Forest Mensuration*; von Gadow, K., Pukkala, T., Tome, M., Eds.; Springer: Dordrecht, The Netherlands, 2007; Volume 13.
83. IIASA Russian Forests & Forestry. Live Biomass & Net Primary Production—Measurements of Forest Phytomass *in situ*. Available online: http://webarchive.iiasa.ac.at/Research/FOR/forest_cdrom/english/for_prod_en.html (accessed on 20 May 2013).
84. Ulander, L.M.H. Radiometrie slope correction of synthetic-aperture radar images. *IEEE Trans. Geosci. Remote Sens.* **1996**, *34*, 1115–1122. [CrossRef]
85. Rignot, E.J.; Zimmermann, R.; Zyl, J.J. Van Spaceborne applications of P-band imaging radars for measuring forest biomass. *IEEE Trans. Geosci. Remote Sens.* **1995**, *33*, 1162–1169. [CrossRef]
86. Pulliainen, J.T.; Mikkela, P.J.; Hallikainen, M.T.; Ikonen, J. Seasonal dynamics of C-band backscatter of boreal forests with applications to biomass and soil moisture estimation. *IEEE Trans. Geosci. Remote Sens.* **1996**, *34*, 758–770. [CrossRef]
87. Quegan, S.; Le Toan, T.; Yu, J.J.; Ribbes, F.; Floury, N. Multitemporal ERS SAR analysis applied to forest mapping. *IEEE Trans. Geosci. Remote Sens.* **2000**, *38*, 741–753. [CrossRef]
88. Born, M.; Wolf, E. *Principles of Optics*, 7th ed.; Cambridge University Press: Cambridge, UK, 1999.
89. Bamler, R.; Hartl, P. Synthetic aperture radar interferometry. *Inverse Probl.* **1998**, *14*, R1–R54. [CrossRef]
90. Jarvis, A.; Reuter, H.I.; Nelson, A.; Guevara, E. Hole-Filled Seamless SRTM Data V4, International Centre for Tropical Agriculture (CIAT). Available online: http://srtm.csi.cgiar.org (accessed on 4 February 2013).
91. Reuter, H.I.; Nelson, A.; Jarvis, A. An evaluation of void filling interpolation methods for SRTM data. *Int. J. Geogr. Inf. Sci.* **2007**, *21*, 983–1008. [CrossRef]
92. Wegmüller, U.; Werner, C.; Strozzi, T. SAR Interferometric and Differential Interferometric Processing Chain. In Proceedings of the IGARSS'98; IEEE Publications: Seattle, WA, USA, 1998; pp. 1106–1108. [CrossRef]
93. Breiman, L.; Cutler, A. Breiman and Cutler's random forests for classification and regression. Available online: https://cran.r-project.org/web/packages/randomForest/randomForest.pdf (accessed on 18 February 2014).
94. Federal Forestry Agency. *Manual on Forest Inventory and Planning in Russian Forest*; Federal Forestry Agency: Moscow, Russia, 1995.
95. Shvidenko, A.Z.; Gustafson, E.; Mcguire, A.D.; Kharuk, V.I.; Schepaschenko, D.G.; Shugart, H.H.; Tchebakova, N.M.; Vygodskaya, N.N.; Onuchin, A.A.; Hayes, D.J.; *et al*. Terrestrial ecosystems and their change. In *Regional Environmental Changes in Siberia and Their Global Consequences*; Groisman, P.Y., Gutman, G., Eds.; Springer Environmental Science and Engineering: Dordrecht, The Netherlands, 2013; pp. 171–249.
96. Fielding, A.H.; Bell, J.F. A review of methods for the assessment of prediction errors in conservation presence/absence models. *Environ. Conserv.* **1997**, *24*, 38–49. [CrossRef]

4.4 Multi-frequency SAR for estimation of aboveground biomass

This section presents the recent research contribution the manuscript entitled "Estimation of above-ground biomass over boreal forests in Siberia using updated in situ, ALOS-2 PALSAR-2, and RADARSAT-2 data" prepared and written by Stelmaszczuk-Górska, M. A., Urbazaev, M., Schmullius C. & Thiel, C.

The manuscript was peer-reviewed and published in
Remote Sensing 10(10), *1550: 1-20;* Special Issue: *The Kyoto and Carbon Initiative—Environmental Applications by ALOS-2 PALSAR-2*
doi: 10.3390/rs10101550

remote sensing

MDPI

Article

Estimation of Above-Ground Biomass over Boreal Forests in Siberia Using Updated In Situ, ALOS-2 PALSAR-2, and RADARSAT-2 Data

Martyna A. Stelmaszczuk-Górska [1,*], Mikhail Urbazaev [1,2], Christiane Schmullius [1] and Christian Thiel [1]

[1] Department for Earth Observation, Friedrich-Schiller-University Jena, Loebdergraben 32, 07743 Jena, Germany; mikhail.urbazaev@uni-jena.de (M.U.); c.schmullius@uni-jena.de (C.S.); christian.thiel@uni-jena.de (C.T.)

[2] International Max Planck Research School for Global Biogeochemical Cycles, Max Planck Institute for Biogeochemistry, Hans-Knoell-Str. 10, 07745 Jena, Germany

* Correspondence: m.stelmas@uni-jena.de; Tel.: +49-3641-9488-71

Received: 12 August 2018; Accepted: 19 September 2018; Published: 26 September 2018

check for updates

Abstract: The estimation of above-ground biomass (AGB) in boreal forests is of special concern as it constitutes the highest carbon pool in the northern hemisphere. Particularly, monitoring of the forests in the Russian Federation is important as some regions have not been inventoried for many years. This study explores the combination of multi-frequency, multi-polarization, and multi-temporal radar data as one key approach to provide an accurate estimate of forest biomass. The data from L-band Advanced Land Observing Satellite 2 (ALOS-2) Phased Array L-Band Synthetic Aperture Radar 2 (PALSAR-2), together with C-band RADARSAT-2 data, were applied for AGB estimation. Backscatter coefficients from L- and C-band radar were used independently and in combination with a non-parametric model to retrieve AGB data for a boreal forest in Siberia (Krasnoyarskiy Kray). AGB estimation was performed using the random forests machine learning algorithm. The results demonstrated that high estimation accuracies can be achieved at a spatial resolution of 0.25 ha. When the L-band data alone were used for the retrieval, a corrected root-mean-square error ($RMSE_{cor}$) of 29.4 t ha^{-1} was calculated. A marginal decrease in $RMSE_{cor}$ was observed when only the filtered L-band backscatter data, without ratio and texture, were used (29.1 t ha^{-1}). The inclusion of the C-band data reduced the over and underestimation; the bias was reduced from 5.5 t ha^{-1} to 4.7 t ha^{-1}; and a $RMSE_{cor}$ of 30.2 t ha^{-1} was calculated.

Keywords: SAR; boreal forest; above-ground biomass; backscatter; ALOS-2 PALSAR-2; RADARSAT-2

1. Introduction

The importance of forests and above-ground forest biomass (AGB) are manifold. On the one hand, they strongly influence climate change as they act as a carbon sink taking part in the global carbon cycle. However, on the other hand, they are essential to the economy as a source of renewable energy and valuable forest products such as wood, paper, and pulp. Since one-third of the total forest area is used for production purposes, forest policies rely on quantitative estimates of the current and future forest biomass.

Above-ground biomass is defined as the amount of all organic matter growing above ground per unit area at a particular time (t ha^{-1}, Mg ha^{-1} or kg m^{-2}) [1]. It is an essential climate variable [2] that is applied in climate-related global vegetation models [3]. In forestry, the total tree AGB is measured either from ground measurements by felling a tree or using tree-level regression models [4]. The models are based on the allometric relation between biomass and tree elements such as the height and/or

diameter at the breast height (dbh). However, due to the sampling nature of the field measurements, and their high acquisition costs, they are limited in time and space. The measurements are carried out by the national forest inventories which are afterwards used for producing forest policies at local, regional, and national levels. Furthermore, the national forest inventories are obligated to report the distribution of the forest AGB to the Food and Agriculture Organization of the United Nations (FAO) as per the Global Forest Resources Assessment (FRA) [5]. The estimation of AGB in boreal forests is of special concern as it constitutes the highest carbon pool in the northern hemisphere. The total forest carbon in boreal forests in Asia was estimated to be 22.1 ± 8.3 Pg C, with a mean carbon density of 4.00 ± 1.54 kg C m^{-2} [6]. Data collection for the FRA 2020 has begun in 2018, even though in many countries up-to-date quantitative estimates on the AGB are not available. For example, in the Russian Federation, which has the largest forest area in the world, some forest regions have not been recorded for more than 25 years [7]. At the same time, due to more frequent fires and illegal logging, (which is estimated to make up approximately 20% of all logging activity in Russia), according to the World Bank and the World Wide Fund for Nature (WWF) [8], the AGB experiences dynamic change within a given period of time. Therefore, it is crucial to support national efforts in providing accurate and up-to-date AGB estimates. This can be achieved by means of e earth observation techniques. Even though remote sensing does not provide a direct measurement of AGB, satellite technology together with prior information, e.g., insitu measurements, allow accurate and relatively cost-efficient AGB estimates. In particular, synthetic aperture radar (SAR) systems are of interest as they provide systematic, weather and sun independent observations. Moreover, SAR shows higher sensitivity to AGB in comparison with the optical sensors [9]. The latest results of biomass estimation using optical data (Landsat) showed measures of moderate accuracy, with a relative mean absolute error (*rMAE*) of approximately 36%, in the boreal zone [10].

For more than 30 years SAR data have been investigated in the context of forest biomass or volume retrieval. In the early 1990s, the airborne platforms (HUTSCAT scatterometer, AIRSAR flying laboratory) were used, after which data from the spaceborne sensors were investigated (ERS-1/2, JERS-1). Studies were mainly conducted over boreal forests because the spaceborne SAR data, despite the saturation effect, were found to have sufficient sensitivity for the estimated biomass ranges, showing correlation coefficients of up to approximately 0.9 [11–14]. Forest biomass has been estimated using parametric empirical [15–17], semi-empirical and physical models [18–20]. With the availability of new algorithms, e.g., machine learning, non-parametric models have been introduced [21–23].

In boreal forests the focus was mainly on the estimation of growing stock volume (GSV); i.e., wood volume above ground per unit area in m^3 ha^{-1}. However, only a few studies were about AGB retrieval. The researchers successfully applied the following SAR properties to estimate the GSV or AGB: backscattering intensity [24–26], interferometric SAR (InSAR) [20,27–30], polarimetric signature [31–33], as well as SAR tomography and radargrammetry [34–36]. It was found that the backscatter data acquired under unfrozen conditions are superior to winter acquisitions [37,38]. In particular, spaceborne SAR data at longer wavelengths, e.g., L-band due to its deeper penetration into the forest canopy and higher saturation level, have provided accurate estimates of GSV or AGB [39,40]. Data in one frequency were mainly used. Multi-frequency approaches were investigated estimating AGB from the airborne AIRSAR sensor (C-, L-, and P-band) [40,41], as well as using data acquired by the spaceborne imaging radar mission SIR-C/X-SAR [14,42–44], or classifying GSV levels from the ERS-1/2 InSAR coherence and JERS-1 backscatter data [45]. No further research using multi-frequency approach has been found over boreal forests. Recent multi-frequency SAR analyses have been reported only in the case of AGB estimation over temperate and Mediterranean forests [46–48], tropical forests [49–51], mangrove forests [52], and mapping savannah woody structures [53].

For the boreal forests, a biomass (AGB or GSV) estimation error of approximately 20% was calculated for forest stands greater than 10 ha [40,54–57] or approximately 40% for a spatial resolution of 25 m [7,22]. Current studies using X-band interferometric SAR height information derived over highly managed forest, reported an estimation error of 16% [20]. Over poorly managed Siberian

boreal forests the GSV or AGB estimation error can range from 15% to more than 50% depending on: (i) spatial resolution; (ii) type and number of observations; (iii) environmental and forest stand conditions; and (iv) quality of reference data [7,19,22,55–61]. The lowest estimation error for GSV of 15%was calculated using hyper-temporal C-band data at a resolution of 0.5° [19]. Multi-temporal approaches performed better than mono-temporal as they compensate for changing weather conditions, and show better model transferability [25,62]. For L-band data the retrieval error was calculated to be 25% in the best cases using backscatter data (46 t ha^{-1}) [56], or InSAR coherence (44 m^3 ha^{-1}) [61]. The root-mean-square error (*RMSE*) of 16 m^3 ha^{-1} was calculated using the polarimetric HHVV-coherence for forest stands larger than 30 ha and relative stocking greater than 70% [57]. When multi-temporal HHVV-coherence was combined with multi-temporal HV-backscatter the *RMSE* of 32.2 m^3 ha^{-1} was reported [33]. The L-band data in HV polarization showed only slightly better potential for GSV or AGB estimation than backscatter in HH polarization for Siberian boreal forests [23,61]. The InSAR coherence and the multi-temporal speckle filtered backscatter data have been shown to be of the highest importance for AGB estimation [23]. The repeat-pass coherence calculated from data acquired under frozen (winter) and stable conditions demonstrated potential for use for biomass estimation over Siberian forests [23,61,63].

Analysis of the previous mentioned results showed that only a few studies implemented multi-frequency SAR data for biomass retrieval over boreal forests. As also highlighted by Santoro and Cartus [64] in their survey study, there is still "an almost unexplored field of investigation for forest biomass retrieval" using multi-frequency, multi-temporal SAR as well as multi-temporal metrics, textural parameters, and *n*-th intensity moment of histograms.

This paper discusses the application of multi-frequency, multi-polarization, and multi-temporal data for forest biomass estimation. Therefore, the results should be of special interest for researchers dealing with AGB estimation. The use of multi-frequency, multi-polarization, and multi-temporal SAR data is of particular interest, due to the long-term data security within new and upcoming SAR missions; e.g., PAZ, Sentinel-1-C/D, NISAR, SAOCOM, ALOS-4 PALSAR-3, TanDEM-L, and BIOMASS. In summary, the aim of this paper is to:

1. investigate for the first time the multi-frequency, multi-polarization, and multi-temporal SAR observations from SAR C- and L-band backscatter using a non-parametric algorithm for AGB estimation over boreal forests;
2. examine the merit of the additional measures from the SAR backscatter for AGB retrieval.

2. Study Area and Data

2.1. Study Area

Siberia is a vast region in Russia that accounts for more than three-quarters of the country's land. The region is divided into three main parts: Western, Central and Eastern Siberia. In this study, a research area located in the southern part of Central Siberia was investigated for AGB estimation (Figure 1). The study area belongs to the Bolshe Murtinsky forest enterprise, located in the boreal forest ecosystem with a total carbon density (tree stems + branches + roots + foliage) of more than 6 kg C m^{-2} [6]. Forests in the area of interest are dense and partially managed with dynamic logging activities. They are characterized by a continental climate with long, severe winters and short, warm, and wet summers. From mid-October until the beginning of April, the mean temperature is approximately −15 °C, while in summer the mean temperature is approximately +15 °C. The annual precipitation is below 450 millimetres. The dominant tree species are Fir (*Abies sibirica*), Birch (*Betula pendula, Betula pubescens*), Aspen (*Populus tremula*), Siberian Pine (*Pinus sibirica*), Pine (*Pinus sylvestris*), Spruce (*Picea obovota*) and Larch (*Larix sibirica, Larix dahurica*). In terms of topography, the study area has a gentle relief with heights from 150 m above sea level (a.s.l.) up to 520 m a.s.l., with an average height of 280 m a.s.l. The slopes range from 0° to 36°, with a mean value of 8°.

The research covered an area of more than 210 km^2 and consisted of overlapping remote sensing data along with updated inventory data.

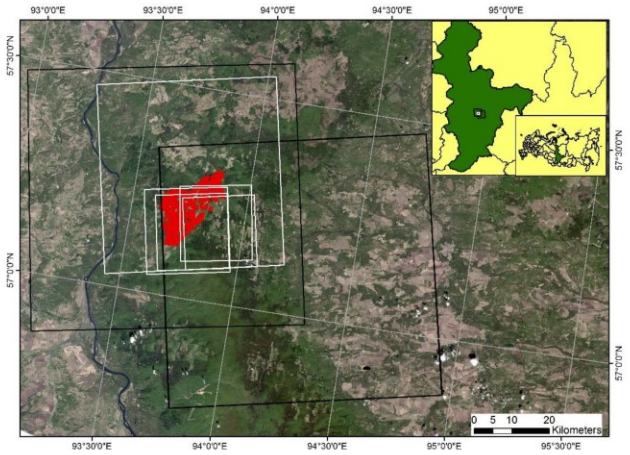

Figure 1. Location of the study area: footprints in black and white represent ALOS-2 PALSAR-2 and RADARSAT-2, respectively; the in situ measurements are presented in red. Landsat 5 Imagery acquired on 2 June 2007 is shown in the background. Landsat Image courtesy of the U.S. Geological Survey.

2.2. Above-Ground Biomass Reference Data

AGB reference data were derived from the growing stock volume (GSV) values collected and reported in the State Forest Account [65]. The forest inventory consisted of a polygon layer and the associated attribute table. For each forest stand, i.e., homogenous area in terms of forest structure and composition as well as geology, the following information was available: land category, density, age of dominant species, mean height, mean diameter at 1.3 meters above ground (dbh), and GSV calculated from these measurements. This inventory dated back to 1998. Because of the gap of 16 years between the inventory and the SAR data acquisitions, the field data were updated to = 2014 (see Section 3.1 for more details). The resulting AGB values are presented in the histogram (Figure 2) and ranged from 0 (non-forest) to 211 t ha^{-1}, with a mean value of 94 t ha^{-1}. The forest stand size varied from 3 ha to 127 ha, with a mean value of 18.5 ha. The stand age varied from 0 years to 292 years. In total, 494 forest stands were available for the investigation.

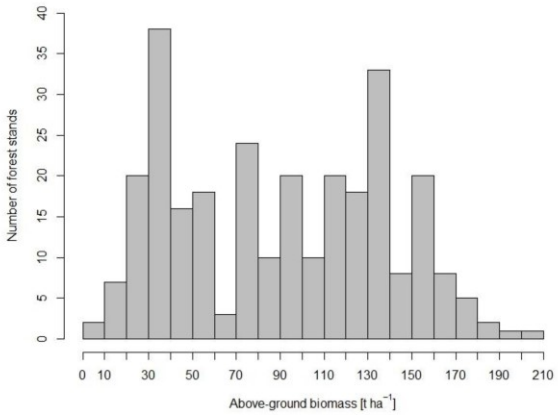

Figure 2. Number of forest stands per above-ground biomass class.

2.3. SAR Data

Data from two SAR satellites were used: Data from the L-band radar of the Phased Array Type L-band Synthetic Aperture Radar 2 (PALSAR-2) aboard the Advanced Land Observing Satellite (ALOS-2) of the Japan Aerospace Exploration Agency (JAXA) were combined with the C-band data from the RADARSAT-2 satellite of the Canadian Space Agency (CSA). The ALOS-2 PALSAR-2 data were available within the Kyoto and Carbon Initiative [66], whereas the RADARSAT-2 data were provided by the European Space Agency and CSA within the Second Call of the Sciences and Operational Application Research over Europe and Canada (SOAR-2). The ALOS-2 PALSAR-2 is an active sensor that has been in operation since 2014. It acquires SAR data from the sun-synchronous orbit (mean altitude 628 km) with a 14-day revisit time. The RADARSAT-2 mission has been active since 2007 and acquires data from the sun-synchronous polar orbit (mean altitude 798 km) with a 24-day revisit time. Both data sources were used to estimate AGB for the study area for the year 2014.

The data were acquired in single (horizontal transmitted, horizontal received, HH) and dual (HH and horizontal transmitted, vertical received, HV) polarizations in single look complex format (SLC). The ALOS-2 PALSAR-2 data were acquired in stripmap fine observation mode and the RADARSAT-2 data in ultrafine and fine mode. In total, four ALOS-2 PALSAR-2 and seven RADARSAT-2 images were available for this study (see Table 1 for summary).

Table 1. Summary of SAR data available for the study area.

Satellite	Scene/Product ID	Image Name	Acquisition Time (YYYY/MM/DD; HH:MM UTC)	Observation Mode (Polarization)	Incidence Angle [°]/Ground Range; Azimuth [m]
ALOS-2 PALSAR-2	ALOS2018571143-140926	PSAR2_20140926_HH PSAR2_20140926_HV	2014/09/26; 17:16	Fine Dual (HH, HV)	31.4/ 4.3; 3.2
	ALOS2019311140-141001	PSAR2_20141001_HH PSAR2_20141001_HV	2014/10/01; 17:23	Fine Dual (HH, HV)	36.3/ 4.3; 3.7
RADARSAT-2	PDS_03827460	RSAT2_20140625_HV	2014/06/25; 11:21	Ultrafine (HV)	32.2/ 2.5; 2.1
	PDS_03827470	RSAT2_20140719_HH RSAT2_20140719_HV	2014/07/19; 19:21	Fine (HH, HV)	32.0/ 8.9; 4.8
	PDS_03932440	RSAT2_20140729_HV	2014/07/29;11:30	Ultrafine (HV)	39.2/ 2.1; 2.1
	PDS_03932470	RSAT2_20140805_HH	2014/08/05; 11:25	Ultrafine (HH)	35.4/ 2.3; 2.1
	PDS_04058330	RSAT2_20141002_HH RSAT2_20141002_HV	2014/10/02; 11:34	Fine (HH, HV)	42.1/ 7.1; 4.7

The comparison of the C- and L-band data acquired in different image modes can be seen in Figure 3. Based on these examples, the influence of the radar frequency can be observed. The influence of the incidence angle can be ignored, as it is similar for all presented examples. The radiation from the C-band sensor penetrates only small objects, such as tree leaves on top of the tree canopy, that equal the wavelength, $\lambda = 5.5$ cm. On the other hand, data acquired with the L-band ($\lambda = 23.8$ cm) radar enables deeper imaging depth providing information related to branches and eventually tree trunks.

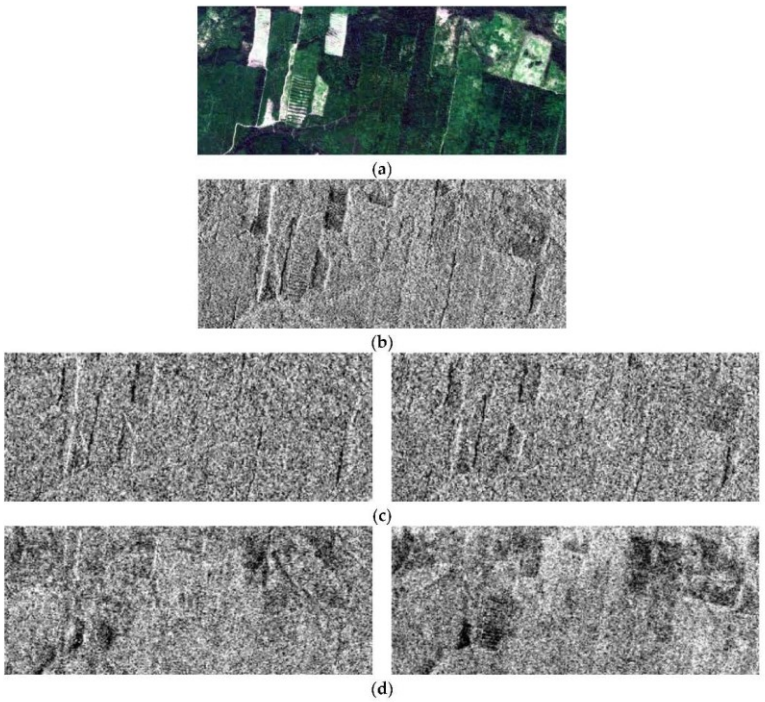

Figure 3. Multi-looked backscattering coefficient calculated for C- and L-band data: (**a**) optical image acquired by RapidEye on 11 June 2012; (**b**) C-band RADARSAT-2 image acquired in ultrafine mode on 5 August 2014; (**c**) C-band RADARSAT-2 image acquired in fine mode HH (on the left), HV (on the right) on 19 July 2014; (**d**) ALOS-2 PALSAR-2 image acquired in fine mode dual HH (on the left), HV (on the right) on 26 September 2014. The scale of images is 1:40,000.

Both HH and HV polarizations were applied for above-ground biomass (AGB) estimation. Due to the lack of data acquired under frozen stable conditions, calculation of the InSAR coherence was not considered in this study.

The digital elevation model (DEM) from the Shuttle Radar Topography Mission (SRTM) version 4.1 [67,68] was used to pre-process the SAR data; i.e., for terrain correction and geocoding.

2.4. Weather Data

Since the penetration depth of the electromagnetic wave in an object is inversely proportional to its dielectric properties (water content), information about the weather conditions during the acquisition

time were recorded. The corresponding weather conditions during data acquisition were available from the Kazachinskoye weather station, collected from http://www.sibessc.uni-jena.de/ (Table 2). The weather parameters are given as a mean from eight daily measurements.

Table 2. Weather conditions during SAR data acquisition. (Data source: NOAA National Climatic Data Center).

Image Name	Weather Conditions (Temperature Temp. in °C; mean wind speed WDSP in m s^{-1}; Precipitation PRCP in mm)
PSAR_20140926_HH PSAR_20140926_HV	Temp. −1.3 °C; WDSP 1.2; PRCP 0
PSAR2_20141001_HH PSAR2_20141001_HV	Temp. 7.7 °C; WDSP 1.1; PRCP 0
RSAT2_20140625_HV	Temp. 22.2 °C; WDSP 1.6; PRCP 0
RSAT2_20140719_HH RSAT2_20140719_HV	Temp. 17.4 °C; WDSP 1.9; PRCP 0.5
RSAT2_20140729_HV	Temp. 17.8 °C; WDSP 1.9; PRCP 3
RSAT2_20140805_HH	Temp. 19.9 °C; WDSP 1; PRCP 0; 4 days before high PRCP
RSAT2_20141002_HH RSAT2_20141002_HV	Temp. 8.6 °C; WDSP 1.2; PRCP 0

3. Methods

3.1. Above-Ground Biomass Data

For updating the available forest inventory data, the semi-empirical phytomass models and growth (i.e., yield) tables that were developed by the International Institute for Applied Systems Analyses (IIASA) in collaboration with V.N. Sukachev Institute of Forests, Siberian Branch, Russian Academy of Sciences, and Moscow State Forest University, were used [69,70]. The implementation of the models and tables in forestry and forest management in Russia has been recommended by the Council of the Federal Agency of Forest Management (Protocol No 2 dated 8 June 2006). The yield models satisfactorily, i.e., root-sum-square difference did not exceed ±3%, represented growth of Northern Eurasia's boreal forests [70]. The improvement of the old inventory data was done using the information about mean tree height and mean age of a stand. In the first step, the site index (SI) of a forest stand was calculated. SI is defined as the edaphic and climatic characteristics of a site which have an impact on the growth and yield of a given tree species [4]. Next, the growth rate was derived by implementing the growth function. The new GSV was calculated as a sum of the GSV measured in the field and the GSV growth derived for an age difference between the available forest inventory and the reference year 2010. In the final step, the GSV was converted to AGB using a regional allometric model. The model was developed using freely available in situ measurements of forest live biomass (phytomass) [71]. Details about the insitu data update and conversion from the GSV into the AGB are given in Reference [23]. Additionally, the forest stands with logging areas after 2010 were removed by means of visual interpretation against the SAR data available for this study. The forest stands were buffered by 2 pixels, and the updated forest inventory database was used for AGB model calibration and validation. In total, 349 polygons were used for further analysis.

3.2. SAR Data Processing and Analysis

First, the SAR data were calibrated and multi-looked. The multi-looking factor (MLI) in the case of the ALOS-2 PALSAR-2 data was 2 × 4 and 2 × 5 in range and azimuth, for an image acquired in September and in October, respectively. The resulting resolution was approximately 15 m. Similarly, the RADARSAT-2 data were multi-looked with the MLI 5 × 5 and 2 × 4 in range and azimuth in the case of the ultrafine and fine acquisition modes, respectively. This produced a spatial resolution of

15 m and 20 m. Next, the backscattering coefficient γ^0 was calculated in dB which includes a correction taking into account the local incidence angle [72].

Additionally, the ratio between the polarizations HH and HV was calculated. It was observed that integration of the ratios improves the estimation of AGB by increasing the saturation level [13,14,47]. Furthermore, ratios can reduce errors resulting from topography [73–75] and forest structure [13,14].

In order to decrease the speckle effect in the images, the enhanced Lee filter [76] was used. The filter uses local statistics (coefficient of variation), reducing speckle and at the same time preserving texture information in the radar data. In the case of homogenous areas, the pixel value is replaced by the average of the filter window; in the case of heterogeneous areas, the pixel value is replaced by a weighted average; and in the case of point objects, the pixel value is not changed. This filter outperformed other speckle filtering methods [77]. A window size of 5×5 and 3×3 was used for ALOS-2 PALSAR-2 and RADARSAT-2 data, respectively. As a result of filtering, the equivalent number of looks (ENL) of the images increased from two to three times. The ENL was estimated from the image statistics for a homogenous region, where the backscatter coefficient is assumed to be constant.

Additionally, texture measures were calculated to produce additional features by making use of spatial variations within the image. The gray level co-occurrence matrix (GLCM) proposed by Haralick et al. [78] is one of the most widely used methods to compute second-order texture measures. The measures were calculated as a probability of the occurrence of two gray levels separated by a given distance in a given direction. The texture measures were performed using data without speckle filtering because filtering reduces texture characteristics. The texture measures showed potential for biomass estimation [79]. The following measures were computed: sum average (mean), variance, homogeneity, contrast, dissimilarity, entropy, second moment, and correlation. For AGB estimation, the sum average co-occurrence matrix was selected by means of visual interpretation.

Altogether, forty-five SAR products were generated, out of which eighteen were from the ALOS-2 PALSAR-2 and twenty-seven were from the RADARSAT-2 data. The SAR products were resampled to a resolution of 50 m (0.25 ha) using the nearest neighbor method.

3.3. Above-Ground Biomass Retrieval

The SAR data and the forest inventory data were used as inputs for a non-parametric data fusion machine learning algorithm, random forests (RF) [80]. The workflow used for AGB estimation is shown graphically in Figure 4. The RF algorithm is widely used in ecology [81–83] as well as in forestry research [84–86]. Recent studies [87,88] have shown that RF is superior to other methods such as support vector machine (SVM), back propagation neural networks (BPNN), k-nearest neighbor (KNN), Gaussian processes (GP), and step-wise linear models (SLM).

RF is an ensemble learning method, which operates by combining random decision trees with bootstrap aggregation (bagging). The predictors are aggregated using bootstrap samples from training sets, and it has been shown that this method produces more accurate resultant predictors than the original predictor [89].

In general, five models using the regression mode of RF were constructed. The models consisted of: L-band data (Model 1); C-band data acquired in two modes ultrafine and fine (Model 2); C-band data in ultrafine mode (Model 3); C-band data in fine mode (Model 4); and L- and C-band data combined (Model 5).

In addition to bagging, the models were resampled during the model tuning using 10-fold cross-validation. Two thousand samples were used per AGB class for model calibration. The sample points within the AGB class were randomly distributed.

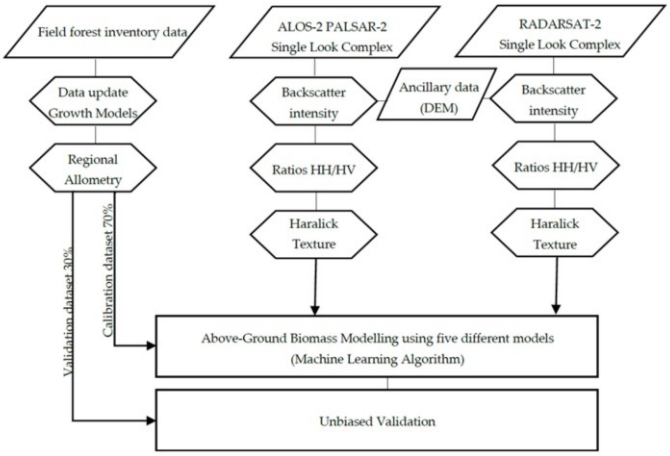

Figure 4. Above-ground biomass estimation processing steps.

3.4. Unbiased Validation

An independent validation was performed using approximately 30% of the forest inventory data (117 forest stands). The prediction models were evaluated using the following four quantitative measures:

(a) corrected root mean squared error, defined as:

$$RMSE_{cor} = \sqrt{RMSE_{Sat}^2 - RMSE_{Ref}^2}, \quad (1)$$

where $RMSE_{Sat}$ represents the root mean squared error in satellite-derived estimation of AGB and $RMSE_{Ref}$ is the root mean square error in forest inventory data. According to the manual on forest inventory and planning in Russian forests, the maximum error of $RMSE_{Ref}$ is expected to be 15% [90].

(b) corrected relative root-mean-square error, defined as:

$$relRMSE_{cor} = \frac{RMSE_{cor}}{\overline{AGB}_{Ref}} \quad (2)$$

shows that $RMSE_{cor}$ is divided by the mean of reference AGB.

(c) bias of the mean estimation error, defined as:

$$bias = \frac{\sum_{i=1}^{n}\left(\hat{AGB}_i - AGB_{ref(i)}\right)}{n} \quad (3)$$

represents $AGB_{ref(i)}$ as AGB reference value for stand i, $\hat{AGB}_i$ as predicted AGB, and n as the number of AGB observations. Positive values of bias express overestimation, and vice versa.

(d) coefficient of determination, shown as:

$$R^2 = 1 - \frac{SS_{res}}{SS_{tot}}, \quad (4)$$

where SS_{res} is the sum of squares of the residuals and SS_{tot} represents the total sum of squares.

The validation was performed using 1000 randomly distributed samples per AGB class.

4. Results

4.1. SAR Data Analysis

The results of the SAR data analysis are presented in Figures 5 and 6. The boxplots show the backscattering coefficient statistics for available forest stands: the minimum (the horizontal line at the bottom of each plot), the median (50th percentile), the 25th and 75th percentile (the lower and upper quartile, respectively), the SAR image maximum (the horizontal line at the top of each plot) as well as outliers. A dynamic range of 7 dB and 4 dB was observed for ALOS-2 PALSAR-2 and RADARSAT-2 data, respectively. We present three examples of the data acquired in fine and ultrafine mode to show the correlation of the SAR backscatter with the AGB. An exponential model was applied to express these relations as described in [29,37].

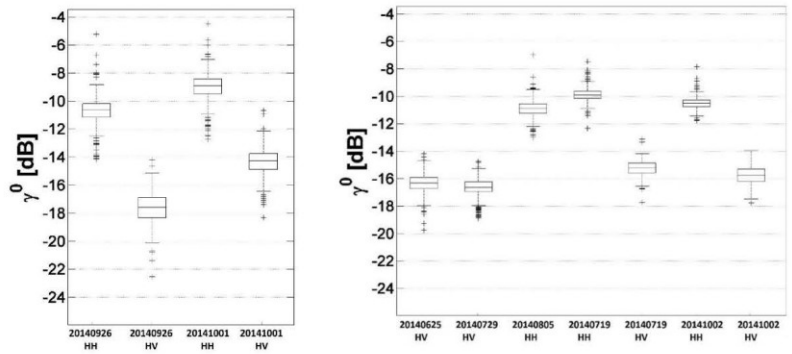

Figure 5. Backscattering coefficient statistics given for the data acquisition time (YYYYMMDD) and polarization (HH or HV): (**a**) ALOS-2 PALSAR-2 data; (**b**) RADARSAT-2 data.

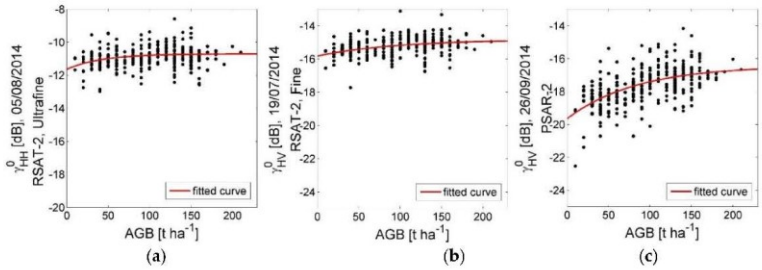

Figure 6. Synthetic Aperture Radar (SAR) backscatter as a function of forest above-ground biomass (AGB); red line represents exponential fit. Data from: (**a**) RADARSAT-2 ultrafine mode; (**b**) RADARSAT-2 fine mode; (**c**) ALOS-2 PALSAR-2 fine dual mode.

The following exponential model was applied:

$$\gamma^0(AGB) = ae^{-cAGB} + b(1 - e^{-cAGB}) \quad (5)$$

where a and b are unknown coefficients that can be derived from the training data; a represents backscatter from ground, b represents backscatter from forest, and c represents the empirical coefficient that depends on forest structure and dielectric properties of the canopy. For unfrozen conditions an approximation of 0.008 was found to be reasonable [91]. The model corresponds to the simplified version of the water cloud model by Attema and Ulaby [92]. As expected, the C-band data showed the well-known saturation effect earlier. No significant relations were observed between the C-band data and field-estimated AGB.

4.2. Above-Ground Biomass Maps

Figure 7 shows the resulting AGB maps with a pixel spacing of 50 m. The maps were derived using Models 1 to 5. The predicted results were expressed in t ha^{-1}. The statistics of the estimated AGB are given in Table 3. When examining the results visually, differences could be observed among the maps in terms of the spatial variability of AGB values and the AGB value range. The AGB maps estimated from the C-band data acquired in ultrafine mode (Model 3) were characterized by the homogenous AGB values, whereas the AGB values estimated from the L-band (Model 1) and combined L- and C-band data (Model 5) showed the highest heterogeneity.

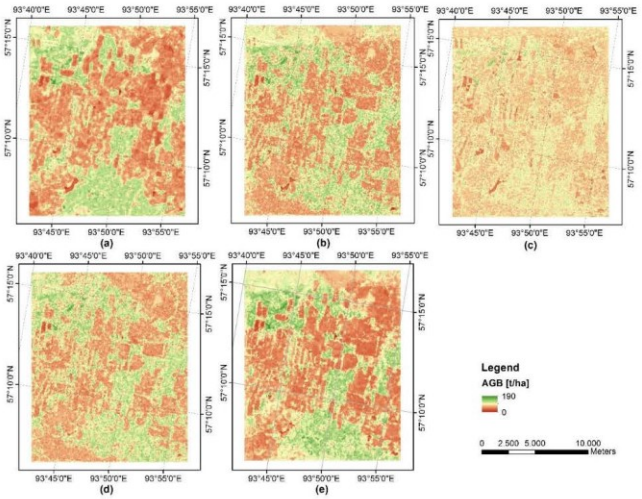

Figure 7. Above-ground biomass maps: (**a**) estimated from ALOS-2 PALSAR-2 data (Model 1); (**b**) estimated from RADARSAT-2 data (Model 2); (**c**) estimated from RADARSAT-2 data acquired in ultrafine mode (Model 3); (**d**) estimated from RADARSAT-2 data acquired in fine mode (Model 4); (**e**) estimated from ALOS-2 PALSAR-2 data combined with RADARSAT-2 data (Model 5).

Table 3. Estimated AGB values for forest stands.

Model	Data	AGB Statistics [t ha^{-1}]		
		Min	Max	Mean
Model 1	PALSAR-2 18 products	8.8	166.7	89.5
Model 2	RADARSAT-2 27 products	14.8	166.5	89.5
Model 3	RADARSAT-2 Ultrafine 9 products	21.3	155	86.7
Model 4	RADARSAT-2 Fine 18 Products	21.7	161.4	89.7
Model 5	PALSAR-2 and RADARSAT-2 45 products	6.8	173.8	90.1

The AGB ranges from Model 1 (L-band data) and Model 5 (combination of L- and C-band data) corresponded most highly with the reference AGB values. This could be also observed on the scatterplots of estimated AGB displayed against the reference (Figure 8). All plots showed overestimation of AGB values < 80 t ha^{-1} and underestimation > 80 t ha^{-1}. However, the AGB values estimated using the C-band data showed larger over and underestimation than the L-band based results.

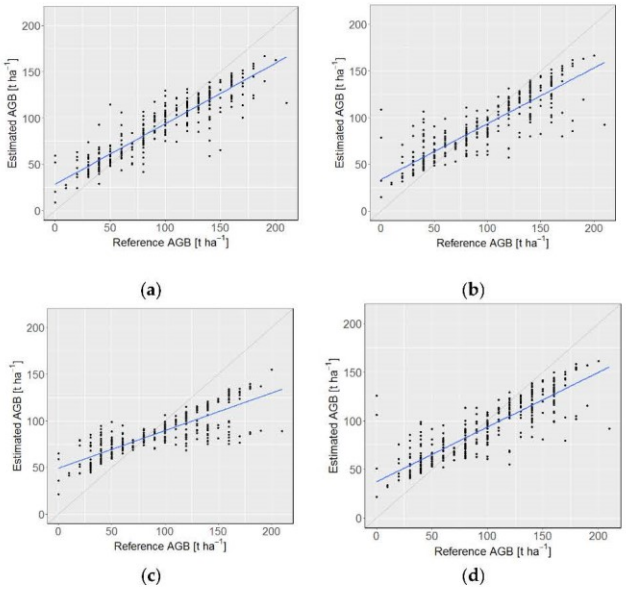

Figure 8. *Cont.*

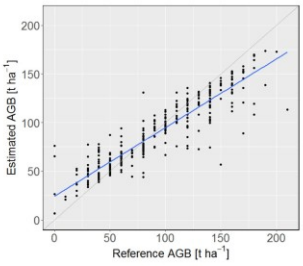

(**e**)

Figure 8. Estimated AGB vs. reference AGB: (**a**) estimated from ALOS-2 PALSAR-2 data (Model 1); (**b**) estimated from RADARSAT-2 data (Model 2); (**c**) estimated from RADARSAT-2 data acquired in ultrafine mode (Model 3); (**d**) estimated from RADARSAT-2 data acquired in fine mode (Model 4); (**e**) estimated from ALOS-2 PALSAR-2 data combined with RADARSAT-2 data (Model 5). Gray line represents 1:1 line; blue line represents linear fit.

It could be observed that the inclusion of the C-band data reduced the over and underestimation to some extent. The over and underestimation were partly caused by the ensemble (averaging) of regression trees, and partly by SAR saturation effects at high AGB ranges, and moisture and roughness effects at low AGB values.

The feature importance of the multi-looked backscattering coefficient calculated from C- and L-band data was presented and discussed in Reference [93]. The authors reported that the PALSAR-2 data acquired on 26/09/2014 in HV polarization were the most important for the retrieval of AGB, while the least important variable was the RADARSAT-2 data acquired on 19/07/2014 in fine mode, in HH polarization.

4.3. Unbiased Validation

Table 4 summarizes the validation results of the predicted AGB using the machine learning algorithm from the L-band ALOS-2 PALSAR-2 and C-band RADARSAT-2 backscatter data.

Table 4. Validation statistics.

Model	Data	$RMSE_{cor}$ [t ha^{-1}]	rel. $RMSE_{cor}$	R^2	Bias [t ha^{-1}]
Model 1	PALSAR-2 18 products	29.4	0.31	0.53	5.5
Model 2	RADARSAT-2 27 products	39.5	0.42	0.23	5.6
Model 3	RADARSAT-2 Ultrafine 9 products	44.6	0.47	0.04	10.6
Model 4	RADARSAT-2 Fine 18 Products	41.1	0.44	0.17	3.9
Model 5	PALSAR-2 and RADARSAT-2 45 products	30.2	0.32	0.51	4.7

Additionally, a detailed investigation of the $RMSE_{cor}$ in the case of the L-band data was performed (Figure 9). The comparison of the $RMSE_{cor}$ has shown that it is sufficient to use the filtered L-band data in HH and HV polarization for the estimation of AGB. Inclusion of the ratio and texture measure in the retrieval slightly increased the AGB estimation error.

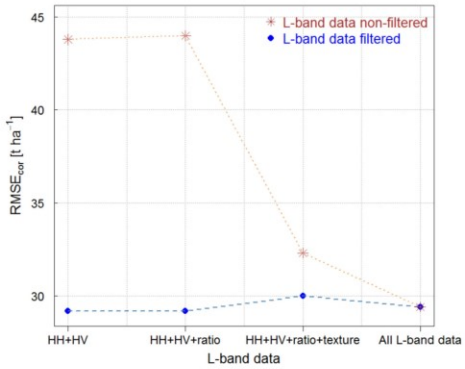

Figure 9. Comparison of corrected relative root-mean-square error $RMSE_{cor}$ between the multi-looked and filtered backscatter from L-band data. All data means data acquired in HH, HV polarization, and ratio HH/HV multi-looked and filtered as well as texture measure (sum average).

In general, the results obtained from L-Band data (Model 1) and combined L- and C-band data (Model 5) showed lower estimation errors. The $RMSE_{cor}$ of 29.4 t ha^{-1} (29.1 t ha^{-1} in case of L-band filtered data used alone) and of 30.2 t ha^{-1} (combination of L- and C-band backscatter intensities) were calculated, respectively. The highest $RMSE_{cor}$ was derived when the C-band data alone were used; 44.6 t ha^{-1} for C-band data acquired in ultrafine mode (Model 3), 41.1 t ha^{-1} for C-band data acquired in fine mode (Model 4), and 39.5 t ha^{-1} for all available C-band data (Model 2). The coefficient of determination (R^2) varied from 0.53 to 0.04 in the case of AGB estimations using Model 1 (L-band data) and that with Model 3 (C-band ultrafine mode). Overall, all models provided overestimated AGB values, with bias varying from 3.9 (C-band in fine mode) to 10.6 (C-band in ultrafine mode).

5. Discussion

Multi-frequency, multi-polarization, and multi-temporal data from L-band ALOS-2 PALSAR-2 and from C-band RADARSAT-2, together with updated in situ data were utilized for the first time to evaluate the improvement of above-ground biomass (AGB) estimation using a non-parametric biomass model. This allowed us to isolate the data source that provided the most information on forest biomass. Backscatter coefficients from L- and C-band radar were used independently, and in combination, to assess a boreal forest study area in, Siberia (Krasnoyarskiy Kray). Furthermore, the effects of including texture measures in AGB retrieval were investigated. The data from both SAR systems, as well as the additional generated SAR features, were combined in a machine learning algorithm (random forests).

As expected, the AGB modeling results indicated that the longer wavelength L-band data in HH and HV polarizations performed better than C-band data in HH and HV polarizations. This finding is in line with previous studies (e.g., References [25,44,62,93,94]). When the L-band data alone were used for the retrieval, a corrected relative root-mean-square error ($RMSE_{cor}$) of 29.4 t ha^{-1} was calculated. The $RMSE_{cor}$ decreased when only the filtered L-band backscatter data, without ratio and texture, were applied (29.1 t ha^{-1}). The ratio of backscatter was not found to be effective, similar to the research results reported in Reference [79]. The first multi-frequency approaches for boreal forests reported errors of 37.6 t ha^{-1} [44] or 25.7 t ha^{-1} [43] using the SIR-C/X-SAR data. It was shown that the L-band in HV polarization was the most important variable for AGB estimation [95], the same as in Reference [42]. Using the empirical parametric model (stepwise regression procedure) the L-band data in HV polarization were selected as the best information for biomass estimation

for boreal forests, followed by the L-band in HH, L-band in VV, and C-band in HV polarization. Moreover, the ratio of HV backscatter from a longer wavelength to that from a shorter wavelength, as well as the ratio of texture measures, have been reported to provide good results for mapping the biomass [14,73,75,96]. The inclusion of the C-band data for AGB estimation only marginally improved the retrieval results. The over and underestimation was reduced, the bias decreased from 5.5 t ha^{-1} to 4.7 t ha^{-1}, and the estimated AGB range corresponded to the reference data. However, the $RMSE_{cor}$ increased by approximately 1% when calculated in combination with C-band and L-band data (30.2 t ha^{-1}) as opposed to when only using the latter (29.4 t ha^{-1}). In the case of African savannah a small improvement of 0.6 t ha^{-1} was reported [53]. Moreover, the authors observed an improvement in the modeling estimations of the complete savannah vegetation structure. It is expected that integration of seasonal and/or annual time series of C-band acquisitions, i.e., from Sentinel-1, should improve the AGB retrieval. Hyper-temporal or multi-temporal (10 stacks of 3-month scenes) approaches using C-band data can provide accurate AGB estimations of approximately 15–20% *RMSE*, as reported in References [48,60].

The better performance in the first scenario, i.e., when only L-band data were used, was due to deeper wavelength penetration into the canopy, providing information from trunks and big branches that are better correlated with the forest AGB, especially in case of dense forests. The information from the C-band data comes mainly from tree leaves and small branches at the top of the canopy. Moreover, the RADARSAT-2 data acquired in the ultrafine mode showed more sensitivity to the roughness of the objects, decreasing the correlation between the SAR and the reference data, and thus generating higher estimation errors. This shows that the long wavelength SAR is better suited for the high forest biomass values and the short wavelength SAR for low biomass ranges. This finding also corresponds to recently reported results in the case of the African savannah test site [53], as well as tropical forests in Indonesia, where instead of C-band the X-band data were combined with L-band [49].

In general, the AGB estimation using L-band data alone, and in combination with C-band data was successful. However, it is important to mention the additional sources of error which were not taken into account in this study. The first source of error relates to the time difference between the SAR datasets and the insitu data, as well as the implementation of yield models. Even though the reference data have been updated using recommended growth models and include removal of the forest stands with extensive logging activities, it is very probable that local changes in the forest structure caused by smaller events, such as selective logging and local fires, were not taken into account. However, it was assumed that the main forest structure had not been changed. Different time and weather conditions resulting in different forest states during the SAR acquisitions could also influence the obtained AGB estimates.

AGB estimations in boreal forests using multi-frequency, multi-polarization and multi-temporal data are not very common. It is assumed that retrieval of AGB over boreal forests can be further improved by using texture ratio and multi-temporal InSAR coherence, and by implementing further SAR frequencies (X-band and P-band) in the analysis. The use of multi-frequency data should improve AGB estimation, as the biomass-related information in the SAR data acquired using different wavelengths comes from different forest compartments; i.e., trunks, branches, and foliage. Moreover, the inclusion of optical data can further reduce the estimation error, as this type of data provide important information on the deciduous/evergreen dominance [48]. Additionally, the use of a deep learning based workflow can increase the AGB accuracy as reported by Reference [88].

6. Conclusions

This study investigated the potential use of multi-frequency (C- and L-band), multi-polarization (HH and HV), and multi-temporal SAR data for AGB estimation in boreal forests. In total forty-five predictor layers were generated using RADARSAT-2 and ALOS-2 PALSAR-2 data, including texture measures.

The research showed that the inclusion of C-band data to the AGB non-parametric retrieval procedure marginally improved the estimation. It is assumed that the use of longer time series of the multi-frequency data will improve the AGB estimation, as the biomass-related information in the SAR data acquired using different wavelengths represents different tree parts and forest structures. The lowest estimation error $RMSE_{cor}$ was calculated for L-band filtered data alone and was 29.1 t ha^{-1} (*rel* $RMSE_{cor}$ of 30%). In previous studies where mono-frequency or multi-frequency data were applied, relative estimation errors in the range of 30–40% for Siberian boreal forests were reported [e.g., References 7,23,57,61]. However, the lowest estimation error was obtained for coarse spatial resolutions (e.g., 1 km). This study showed that for local applications at a scale of 0.25 ha highly accurate AGB estimations can be obtained.

It is expected that AGB estimations could be further improved by including multi-temporal metrics, texture ratio, and InSAR coherence as predictor variables, as well as optical data. Moreover, the use of hyper-temporal C-band data with long wavelength SAR data can further reduce the over and underestimation that is presented when using non-parametric, i.e., machine or deep learning, algorithms.

Author Contributions: Conceptualization, M.A.S.-G.; Data acquisition and data processing, M.A.S.-G.; Methodology, M.A.S.-G.; Writing-original draft preparation, M.A.S.-G.; Writing-review and editing, M.A.S.-G., M.U. and C.T.; Supervision, C.T., C.S.

Funding: This work began within the framework of the GMES Initial Operations—Network for Earth Observation Research Training GIONET project, grant agreement PITN-GA-2010-264509.

Acknowledgments: The authors would like to thank the Japan Aerospace Exploration Agency (JAXA) for providing ALOS-2 PALSAR-2 data within the Kyoto & Carbon Initiative, as well as MacDonald, Dettwiler and Associates Ltd. for supplying the RADARSAT-2 data within the RADARSAT-2 Science and Operational Applications Research and Development Program (SOAR2)—RADARSAT-2 Data and Products MacDonald, Dettwiler and Associates Ltd. (2014)—All Rights Reserved. RADARSAT is an official trademark of the Canadian Space Agency. The authors would like to thank Kokila Egodage for English proof-reading of this manuscript as well as Nesrin Salepci and Jakob Wernicke for their support.The authors wish to express their appreciation to the anonymous reviewers and the editors for their valuable comments.

Conflicts of Interest: The authors declare no conflicts of in terest. The funders had no role in the design of the study, in the collection, analyses, or interpretation of data, in the writing of the manuscript, or in the decision to publish the results.

References

1. FAO. *Terrestrial Essential Climate Variables. For Climate Change Assessment, Mitigation and Adaptation—BIOMASS*; FAO: Rome, Italy, 2009.
2. Bojinski, S.; Verstraete, M.; Peterson, T.C.; Richter, C.; Simmons, A.; Zemp, M. The concept of essential climate variables in support of climate research, applications, and policy. *Bull. Am. Meteorol. Soc.* **2014**, *95*, 1431–1443. [CrossRef]
3. Thurner, M.; Beer, C.; Ciais, P.; Friend, A.D.; Ito, A.; Kleidon, A.; Lomas, M.R.; Quegan, S.; Rademacher, T.T.; Schaphoff, S.; et al. Evaluation of climate-related carbon turnover processes in global vegetation models for boreal and temperate forests. *Glob. Chang. Biol.* **2017**, *23*, 3076–3091. [CrossRef] [PubMed]
4. Van Laar, A.; Akca, A. *Forest Mensuration: Chapter 8 Tree and Stand Biomass*; von Gadow, K., Pukkala, T., Tome, M., Eds.; Springer: Dordrecht, The Netherlands, 2007; Volume 13, pp. 183–199.
5. FAO. *Global Forest Resources Assessment 2015*; FAO: Rome, Italy, 2015.
6. Thurner, M.; Beer, C.; Santoro, M.; Carvalhais, N.; Wutzler, T.; Schepaschenko, D.; Shvidenko, A.; Kompter, E.; Ahrens, B.; Levick, S.R.; et al. Carbon stock and density of northern boreal and temperate forests. *Glob. Ecol. Biogeogr.* **2014**, *23*, 297–310. [CrossRef]
7. Hüttich, C.; Korets, M.; Bartalev, S.; Zharko, V.; Schepaschenko, D.; Shvidenko, A.; Schmullius, C. Exploiting Growing Stock Volume Maps for Large Scale Forest Resource Assessment: Cross-Comparisons of ASAR- and PALSAR-Based GSV Estimates with Forest Inventory in Central Siberia. *Forests* **2014**, *5*, 1753–1776. [CrossRef]
8. FAO. *The Russian Federation Forest Sector Outlook Study to 2030*; FAO: Rome, Italy, 2012.

9. Stelmaszczuk-Górska, M.; Thiel, C.; Schmullius, C. Remote Sensing for Aboveground Biomass Estimation in Boreal Forests. In *Earth Observation for Land and Emergency Monitoring.*; Balzter, H., Ed.; John Wiley & Sons Ltd.: West Sussex, UK, 2017; pp. 33–55.
10. Ji, L.; Wylie, B.K.; Nossov, D.R.; Peterson, B.; Waldrop, M.P.; McFarland, J.W.; Rover, J.; Hollingsworth, T.N. Estimating aboveground biomass in interior Alaska with Landsat data and field measurements. *Int. J. Appl. Earth Obs. Geoinf.* **2012**, *18*, 451–461. [CrossRef]
11. Le Toan, T.; Beaudoin, A.; Riom, J.; Guyon, D. Relating forest biomass to SAR data. *IEEE Trans. Geosci. Remote Sens.* **1992**, *30*, 403–411. [CrossRef]
12. Beaudoin, A.; Le Toan, T.; Goze, S.; Nezry, E.; Lopes, A.; Mougin, E.; Hsu, C.C.; Han, H.C.; Kong, J.A.; Shin, R.T. Retrieval of forest biomass from SAR data. *Int. J. Remote Sens.* **1994**, *15*, 2777–2796. [CrossRef]
13. Dobson, M.C.; Ulaby, F.T.; Pierce, L.E.; Sharik, T.L.; Bergen, K.M.; Kellndorfer, J.; Kendra, J.R.; Li, E.; Lin, Y.C.; Nashashibi, A.; et al. Estimation of forest biophysical characteristics in Northern Michigan with SIR-C/X-SAR. *IEEE Trans. Geosci. Remote Sens.* **1995**, *33*, 877–895. [CrossRef]
14. Ranson, K.J.; Sun, G. Mapping biomass of a northern forest using multifrequency SAR data. *IEEE Trans. Geosci. Remote Sens.* **1994**, *32*, 388–396. [CrossRef]
15. Fransson, J.E.S.; WaLter, F.; Ulander, L.M.H. Estimation of forest parameters using CARABAS-II VHF SAR data. *IEEE Trans. Geosci. Remote Sens.* **2000**, *38*, 720–727. [CrossRef]
16. Rauste, Y. Multi-temporal JERS SAR data in boreal forest biomass mapping. *Remote Sens. Environ.* **2005**, *97*, 263–275. [CrossRef]
17. Soja, M.J.; Sandberg, G.; Ulander, L.M.H.; Member, S. Regression-based retrieval of boreal forest biomass in sloping terrain using P-band SAR backscatter intensity data. *IEEE Trans. Geosci. Remote Sens.* **2013**, *51*, 2646–2665. [CrossRef]
18. Soja, M.J.; Persson, H.J.; Ulander, L.M.H. Estimation of forest biomass from two-level model inversion of single-pass InSAR data. *IEEE Int. Geosci. Remote Sens. Symp.* **2015**, *53*, 3886–3889. [CrossRef]
19. Santoro, M.; Cartus, O.; Fransson, J.; Shvidenko, A.; McCallum, I.; Hall, R.; Beaudoin, A.; Beer, C.; Schmullius, C. Estimates of Forest Growing Stock Volume for Sweden, Central Siberia, and Québec Using Envisat Advanced Synthetic Aperture Radar Backscatter Data. *Remote Sens.* **2013**, *5*, 4503–4532. [CrossRef]
20. Askne, J.; Fransson, J.; Santoro, M.; Soja, M.; Ulander, L. Model-based biomass estimation of a hemi-boreal forest from multitemporal TanDEM-X acquisitions. *Remote Sens.* **2013**, *5*, 5574–5597. [CrossRef]
21. Karjalainen, M.; Kankare, V.; Vastaranta, M.; Holopainen, M.; Hyyppä, J. Prediction of plot-level forest variables using TerraSAR-X stereo SAR data. *Remote Sens. Environ.* **2012**, *117*, 338–347. [CrossRef]
22. Wilhelm, S.; Hüttich, C.; Korets, M.; Schmullius, C. Large area mapping of boreal Growing Stock Volume on an annual and multi-temporal level using PALSAR L-band backscatter mosaics. *Forests* **2014**, *5*, 1999–2015. [CrossRef]
23. Stelmaszczuk-Górska, M.; Rodriguez-Veiga, P.; Ackermann, N.; Thiel, C.; Balzter, H.; Schmullius, C. Non-Parametric Retrieval of Aboveground Biomass in Siberian Boreal Forests with ALOS PALSAR Interferometric Coherence and Backscatter Intensity. *J. Imaging* **2016**, *2*, 24. [CrossRef]
24. Pulliainen, J.T.; Heiska, K.; Hyyppa, J.; Hallikainen, M.T. Backscattering properties of boreal forests at the C- and X-bands. *IEEE Trans. Geosci. Remote Sens.* **1994**, *32*, 1041–1050. [CrossRef]
25. Fransson, J.E.S.; Israelsson, H. Estimation of stem volume in boreal forests using ERS-1 C- and JERS-1 L-band SAR data. *Int. J. Remote Sens.* **1999**, *20*, 123–137. [CrossRef]
26. Antropov, O.; Rauste, Y.; Ahola, H.; Häme, T. Stand-level stem volume of boreal forests from spaceborne SAR imagery at L-band. *IEEE Trans. Geosci. Remote Sens.* **2013**, *6*, 4776–4779. [CrossRef]
27. Solberg, S.; Astrup, R.; Gobakken, T.; Næsset, E.; Weydahl, D.J. Estimating spruce and pine biomass with interferometric X-band SAR. *Remote Sens. Environ.* **2010**, *114*, 2353–2360. [CrossRef]
28. Koskinen, J.T.; Pulliainen, J.T.; Hyyppä, J.M.; Engdahl, M.E.; Hallikainen, M.T. The seasonal behavior of interferometric coherence in boreal forest. *IEEE Trans. Geosci. Remote Sens.* **2001**, *39*, 820–829. [CrossRef]
29. Santoro, M.; Askne, J.; Smith, G.; Fransson, J.E.S. Stem volume retrieval in boreal forests from ERS-1/2 interferometry. *Remote Sens. Environ.* **2002**, *81*, 19–35. [CrossRef]
30. Næsset, E.; Bollandsås, O.M.; Gobakken, T.; Solberg, S.; McRoberts, R.E. The effects of field plot size on model-assisted estimation of aboveground biomass change using multitemporal interferometric SAR and airborne laser scanning data. *Remote Sens. Environ.* **2015**, *168*, 252–264. [CrossRef]

31. Papathanassiou, K.P.; Cloude, S.R. Single-baseline polarimetric SAR interferometry. *IEEE Trans. Geosci. Remote Sens.* **2001**, *39*, 2352–2363. [CrossRef]
32. Neumann, M.; Saatchi, S.S.; Ulander, L.M.H.; Fransson, J.E.S. Assessing performance of L- and P-Band polarimetric interferometric SAR data in estimating boreal forest above-ground biomass. *IEEE Trans. Geosci. Remote Sens.* **2012**, *50*, 714–726. [CrossRef]
33. Antropov, O.; Rauste, Y.; Häme, T.; Praks, J. Polarimetric ALOS PALSAR Time Series in Mapping Biomass of Boreal Forests. *Remote Sens.* **2017**, *9*, 999. [CrossRef]
34. Tebaldini, S.; Rocca, F. Multibaseline polarimetric SAR tomography of a boreal forest at P- and L-bands. *IEEE Trans. Geosci. Remote Sens.* **2012**, *50*, 232–246. [CrossRef]
35. Persson, H.; Fransson, J. Forest variable estimation using radargrammetric processing of TerraSAR-X images in boreal forests. *Remote Sens.* **2014**, *6*, 2084–2107. [CrossRef]
36. Vastaranta, M.; Niemi, M.; Karjalainen, M.; Peuhkurinen, J.; Kankare, V.; Hyyppä, J.; Holopainen, M. Prediction of forest stand attributes using TerraSAR-X stereo imagery. *Remote Sens.* **2014**, *6*, 3227–3246. [CrossRef]
37. Santoro, M.; Eriksson, L.; Fransson, J. Reviewing ALOS PALSAR Backscatter Observations for Stem Volume Retrieval in Swedish Forest. *Remote Sens.* **2015**, *7*, 4290–4317. [CrossRef]
38. Eriksson, L.E.B. Satellite-borne L-band Interferometric Coherence for Forestry Applications in the Boreal Zone. Doctoral Thesis, University of Jena, Jena, Germany, 2004.
39. Le Toan, T.; Beaudoin, A.; Riom, J.; Guyon, D. Relating Forest Biomass to SAR Data. *IEEE Trans. Geosci. Remote Sens.* **1994**, *30*, 403–411. [CrossRef]
40. Rignot, E.; Way, J.; Williams, C.; Viereck, L. Radar estimates of aboveground biomass in boreal forests of interior Alaska. *IEEE Trans. Geosci. Remote Sens.* **1994**, *32*, 1117–1124. [CrossRef]
41. Saatchi, S.S.; Moghaddam, M. Estimation of crown and stem water content and biomass of boreal forest using polarimetric SAR imagery. *IEEE Trans. Geosci. Remote Sens.* **2000**, *38*, 697–709. [CrossRef]
42. Ranson, K.J.; Sun, G.; Lang, R.H.; Chauhan, N.S.; Cacciola, R.J.; Kilic, O. Mapping of boreal forest biomass from spaceborne synthetic aperture radar. *J. Geophys. Res.* **1997**, *102*, 29599–29610. [CrossRef]
43. Ranson, K.J.; Sun, G.; Member, S. Effects of Environmental Conditions on Boreal Forest Classification and Biomass Estimates with SAR. *IEEE Geosci. Remote Sens.* **2000**, *38*, 1242–1252. [CrossRef]
44. Ranson, K.J.; Sun, G.; Lang, R.H.; Chauhan, N.S.; Cacciola, R.J.; Kilic, O. An evaluation of AIRSAR and SIR-C/X-SAR images for mapping northern forest attributes in Maine, USA. *Remote Sens. Environ.* **1997**, *59*, 203–222. [CrossRef]
45. Wagner, W.; Luckman, A.; Vietmeier, J.; Tansey, K.; Balzter, H.; Schmullius, C.; Davidson, M.; Gaveau, D.; Gluck, M.; Le, T.; et al. Large-scale mapping of boreal forest in SIBERIA using ERS tandem coherence and JERS backscatter data. *Remote Sens. Environ.* **2003**, *85*, 125–144. [CrossRef]
46. Tsui, O.W.; Coops, N.C.; Wulder, M.A.; Marshall, P.L.; McCardle, A. Using multi-frequency radar and discrete-return LiDAR measurements to estimate above-ground biomass and biomass components in a coastal temperate forest. *ISPRS J. Photogramm. Remote Sens.* **2012**, *69*, 121–133. [CrossRef]
47. Harrell, P.A.; Kasischke, E.S.; Bourgeau-Chavez, L.L.; Haney, E.M.; Christensen, N.L. Evaluation of approaches to estimating aboveground biomass in Southern pine forests using SIR-C data. *Remote Sens. Environ.* **1997**, *59*, 223–233. [CrossRef]
48. Laurin, G.V.; Balling, J.; Corona, P.; Mattioli, W.; Papale, D.; Puletti, N.; Rizzo, M.; Truckenbrodt, J.; Urban, M. Above-ground biomass prediction by Sentinel-1 multitemporal data in central Italy with integration of ALOS2 and Sentinel-2 data. *J. Appl. Remote Sens.* **2018**, *12*, 18. [CrossRef]
49. Englhart, S.; Keuck, V.; Siegert, F. Aboveground biomass retrieval in tropical forests—The potential of combined X- and L-band SAR data use. *Remote Sens. Environ.* **2011**, *115*, 1260–1271. [CrossRef]
50. Englhart, S.; Member, S.; Keuck, V.; Siegert, F. Modeling Aboveground Biomass in Tropical Forests Using Multi-Frequency SAR Data—A Comparison of Methods. *IEEE J. Sel. Top. Appl. Earth Obs. Remote Sens.* **2012**, *5*, 298–306. [CrossRef]
51. Backscatter, P.R.; Neeff, T.; Dutra, L.V.; Freitas, C. Tropical Forest Measurement by Interferometric Height Modeling and P-Band Radar Backscatter. *Biomass* **2005**, *51*, 585–594.
52. Mougin, E.; Proisy, C.; Marty, G.; Fromard, F.; Puig, H.; Betoulle, J.L.; Rudant, J.P. Multifrequency and multipolarization radar backscattering from mangrove forests. *IEEE Trans. Geosci. Remote Sens.* **1999**, *37*, 94–102. [CrossRef]

53. Naidoo, L.; Mathieu, R.; Main, R.; Kleynhans, W.; Wessels, K.; Asner, G.; Leblon, B. Savannah woody structure modelling and mapping using multi-frequency (X-, C- and L-band) Synthetic Aperture Radar data. *ISPRS J. Photogramm. Remote Sens.* **2015**, *105*, 234–250. [CrossRef]
54. Askne, J.; Santoro, M.; Smith, G.; Fransson, J.E.S. Multitemporal repeat-rass SAR interferometry of boreal forests. *IEEE Trans. Geosci. Remote Sens.* **2003**, *41*, 1540–1550. [CrossRef]
55. Santoro, M.; Shvidenko, A.; Mccallum, I.; Askne, J.; Schmullius, C. Properties of ERS-1/2 coherence in the Siberian boreal forest and implications for stem volume retrieval. *Remote Sens. Environ.* **2007**, *106*, 154–172. [CrossRef]
56. Peregon, A.; Yamagata, Y. The use of ALOS/PALSAR backscatter to estimate above-ground forest biomass: A case study in Western Siberia. *Remote Sens. Environ.* **2013**, *137*, 139–146. [CrossRef]
57. Chowdhury, T.A.; Thiel, C.; Schmullius, C. Growing stock volume estimation from L-band ALOS PALSAR polarimetric coherence in Siberian forest. *Remote Sens. Environ.* **2014**, *155*, 129–144. [CrossRef]
58. Rodriguez-Veiga, P.; Stelmaszczuk-Górska, M.; Hüttich, C.; Schmullius, C.; Tansey, K.; Balzter, H. Aboveground Biomass Mapping in Krasnoyarsk Kray (Central Siberia) using Allometry, Landsat, and ALOS PALSAR. In Proceedings of the RSPSoc Annual Conference, Aberystwyth, UK, 15 June 2014.
59. Santoro, M.; Eriksson, L.; Askne, J.; Schmullius, C. Assessment of stand-wise stem volume retrieval in boreal forest from JERS-1 L-band SAR backscatter. *Int. J. Remote Sens.* **2006**, *27*, 3425–3454. [CrossRef]
60. Santoro, M.; Beer, C.; Cartus, O.; Schmullius, C.; Shvidenko, A.; McCallum, I.; Wegmüller, U.; Wiesmann, A. Retrieval of growing stock volume in boreal forest using hyper-temporal series of Envisat ASAR ScanSAR backscatter measurements. *Remote Sens. Environ.* **2011**, *115*, 490–507. [CrossRef]
61. Thiel, C.; Schmullius, C. The potential of ALOS PALSAR backscatter and InSAR coherence for forest growing stock volume estimation in Central Siberia. *Remote Sens. Environ.* **2016**, *173*, 258–273. [CrossRef]
62. Kurvonen, L.; Pulliainen, J.; Hallikainen, M. Retrieval of biomass in boreal forests from multitemporal ERS-1 and JERS-1 SAR images. *IEEE Trans. Geosci. Remote Sens.* **1999**, *37*, 198–205. [CrossRef]
63. Eriksson, L.E.B.; Santoro, M.; Wiesmann, A.; Schmullius, C.C. Multitemporal JERS repeat-pass coherence for growing-stock volume estimation of Siberian forest. *IEEE Trans. Geosci. Remote Sens.* **2003**, *41*, 1561–1570. [CrossRef]
64. Santoro, M.; Cartus, O. Research pathways of forest above-ground biomass estimation based on SAR backscatter and interferometric SAR observations. *Remote Sens.* **2018**, *10*, 608. [CrossRef]
65. Schmullius, C.; Baker, J.; Balzter, H.; Davidson, M.; Eriksson, L.; Gaveau, D.; Gluck, M.; Holz, A.; Le Toan, T.; Luckman, A.; et al. *SAR Imaging for Boreal Ecology and Radar Interferometry Applications SIBERIA Project (Contract No. ENV4-CT97-0743-SIBERIA)—Final Report*; Microwaves and Radar Institute: Jena, Germany, 2001.
66. Rosenqvist, Å.; Milne, A.; Lucas, R.; Imhoff, M.; Dobson, C. A review of remote sensing technology in support of the Kyoto Protocol. *Environ. Sci. Policy* **2003**, *6*, 441–455. [CrossRef]
67. CGIAR CSI. Available online: http://srtm.csi.cgiar.org (accessed on 15 April 2014).
68. Reuter, H.I.; Nelson, A.; Jarvis, A. An evaluation of void filling interpolation methods for SRTM data. *Int. J. Geogr. Inf. Sci.* **2007**, *21*, 983–1008. [CrossRef]
69. Shvidenko, A.; Schepaschenko, D.; Nilsson, S.; Bouloui, Y. Semi-empirical models for assessing biological productivity of Northern Eurasian forests. *Ecol. Modell.* **2007**, *204*, 163–179. [CrossRef]
70. Shvidenko, A.; Schepaschenko, D.; Nilsson, S.; Boului, Y. *Tables and Models of Growth and Productivity of Forests of Major Forming Species of Northern Eurasia (Standard and Reference Materials)*; Federal Agency of Forest Management: Moscow, Russia, 2008.
71. IIASA Russian Forests & Forestry. Live Biomass & Net Primary Production—Measurements of Forest Phytomass in Situ. Available online: http://webarchive.iiasa.ac.at/Research/FOR/forest_cdrom/english/for_prod_en.html (accessed on 10 January 2014).
72. Ulander, L.M.H. Radiometrie slope correction of synthetic-aperture radar images. *IEEE Trans. Geosci. Remote Sens.* **1996**, *34*, 1115–1122. [CrossRef]
73. Ranson, K.J.; Saatchi, S.S.; Sun, G. Boreal Forest Ecosystem Characterization with SIR-C / XSAR. *IEEE Trans. Geosci. Remote Sens.* **1995**, *33*, 867–876. [CrossRef]
74. Soja, M.J.; Sandberg, G.; Ulander, L.M.H. Topographic correction for biomass retrieval from P-band SAR data in boreal forests. *IEEE Int. Geosci. Remote Sens. Symp.* **2010**, 4776–4779. [CrossRef]

75. Ranson, K.J.; Sun, G.; Kharuk, V.I.; Kovacs, K. Characteristics of Forests in Western Sayani Mountains, Siberia from SAR Data. *Remote Sens. Environ.* **2001**, *75*, 188–200. [CrossRef]
76. Lopes, A.; Touzi, R.; Nezry, E. Adaptive Speckle Filters and Scene Heterogeneity. *IEEE Trans. Geosci. Remote Sens.* **1990**, *28*, 992–1000. [CrossRef]
77. Joshi, N.; Mitchard, E.; Schumacher, J.; Johannsen, V.; Saatchi, S.; Fensholt, R. L-band SAR backscatter related to forest cover, height and aboveground biomass at multiple spatial scales across Denmark. *Remote Sens.* **2015**, *7*, 4442–4472. [CrossRef]
78. Haralick, R.M.; Shanmugam, K.; Dinstein, I. Textural Features for Image Classification. *IEEE Trans. Syst. Man. Cybern.* **1973**, *SMC-3*, 610–621. [CrossRef]
79. Sarker, M.L.R.; Nichol, J.; Ahmad, B.; Busu, I.; Rahman, A.A. Potential of texture measurements of two-date dual polarization PALSAR data for the improvement of forest biomass estimation. *ISPRS J. Photogramm. Remote Sens.* **2012**, *69*, 146–166. [CrossRef]
80. Breiman, L. Random Forests. *Mach. Learn.* **2001**, *45*, 5–32. [CrossRef]
81. Prasad, A.M.; Iverson, L.R.; Liaw, A. Newer classification and regression tree techniques: Bagging and random forests for ecological prediction. *Ecosystems* **2006**, *9*, 181–199. [CrossRef]
82. Hüttich, C.; Herold, M.; Strohbach, B.J.; Dech, S. Integrating in-situ, Landsat, and MODIS data for mapping in Southern African savannas: Experiences of LCCS-based land-cover mapping in the Kalahari in Namibia. *Environ. Monit. Assess.* **2011**, *176*, 531–547. [CrossRef] [PubMed]
83. Cutler, D.R.; Edwards, T.C.; Beard, K.H.; Cutler, A.; Hess, K.T.; Gibson, J.; Lawler, J.J. Random forests for classification in ecology. *Ecology* **2007**, *88*, 2783–2792. [CrossRef] [PubMed]
84. Cartus, O.; Kellndorfer, J.; Rombach, M.; Walker, W. Mapping Canopy Height and Growing Stock Volume Using Airborne Lidar, ALOS PALSAR and Landsat ETM+. *Remote Sens.* **2012**, *4*, 3320–3345. [CrossRef]
85. Cartus, O.; Kellndorfer, J.; Walker, W.; Franco, C.; Bishop, J.; Santos, L.; Fuentes, J. A National, Detailed Map of Forest Aboveground Carbon Stocks in Mexico. *Remote Sens.* **2014**, *6*, 5559–5588. [CrossRef]
86. Baccini, A.; Laporte, N.; Goetz, S.J.; Sun, M.; Dong, H. A first map of tropical Africa's above-ground biomass derived from satellite imagery. *Environ. Res. Lett.* **2008**, *3*, 9. [CrossRef]
87. Fassnacht, F.E.; Hartig, F.; Latifi, H.; Berger, C.; Hernández, J.; Corvalán, P.; Koch, B. Importance of sample size, data type and prediction method for remote sensing-based estimations of aboveground forest biomass. *Remote Sens. Environ.* **2014**, *154*, 102–114. [CrossRef]
88. Shao, Z.; Zhang, L.; Wang, L. Stacked Sparse Autoencoder Modeling Using the Synergy of Airborne LiDAR and Satellite Optical and SAR Data to Map Forest Above-Ground Biomass. *IEEE J. Sel. Top. Appl. Earth Obs. Remote Sens.* **2017**, *10*, 5569–5582. [CrossRef]
89. Breiman, L. Bagging predictors. *Mach. Learn.* **1996**, *24*, 123–140. [CrossRef]
90. Federal Forestry Agency. *Manual on Forest Inventory and Planning in Russian Forest*; Federal Forestry Agency: Moscow, Russia, 1995.
91. Cartus, O.; Santoro, M.; Kellndorfer, J. Mapping forest aboveground biomass in the Northeastern United States with ALOS PALSAR dual-polarization L-band. *Remote Sens. Environ.* **2012**, *124*, 466–478. [CrossRef]
92. Attema, E.P.W.; Ulaby, F.T. Vegetation Modeled as a Water Cloud. *Radio Sci.* **1978**, *13*, 357–364. [CrossRef]
93. Harrell, P.A.; Bourgeau-Chavez, L.L.; Kasischke, E.S.; French, N.H.F.; Christensen, N.L., Jr. Sensitivity of ERS-1 and JERS-1 radar data to biomass and stand structure in Alaskan boreal forest. *Remote Sens. Environ.* **1995**, *54*, 247–260. [CrossRef]
94. Balzter, H.; Baker, J.R.; Hallikainen, M.; Tomppo, E. Retrieval of timber volume and snow water equivalent over a Finnish boreal forest from airborne polarimetric Synthetic Aperture Radar. *Int. J. Remote Sens.* **2002**, *23*, 3185–3208. [CrossRef]
95. Stelmaszczuk-Górska, M.; Thiel, C.; Schmullius, C. Retrieval of aboveground biomass using multi-frequency SAR. In Proceedings of the ESA Living Planet Symposium 2016, Prague, Czech Republic, 9–13 May 2016.
96. Sarker, L.R.; Nichol, J.; Iz, H.B.; Ahmad, B.; Rahman, A.A. Forest Biomass Estimation Using Texture Measurements of High-Resolution Dual-Polarization C-Band SAR Data. *IEEE Trans. Geosci. Remote Sens.* **2013**, *51*, 3371–3384. [CrossRef]

Chapter 5

Synthesis

Discussion and conclusions

Outlook

5.1 Discussion and conclusions

The overall goal of this work was *to develop methods for forest parameter estimation from SAR*. For this, different models were developed. Multi-temporal, multi-polarization, and multi-frequency backscattering coefficients and multi-temporal coherence images were used independently and in combination with the non-parametric models to retrieve AGB. Additionally, polarimetric ratios and texture measures were used as predictor variables. Moreover, an effort to establish an improved operational large-scale mapping of forest loss has been made.

In the following, the achievements of this study with respect to the research questions stated in Chapter 3.2 are discussed and concluded. The potential future research needs that resulted from this work are given in the next section.

Research question #1: How to improve large-scale mapping of boreal forest changes using SAR L-band products?

To answer this research question, three forest loss maps were derived. Moreover, the results were compared with a global forest loss generated by Hansen et al. (Hansen et al., 2013). The study demonstrated that the L-band SAR data have a great potential for automated large-scale forest change/aboveground biomass loss monitoring applying a simple thresholding method in the Siberian forests with a high spatial resolution. Using ALOS PALSAR mosaics with 25 m spatial resolution, forest cover loss was mapped with reasonable accuracy.

To map human induced forest change areas, an integrated GIS and pre-classification approach was implemented. In total 364 1-degree tiles of yearly mosaics of ALOS PALSAR were applied. The data were provided by the ALOS K&C Initiative as level 1.5, co-registered tiles. The dataset is released by JAXA on annual basis. Only HV-polarized mosaic data were used for the yearly forest loss monitoring. Different temporal metrics were employed in order to evaluate change (non-forest) and no change (forest) class separability. For the final automatic forest change mapping a simple thresholding approach based on ratio of SAR mosaics was implemented. The difference between the acquisitions of 2 dB was implemented. To eliminate the misclassifications, a reference map and LC information were used. The data were employed to mask changes in non-forest class that were not relevant (e.g., related to data quality). Further improvement of the classification results was done by removing small patches (<2 ha) and by employing a shape compactness (Bogaert et al., 2000).

The reported high potential for L-band sensors using HV cross-polarization data for large-scale forest mapping, was in line with previous studies (e.g., Santoro et al., 2012). The changes in the study area were identified with approximately 70% accuracy. The majority of forest loss could be observed in 2008 and in 2010 in the north-eastern region of the study area. Hansen's global forest loss map showed the same trend and pattern of changes.

Research question #2: What are the research pathways of boreal forest aboveground biomass estimation using SAR data?

In general, it was difficult to compare the reviewed studies due to the differences between them, which concerned: (i) study area and its characteristics, (ii) spatial resolution of analysis (e.g., forest stand vs forest plot or pixel size), (iii) properties of SAR data (e.g., different frequency, polarization), (iv) SAR acquisition geometry (e.g., different incident angle), weather conditions during the data acquisition, (v) validation procedures, (vi) model applied. However, general conclusions and research pathways could be drawn out.

The conducted review of published research papers showed that most of the studies employed data acquired by C-band satellite missions followed by L-band, and X-band data and were focused on European sites. This was related to the data availability. Only 12% applied data acquired over Siberian sites. Biomass estimation error varied from 119% (M. Santoro et al., 2002) to 5.1%, when multi-temporal combination of ALOS PALSAR backscattering coefficient data at a forest plot in machine-learning approach was used (Andersen et al., 2011). The reported accuracy depended on the (i) frequency of the SAR data, (ii) number and quality of SAR data, (iii) spatial resolution of the analysis. Most of the reported models used semi-empirical models (54%). Fransson and Israelsson (Fransson & Israelsson, 1999) showed that backscatter can be modelled by a semi-empirical model as well as through empirical models, providing equally good results. Most of the reported models employed ground reference data for forest AGB/GSV estimation.

Although greater wavelengths are preferable for forest aboveground biomass estimation, recently the highest accuracies have been reported using X-band data. The lowest estimation errors were reported employing semi-empirical models based on X-band data using InSAR height (12%, at forest plot, (Maciej, Soja, & Persson, 2015)) and radargrammetry method (26.4%, at forest plot, (H. J. Persson & Fransson, 2017)) for European forest sites. For Siberian forests an estimation error of 25% at stand level using ALOS PALSAR InSAR coherence data was reported (Christian Thiel & Schmullius, 2016). According to the author's knowledge, to date

no study has been conducted that would compare different types of models for forest aboveground biomass estimation on one study site using different SAR datasets.

The highest estimation accuracies are anticipated using a combination of data from multiple sources (Maurizio Santoro & Cartus, 2018; Maurizio Santoro et al., 2019).

Research question #3: How to combine multi-temporal InSAR coherence and backscatter data to improve aboveground biomass estimation in boreal forests?

In this study, the feasibility of synergistic usage of backscatter and coherence for AGB retrieval for boreal forests in Siberia at a local scale of 0.25 ha was demonstrated. Four AGB maps were generated and validated. The maps were produced using ALOS PALSAR L-band backscatter in combination with coherence data. New backscatter-coherence normalized ratio was introduced. It was developed based on statistical SAR data analysis. The results showed that relatively high estimation accuracy (down to 30%) can be obtained at a local scale. Moreover, in order to update the available reference data a regional allometric model was developed.

In total 13 variables were used for the AGB estimation. For the AGB retrieval, two popular machine-learning algorithms were implemented. The MaxEnt and RF models performed good showing promising AGB estimations. The RMSEs were 35.8 tons/ha (38.8%) and 35 tons/ha (36.9%) for the MaxEnt and RF, respectively. The models provided different variable importance rankings. However, in both cases the normalized ratio products seem to contain important information in the model development. Coherence data were most important in the low and high AGB ranges, whereas the ratio in the medium to high AGB ranges. Thus, a strategy of using different data sets for estimation of different levels of AGB could further increase biomass retrieval accuracy. It was observed that the backscatter data increased their contribution in the model construction after filtering. In terms of the retrieved AGB values the RF algorithm provided AGB mean estimation almost the same as the reference value. MaxEnt, on the other hand, provided a more realistic spatial distribution of AGB values.

The inventory data dated back to 1998. Because of the time difference between inventory data and the SAR data acquisitions (8-14 years) the *in situ* data were updated. It was done using semi-empirical phytomass models (Shvidenko et al., 2007) and freely available measurements of forest live biomass (phytomass) (IIASA, 2007). Even though, the reference data have been updated using recommended growth models and including removal of the forest stands with extensive logging

activities it is very probable that the local changes in forest structure caused by smaller events, such as selective logging and local fire events, were not taken into account. In this study, it was assumed that the main forest structure has not been changed.

Research question #4: How can fusing of multi-temporal and multi-frequency SAR data improve aboveground biomass estimation?

This study investigated the potential use of multi-frequency (C- and L-band), multi-polarization (HH and HV) and multi-temporal SAR data for AGB estimation in boreal forests. In total forty-five predictor layers were generated using RADARSAT-2 and ALOS-2 PALSAR-2 data, including the multi-temporal metrics and texture measures. The study demonstrated that the high accuracy of AGB estimation could be obtained at local scale of 0.25 ha. Moreover, the use of new acquisition modes of RADARSAT-2 for AGB estimation was investigated.

In total, five models for AGB estimation were developed using from nine to forty-five SAR products. As expected, the AGB modelling results indicated that the longer wavelength L-band data in HH and HV polarizations performed better than C-band data in HH and HV polarizations. The better performance in the first scenario, i.e., when only L-band data were used, was due to the wavelength deeper penetration into canopy providing information from trunks and big branches that are better correlated with the forest AGB, especially in case of dense forests. Comparison of estimation errors showed that filtered L-band data co- and cross-polarized are sufficient to estimate AGB with good accuracy. The inclusion of ratio and texture measure as well as C-band data did not improve the estimation. RADARSAT-2 data acquired in the Ultrafine mode showed greater sensitivity to roughness of objects, reducing the correlation between SAR and reference data, thus generating higher estimation errors.

The lowest estimation error was calculated for L-band filtered data alone and was 29.1 tons/ha (30%). Overall, all models provided the overestimated AGB values with a bias ranging from 3.9 tons/ha (C-band in Fine mode) to 10.6 tons/ha (C-band in Ultrafine mode). In previous studies where the mono-frequency L-band data were applied using the same machine-learning approach and at 25 m spatial resolution, the relative estimation errors from 33.4% to 42.44% for Siberian boreal forests were reported (C. Hüttich et al., 2014; Wilhelm et al., 2014).

The research achievements, along with the research pathways described in Chapter 2.3 can be synthesized as follow:

1. SAR systems have provided reliable information on changes in carbon storage that can contribute to the reduction of the uncertainties in terrestrial carbon pools and current timber volume through mapping of forest cover and estimates of aboveground biomass. The accuracies obtained are higher than previously reported for the boreal Siberian forests for a spatial resolution of 0.25 ha (RMSE of ~30%).
2. The use of multi-looked or/and multi-temporally averaged/filtered SAR data has reduced errors resulted from, e.g., the environmental conditions, geolocation discrepancies between the SAR and *in situ* data.
3. AGB estimations have been improved by including texture, SAR ratios, InSAR coherence and height as a predictor variable. Moreover, the use of longer time series of short wavelength SAR data together with long wavelength data reduced the over- and underestimation that is present when using the non-parametric, i.e., machine learning methods.
4. The known limitation of SAR data, saturation of the signal, has been minimized by the integration of multi-temporal, multi-polarization, and multi-frequency data. The use of the multi-frequency data improved the AGB estimation, as the biomass-related information in the SAR data acquired using different wavelengths comes from different tree compartments, i.e., trunks, branches, and foliage. The C-band data are recommended to estimate AGB of low-biomass vegetation, L-band low to moderate, and P-band moderate to high-biomass vegetation (SERVIR Global Science Coordination Office & National Space Science and Technology Center, 2019).
5. It is also known that the errors in the AGB estimation and its loss monitoring increase due to the topography. Hence, only radiometrically and slope corrected data have been used for AGB estimations. Moreover, the data from both ascending and descending orbits can be applied.
6. The time gap between the SAR and reference data has been minimized. It was done by updating the outdated inventory data using a new regional allometric model. It is recommended to conduct field measurements or use alternative data sources, e.g., optical data, LiDAR data, on the basis of which AGB or other forest parameters can be calculated. The changes in AGB and forest structure influence the SAR signal and thus the accuracy of the estimates. When conducting the forest inventory, the size of reference data should be considered. In general, plots larger than SAR pixel are recommended (SERVIR Global Science Coordination Office & National Space Science and Technology Center, 2019).

7. The applied ML approaches have provided good results of AGB estimation (RMSE of ~30%). ML outperforms parametric methods in case of integration of large number of data with different statistical properties, e.g., distribution and autocorrelation, providing accurate AGB estimates. These methods, however, can provide accurate results for areas for which a comprehensive set of reference data are available. Due to the strong dependence of model performance related to the availability of representative *in situ* data, the methods are characterized by the limited transferability to other regions with different forest structure. In case there is not enough training data available, the use of other methods, e.g., semi-empirical models, should be prioritized.
8. SAR L-band mosaics have provided acceptable mapping results for forest cover changes (accuracy above 70%). The HV-backscatter showed good contrast between forest and non-forested area. Moreover, it was less affected by variations of the environmental conditions. It is recommended, however, to use multiple single-date L-band data instead of annually generated mosaics for accurate forest change mapping. In this way, the errors related to the heterogeneous environmental conditions at the time of data acquisition will be minimized. Furthermore, data acquired using new SAR L-band acquisition modes with higher spatial resolution should further decrease the number of misclassifications. Time series analysis of SAR data should be implemented.

5.2 Outlook

More accurate results are expected in the near future with the launch of new satellite missions BIOMASS, NISAR, and potentially Tandem-L and availability of global LiDAR measurements. These missions are designed in particular to measure forest structure, biomass, and its temporal variations. The use of multi-temporal, multi-frequency and InSAR data is strongly recommended for future forest monitoring studies. In 2022, spaceborne missions collecting data in the X-, C-, and L-band will be complemented by the spaceborne P-band (BIOMASS with new technique tomography SAR) and new L-band (e.g., potentially Tandem-L) missions. The availability of single-pass InSAR L- and P-band data will improve forest change and biomass estimation.

It is known that information on biomass in SAR data obtained using different wavelengths comes from various elements of trees, i.e., trunks, branches, and foliage. The X- and C-band data are recommended to estimate AGB of low-biomass

vegetation, L-band low to moderate, and P-band moderate to high-biomass vegetation. This research showed that the inclusion of C-band data did not improve the estimation. It should be mentioned, however, that only a limited number of C-band images was available for this study. Therefore, the use of ever-growing archive of spaceborne C-band data should be further investigated. In addition, the inclusion of data acquired by complementary short and long frequencies X- and soon available P-band sensors should be assessed. Moreover, data acquired in the C-band with increased spatial resolution (Ultrafine mode) showed more sensitivity to roughness of objects, reducing the correlation between the SAR and the forest biomass, thus generating higher estimation errors. Analysis of multi-temporal observations at multiple frequencies will contribute to improving our understanding of the scattering mechanism from forests, and will allow more accurate biomass estimation using satellite SAR systems. The use of multi-temporal and multi-frequency data will also reduce the over and underestimation that occurs when using non-parametric algorithms, i.e., machine or deep learning. Thus, the research needs that should be formulated in the future would be which frequencies and acquisition modes should be preferred for which forest characteristics (e.g., forest structure and type) and what would be the minimum required number of SAR acquisitions to achieve a certain accuracy.

Complementary and new information to the backscattering intensity provides SAR interferometry. Both interferometric height information and coherence were used for forest applications. This study demonstrated the feasibility of synergistic use of backscatter and coherence for AGB estimation for boreal forests. AGB was calculated using ALOS PALSAR L-band backscatter in combination with coherence data. The results showed that relatively high estimation accuracy can be obtained at a local scale. Coherence data were most important in the low and maximum AGB ranges, while backscatter in the low and normalized backscatter-coherence ratio in the medium to high AGB ranges. This approach of analyzing various SAR products compared to different AGB ranges may be the subject of further research, including integrating time series of multi-frequency backscatter and coherence data. Thus, a strategy of using different data sets to estimate different AGB levels can further increase the accuracy of biomass retrieval using SAR data.

Integration of coherence image should improve the accuracy of forest/non-forest mapping. The use of repeat-pass interferometry is not a limitation in the Siberian boreal forests due to the stable environmental conditions during winter. Integration of InSAR coherence is of particular importance in order to fully use the potential of SAR data within an operational large-scale forest-monitoring system. Fusion of further additional data sources, e.g., up-to-date forest mask, tree height information,

could be considered in a future as a refinement of the automated mapping system. The results could be further improved by employing the image segmentation in the classification procedure.

Recommended future studies of the complementarity of different SAR products for forest monitoring, in particular forest biomass estimation with different forest structural characteristics, are not possible without reliable and extensive reference data. In this study, due to the time difference between inventory data and the SAR data acquisitions, the *in situ* data were updated using a new regional allometric equation. No other data or solutions were available at the time the forest inventory was updated. Currently new ground data acquisition technologies are possible. In the near future, these technologies can replace the standard techniques used for inventory of forest resources and eliminate unknown errors in human measurements. The costs of LiDAR data have decreased and can be obtained not only from airborne platforms carrying large heavy sensor, but also from Unmanned Aerial Vehicles (UAVs). The UAV LiDAR system for 3D vegetation mapping is cost-effective compared to renting an aircraft. UAV photogrammetry is a technology closely related to UAV LiDAR but cheaper. Using overlapping images (80 to 90% overlap) of the ground, tree height can be generated. Terrestrial laser scanning (TLS) can also be used to analyze a small area. It is a ground-based version of the airborne or UAV LIDAR often used for terrain and landscape mapping. UAV LiDAR, UAV photogrammetry and TLS are relatively new developments for high-resolution mapping and can support the collection of reliable and representative reference data. This kind of data will not only contribute to a better understanding of the interaction of multi-frequency SAR products with forests, but will also provide important input to machine learning algorithms.

References

Achard, F., & Hansen, M. C. (Eds.). (2013). *Global Forest Monitoring from Earth Observation*. Boca Raton, USA: CRC Press.

Allen, C. D., Macalady, A. K., Chenchouni, H., Bachelet, D., McDowell, N., Vennetier, M., … Cobb, N. (2010). A global overview of drought and heat-induced tree mortality reveals emerging climate change risks for forests. *Forest Ecology and Management*, *259*(4), 660–684. https://doi.org/10.1016/j.foreco.2009.09.001

Andersen, H. E., Strunk, J., Temesgen, H., Atwood, D., & Winterberger, K. (2011). Using multilevel remote sensing and ground data to estimate forest biomass resources in remote regions: A case study in the boreal forests of interior Alaska. *Canadian Journal of Remote Sensing*, *37*(6), 596–611. https://doi.org/10.5589/m12-003

Antropov, O., Rauste, Y., Ahola, H., & Häme, T. (2013). Stand-level stem volume of boreal forests from spaceborne SAR imagery at L-band. *IEEE Transactions on Geoscience and Remote Sensing*, *6*(1), 4776–4779.

Antropov, O., Rauste, Y., Häme, T., & Praks, J. (2017). Polarimetric ALOS PALSAR time series in mapping biomass of boreal forests. *Remote Sensing*, *9*(10), 1–24. https://doi.org/10.3390/rs9100999

Askne, J., & Smith, G. (1996). Forest InSAR decorrelation and classification properties. In *FRINGE 96 Workshop on ERS SAR Interferometry*. Zurich.

Askne, J. I. H., Dammert, P. B. G., Ulander, L. M. H., & Smith, G. (1997). C-band repeat-pass interferometric SAR observations of the forest. *IEEE Transactions on Geoscience and Remote Sensing*, *35*(1), 25–35.

Askne, J., Santoro, M., Smith, G., & Fransson, J. E. S. (2003). Multitemporal repeat-rass SAR interferometry of boreal forests. *IEEE Transactions on Geoscience and Remote Sensing*, *41*(7), 1540–1550.

Askne, J. I. H., & Santoro, M. (2009). Automatic model-based estimation of boreal forest stem volume from repeat pass C-band InSAR coherence. *IEEE Transactions on Geoscience and Remote Sensing*, *47*(2), 513–516.

Askne, J., Fransson, J., Santoro, M., Soja, M., & Ulander, L. (2013). Model-based biomass estimation of a hemi-boreal forest from multitemporal TanDEM-X acquisitions. *Remote Sensing*, *5*(11), 5574–5597. https://doi.org/10.3390/rs5115574

Askne, J. I. H., & Santoro, M. (2015). On the Estimation of Boreal Forest Biomass From TanDEM-X Data Without Training Samples. *IEEE Geoscience and Remote Sensing Letters*, *12*(4), 771–775. Retrieved from http://ieeexplore.ieee.org/stamp/stamp.jsp?tp=&arnumber=6934977&tag=1

Askne, J. I. H., Soja, M. J., & Ulander, L. M. H. (2017). Biomass estimation in a boreal forest from TanDEM-X data, lidar DTM, and the interferometric water cloud model. *Remote Sensing of Environment*, *196*, 265–278. https://doi.org/10.1016/j.rse.2017.05.010

Askne, J. I. H., & Persson, H. J. (2019). On the Sensitivity of TanDEM-X-Observations to Boreal Forest Structure. *Remote Sensing*, *11*(14), 1–22.

Atwood, D. K., Andersen, H. E., Matthiss, B., & Holecz, F. (2014). Impact of topographic correction on estimation of aboveground boreal biomass using multi-temporal, L-band backscatter. *IEEE Journal of Selected Topics in Applied Earth Observations and Remote Sensing*, *7*(8), 3262–3273. https://doi.org/10.1109/JSTARS.2013.2289936

Avitabile, V., Herold, M., Henry, M., & Schmullius, C. (2011). Mapping biomass with remote sensing: a comparison of methods for the case study of Uganda. *Carbon Balance and Management*, *6*(1), 7. https://doi.org/10.1186/1750-0680-6-7

Avitabile, V., Baccini, A., Friedl, M. a., & Schmullius, C. (2012). Capabilities and limitations of Landsat and land cover data for aboveground woody biomass estimation of Uganda. *Remote Sensing of Environment*, *117*, 366–380. https://doi.org/10.1016/j.rse.2011.10.012

Babcock, C., Finley, A. O., Cook, B. D., Weiskittel, A., & Woodall, C. W. (2016). Modeling forest biomass and growth: Coupling long-term inventory and LiDAR data. *Remote Sensing of Environment*, *182*, 1–12. https://doi.org/10.1016/j.rse.2016.04.014

Baccini, A., Laporte, N., Goetz, S. J., Sun, M., & Dong, H. (2008). A first map of tropical Africa's above-ground biomass derived from satellite imagery. *Environmental Research Letters*, *3*(045011), 9. https://doi.org/10.1088/1748-9326/3/4/045011

Balzter, H. (2001). Forest mapping and monitoring with interferometric synthetic aperture radar (InSAR). *Progress in Physical Geography*, *25*(2), 159–177. https://doi.org/10.1177/030913330102500201

Balzter, H., Talmon, E., Wagner, W., Gaveau, D., Plummer, S., Yu, J. J., … Schmullius, C. (2002). Accuracy assessment of a large-scale forest cover map of

central Siberia from synthetic aperture radar. *Canadian Journal of Remote Sensing*, *28*, 719–737.

Bamler, R., & Hartl, P. (1998). Synthetic aperture radar interferometry. *Inverse Problems*, *14*(4), R1–R54. https://doi.org/10.1088/0266-5611/14/4/001

Bamler, R., Bruzzone, L., Camp-Valls, G., Cavallaro, G., Corpetti, T., Datcu, M., … Zhu, X. (2018). *Towards a European AI4EO R&I Agenda*. Retrieved from https://eo4society.esa.int/wp-content/uploads/2018/09/ai4eo_v1.0.pdf

Bar-On, Y. M., Phillips, R., & Milo, R. (2018). The biomass distribution on Earth. *Proceedings of the National Academy of Sciences of the United States of America*, *115*(25), 6506–6511. https://doi.org/10.1073/pnas.1711842115

Bastin, J. F., Finegold, Y., Garcia, C., Mollicone, D., Rezende, M., Routh, D., … Crowther, T. W. (2019). The global tree restoration potential. *Science*, *364*(6448), 76–79. https://doi.org/10.1126/science.aax0848

Beaudoin, A., Le Toan, T., Goze, S., Nezry, E., Lopes, A., Mougin, E., … Shin, R. T. (1994). Retrieval of forest biomass from SAR data. *International Journal of Remote Sensing*, *15*(14), 2777–2796.

Beck, P. S. A., Juday, G. P., Alix, C., Barber, V. A., Winslow, S. E., Sousa, E. E., … Goetz, S. J. (2011). Changes in forest productivity across Alaska consistent with biome shift. *Ecology Letters*, *14*(4), 373–379. https://doi.org/10.1111/j.1461-0248.2011.01598.x

Belgiu, M., & Drăgu, L. (2016). Random forest in remote sensing: A review of applications and future directions. *ISPRS Journal of Photogrammetry and Remote Sensing*, *114*, 24–31. https://doi.org/10.1016/j.isprsjprs.2016.01.011

Bogaert, J., Rousseau, R., Van Hecke, P., & Impens, I. (2000). Alternative area-perimeter ratios for measurement of 2D shape compactness of habitats. *Applied Mathematics and Computation*, *111*(1), 71–85. https://doi.org/10.1016/S0096-3003(99)00075-2

Bojinski, S., Verstraete, M., Peterson, T. C., Richter, C., Simmons, A., & Zemp, M. (2014). The concept of essential climate variables in support of climate research, applications, and policy. *Bulletin of the American Meteorological Society*, *95*(9), 1431–1443. https://doi.org/10.1175/BAMS-D-13-00047.1

Bonan, G. B. (2008). Forests and climate change: Forcings, feedbacks, and the climate benefits of forests. *Science*, *320*(5882), 1444–1449. https://doi.org/10.1126/science.1155121

Born, M., & Wolf, E. (1999). *Principles of optics* (Seventh). Cambridge University Press.

Bortolot, Z. J., & Wynne, R. H. (2005). Estimating forest biomass using small footprint LiDAR data: An individual tree-based approach that incorporates training data. *ISPRS Journal of Photogrammetry and Remote Sensing*, *59*(6),

342–360. https://doi.org/10.1016/j.isprsjprs.2005.07.001

Boyd, D. S., Foody, G. M., & Curran, P. J. (1999). The relationship between the biomass of Cameroonian tropical forests and radiation reflected in middle infrared wavelengths (3.0-5.0 μm). *International Journal of Remote Sensing*, *20*(5), 1017–1023. https://doi.org/10.1080/014311699213055

Breckle, S.-W. (2002). *Walter's Vegetation of the Earth. The Ecological Systems of the Geo-Biosphere* (4th ed.). Springer-Verlag Berlin Heidelberg.

Breiman, L. (2001). Random Forests. *Machine Learning*, *45*(1), 5–32. https://doi.org/10.1023/A:1010933404324

Bruzzone, L., Gamba, P., Hayden, L., Inggs, M., Kerekes, J., Le Vine, D. M., … (eds.). (2016). Learning the Data: A special Issue on Advances in Machine Learning for Remote Sensing and Geosciences. *IEEE Geoscience and Remote Sensing Magazine*, p. 116. https://doi.org/10.1109/MGRS.2016.2547659

Burton, P. J., Bergeron, Y., Bogdanski, B. E. C., Juday, G. P., Kuuluvainen, T., McAfee, B. J., … Hantula, J. (2010). Sustainability of boreal forests and forestry in a changing environment. In G. Mery, P. Katila, G. Galloway, R. I. Alfaro, M. Kanninen, M. Lobovikov, & J. Varjo (Eds.), *Forests and Society - Responding to Global Drivers of Change* (pp. 249–282). Vienna, Austria: International Union of Forest Research Organizations, IUFRO World Series.

CSA. (2017). RADARSAT-2. Retrieved August 1, 2019, from http://www.asc-csa.gc.ca/eng/satellites/radarsat2/Default.asp

Cartus, O., Kellndorfer, J., Rombach, M., & Walker, W. (2012). Mapping Canopy Height and Growing Stock Volume Using Airborne Lidar, ALOS PALSAR and Landsat ETM+. *Remote Sensing*, *4*(11), 3320–3345. https://doi.org/10.3390/rs4113320

Cartus, O., & Santoro, M. (2019). Exploring combinations of multi-temporal and multi-frequency radar backscatter observations to estimate above-ground biomass of tropical forest. *Remote Sensing of Environment*, *232*(March), 111313. https://doi.org/10.1016/j.rse.2019.111313

Cartus, O., Santoro, M., Wegmüller, U., & Rommen, B. (2019). Benchmarking the Retrieval of Biomass in Boreal Forests Using P-Band SAR Backscatter with Multi-Temporal C- and L-band Observations. *Remote Sensing*, *11*(14), 20. https://doi.org/https://doi.org/10.3390/rs11141695

Carvalhais, N., Forkel, M., Khomik, M., Bellarby, J., Jung, M., Migliavacca, M., … Reichstein, M. (2014). Global covariation of carbon turnover times with climate in terrestrial ecosystems. *Nature*, *514*(7521), 213–217. https://doi.org/10.1038/nature13731

Chowdhury, T. A., Thiel, C., & Schmullius, C. (2014). Growing stock volume estimation from L-band ALOS PALSAR polarimetric coherence in Siberian forest. *Remote Sensing of Environment*, *155*, 129–144.

https://doi.org/10.1016/j.rse.2014.05.007

Ciais, P., Sabine, C., Bala, G., Bopp, L., Brovkin, V., Canadell, A., … Thornton, P. (2013). Carbon and Other Biogeochemical Cycles - Climate Change The physical Science Basis. Contribution of Working Group I to the Fifth Assessment Report of the intergovernmental Panel on Climate Change. In T. F. Stocker, D. Qin, G.-K. Plattner, M. Tignor, S. K. Allen, J. Boschung, … P. M. Midgle (Eds.), *The physical Science Basis. Contribution of Working Group I to the Fifth Assessment Report of the intergovernmental Panel on Climate Change* (pp. 465–570). Cambridge, United Kingdom and New York, NY, USA: Cambridge University Press. Retrieved from http://ebooks.cambridge.org/ref/id/CBO9781107415324A023%0Apapers3://publication/doi/10.1017/cbo9781107415324.015

Cihlar, J., Denning, S., Ahem, F., Arino, O., Belward, A., Bretherton, F., … Wickland, D. (2002). Initiative to quantify terrestrial carbon sources and sinks. *Eos, Transactions American Geophysical Union*, *83*(1), 6–7. https://doi.org/10.1029/2002EO000002

Coppin, P., & Bauer, M. E. (1996). Digital Change Detection in Forest Ecosystems with Remote Sensing Imagery. *Remote Sensing Reviews*, *13*(3–4), 207–234. https://doi.org/10.1080/02757259609532305

Coppin, P., Jonckheere, I., Nackaerts, K., Muys, B., & Lambin, E. (2004). Digital change detection methods in ecosystem monitoring: A review. *International Journal of Remote Sensing*, *25*(9), 1565–1596. https://doi.org/10.1080/0143116031000101675

Cremer, F., Urbazaev, M., Berger, C., Mahecha, M. D., Schmullius, C., & Thiel, C. (2018). An Image Transform Based on Temporal Decomposition. *IEEE Geoscience and Remote Sensing Letters*, *15*(4), 537–541. https://doi.org/10.1109/LGRS.2018.2791658

Cumming, I. G., & Wong, F. H. (2005). *Digital Processing of Synthetic Aperture Radar Data. Algorithms and Implementation.* Artech House, Inc.

Dammert, B. G., & Askne, J. (1998). Interferometric tree height observations in boreal forests with SAR interferometry. In *IEEE International Geoscience and Remote Sensing Symposium 1998* (pp. 1363–1366). Seattle, WA, USA.

De Zan, F., & Guarnieri, A. M. (2006). TOPSAR: Terrain observation by progressive scans. *IEEE Transactions on Geoscience and Remote Sensing*, *44*(9), 2352–2360. https://doi.org/10.1109/TGRS.2006.873853

DeFries, R. (2013). Why Forest Monitoring Matters for People and the Planet. In Frederic Achard & R. A. Houghton (Eds.), *Global Forest Monitoring from Earth Observation* (pp. 1–14). CRC Press.

Dobson, M. C., Ulaby, F. T., Beaudoin, A., Kasischke, E. S., & Christensen, N. (1992). Dependence of radar backscatter on coniferous forest biomass. *IEEE*

Transactions on Geoscience and Remote Sensing, *30*(2), 412–415.

Dong, J., Kaufmann, R. K., Myneni, R. B., Tucker, C. J., Kauppi, P. E., Liski, J., … Hughes, M. K. (2003). Remote sensing estimates of boreal and temperate forest woody biomass: carbon pools, sources, and sinks. *Remote Sensing of Environment*, *84*, 393–410. https://doi.org/10.1016/S0034-4257(02)00130-X

Dubayah, R., Blair, J. B., Goetz, S., Fatoyinbo, L., Hansen, M., Healey, S., … Silva, C. (2020). The Global Ecosystem Dynamics Investigation: High-resolution laser ranging of the Earth's forests and topography. *Science of Remote Sensing*, *1*(September 2019), 100002. https://doi.org/10.1016/j.srs.2020.100002

Eberle, J., Clausnitzer, S., Hüttich, C., & Schmullius, C. (2013). Multi-source data processing middleware for land monitoring within a web-based spatial data infrastructure for Siberia. *ISPRS International Journal of Geo-Information*, *2*(3), 553–576. https://doi.org/10.3390/ijgi2030553

Erb, K. H., Kastner, T., Plutzar, C., Bais, A. L. S., Carvalhais, N., Fetzel, T., … Luyssaert, S. (2018). Unexpectedly large impact of forest management and grazing on global vegetation biomass. *Nature*, *553*(7686), 73–76. https://doi.org/10.1038/nature25138

Eriksson, L. E. B., Santoro, M., Wiesmann, A., & Schmullius, C. C. (2003). Multitemporal JERS repeat-pass coherence for growing-stock volume estimation of Siberian forest. *IEEE Transactions on Geoscience and Remote Sensing*, *41*(7), 1561–1570.

ESA. (2019). Biomass - Satellite Missions - eoPortal Directory Biomass.

EU. Regulation (EU) No 377/2014 of the European Parliament and of the Council of 3 April 2014 establishing the Copernicus Programme and repealing Regulation (EU) No 911/2010 (Text with EEA relevance), 2014 § (2014). Retrieved from http://www.copernicus.eu/pages-principales/library/

FAO. (2006). *Global Forest Resources Assessment 2005: Progress towards sustainable forest management. FAO Forestry Paper.*

FAO. (2009). *Essential Climate Variables. Assessment of the status of the development of the standards for the terretrial Essential Climate Variables. GTOS Essential Climate Variable Reports* (Vol. T8).

FAO. (2010). *Global Forest Resources. Assesment 2010. Main report.* Rome. Retrieved from http://www.fao.org/docrep/013/i1757e/i1757e00.htm

FAO. (2012). *The Russian Federation forest sector outlook study to 2030.* Rome.

FAO. (2015). *Global Forest Resources Assessment 2015. FAO.* Rome, Italy. https://doi.org/10.1002/2014GB005021

FAO. (2016). *State of the World's Forests 2016. Forests and agriculture: land-use challenges and opportunities. State of the World'S Forests Forests and Agriculture: Land-Use Challenges and Opportunities* (Vol. 45).

https://doi.org/10.1146/annurev-environ-020411-130608

FAO. (2018). *Global Forest Resources Assessment 2020. Guidelines and specifications*. Retrieved from www.fao.org/forestry%0Ahttp://www.fao.org/3/I8699EN/i8699en.pdf

FAO FRA. (2012). Forest Resources Assessment 2015: Terms and Definitions. *FAO Report*, 36. Retrieved from http://www.fao.org/docrep/017/ap862e/ap862e00.pdf

Fassnacht, F. E., Latifi, H., Sterenczak, K., Modzelewska, A., Lefsky, M., Waser, L. T., … Ghosh, A. (2016). Review of studies on tree species classification from remotely sensed data. *Remote Sensing of Environment*, *186*, 64–87. https://doi.org/10.1016/j.rse.2016.08.013

Fassnacht, F. E., Mangold, D., Schäfer, J., Immitzer, M., Kattenborn, T., Koch, B., & Latifi, H. (2017). Estimating stand density, biomass and tree species from very high resolution stereo-imagery – towards an all-in-one sensor for forestry applications? *Forestry: An International Journal of Forest Research*, (March), 1–19. https://doi.org/10.1093/forestry/cpx014

Fatoyinbo, T. (Ed.). (2012). *Remote sensing of biomass - Principles and applications*. InTech. https://doi.org/10.5772/696

Folkesson, K., Smith-jonforsen, G., & Ulander, L. M. H. (2009). Model-based compensation of topographic effects for improved stem-volume retrieval from CARABAS-II VHF-band SAR images. *IEEE Transactions on Geoscience and Remote Sensing*, *47*(4), 1045–1055. https://doi.org/10.1109/TGRS.2008.2009531

FRA. (2018). *Global Forest Resources Assessment 2020: Terms and Definition. Resources Assessment Working Paper 188*.

Fransson, J. E. S., & Israelsson, H. (1999). Estimation of stem volume in boreal forests using ERS-1 C- and JERS-1 L- band SAR data. *International Journal of Remote Sensing*, *20*(1), 123–137.

Fransson, J. E. S., WaLter, F., & Ulander, L. M. H. (2000). Estimation of forest parameters using CARABAS-II VHF SAR data. *IEEE Transactions on Geoscience and Remote Sensing*, *38*(2), 720–727. https://doi.org/10.1109/36.842001

Fransson, J. E. S., Smith, G., Askne, J., & Olsson, H. (2001). Stem volume estimation in boreal forests using ERS-1/2 coherence and SPOT XS optical data. *International Journal of Remote Sensing*, *22*(14), 2777–2791. https://doi.org/10.1080/01431160010006872

Fransson, J. E. S., Magnusson, M., Eriksson, L. E. B., Sandberg, G., Smith-, G., & Ulander, L. M. H. (2007). Detection of forest changes using ALOS PALSAR satellite images. In *Geoscience and Remote Sensing Symposium, IGARSS 2007* (pp. 2330–2333). Retrieved from

http://ieeexplore.ieee.org/stamp/stamp.jsp?tp=&arnumber=4423308

Freeman, A. (2004). Calibration of linearly polarized polarimetric SAR data subject to Faraday rotation. *IEEE Transactions on Geoscience and Remote Sensing*, *42*(8), 1617–1624. https://doi.org/10.1109/TGRS.2004.830161

Frey, O., Santoro, M., Werner, C. L., & Wegmüller, U. (2013). DEM-based SAR pixel-area estimation for enhanced geocoding refinement and radiometric Normalization. *IEEE Geoscience and Remote Sensing Letters*, *10*(1), 48–52. https://doi.org/10.1109/LGRS.2012.2192093

Garrison, J. L., Melgani, F., Hayden, L., Hajnsek, I., Inggs, M., Kerekes, J., … (eds.). (2019). Special Issue on Data Fusion in Remote Sensing. *IEEE Transactions on Geoscience and Remote Sensing Magazine*, *7*(1), 116. https://doi.org/10.1109/tgrs.2014.2383297

Garvin, J., Bufton, J., Blair, J., Harding, D., Luthcke, S., Frawley, J., & Rowlands, D. (1998). Observations of the earth's topography from the Shuttle Laser Altimeter (SLA): Laser-pulse echo-recovery measurements of terrestrial surfaces. *Physics and Chemistry of the Earth*, *23*(9–10), 1053–1068. https://doi.org/10.1016/S0079-1946(98)00145-1

Gauthier, S., Bernier, P., Kuuluvainen, T., Shvidenko, A. Z., & Schepaschenko, D. G. (2015). Boreal forest health and global change. *Science*, *349*(6250), 819–822. https://doi.org/10.1126/science.aaa9092

GCOS. (2016). *The Global Observing System For Climate: Implementation Needs. World Meteorological Organization* (Vol. 200). Geneva, Switzerland. https://doi.org/GCOS-200

Geudtner, D. (2014). *Implementation of the TOPS Mode on RADARSAT-2 in Support of the Copernicus Sentinel-1 Mission. RADARSAT-2 TOPS SAR Interferometry (InSAR) Data Satck Acquisitions. ESA Tecnical Note* (Vol. 1).

Goetz, S., & Dubayah, R. (2011). Advances in remote sensing technology and implications for measuring and monitoring forest carbon stocks and change. *Carbon Management*, *2*(3), 231–244. https://doi.org/10.4155/cmt.11.18

GOFC-GOLD. (2009). *A sourcebook of methods and procedures for monitoring and reporting anthropogenic greenhouse gas emissions and removals caused by deforestation, gains and losses of carbon stocks in forests remaining forests, and forestation.* Retrieved from http://www.gofc-gold.uni-jena.de/redd/sourcebook/Sourcebook_Version_Nov_2009_cop15-1.pdf

Goldstein, R. M., Zebker, H. A., & Werner, C. L. (1988). Radar interferometry: Two-dimensional phase unwrapping. *Radio Science*, *23*(4), 713–720.

Hagberg, J., Ulander, L. M. H., & Askne, J. (1995). Repeat-pass SAR interferometry over forested terrain. *IEEE Transactions on Geoscience and Remote Sensing*, *33*(2), 331–340.

Hanssen, R. F. (2001). *Radar Interferometry. Data Interpretation and Error Analysis*. Dordrecht, The Netherlands: Kluwer Academic Publishers. Retrieved from http://weekly.cnbnews.com/news/article.html?no=124000

Hansen, M. C., Potapov, P. V, Moore, R., Hancher, M., Turubanova, S. a, Tyukavina, a, … Townshend, J. R. G. (2013). High-resolution global maps of 21st-century forest cover change. *Science (New York, N.Y.)*, *342*(6160), 850–853. https://doi.org/10.1126/science.1244693

Hansen, M. C., Krylov, A., Tyukavina, A., Potapov, P. V., Turubanova, S., Zutta, B., … Moore, R. (2016). Humid tropical forest disturbance alerts using Landsat data. *Environmental Research Letters*, *11*(3). https://doi.org/10.1088/1748-9326/11/3/034008

Harding, D., Dabney, P., Abshire, J., Huss, T., Jodor, G., Machan, R., … Zheng, Y. (2010). The slope imaging multi-polarisation photon-counting LiDAR: an advanced technology airborne laser altimeter. In *NASA Earth Science Technology Forum*. Arlington.

Hare, F. K., & Ritchie, J. C. (1972). The Boreal Bioclimates. *American Geographical Society*, *62*(3), 333–365. https://doi.org/10.1126/science.15.370.195

Harrell, P. A., Bourgeau-Chavez, L. L., Kasischke, E. S., French, N. H. F., & Christensen Jr., N. L. (1995). Sensitivity of ERS-1 and JERS-1 radar data to biomass and stand structure in Alaskan boreal forest. *Remote Sensing of Environment*, *54*(3), 247–260. https://doi.org/10.1016/0034-4257(95)00127-1

Harrell, P. a., Kasischke, E. S., Bourgeau-Chavez, L. L., Haney, E. M., & Christensen, N. L. (1997). Evaluation of approaches to estimating aboveground biomass in Southern pine forests using SIR-C data. *Remote Sensing of Environment*, *59*(2), 223–233. https://doi.org/10.1016/S0034-4257(96)00155-1

Henderson, F. M., & Lewis, A. J. (1998). *Principles and Applications of Imaging Radar, Vol. 2* (Third). John Wiley an Sons Inc.

Herold, M., Carter, S., Avitabile, V., Espejo, A. B., Jonckheere, I., Lucas, R., … De Sy, V. (2019). The Role and Need for Space-Based Forest Biomass-Related Measurements in Environmental Management and Policy. *Surveys in Geophysics*, 757–778. https://doi.org/10.1007/s10712-019-09510-6

Hess, L. L., Melack, J. M., & Simonett, D. S. (1990). Radar detection of flooding beneath the forest canopy: A review. *International Journal of Remote Sensing*, *11*(7), 1313–1325. https://doi.org/10.1080/01431169008955095

Houghton, R. A. (2007). Balancing the Global Carbon Budget. *Annual Review of Earth and Planetary Sciences*, *35*(1), 313–347. https://doi.org/10.1146/annurev.earth.35.031306.140057

Houghton, R. A., Hall, F., & Goetz, S. J. (2009). Importance of biomass in the global carbon cycle. *Journal of Geophysical Research*, *114*, 1–13.

https://doi.org/10.1029/2009JG000935

Houghton, R. A. (2013). Role of Forests and Impact of Deforestation in the Global Carbon Cycle. In Frédéric Achard & M. C. Hansen (Eds.), *Global Forest Monitoring from Earth Observation* (pp. 15–38). CRC Press.

Hu, T., Su, Y., Xue, B., Liu, J., Zhao, X., Fang, J., & Guo, Q. (2016). Mapping global forest aboveground biomass with spaceborne LiDAR, optical imagery, and forest inventory data. *Remote Sensing*, *8*(7). https://doi.org/10.3390/rs8070565

Hughes, G. F. (1968). On the mean accuracy of statistical pattern recognizers. *IEEE Transactions on Information Theory*, *14*, 55.

Hüttich, C, Schmullius, C., Thiel, C., Bartalev, S., Emelyanov, K., Korets, M., & Shvidenko, A. (2012). Assessment and monitoring of Siberian forest recources in the framework of the EU-Russia ZAPÁS project. In *IGARSS 2012 Geoscience and Remote Sensing Symposium* (Vol. 5, pp. 7208–7211). Munich, Germany. Retrieved from http://ieeexplore.ieee.org/stamp/stamp.jsp?tp=&arnumber=6351999

Hüttich, C., Korets, M., Bartalev, S., Zharko, V., Schepaschenko, D., Shvidenko, A., & Schmullius, C. (2014). Exploiting Growing Stock Volume Maps for Large Scale Forest Resource Assessment: Cross-Comparisons of ASAR- and PALSAR-Based GSV Estimates with Forest Inventory in Central Siberia. *Forests*, *5*, 1753–1776. https://doi.org/10.3390/f5071753

Hüttich, Christian, Stelmaszczuk-Górska, M., Eberle, J., Kotzerke, P., & Schmullius, C. C. (2014). Operational forest monitoring in Siberia using multi-source Earth Observation data. *Siberian Journal of Forest Science*, *5*, 38–52. Retrieved from http://sibjforsci.com/articles/h-ttich-c-stelmaszczuk-g-rska-m-a-eberle-j-kotzerke-p-schmullius-c-operational-forest-monitoring-in-/

IIASA. (2007). Russian Forests & Forestry. Live biomass & net primary production – measurements of forest phytomass in situ. Retrieved from http://webarchive.iiasa.ac.at/Research/FOR/forest_cdrom/english/for_prod_en.html

Imhoff, M. L. (1995). Radar backscatter and biomass saturation: ramifications for global biomass inventory. *IEEE Transactions on Geoscience and Remote Sensing*, *33*(2), 511–518. https://doi.org/10.1109/36.377953

IPCC. (2007). *Climate Change 2007: An Assessment of the Intergovernmental Panel on Climate Change. IPCC.*

IPCC. (2013). *Climate Change 2013: The physical science basis. Working Group I contribution to the fifth assessment report of the Intergovermental Panel on Climate Change.*

IPCC. (2014). *Climate Change 2014: Synthesis Report.* (R. K. Pachauri & L. A. Meyer, Eds.), *Contribution of Working Groups I, II and III to the Fifth*

Assessment Report of the Intergovernmental Panel on Climate Change (Vol. 40). Geneva, Switzerland: Intergovernmental Panel on Climate Change. Retrieved from https://www.ipcc.ch/site/assets/uploads/2018/02/SYR_AR5_FINAL_full.pdf

IPCC. (2018a). *Global Warming of 1.5°C. An IPCC Special Report on the impacts of global warming of 1.5°C above pre-industrial levels and related global greenhouse gas emission pathways, in the context of strengthening the global response to the threat of climate change,*. Retrieved from https://www.ipcc.ch/site/assets/uploads/sites/2/2019/06/SR15_Full_Report_High_Res.pdf

IPCC. (2018b). *Summary for Policymakers. In: Global warming of 1.5°C. An IPCC Special Report on the impacts of global warming*. Retrieved from https://www.ipcc.ch/

JAXA Earth Observation Research Center. (2018). *Global 25m Resolution PALSAR-2/PALSAR Mosaic and Forest/Non-Forest Map (FNF): Dataset Description*. Retrieved from https://www.eorc.jaxa.jp/ALOS/en/palsar_fnf/DatasetDescription_PALSAR2_Mosaic_FNF_revH.pdf

Jensen, J. R. (2007). *Remote Sensing of the Environment: An Earth Resource Perspective* (2nd ed.). New York, USA.: PEARSON Prentice Hall, Upper Saddle River.

Joshi, C., Leeuw, J. De, Skidmore, A. K., Duren, I. C. Van, & van Oosten, H. (2006). Remotely sensed estimation of forest canopy density: A comparison of the performance of four methods. *International Journal of Applied Earth Observation and Geoinformation*, *8*, 84–95. https://doi.org/10.1016/j.jag.2005.08.004

Joshi, N., Mitchard, E. T. A., Brolly, M., Schumacher, J., Fernández-Landa, A., Johannsen, V. K., … Fensholt, R. (2017). Understanding "saturation" of radar signals over forests. *Scientific Reports*, *7*(1), 1–11. https://doi.org/10.1038/s41598-017-03469-3

Kankaku, Y., Suzuki, S., & Osawa, Y. (2013). ALOS-2 mission and development status. In *International Geoscience and Remote Sensing Symposium (IGARSS)* (pp. 2396–2399). IEEE. https://doi.org/10.1109/IGARSS.2013.6723302

Karila, K., Vastaranta, M., Karjalainen, M., & Kaasalainen, S. (2015). Tandem-X interferometry in the prediction of forest inventory attributes in managed boreal forests. *Remote Sensing of Environment*, *159*, 259–268. https://doi.org/10.1016/j.rse.2014.12.012

Karjalainen, M., Kankare, V., Vastaranta, M., Holopainen, M., & Hyyppä, J. (2012). Prediction of plot-level forest variables using TerraSAR-X stereo SAR data. *Remote Sensing of Environment*, *117*, 338–347.

https://doi.org/10.1016/j.rse.2011.10.008

Kellndorfer, J., Cartus, O., Bishop, J., Walker, W., & Holecz, F. (2011). Large Scale Mapping of Forests and Land Cover with Synthetic Aperture Radar Data. In F. Holecz, P. Pasquali, N. Milisavljevic, & D. Closson (Eds.), *Land applications of radar remote sensing* (p. 36). InTech. Retrieved from http://www.intechopen.com/books/land-applications-of-radar-remote-sensing/large-scale-mapping-of-forests-and-land-cover-with-synthetic-aperture-radar-data

Kessler, R. (1987). Applicabilities of imaging radar for classification of forest vegetation. *Photogrammetria*, *41*(4), 221–232. https://doi.org/10.1016/0031-8663(87)90013-5

Koskinen, J. T., Pulliainen, J. T., Hyyppä, J. M., Engdahl, M. E., & Hallikainen, M. T. (2001). The seasonal behavior of interferometric coherence in boreal forest. *IEEE Transactions on Geoscience and Remote Sensing*, *39*(4), 820–829.

Kramer, H. J. (2002). *Observation of the Earth and its Environment. Observation of the Earth and its Environment* (4th Editio). Springer Berlin Heidelberg New York. https://doi.org/10.1007/978-3-662-09038-1

Kurvonen, L., Pulliainen, J., & Hallikainen, M. (1999). Retrieval of biomass in boreal forests from multitemporal ERS-1 and JERS-1 SAR images. *IEEE Transactions on Geoscience and Remote Sensing*, *37*(1), 198–205. https://doi.org/10.1109/36.739154

Langanke, T. (2015). *GIO Land (GMES/Copernicus initial operations land) High Resolution Layers (HRLs) - summary of product specifications. GIO land team at the EEA.*

Lary, D. J., Alavi, A. H., Gandomi, A. H., & Walker, A. L. (2016). Machine learning in geosciences and remote sensing. *Geoscience Frontiers*, *7*(1), 3–10. https://doi.org/10.1016/j.gsf.2015.07.003

Lary, D. J., Zewdie, G. K., Liu, X., Wu, D., Levetin, E., Allee, R. J., … Aurin, D. (2018). Machine Learning Applications for Earth Observation. In *Earth Observation Open Science and Innovation* (pp. 165–218). https://doi.org/10.1007/978-3-319-65633-5_8

Le Quéré, C., Moriarty, R., Andrew, R. M., Canadell, J. G., Sitch, S., Korsbakken, J. I., … Zeng, N. (2015). Global Carbon Budget 2015. *Earth System Science Data*, *7*(2), 349–396. https://doi.org/10.5194/essd-7-349-2015

Le Toan, T, Beaudoin, A., Riom, J., & Guyon, D. (1992). Relating forest biomass to SAR data. *IEEE Transactions on Geoscience and Remote Sensing*, *30*(2), 403–411.

Le Toan, T., Tanase, M., Riva, J. De, Bouvet, A., Santoro, M., & Schmullius, C. (2009). *K & C Science Report – Phase 1 Change in forest cover in Central Siberia using ALOS / PALSAR.* Retrieved from

http://www.eorc.jaxa.jp/ALOS/en/kyoto/phase_1/KC-Phase1-report_LeToan.pdf

Lee, J. Sen, Wen, J. H., Ainsworth, T. L., Chen, K. S., & Chen, A. J. (2009). Improved sigma filter for speckle filtering of SAR imagery. *IEEE Transactions on Geoscience and Remote Sensing*, *47*(1), 202–213. https://doi.org/10.1109/TGRS.2008.2002881

Lefsky, M.A., Cohen, W. B., Acker, S. A., Parker, G. G., Spies, T. A., & Harding, D. (1999). Lidar remote sensing of the canopy structure and biophysical properties of Douglas-Fir Western Hemlock forests. *Remote Sensing of Environment*, *70*(3), 339–361. https://doi.org/10.1016/S0034-4257(99)00052-8

Lefsky, M. A., Cohen, W. B., Parker, G. G., & Harding, D. J. (2002). Lidar Remote Sensing for Ecosystem Studies. *BioScience*, *52*(1), 19. https://doi.org/10.1641/0006-3568(2002)052[0019:lrsfes]2.0.co;2

Lefsky, M. A., Harding, D. J., Keller, M., Cohen, W. B., Carabajal, C. C., Del Bom Espirito-Santo, F., … de Oliveira, R. (2005). Estimates of forest canopy height and aboveground biomass using ICESat. *Geophysical Research Letters*, *32*, 22–25. https://doi.org/10.1029/2005GL023971

Lefsky, M. A. (2010). A global forest canopy height map from the Moderate Resolution Imaging Spectroradiometer and the Geoscience Laser Altimeter System. *Geophysical Research Letters*, *37*. https://doi.org/10.1029/2010GL043622

Ling, F., Li, Z. L., Chen, E., & Wang, Q. (2008). Forest mapping with multi-temporal dual polarization ALOS PALSAR data. In *Proc. SPIE 7285, International Conference on Earth Observation Data Processing and Analysis (ICEODPA).*

Loew, A., & Mauser, W. (2007). Generation of geometrically and radiometrically terrain corrected SAR image products. *Remote Sensing of Environment*, *106*(3), 337–349. https://doi.org/10.1016/j.rse.2006.09.002

Lu, D., Mausel, P., Brondizio, E., & Moran, E. F. (2004). Change detection techniques. *International Journal of Remote Sensing*, *25*, 2365–2407. https://doi.org/10.1080/0143116031000139863

Lucas, R., Clewley, D., Rosenqvist, A., Kellndorfer, J., Walker, W., Hoekman, D., … Navarro de Mesquita Jr., H. (2013). Global Forest Monitoring with Synthetic Aperture Radar (SAR) Data. In F. Achard & M. C. Hansen (Eds.), *Global Forest Monitoring from Earth Observation* (p. 26). CRC Press.

Luckman A. (1998). Correction of SAR Imagery for Variation in Pixel Scattering Area Caused by Topography. *IEEE Transactions on Geoscience and Remote Sensing*, *36*(1), 344–350.

Markus, T., Neumann, T., Martino, A., Abdalati, W., Brunt, K., Csatho, B., … Zwally, J. (2017). The Ice, Cloud, and land Elevation Satellite-2 (ICESat-2):

Science requirements, concept, and implementation. *Remote Sensing of Environment*, *190*, 260–273. https://doi.org/10.1016/j.rse.2016.12.029

Martone, M., Rizzoli, P., Wecklich, C., González, C., Bueso-Bello, J. L., Valdo, P., … Moreira, A. (2018). The global forest/non-forest map from TanDEM-X interferometric SAR data. *Remote Sensing of Environment*, *205*(December 2017), 352–373. https://doi.org/10.1016/j.rse.2017.12.002

Maxar Technologies Ltd. (2018). *RADARSAT-2 Product Description*. Retrieved from https://mdacorporation.com/docs/default-source/technical-documents/geospatial-services/52-1238_rs2_product_description.pdf?sfvrsn=10

Maxwell, A. E., Warner, T. A., & Fang, F. (2018). Implementation of machine-learning classification in remote sensing: An applied review. *International Journal of Remote Sensing*, *39*(9), 2784–2817. https://doi.org/10.1080/01431161.2018.1433343

McDonald, K. C., Zimmermann, R., Way, J., & Chun, W. (1999). Automated instrumentation for continuous monitoring of the dielectric properties of woody vegetation: System design, implementation, and selected in situ measurements. *IEEE Transactions on Geoscience and Remote Sensing*, *37*(4), 1880–1894. https://doi.org/10.1109/36.774701

Means, J. E., Acker, S. A., Harding, D. J., Blair, J. B., Lefsky, M. A., Cohen, W. B., … Mckee, W. A. (1999). Use of large-footprint scanning airborne lidar to estimate forest stand characteristics in the western cascades of Oregon. *Remote Sensing of Environment*, *67*, 298–308.

Microwaves and Radar Institute. (2019). *TanDEM-X Forest/Non-Forest Map Product Description*.

Mitchell, A. L., Rosenqvist, A., & Mora, B. (2017). Current remote sensing approaches to monitoring forest degradation in support of countries measurement, reporting and verification (MRV) systems for REDD+. *Carbon Balance and Management*, *12*(1). https://doi.org/10.1186/s13021-017-0078-9

Moghaddam, M., & Saatchi, S. (1995). Analysis of Scattering Mechanisms in SAR Imagery over Boreal Forest. *IEEE Transactions on Geoscience and Remote Sensing*, *33*(5).

Moore, R. K. (1966). Radar Scatterometry. An active remote sensing tool. In *Fourth Symposium on Remote Sensing of the Environment* (p. 35). Ann Arbor, Michigan.

Moser, G., & Serpico, S. B. (2009). Unsupervised change detection from multichannel SAR data by Markovian data fusion. *IEEE Transactions on Geoscience and Remote Sensing*, *47*(7), 2114–2128. https://doi.org/10.1109/TGRS.2009.2012407

Mukhortova, L., Schepaschenko, D., Shvidenko, a., McCallum, I., & Kraxner, F.

(2015). Soil contribution to carbon budget of Russian forests. *Agricultural and Forest Meteorology*, *206*, 97–108. https://doi.org/10.1016/j.agrformet.2014.09.017

Næsset, E., Gobakken, T., Solberg, S., Gregoire, T. G., Nelson, R., Ståhl, G., & Weydahl, D. (2011). Model-assisted regional forest biomass estimation using LiDAR and InSAR as auxiliary data: A case study from a boreal forest area. *Remote Sensing of Environment*, *115*(12), 3599–3614. https://doi.org/10.1016/j.rse.2011.08.021

NASA, & University of Maryland. (2020). GEDI Ecosystem Lidar. Retrieved January 21, 2020, from https://gedi.umd.edu/

NSIDC. (2019). Ice, Cloud, and land Elevation Satellite-2, ICESat-2. Retrieved August 29, 2019, from https://nsidc.org/data/icesat-2/

Neigh, C. S. R., Nelson, R. F., Ranson, K. J., Margolis, H. A., Montesano, P. M., Sun, G., … Andersen, H. E. (2013). Taking stock of circumboreal forest carbon with ground measurements, airborne and spaceborne LiDAR. *Remote Sensing of Environment*, *137*, 274–287. https://doi.org/10.1016/j.rse.2013.06.019

Nelson, R., Ranson, K. J., Sun, G., Kimes, D. S., Kharuk, V., & Montesano, P. (2009). Estimating Siberian timber volume using MODIS and ICESat/GLAS. *Remote Sensing of Environment*, *113*(3), 691–701. https://doi.org/10.1016/j.rse.2008.11.010

Nelson, Ross, Krabill, W., & Tonelli, J. (1988). Estimating forest biomass and volume using airborne laser data. *Remote Sensing of Environment*, *24*(2), 247–267. https://doi.org/10.1016/0034-4257(88)90028-4

Neumann, M., Saatchi, S. S., Ulander, L. M. H., & Fransson, J. E. S. (2012). Assessing performance of L- and P-Band polarimetric interferometric SAR data in estimating boreal forest above-ground biomass. *IEEE Transactions on Geoscience and Remote Sensing*, *50*(3), 714–726.

Nilsson, M. (1996). Estimation of tree heights and stand volume using an airborne Lidar system. *Remote Sensing of Environment*, *56*(1), 1–7.

Nilsson, S. (1997). Challenges for the boreal forest zone and IBFRA. In S. G. Conard (Ed.), *Disturbance in Boreal Forest Ecosystems: Human Impacts and Natural Processes. International Boreal Forest Research Association. Annual Meeting Proceedings*. Duluth, Minnesota, USA: North Central Research Station, Forest Service-U.S. Department of Agriculture. Retrieved from https://www.nrs.fs.fed.us/pubs/gtr/gtr_nc209.pdf

Okada, Y., Nakamura, S., Iribe, K., Yokota, Y., Tsuji, M., Tsuchida, M., … Shimada, M. (2013). System design of wide swath, high resolution, full polarimietoric L-band SAR onboard ALOS-2. *International Geoscience and Remote Sensing Symposium (IGARSS)*, *2*(1), 2408–2411. https://doi.org/10.1109/IGARSS.2013.6723305

Oliver, C., & Quegan, S. (2004). *Understanding Synthetic Aperture Radar Images*. SciTech Publishing, INC.

Pal, M., & Mather, P. M. (2005). Support vector machines for classification in remote sensing. *International Journal of Remote Sensing*, *26*(5), 1007–1011. https://doi.org/10.1080/01431160512331314083

Pan, Y., Birdsey, R. A., Fang, J., Houghton, R., Kauppi, P. E., Kurz, W. A., … Hayes, D. (2011). A large and persistent carbon sink in the world's forests. *Science (New York, N.Y.)*, *333*(6045), 988–993. https://doi.org/10.1126/science.1201609

Pantze, A., Fransson, J. E. S., & Santoro, M. (2010). Forest change detection from L-band satellite SAR images using iterative histogram matching and thresholding together with data fusion. In *International Geoscience and Remote Sensing Symposium (IGARSS)* (Vol. 25, pp. 1226–1229). https://doi.org/10.1109/IGARSS.2010.5650677

Papathanassiou, K. P., & Cloude, S. R. (2001). Single-baseline polarimetric SAR interferometry. *IEEE Transactions on Geoscience and Remote Sensing*, *39*(11), 2352–2363. https://doi.org/10.1109/36.964971

Patenaude, G., Hill, R. ., Milne, R., Gaveau, D. L. a., Briggs, B. B. J., & Dawson, T. P. (2004). Quantifying forest above ground carbon content using LiDAR remote sensing. *Remote Sensing of Environment*, *93*(3), 368–380. https://doi.org/10.1016/j.rse.2004.07.016

Patenaude, Genevieve, Milne, R., & Dawson, T. P. (2005). Synthesis of remote sensing approaches for forest carbon estimation: reporting to the Kyoto Protocol. *Environmental Science & Policy*, *8*(2), 161–178. https://doi.org/10.1016/j.envsci.2004.12.010

Peregon, A., & Yamagata, Y. (2013). The use of ALOS/PALSAR backscatter to estimate above-ground forest biomass: A case study in Western Siberia. *Remote Sensing of Environment*, *137*, 139–146. https://doi.org/10.1016/j.rse.2013.06.012

Persson, H., & Fransson, J. (2014). Forest variable estimation using radargrammetric processing of TerraSAR-X images in boreal forests. *Remote Sensing*, *6*(3), 2084–2107. https://doi.org/10.3390/rs6032084

Persson, H. J., & Fransson, J. E. S. (2017). Comparison between TanDEM-X- and ALS-based estimation of aboveground biomass and tree height in boreal forests. *Scandinavian Journal of Forest Research*, *32*(4), 306–319. https://doi.org/10.1080/02827581.2016.1220618

Pulliainen, J. T., Heiska, K., Hyyppa, J., & Hallikainen, M. T. (1994). Backscattering properties of boreal forests at the C- and X-bands. *IEEE Transactions on Geoscience and Remote Sensing*, *32*(5), 1041–1050.

Pulliainen, J. T., Mikkela, P. J., Hallikainen, M. T., & Ikonen, J. (1996). Seasonal

dynamics of C-band backscatter of boreal forests with applications to biomass and soil moisture estimation. *IEEE Transactions on Geoscience and Remote Sensing*, *34*(3), 758–770.

Pulliainen, J. T., Kurvonen, L., & Hallikainen, M. T. (1999). Multitemporal behavior of L- and C-band SAR observations of boreal forests. *IEEE Transactions on Geoscience and Remote Sensing*, *37*(2), 927–937.

Pulliainen, J., Engdahl, M., & Hallikainen, M. (2003). Feasibility of multi-temporal interferometric SAR data for stand-level estimation of boreal forest stem volume. *Remote Sensing of Environment*, *85*, 397–409. https://doi.org/10.1016/S0034-4257(03)00016-6

Quegan, S., & Yu, J. J. (2001). Filtering of multichannel SAR images. *IEEE Transactions on Geoscience and Remote Sensing*, *39*(11), 2373–2379. https://doi.org/10.1109/36.964973

Quegan, Shaun, & Lomas, M. R. (2015). The interaction between Faraday rotation and system effects in synthetic aperture radar measurements of backscatter and biomass. *IEEE Transactions on Geoscience and Remote Sensing*, *53*(8), 4299–4312. https://doi.org/10.1109/TGRS.2015.2395138

Rahlf, J., Breidenbach, J., Solberg, S., Næsset, E., & Astrup, R. (2014). Comparison of four types of 3D data for timber volume estimation. *Remote Sensing of Environment*, *155*, 325–333. https://doi.org/10.1016/j.rse.2014.08.036

Ranson, K. J., & Sun, G. (1994a). Northern Forest Classification using Temporal Multifrequency and Multipolarimetric SAR Images. *Remote Sensing of Environment*, *47*(2), 142–153. https://doi.org/http://dx.doi.org/10.1016/0034-4257(94)90151-1

Ranson, K. J., & Sun, G. (1994b). Mapping biomass of a northern forest using multifrequency SAR data. *IEEE Transactions on Geoscience and Remote Sensing*, *32*(2), 388–396.

Ranson, K. J., Sun, G., Lang, R. H., Chauhan, N. S., Cacciola, R. J., & Kilic, O. (1997). Mapping of boreal forest biomass from spaceborne synthetic aperture radar. *Journal of Geophysical Research*, *102*(D24), 29599–29610.

Ranson, K. J., Sun, G., Kharuk, V. I., & Kovacs, K. (2001). Characteristics of Forests in Western Sayani Mountains, Siberia from SAR Data. *Remote Sensing of Environment*, *75*, 188–200. Retrieved from https://ntrs.nasa.gov/search.jsp?R=20000033365&hterms=siberia+forest+limit&qs=Nm%3D123%7CCollection%7CNASA%2520STI%7C%7C17%7CCollection%7CNACA%26Ntx%3Dmode%2520matchallpartial%26Ntk%3DAll%26N%3D0%26No%3D10%26Ntt%3Dsiberia%2520forest%2520limit

Ranson, K J, Kovacs, K., Sun, G., & Kharuk, V. I. (2003). Disturbance recognition in the boreal forest using radar and Landsat-7. *Canadian Journal of Remote Sensing*, *29*(2), 271–285. https://doi.org/10.5589/m02-096

Rauste, Y., Häme, T., Pulliainen, J., Heiska, K., & Hallikainen, M. (1994). Radar-based forest biomass estimation. *International Journal of Remote Sensing*, *15*(14), 2797–2808. https://doi.org/10.1080/01431169408954285

Rauste, Y. (2005). Multi-temporal JERS SAR data in boreal forest biomass mapping. *Remote Sensing of Environment*, *97*(2), 263–275. https://doi.org/10.1016/j.rse.2005.05.002

Rawlings, J. O., Pantula, S. G., & Dickey, D. A. (1998). *Applied Regression Analysis : A Research Tool* (Second Edi). Springer.

Rees, W. G. (2001). *Physical Principles of Remote Sensing* (2nd ed.). Cambridge University Press.

Reiche, J., Verbesselt, J., Hoekman, D., & Herold, M. (2015). Remote Sensing of Environment Fusing Landsat and SAR time series to detect deforestation in the tropics. *Remote Sensing of Environment*, *156*, 276–293. https://doi.org/10.1016/j.rse.2014.10.001

Reiche, J., Hamunyela, E., Verbesselt, J., Hoekman, D., & Herold, M. (2018). Improving near-real time deforestation monitoring in tropical dry forests by combining dense Sentinel-1 time series with Landsat and ALOS-2 PALSAR-2. *Remote Sensing of Environment*, *204*(October 2017), 147–161. https://doi.org/10.1016/j.rse.2017.10.034

Reichstein, M., & Carvalhais, N. (2019). Aspects of Forest Biomass in the Earth System: Its Role and Major Unknowns. *Surveys in Geophysics*, *40*(4), 693–707. https://doi.org/10.1007/s10712-019-09551-x

Richards, J. A. (1990). Radar backscatter modelling of forests: A review of current trends. *International Journal of Remote Sensing*, *11*(7), 1299–1312. https://doi.org/10.1080/01431169008955094

Rignot, E., Way, J., Williams, C., & Viereck, L. (1994). Radar estimates of aboveground biomass in boreal forests of interior Alaska. *IEEE Transactions on Geoscience and Remote Sensing*, *32*(5), 1117–1124. https://doi.org/10.1109/36.312903

Rignot, E. J., Zimmermann, R., & Zyl, J. J. Van. (1995). Spaceborne applications of P-band imaging radars for measuring forest biomass. *IEEE Transactions on Geoscience and Remote Sensing*, *33*(5), 1162–1169.

Rignot, E., Salas, W. A., & Skole, D. L. (1997). Mapping Deforestation and Secondary Growth in Rondonia, Brazil, Using Imaging Radar and Thematic Mapper Data. *Remote Sensing of Environment*, *59*(2), 167–179. https://doi.org/10.1016/S0034-4257(1996)00150-2

Rodríguez-Veiga, P., Quegan, S., Carreiras, J., Persson, H. J., Fransson, J. E. S., Hoscilo, A., … Balzter, H. (2019). Forest biomass retrieval approaches from earth observation in different biomes. *International Journal of Applied Earth Observation and Geoinformation*, *77*(December 2018), 53–68.

https://doi.org/10.1016/j.jag.2018.12.008

Rosenqvist, A., Shimada, M., Chapman, B., Freeman, A., De Grandi, G., Saatchi, S., & Rauste, Y. (2000). The Global Rain Forest Mapping project - A review. *International Journal of Remote Sensing*, *21*(6–7), 1375–1387. https://doi.org/10.1080/014311600210227

Rosenqvist, A., Ogawa, T., Shimada, M., & Igarashi, T. (2001). Initiating the ALOS Kyoto & Carbon Initiative. In *International Geoscience and Remote Sensing Symposium (IGARSS)* (pp. 546–548). Sydney, Australia. https://doi.org/10.1109/igarss.2001.976217

Rosenqvist, Å., Milne, A., Lucas, R., Imhoff, M., & Dobson, C. (2003). A review of remote sensing technology in support of the Kyoto Protocol. *Environmental Science & Policy*, *6*(5), 441–455. https://doi.org/10.1016/S1462-9011(03)00070-4

Rosenqvist, A., Shimada, M., & Watanabe, M. (2004). ALOS PALSAR: Technical outline and mission concepts. In *International Symposium on Retrieval of Bio- and Geophysical Parameters from SAR Data for Land Applications* (Vol. 1, pp. 1–7).

Rosenqvist, A., Shimada, M., Suzuki, S., Ohgushi, F., Tadono, T., Watanabe, M., … Aoki, E. (2014). Operational performance of the ALOS global systematic acquisition strategy and observation plans for ALOS-2 PALSAR-2. *Remote Sensing of Environment*, *155*, 3–12. https://doi.org/10.1016/j.rse.2014.04.011

Saatchi, S. S., Harris, N. L., Brown, S., Lefsky, M., Mitchard, E. T. a, Salas, W., … Morel, A. (2011). Benchmark map of forest carbon stocks in tropical regions across three continents. *Proceedings of the National Academy of Sciences of the United States of America*, *108*(24), 9899–9904. https://doi.org/10.1073/pnas.1019576108

Sader, S. A. (1987). Forest biomass, canopy structure, and species composition relationships with multipolarization L-Band Synthetic Aperture Radar data. *Photogrammetric Engineering and Remote Sensing*, *53*(2), 193–202.

Sader, S. A., Waide, R. B., Lawrence, W. T., & Joyce, A. T. (1989). Tropical Forest Biomass and Successional Age Class Relationships to a Vegetation Index Derived from Landsat TM Data. *Remote Sensing of Environment*, *28*, 143–156.

Sandberg, Gustaf, Eriksson, L. E. B., & Ulander, L. M. H. (2009). Measurements of faraday rotation using polarimetric PALSAR images. *IEEE Geoscience and Remote Sensing Letters*, *6*(1), 142–146. https://doi.org/10.1109/LGRS.2008.2010062

Sandberg, G., Ulander, L. M. H., Fransson, J. E. S., Holmgren, J., & Le Toan, T. (2011). L- and P-band backscatter intensity for biomass retrieval in hemiboreal forest. *Remote Sensing of Environment*, *115*(11), 2874–2886. https://doi.org/10.1016/j.rse.2010.03.018

Santoro, M., Askne, J., Smith, G., & Fransson, J. E. S. (2002). Stem volume retrieval in boreal forests from ERS-1 / 2 interferometry. *Remote Sensing of Environment*, *81*, 19–35.

Santoro, M. (2003). Estimation of Biophysical Parameters in Boreal Forests from ERS and JERS SAR Interferometry Estimation of Biophysical Parameters in Boreal Forests from ERS and JERS SAR Interferometry, (188), 1–197.

Santoro, M, Eriksson, L., Askne, J., & Schmullius, C. (2006). Assessment of stand-wise stem volume retrieval in boreal forest from JERS-1 L-band SAR backscatter. *International Journal of Remote Sensing*, *27*(16), 3425–3454. https://doi.org/10.1080/01431160600646037

Santoro, M., Shvidenko, A., Mccallum, I., Askne, J., & Schmullius, C. (2007). Properties of ERS-1 / 2 coherence in the Siberian boreal forest and implications for stem volume retrieval. *Remote Sensing of Environment*, *106*, 154–172. https://doi.org/10.1016/j.rse.2006.08.004

Santoro, M., Askne, J., Beer, C., Cartus, O., Schmullius, C., Wegmüller, U., & Wiesmann, A. (2008). Automatic model inversion of multi-temporal C-band coherence and backscatter measurements for forest stem volume retrieval. In *Geoscience and Remote Sensing Symposium, 2008. IGARSS 2008* (pp. 124–127). Boston, MA, USA.

Santoro, M., Fransson, J. E. S., Eriksson, L. E. B., Magnusson, M., Ulander, L. M. H., & Olsson, H. (2009). Signatures of ALOS PALSAR L-band backscatter in Swedish forest. *IEEE Transactions on Geoscience and Remote Sensing*, *47*(12), 4001–4019. https://doi.org/10.1109/TGRS.2009.2023906

Santoro, M., Fransson, J. E. S., Eriksson, L. E. B., & Ulander, L. M. H. (2010). Clear-cut detection in Swedish boreal forest using multi-temporal ALOS PALSAR backscatter data. *IEEE Journal of Selected Topics in Applied Earth Observations and Remote Sensing*, *3*(4), 618–631.

Santoro, M., Beer, C., Cartus, O., Schmullius, C., Shvidenko, A., McCallum, I., … Wiesmann, A. (2011). Retrieval of growing stock volume in boreal forest using hyper-temporal series of Envisat ASAR ScanSAR backscatter measurements. *Remote Sensing of Environment*, *115*(2), 490–507. https://doi.org/10.1016/j.rse.2010.09.018

Santoro, M., Pantze, A., Fransson, J. E. S., Dahlgren, J., & Persson, A. (2012). Nation-wide clear-cut mapping in Sweden using ALOS PALSAR strip images. *Remote Sensing*, *4*(12), 1693–1715. https://doi.org/10.3390/rs4061693

Santoro, M., Cartus, O., Fransson, J., Shvidenko, A., McCallum, I., Hall, R., … Schmullius, C. (2013). Estimates of Forest Growing Stock Volume for Sweden, Central Siberia, and Québec Using Envisat Advanced Synthetic Aperture Radar Backscatter Data. *Remote Sensing*, *5*(9), 4503–4532. https://doi.org/10.3390/rs5094503

Santoro, M., Eriksson, L., & Fransson, J. (2015). Reviewing ALOS PALSAR Backscatter Observations for Stem Volume Retrieval in Swedish Forest. *Remote Sensing*, *7*(4), 4290–4317. https://doi.org/10.3390/rs70404290

Santoro, M., Beaudoin, A., Beer, C., Cartus, O., Fransson, J. E. S., Hall, R. J., … Wegmüller, U. (2015). Forest growing stock volume of the northern hemisphere: Spatially explicit estimates for 2010 derived from Envisat ASAR. *Remote Sensing of Environment*, *168*, 316–334. https://doi.org/10.1016/j.rse.2015.07.005

Santoro, M., & Cartus, O. (2018). Research pathways of forest above-ground biomass estimation based on SAR backscatter and interferometric SAR observations. *Remote Sensing*, *10*(4). https://doi.org/10.3390/rs10040608

Santoro, M. (2018). GlobBiomass - global datasets of forest biomass. PANGAEA. https://doi.org/10.1594/PANGAEA.894711

Santoro, M., & Cartus, O. (2018). Research Pathways of Forest Above-Ground Biomass Estimation Based on SAR Backscatter and Interferometric SAR Observations. *Remote Sensing*, *10*(4), 608. https://doi.org/10.3390/rs10040608

Santoro, M., Cartus, O., Fransson, J. E. S., & Wegmüller, U. (2019). Complementarity of X-, C-, and L-band SAR Backscatter Observations to Retrieve Forest Stem Volume in Boreal Forest. *Remote Sensing*, *11*(13), 1–25. https://doi.org/https://doi.org/10.3390/rs11131563

Schmullius, C., Baker, J., Balzter, H., Davidson, M., Eriksson, L., Gaveau, D., … Wegmuller, U. (2001). *SAR Imaging for Boreal Ecology and Radar Interferometry Applications SIBERIA project (Contract No. ENV4-CT97-0743-SIBERIA) – Final Report*. Retrieved from http://www.siberia1.uni-jena.de/

Schutz, B. E., Zwally, H. J., Shuman, C. A., Hancock, D., & DiMarzio, J. P. (2005). Overview of the ICESat mission. *Geophysical Research Letters*, *32*(21), 1–4. https://doi.org/10.1029/2005GL024009

SERVIR Global Science Coordination Office, & National Space Science and Technology Center. (2019). *The Synthetic Aperture Radar (SAR) Handbook: Comprehensive Methodologies for Forest Monitoring and Biomass Estimation*. https://doi.org/10.25966/nr2c-s697

Shimada, M. (2010). Ortho-Rectification and Slope Correction of SAR Data Using DEM and Its Accuracy Evaluation. *IEEE Transactions on Geoscience and Remote Sensing*, *3*(4), 657–671.

Shimada, M., Itoh, T., Motooka, T., Watanabe, M., Shiraishi, T., Thapa, R., & Lucas, R. (2014). New global forest/non-forest maps from ALOS PALSAR data (2007–2010). *Remote Sensing of Environment*, *155*, 13–31. https://doi.org/10.1016/j.rse.2014.04.014

Shvidenko, A., Schepaschenko, D., Nilsson, S., & Bouloui, Y. (2007). Semi-empirical

models for assessing biological productivity of Northern Eurasian forests. *Ecological Modelling*, *204*(1–2), 163–179. https://doi.org/10.1016/j.ecolmodel.2006.12.040

Shvidenko, A., Schepaschenko, D., Nilsson, S., & Boului, Y. (2008). *Tables and models of growth and productivity of forests of major forming species of Northern Eurasia (standard and reference materials)*. Moscow: Federal Agency of Forest Management. Retrieved from http://webarchive.iiasa.ac.at/Research/FOR/forest_cdrom/Articles/THR.pdf

Shvidenko, A., Schepaschenko, D., McCallum, I., & Nilsson, S. (2011a). Can the uncertainty of full carbon accounting of forest ecosystems be made acceptable to policymakers? In *Greenhouse Gas Inventories* (Springer, pp. 137–157). Dordrecht.

Shvidenko, A., Schepaschenko, D., Sukhinin, A., McCallum, I., & Maksyutov, S. (2011b). Carbon emissions from forest fires in boreal Eurasia between 1998-2010. In *5th International Wildland Fire Conference*. Sun City, South Africa.

Simard, M., Pinto, N., Fisher, J. B., & Baccini, A. (2011). Mapping forest canopy height globally with spaceborne lidar. *Journal of Geophysical Research*, *116*(G04021). https://doi.org/10.1029/2011JG001708

Small, D. (2011). Flattening gamma: Radiometric terrain correction for SAR imagery. *IEEE Transactions on Geoscience and Remote Sensing*, *49*(8), 3081–3093. https://doi.org/10.1109/TGRS.2011.2120616

Smith, G., Dammert, P. B. G., & Askne, J. (1996). Decorrelation mechanisms in C-band SAR interferometry over boreal forest. In *Proc.SPIE* (Vol. 2958). Retrieved from https://doi.org/10.1117/12.262703

Smith, G., Dammert, P. B. G., Santoro, M., Fransson, J. E. S., Wegmüller, U., Askne, J., & Federico, N. (1998). Biomass retrieval in boreal forest using ERS and JERS SAR. In *Retrieval of Bio- and Geophysical Parameters from SAR Data for Land Applications* (pp. 293–300). Noordwijk, Netherlands.

Soja, M. J., Sandberg, G., & Ulander, L. M. H. (2013). Regression-based retrieval of boreal forest biomass in sloping terrain using P-band SAR backscatte intensity data. *IEEE Transactions on Geoscience and Remote Sensing*, *51*(5), 2646–2665.

Soja, M. J., H., & Persson, L. M. H. U. (2015). Estimation of Forest Height and Canopy Density From a Single InSAR Correlation Coefficient. *Ieee Geoscience and Remote Sensing Letters*, *12*(3), 646–650. https://doi.org/10.1109/LGRS.2014.2354551

Soja, M. J., Persson, H. J., & Ulander, L. M. H. (2015). Estimation of forest biomass from two-level model inversion of single-pass InSAR data. *2015 IEEE International Geoscience and Remote Sensing Symposium (IGARSS)*, *53*(9), 3886–3889. https://doi.org/10.1109/IGARSS.2015.7326673

Soja, M. J., Persson, H. J., & Ulander, L. M. H. (2018). Modeling and Detection of Deforestation and Forest Growth in Multitemporal TanDEM-X Data. *IEEE Journal of Selected Topics in Applied Earth Observations and Remote Sensing*, *11*(10), 3548–3563. https://doi.org/10.1109/JSTARS.2018.2851030

Solberg, S., Astrup, R., Gobakken, T., Næsset, E., & Weydahl, D. J. (2010). Remote sensing of environment estimating spruce and pine biomass with interferometric X-band SAR. *Remote Sensing of Environment*, *114*(10), 2353–2360. https://doi.org/10.1016/j.rse.2010.05.011

Solberg, S., Astrup, R., Breidenbach, J., Nilsen, B., & Weydahl, D. (2013). Monitoring spruce volume and biomass with InSAR data from TanDEM-X. *Remote Sensing of Environment*, *139*, 60–67. https://doi.org/10.1016/j.rse.2013.07.036

Souza, C., Firestone, L., Silva, L. M., & Roberts, D. (2003). Mapping forest degradation in the Eastern Amazon from SPOT 4 through spectral mixture models. *Remote Sensing of Environment*, *87*, 494–506. https://doi.org/10.1016/j.rse.2002.08.002

Steffen, W., Richardson, K., Rockström, J., Cornell, S. E., Fetzer, I., Bennet, E. M., … Särlin, S. (2015). Planetary boundaries: Guiding human development on a changing planet. *Science*, *348*(6240), 1217–c. https://doi.org/10.1126/science.aaa9629

Stelmaszczuk-Górska, M. A., Rodriguez-Veiga, P., Ackermann, N., Thiel, C., Balzter, H., & Schmullius, C. (2016). Non-Parametric Retrieval of Aboveground Biomass in Siberian Boreal Forests with ALOS PALSAR Interferometric Coherence and Backscatter Intensity. *Journal of Imaging*, *2*(1), 24. https://doi.org/10.3390/jimaging2010001

Stelmaszczuk-Górska, M. A., Sagischewski, H., & Chmara, S. (2017). New opportunities for forest management using Copernicus data Sentinels for Thuringian Information Systems. In V. W. Benoît Otjacques, Patrik Hitzelberger, Stefan Naumann (Ed.), *From Science to Society: The Bridge provided by Environmental Informatics Adjunct Proceedings of the 31st EnviroInfo conference* (pp. 333–339). Shaker Verlag. Retrieved from https://www.shaker.de/de/content/catalogue/index.asp?lang=de&ID=8&ISBN=978-3-8440-5495-8&search=yes

Stelmaszczuk-Górska, M. A., Thiel, C. J., & Schmullius, C. C. (2017). Remote Sensing for Aboveground Biomass Estimation in Boreal Forests. In H. Balzter (Ed.), *Earth Observation for Land and Emergency Monitoring* (1st ed., pp. 33–55). © 2017 John Wiley & Sons Ltd. https://doi.org/10.1002/9781118793787

Stelmaszczuk-Górska, M. A., Urbazaev, M., Schmullius, C., & Thiel, C. (2018). Estimation of Above-Ground Biomass over Boreal Forests in Siberia using updated in situ, ALOS-2 PALSAR-2, and RADARSAT-2 Data. *Remote Sensing*, *10*(10), 1550. https://doi.org/10.3390/rs10101550

Sun, G., Ranson, K. J., Guo, Z., Zhang, Z., Montesano, P., & Kimes, D. (2011). Forest biomass mapping from lidar and radar synergies. *Remote Sensing of Environment*, *115*(11), 2906–2916. https://doi.org/10.1016/j.rse.2011.03.021

Suzuki, S., Kankaku, Y., & Shimada, M. (2013). ALOS-2 acquisition strategy. In *International Geoscience and Remote Sensing Symposium (IGARSS)* (Vol. 2, pp. 2412–2415). IEEE. https://doi.org/10.1109/IGARSS.2013.6723306

Tanase, M. A., Panciera, R., Lowell, K., Tian, S., García-martín, A., & Walker, J. P. (2014). Sensitivity of L-Band Radar Backscatter to Forest Biomass in Semiarid Environments : A Comparative Analysis of Parametric and Nonparametric Models. *IEEE Transactions on Geoscience and Remote Sensing*, *52*(8), 4671–4685.

Tang, X., Bullock, E. L., Olofsson, P., Estel, S., & Woodcock, C. E. (2019). Near real-time monitoring of tropical forest disturbance: New algorithms and assessment framework. *Remote Sensing of Environment*, *224*(February), 202–218. https://doi.org/10.1016/j.rse.2019.02.003

Tebaldini, S., & Rocca, F. (2012). Multibaseline polarimetric SAR tomography of a boreal forest at P- and L-bands. *IEEE Transactions on Geoscience and Remote Sensing*, *50*(1), 232–246. https://doi.org/10.1109/TGRS.2011.2159614

Thiel, C., Drezet, P., Weise, C., Quegan, S., & Schmullius, C. (2006). Radar remote sensing for the delineation of forest cover maps and the detection of deforestation. *Forestry*, *79*(5), 589–597. https://doi.org/10.1093/forestry/cpl036

Thiel, C. J., Thiel, C., & Schmullius, C. C. (2009). Operational Large-Area Forest Monitoring in Siberia Using ALOS PALSAR Summer Intensities and Winter Coherence. *IEEE Geoscience and Remote Sensing*, *47*(12), 3993–4000.

Thiel, C. J., Chowdhury, T., Stelmaszczuk-Górska, M. A., Hüttich, C., & Schmullius, C. (2014). *The ALOS Kyoto & Carbon Initiative Science Team Reports Phase 3 (2011-2014): PALSAR Intensities, Coherence and Polarimetric Parameters for the Delineation of Forest Cover and Forest Cover Change and Growing Stock Volume over Central Siberia.* Retrieved from https://www.eorc.jaxa.jp/ALOS/en/kyoto/phase_3/KC-Phase-3-report_NDX-140008.pdf

Thiel, C., & Schmullius, C. (2016). The potential of ALOS PALSAR backscatter and InSAR coherence for forest growing stock volume estimation in Central Siberia. *Remote Sensing of Environment*, *173*, 258–273. https://doi.org/http://dx.doi.org/10.1016/j.rse.2015.10.030

Thurner, M., Beer, C., Santoro, M., Carvalhais, N., Wutzler, T., Schepaschenko, D., … Schmullius, C. (2014). Carbon stock and density of northern boreal and temperate forests. *Global Ecology and Biogeography*, *23*(3), 297–310. https://doi.org/10.1111/geb.12125

Torres, R., Snoeij, P., Geudtner, D., Bibby, D., Davidson, M., Attema, E., …

Rostan, F. (2012). GMES Sentinel-1 mission. *Remote Sensing of Environment*, *120*, 9–24. https://doi.org/10.1016/j.rse.2011.05.028

Touzi, R., Lopes, a., Bruniquel, J., & Vachon, P. W. (1999). Coherence estimation for SAR imagery. *IEEE Transactions on Geoscience and Remote Sensing*, *37*(1), 135–149. https://doi.org/10.1109/36.739146

Ulaby, F. T., Moore, R. K., & Fung, A. K. (1982). *Microwave Remote Sensing Active and Passive. Volume II. Radar Remote Sensing and Surface Scattering and Emission Theory*. Norwood, MA, USA: Artech House, Inc.

Ulander, L. M. H. (1996). Radiometric slope correction of Synthetic-Aperture Radar images. *IEEE Transactions on Geoscience and Remote Sensing*, *34*(5), 1115–1122. https://doi.org/10.1109/36.536527

Ulander, Lars M.H., Sandberg, G., & Soja, M. J. (2011). Biomass retrieval algorithm based on P-band biosar experiments of boreal forest. In *2011 IEEE International Geoscience and Remote Sensing Symposium* (pp. 4245–4248). Vancouver: Ieee. https://doi.org/10.1109/IGARSS.2011.6050168

UN. (1992). *United Nations Framework Convention on Climate Change* (Vol. 62220).

UN. (1998). *Kyoto Protocol to the United Nations Framework Convention on Climate Change*.

UN. (2019). *The Sustainable Development Goals Report 2019*. New York, USA. https://doi.org/10.29171/azu_acku_pamphlet_k3240_s878_2016

UNFCCC. (2015). *ADOPTION OF THE PARIS AGREEMENT - Conference of the Parties COP 21*. https://doi.org/FCCC/CP/2015/L.9/Rev.1

Urbazaev, M., Cremer, F., Migliavacca, M., Reichstein, M., Schmullius, C., & Thiel, C. (2018). Potential of Multi-Temporal ALOS-2 PALSAR-2 ScanSAR Data for Vegetation Height Estimation in Tropical Forests of Mexico. *Remote Sensing*, *10*(8), 1277. https://doi.org/10.3390/rs10081277

van Laar, A., & Akca, A. (2007). *Forest Mensuration*. (K. von Gadow, T. Pukkala, & M. Tome, Eds.), *Managing Forest Ecosystems* (Vol. 13). Dordrecht, The Netherlands: Springer.

Vastaranta, M., Niemi, M., Karjalainen, M., Peuhkurinen, J., Kankare, V., Hyyppä, J., & Holopainen, M. (2014). Prediction of forest stand attributes using TerraSAR-X stereo imagery. *Remote Sensing*, *6*(4), 3227–3246. https://doi.org/10.3390/rs6043227

Wagner, W., Luckman, A., Vietmeier, J., Tansey, K., Balzter, H., Schmullius, C., … Jiong, J. (2003). Large-scale mapping of boreal forest in SIBERIA using ERS tandem coherence and JERS backscatter data. *Remote Sensing*, *85*, 125–144. https://doi.org/10.1016/S0034-4257(02)00198-0

Wasseige, C. De, & Defourny, P. (2002). Retrieval of tropical forest structure

characteristics from bi-directional reflectance of SPOT images. *Remote Sensing of Environment*, *83*, 362–375.

Wegmuller, U., & Werner, C. L. (1995). SAR interferometric signatures of forest. *IEEE Transactions on Geoscience and Remote Sensing*, *33*(5), 1153–1161. https://doi.org/10.1109/36.469479

Werner, C., Wegmüller, U., Strozzi, T., & Wiesmann, A. (2000). GAMMA SAR and interferometric processing software. In *ERS - ENVISAT Symposium Proceedings* (pp. 211–219). Gothenburg, Sweden.

Wilhelm, S., Hüttich, C., Korets, M., & Schmullius, C. (2014). Large area mapping of boreal Growing Stock Volume on an annual and multi-temporal level using PALSAR L-band backscatter mosaics. *Forests*, *5*(8), 1999–2015. https://doi.org/10.3390/f5081999

Woodhouse, I. H. (2006). *Introduction to Microwave Remote Sensing*. Taylor & Francis.

World Bank Group. (2014). *Turn Down the Heat: Confronting the New Climate Normal*. Washington, DC, USA. Retrieved from https://openknowledge.worldbank.org/handle/10986/20595

World Resources Institute. (2019). Global Forest Watch: Tree cover loss in Russia. Retrieved August 10, 2019, from https://www.globalforestwatch.org/

Wu, S.-T. (1987). Potential Application of Multipolarization SAR for pine-biomass estimation. *IEEE Transactions on Geoscience and Remote Sensing*, *25*(3), 403–409.

Xiong, S., Muller, J. P., & Li, G. (2017). The application of ALOS/PALSAR InSAR to measure subsurface penetration depths in deserts. *Remote Sensing*, *9*(6), 1–19. https://doi.org/10.3390/rs9060638

Yale University. (2019). Boreal Zone. Retrieved from https://globalforestatlas.yale.edu/boreal-zone

Yu, L., Liang, L., Wang, J., Zhao, Y., Cheng, Q., Hu, L., … Gong, P. (2014). Meta-discoveries from a synthesis of satellite-based land-cover mapping research. *International Journal of Remote Sensing*, *35*(13), 4573–4588. https://doi.org/10.1080/01431161.2014.930206

Zebker, H. A., & Villasenor, J. (1992). Decorrelation in Interferometric Radar Echoes. *Jet Propulsion*, (818), 1–19.

Zheng, D., Rademacher, J., Chen, J., Crow, T., Bresee, M., Le Moine, J., & Ryu, S.-R. (2004). Estimating aboveground biomass using Landsat 7 ETM+ data across a managed landscape in northern Wisconsin, USA. *Remote Sensing of Environment*, *93*, 402–411. https://doi.org/10.1016/j.rse.2004.08.008

Appendix A: Proceedings paper

Stelmaszczuk-Górska, M., Thiel, C., Schmullius, C. (2013). Optimization of coherence estimation window size aiming at growing stock volume retrieval in Siberian forest. In Proceedings of the ESA Living Planet Symposium. pp. 1–4.

OPTIMIZATION OF COHERENCE ESTIMATION WINDOW SIZE AIMING AT GROWING STOCK VOLUME RETRIEVAL IN SIBERIAN FORESTS

Martyna Stelmaszczuk-Górska [1], Christian Thiel [1], Christiane Schmullius[1]

[1] *Department of Earth Observation, Friedrich-Schiller-University Jena, Loebdergraben 32, D-07743 Jena, Germany, Email: m.stelmas@uni-jena.de, christian.thiel@uni-jena.de, c.schmullius@uni-jena.de*

ABSTRACT

This study was conducted to determine the optimal coherence estimation window size for growing stock volume retrieval in Siberian Forests. The properties of ALOS PALSAR L-band interferometric coherence for Siberian boreal forest are presented. We observed that the data acquired during frozen conditions are better suited for growing stock volume retrieval, as the data showed high coherence for sparse forest and low coherence for dense forest. It was concluded that at least ~ 60 equivalent number of looks are necessary to achieve a compromise between a good spatial resolution and a reliable estimation of coherence using ALOS PALSAR FBS images for Siberian forests.

1. INTRODUCTION

The basis for the Interferometric Synthetic Aperture Radar (InSAR) system is observation of a target by the radar antenna either from two slightly different positions, or at different times, or both [1]. The main output of InSAR processing is the interferogram, which consists of *magnitude* (i.e. correlation between images, also known as coherence) and *phase* (i.e. interferometric phase). *Complex coherence* (γ) is formed by multiplying a single SAR image with the complex conjugate of a second image. In practice, coherence is obtained using estimators by spatial averaging within a two-dimensional window (Eq. 1) [2]:

$$\gamma = \frac{\left|\sum_{i=1}^{N} g_{1,i} g_{2,i}^{*}\right|}{\sqrt{\sum_{i=1}^{N}\left|g_{1,i}\right|^{2}\sum_{i=1}^{N}\left|g_{2,i}\right|^{2}}} \qquad (1)$$

where γ represents sample coherence and N is the number of pixels within the averaging window. However, this estimation is biased and tends to overestimate the low coherence [1, 3–7] typically associated with forests. Using larger estimation windows decreases estimation bias, approaching the true coherence value. However, an infinite number of samples are required to completely remove bias, a method that is not possible in the case of real SAR data due to the heterogeneity of large areas. Larger window sizes also make resolution coarser. Optimization of coherence estimation window size is therefore a compromise between a good spatial resolution and a reliable estimation of coherence.

2. TEST SITES AND IN-SITU DATA

To investigate coherence estimation window size two forest territories in Central Siberia were used: Primorsky and Chunsky East (E). These areas are situated in the southern taiga sub-zone of the boreal forest, and fall into two Russian Siberian Federal districts: Krasnoyarsk Kray and Irkutsk Oblast, respectively (Fig. 1).

Figure 1. Location of study area (World map source: US National Park Service).

Both areas are characterized by a continental climate with long, severe winters and short, warm and wet summers. The mean temperature in winter is -16°C to-30°C, and in summer is 15°C to 25°C. Annual precipitation is less than 450 millimetres [8]. Both areas are overall flat, with more than 60% of terrain characterized by a slope of less than 5%.

Forest inventory data were used to study coherence estimation for growing stock volume (GSV) retrieval. The database was made available by the Department of Earth Observation, Friedrich-Schiller-University Jena and was acquired within the SIBERIA-II project [9]. The database consists of detailed measurements of several forest biophysical parameters, including GSV (i.e. the volume of tree stem per unit area). To avoid the discrepancies resulting from the time difference between when the inventory dataset and the SAR data were acquired, the inventory database was updated. After optical data were used to exclude changed forest stands (i.e. homogenous groups of trees), models of growth were applied [10]. The key statistics for the updated forest territories are given in Tab. 1.

Table 1 Key statistics for investigated forest territories.

	Primorsky	Chunsky E
Area [km^2]	318	130
Number of stands	1508	363
Mean stand size [ha]	21	35
Stem volume (GSV) [m^3/ha] (min/max/mean/std)	0/500/145/109	0/440/120/110
Mean stem volume for sparse forest (GSV < 50) [m^3/ha]	40	36
Mean stem volume for dense forest (GSV > 250) [m^3/ha]	300	323
Age of stands (min/max/mean/std)	0/300/112/71	0/310/120/73
Relative stocking [%] (min/max/mean/std)	0/100/69/18	0/100/60/19

3. SAR DATASETS AND PROCESSING

Phased Array type L-band Synthetic Aperture Radar (PALSAR) data from the Advanced Land Observing Satellite (ALOS) were used to investigate the coherence estimation.

Example coherence maps are shown in Fig. 2. To compare the coherence estimation between investigated test site data, similar perpendicular baseline were selected, Bn was ~700m. InSAR processing and geocoding were done using the GAMMA ISP, DIFF&GEO and LAT modules [11].

Table 2 PALSAR data acquisition summary

	Primorsky		Chunsky E
	FBD[a]	FBS	FBS
Track/Frame	466/1110	466/1110	473/1150
Acquisition dates	29.07.2010 13.09.2010	26.01.2010 13.03.2010	07.01.2010 22.02.2010
Weather conditions	T_1≈13°C, T_2≈4°C, WS_1≈4 m/s, WS_2≈3 m/s, P_1≈7 mm, P_2≈0.5 mm	T_1≈-30°C, T_2≈-11°C, WS_1≈5 m/s, WS_2≈2.5 m/s, SD≈50 cm	T_1≈-32°C, T_2≈-22°C, WS_1≈0.1 m/s, WS_2≈3.5 m/s, SD≈40 cm
Perpendicular baseline (B_n) [m]	249	703	789

[a] a FBS = Fine Beam Single Polarisation, FBD = Fine Beam Double Polarisation. T, WS, SD, and P stand for temperature, wind speed, snow depth, and precipitation, respectively.

The PALSAR datasets were acquired in 1.1 processing level, a Single Look Complex (SLC) product. The data were provided as complex data including phase history in slant range geometry. Both Fine Beam Double (FBD) and Fine Beam Single (FBS) Polarisation modes were investigated. In Tab. 2 the summary of the SAR data is presented.

Coherence was calculated based on interferometric pairs with 46-day repeat–pass intervals. SAR processing consisted of SLC co-registration at the sub-pixel level (i.e. less than 0.1 pixel [4]), common-band filtering in range and azimuth, and generation of a differential interferogram. To obtain a more square pixel shape the interferogram was calculated using (1) number of looks in range and (3) in azimuth for the FBS data, and using (1) number of looks in range and (5) number of looks in azimuth for the FBD data. Coherence was then calculated over sufficiently large homogenous areas. The same procedure was repeated for different window sizes from 3 x 3 to 85 x 85, and with different coherence and test areas. Afterwards the data were geocoded.

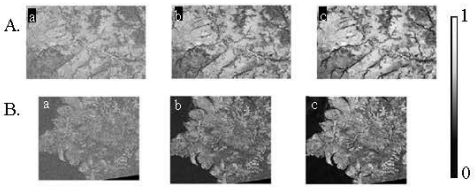

Figure 2. Coherence maps, a. 3x3 window, b. 7x7 window, c. 31x31 window size used, A. Chunsky E, B. Primorsky

To investigate the influence of the implemented coherence estimation window size on GSV retrieval, an exponential regression equation was used (Eq. 2) [12].

$$\Gamma(V) = a_1 e^{-a_2 V} + a_3 (1 - e^{-a_2 V}) \qquad (2)$$

$\Gamma(V)$ is coherence as a function of volume (V), which refers to GSV, and a_1, a_2, a_3 are empirical coefficients.

4. RESULTS

The results regarding the optimal coherence estimation window size for GSV retrieval in Siberian forests are presented in Fig. 3.

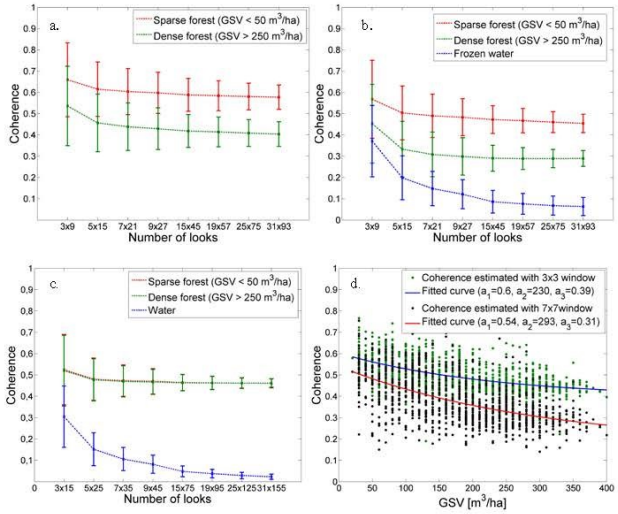

Figure 3. Mean and standard deviation of interferometric coherence as a function of number of looks, a. Chunsky test site (FBS data), b. Primorsky test site (FBS data), c. Primorsky test site (FBD data), d. coherence versus GSV, Primorsky test site.

First, when comparing FBD and FBS coherence during the unfrozen conditions, it is not possible to distinguish between sparse and dense forest (Fig. 3c). This is due to the temporal de-correlation caused by the time difference between the data acquisitions. Hence, as reported in previous studies, the data acquired under stable, frozen conditions are better suited for GSV retrieval [e.g. 13–15]. Second, areas with high and medium interferometric correlations and small averaging windows resulted in reliable coherence estimates. Based on the FBS data it can be observed that at least 75 pixels (~60 equivalent number of looks ENL) are required for a reliable coherence estimate.

Finally, the simple exponential regression equation demonstrates that applied window size can affect the saturation level, change from 230 m^3/ha to 293 m^3/ha (Fig. 3d).

5. CONCLUSIONS AND OUTLOOK

The study was conducted to optimize the coherence estimation in growing stock volume (GSV) retrieval over Siberian forests using ALOS PALSAR data.

It can be concluded that at least ~ 60 equivalent number of looks (ENL) are necessary to achieve a compromise between a good spatial resolution and a reliable estimation of coherence in ALOS PALSAR FBS images over Siberian forests. This high ENL means that future ALOS-2 PALSAR-2 mission with a 3 m resolution (i.e. Ultra-Fine mode) will not only achieve a reliable coherence estimation, but also a very good spatial resolution using less number of looks.

6. ACKNOWLEDGMENTS

This work was performed within the GIONET project, funded by the European Commission, Marie Curie Programme, Initial Training Networks, Grant Agreement Number PITN-GA-2010-264509.

The authors would like to thank the GAMMA Remote Sensing's team for great support and for providing materials.

The ALOS PALSAR data were provided by the Japan Aerospace Exploration Agency (JAXA) within the

Kyoto & Carbon Initiative.
The optical data were provided by the European Space Agency (project id: 13300).
The GIS forest inventory data were available within the FP5 EC-funded SIBERIA II project.

7. REFERENCES

1. Bamler, R., & Hartl, P. (1998). Synthetic aperture radar interferometry. *Inverse Problems* **14**, R1–R54.

2. Seymour, M.S. & Cumming, I.G. (1994). Maximum Likelihood estimator for SAR interferometry. in Proc. 1994 Int. Geosci. Remote Sensing Symp., IGARSS'94, 2272-2275, Pasadena, CA.

3. Wegmüler, U. & Werner, C.L. (1995). SAR Interferometric Signatures of Forest. *IEEE Transactions on Geoscience and Remote Sensing* **33**(5), 1153-1161.

4. Askne, J.I.H., Dammert, P.B.G., Ulander, L.M.H. & Smith, G. (1997). C-band repeat-pass interferometric SAR observations of the forest. *IEEE Transactions on Geoscience and Remote Sensing* **35**(1), 25-35.

5. Touzi, R., Lopes, A., Bruniquel, J. & Vachon, P.W. (1999). Coherence Estimation for SAR Imagery. *IEEE Transactions on Geoscience and Remote Sensing* **37**(1), 135-149.

6. Dammert, P.B.G. (1999). Spaceborne SAR Interferometry: Theory and Applications. Technical Report. Chalmers University of Technology.

7. Lopez-Martinez, C. & Pottier, E. (2007). Coherence estimation in synthetic aperture radar data based on speckle noise modelling. *Applied Optics* **48**(4), 544-558.

8. Thiel, Ch., Thiel, C. & Schmullius, C. (2009). Operational large-area forest monitoring in Siberia using ALOS PALSAR summer intensities and winter coherence. *IEEE Transactions on Geoscience and Remote Sensing* **47**(12), 3993-4000.

9. EC FP5 Project SIBERIA-II: http://www.siberia2.uni-jena.de

10. Shvidenko, A.Z., Schepaschenko, D.G, Nilsson, S. & Buluy Yu.I. (2006). *Tables and models of growth and productivity of forests of major forest forming species of northern Eurasia (standard and reference materials)*, Ministry of Natural Resources of the Russian Federation, Federal Agency of Forest Management, International Institute for Applied Systems Analysis, Moscow, Russia.

11. Wegmüller, U., Werner, C.L. & Strozzi, T. (1998). SAR interferometric and differential interferometric processing chain. in Proc. 2003 Int. Geosci. Remote Sensing Symp. IGARSS'98. 1106-1108, Seattle Washington, USA.

12. Askne, J. & Santoro, M. (2005). Multitemporal Repeat Pass SAR Interferometry of Boreal Forests. *IEEE Transactions on Geoscience and Remote Sensing* **43**(6), 1219-1228.

13. Santoro, M., Askne, J., Smith, G. & Fransson, J. E. S. (2002). Stem volume retrieval in boreal forests from ERS-1/2 interferometry. *Remote Sensing of Environment* **81**, 19-35.

14. Eriksson, L., Wiesmann, A., Schmullius, C. & Santoro, M. (2003). The potential of ALOS single polarisation InSAR for estimation of growing stock volume in Boreal Forest. in Proc. 2003 Int. Geosci. Remote Sensing Symp. IGARSS'03. 1939-1941, Toulouse, France.

15. Eriksson, L.E.B., Santoro, M., Wiesmann, A. & Schmullius, C. (2003) Multi-temporal JERS repeat-pass coherence for growing stock volume estimation of Siberian forest. *IEEE Transactions on Geoscience and Remote Sensing* **41**(7), 1561-1570.

Appendix B: Studies on biomass estimation in boreal forests

This section presents a list of studies on biomass estimation (stem volume and aboveground biomass) in boreal forests reported in the peer-reviewed research papers.

Reference	Sensor *Airborne* Satellite	Wavelength Polarization Incident or off-nadir angle [°]	Location/ site/No. of stands (No. of plots)	No. of images/ measurements	Estimated variable	Range of estimated variable (mean) /range of stand size (mean/plot size) [ha]	Input data	Model used	Spatial resolution	R^2 adjR^2 (r)	RMSE [unit as estimated variable] (rRMSE [%])
Ranson & Sun, 1994/[1]	*AIRSAR*	C-band L-band P-band HH, HV, VV 25, 35, 50	USA/ International Paper's Northern Experiment Forest/49	Multiple acquisitions	AGB [tons/ha]	0-350/-	Backscattering coefficient	Empirical model (simple regression)	353 px (>13 ha)	0.74 (P/C HV)	-
Rauste et al., 1994/[2]	*HUTSCAT*	X-&C-band Quad-Pol -	Finland/ Ruotsinkylä/ (150)	/1	Stem volume [m^3/ha]	0-370/- (0.04)	Backscattering coefficient	Empirical model (multiple regression)	0.04 ha	0.75	47
Rignot et al., 1994/[3]	*AIRSAR*	C-band L-band P-band HH, HV, VV multi-angle	USA, Alaska/ Bonanza Creek Experimental Forest/21	Multiple acquisitions	AGB [tons/ha]	6-218/-	Backscattering coefficient	Empirical model (polynomial regression)	Forest stand	-	(20-39) (19-32) w/o alder stands
Dobson et al., 1995/[4]	SIR-C/X-SAR	C-band L-band X-Band (VV) Quad-Pol 31	USA/Raco Supersite/63	1	AGB [tons/ha]	0-250/>10	Backscattering coefficient	Semi-empirical (sum of crown and trunk biomass)	Forest stand	0.96	14
Rignot et al., 1995/[5]	*AIRSAR*	P-band Quad-Pol -	USA, Alaska/ Bonanza Creek Experimental Forest/21	2	AGB [tons/ha]	4-220/-	Backscattering coefficient	Empirical model (multiple regression)	Forest stand	0.99-0.85	(18-45)
Pulliainen et al., 1996/[6]	ERS-1	C-band VV 23	Finland/ Porvoo/ Mäntsälä/198 Ohkola/ 91	23	Stem volume [m^3/ha]	0-383 (143)/- (2.0) (1.65)	Backscattering coefficient	Semi-empirical model (IUFT model)	Forest stand	(0.63) (0.64)	98 (78*) 90 (58*)

Reference	Sensor *Airborne* Satellite	Wavelength Polarization Incident or off-nadir angle [°]	Location/ site/No. of stands (No. of plots)	No. of images/ measurements	Estimated variable	Range of estimated variable (mean) /range of stand size (mean/plot size) [ha]	Input data	Model used	Spatial resolution	R^2 adjR^2 (r)	RMSE [unit as estimated variable] (rRMSE [%])
Ranson & Sun, 1997/[7]	SIR-C/X-SAR	C-band Quad-Pol L-band Quad-Pol X-band VV -49	Canada/ BOREAS southern study area/62	2 acquisitions: April & October	AGB [tons/ha]	(0-250)/-	Backscattering coefficient	Empirical model (multiple regression)	0.09 ha	0.89	15
Kurvonen et al., 1999/[8]	ERS-1	C-band VV 23	Finland/ Porvoo/*16000* forest blocks	4	Stem volume [m^3/ha]	0-300 (133)/- (4.5)	Backscattering coefficient	Semi-empirical model (HUT model)	Forest. block	(0.09-0.47)	78.3-114 (49.6-77.1)
	JERS-1	L-band HH 35		4						(0.52-0.65)	53.0-94.0 (34.3-60.6)
Pulliainen et al., 1999/[9]	ERS-1	C-band VV 23	Finland/ Porvoo/*16000* forest blocks	8 (4 ERS-1)	Stem volume [m^3/ha]	4-287 (133)/ - (4.5)	Backscattering coefficient	Semi-empirical model (HUT model)	Forest. block	(0.60-0.65)	(27-60)
	JERS-1	L-band HH 35	Finland/Sodankylä/*13400* forest blocks	5 (3 ERS-1)		0-135 (42)/- (6.0)				(0.65-0.85)	(26-52)
Fransson & Israelsson, 1999/[10]	ERS-1	C-band VV 23	Sweden/ northern Sweden/60	5 (2 ERS-1)	Stem volume [m^3/ha]	0-285/2-140	Backscattering coefficient	Empirical model (simple regression)	Forest. stand	-	-
	JERS-1	L-band HH 35								(0.78)	-

Reference	Sensor *Airborne* Satellite	Wavelength Polarization Incident or off-nadir angle [°]	Location/ site/No. of stands (No. of plots)	No. of images/ measurements	Estimated variable	Range of estimated variable (mean) /range of stand size (mean/plot size) [ha]	Input data	Model used	Spatial resolution	R^2 adjR^2 (r)	RMSE [unit as estimated variable] (rRMSE [%])
Fransson et al., 2000/[11]	*CARABAS-II*	VHF HH 45-67	Sweden/Tönnersjöheden/ 30	Multiple acquisitions	Stem volume [m^3/ha]	0-625 (312)/ 2-17 (4.6)	Backscattering coefficient Backscattering amplitude	Empirical model (simple regression)	Forest stand	-	- 65.8 (21)
Saatchi & Moghaddam, 2000/[12]	*AIRSAR*	C-band L-band P-band Quad-Pol 20-60 (40-50)	Canada/ BOREAS southern study area/18 (72)	15	AGB [tons/ha]	(7.42-165.60)/-	Backscattering coefficient	Semi-empirical model (two layer model)	Forest stand	-	(1.50-28.43)
Rauste et al., 2000/[13]	SIR-C/X SAR	X-band VV C-band L-band HH, HV, VV 40.9-47.8	Canada/ BOREAS test site/38	4	AGB [tons/ha]	6.4-150/-	Backscattering coefficient	Empirical model (multiple regression)	Forest stand	0.29-0.69	25.7-38.6
Hyyppä et al., 2000/[14]	ERS-1/2 JERS-1 *HUTSCAT*	C-band VV 23 L-band HH 35 C-band HH, VV, HV 23	Finland/ Kalkkinen/183 /2	18 (9 pairs) 3 8 (4 pairs)	Stem volume [m^3/ha]	0-423.8 (156)/ - (1)	Backscattering coefficient InSAR coherence Backscattering coefficient Backscattering coefficient, height	Empirical model (multiple regression)	Forest stand	0.06 0.24 0.13 0.68	101.9 (65) 90.9 (58) 98.4 (63) 55.7 (34)
Koskinen et al., 2001/[15]	ERS-1/2	C-band VV 23	Finland/ Tuusula/144 Finland/ Kalkkinen/195	10 (5 pairs) 8 (4 pairs)	Stem volume [m^3/ha]	0-550 (155)/- (2.5) 0-430 (156)/- (1.0)	Backscattering coefficient and InSAR coherence	Semi-empirical model (IHUT model)	Forest stand	0.67 -	99 (57) -

Reference	Sensor *Airborne* Satellite	Wavelength Polarization Incident or off-nadir angle [°]	Location/ site/No. of stands (No. of plots)	No. of images/ measurements	Estimated variable	Range of estimated variable (mean) /range of stand size (mean/plot size) [ha]	Input data	Model used	Spatial resolution	R^2 adjR^2 (r)	RMSE [unit as estimated variable] (rRMSE [%])
Fransson et al., 2001/[16]	ERS-1/2	C-band VV 23	Sweden/ Kättböle/43	10 (5 pairs)	Stem volume [m^3/ha]	0-305 (129)/ 1.4-15 (5.2)	InSAR coherence	Empirical model (linear regression)	Forest stand	0.06-0.87	26-82 (20-62)
Balzter et al., 2002/[17]	*EMISAR* L-band Quad-Pol 35-60	C-band	Finland/ Pikkarala/-	2	Stem volume [m^3/ha]	0-150 (50.5)/-	Backscattering coefficient and PolInSAR coherence	Empirical models (nonlinear, multiple regression)	Forest stand	(0.23-0.71) (0.54-0.78)	24.5-43.7 (43-65) 21.6-43.7 (39-65)
Santoro et al., 2002/[18]	ERS-1/2	C-band VV 23	Sweden/ Kättböle/42 (216)	18 (9 pairs)	Stem volume [m^3/ha]	8-335 (135)/2-14 (0.00785-0.03)	Backscattering coefficient and InSAR coherence Backscattering coefficient All data	Semi-empirical model (WCM)	Forest stand	0.04-0.92 0.01-0.36 0.93	20.9-151.5 (15.5-112) 82.4-160.2 (61-119) 10.8 (8*)
Sun et al., 2002/[19]	SIR-C/X SAR	L-band Quad-Pol 46.4	Russia/Siberia Western Sayani Mountains/ 56	1	AGB [tons/ha]	10-240/-	Backscattering coefficient	Empirical model (multiple regression)	Forest stand	0.91	18.1
Pulliainen et al., 2003/[20]	ERS-1/2	C-band VV 23	Finland/ Tuusula/134	28 (14 pairs)	Stem volume [m^3/ha]	0-539.3 (174.1)/ 1.52-13.8 (3.2)	Backscattering coefficient and InSAR coherence	Semi-empirical model (IHUT)	Forest stand	0.79 (0.89)	83.7 (48)

Reference	Sensor *Airborne* Satellite	Wavelength Polarization Incident or off-nadir angle [°]	Location/ site/No. of stands (No. of plots)	No. of images/ measurements	Estimated variable	Range of estimated variable (mean) /range of stand size (mean/plot size) [ha]	Input data	Model used	Spatial resolution	R^2 adjR^2 (r)	RMSE [unit as estimated variable] (rRMSE [%])
Askne et al., 2003/[21]	ERS-1/2	C-band VV 23	Sweden/ Kättbäle/37	18 (9 pairs)	Stem volume [m^3/ha]	8-335 (140)/2-14	Backscattering coefficient and InSAR coherence	Semi-empirical model (IWCM)	Forest stand	-	-
	JERS-1	L-band HH 35		9 (4 pairs)						-	30-35 (21.4-25)
Engdahl et al., 2004/[22]	ERS1/2	C-band VV 23	Finland/ Tuusula/134	28 (14 pairs)	Stem volume [m^3/ha]	0-539.3 (174.4)/(3.2)	Backscattering coefficient and InSAR coherence	Semi-empirical model (HUT)	Forest stand	0.79	-
Askne et al., 2005/[23]	ERS-1/2	C-band VV 23	Finland/ Tuusula/202	16 (8 pairs)	Stem volume [m^3/ha]	0-539 (157.6)/(1)	Backscattering coefficient and InSAR coherence	Semi-empirical model (IWCM)	Forest stand	-	34.7 143.4 (22-91)
Rauste, 2005/ [24]	JERS-1	L-band HH 35	Finland/ Punmala & Ruokolahti/ 206	6	Stem volume [m^3/ha]	0-364 (102)/-	Backscattering coefficient	Empirical model (multiple regression)	Forest stand	0.16-0.66 0.71	59.8 (58.6)
Santoro et al., 2006/[25]	JERS-1	L-band HH 35	Sweden/ Kättbäle/42	9	Stem volume [m^3/ha]	16-344 (144)/ 2-21	Backscattering coefficient	Semi-empirical model (WCM)	Forest stand	0.76	36 (25)
			Finland/ Tuusula/35	3		5-535 (257)/ 0.5-20				0.68	102 (40)
			Russia/ Southern Siberia Bolshe Murtinsky/ 506	13		5-400 (171.15)/8-683				0.73	57 (51)
Askne & Santoro, 2007/[26]	ERS-1/2	C-band VV 23	Finland/ Tuusula/202	30 (15 pairs)	Stem volume [m^3/ha]	0-539	Backscattering coefficient and InSAR coherence	Semi-empirical model (IWCM)	Forest stand	-	(17-63)

Reference	Sensor *Airborne* Satellite	Wavelength Polarization Incident or off-nadir angle [°]	Location/ site/No. of stands (No. of plots)	No. of images/ measurements	Estimated variable	Range of estimated variable (mean) /range of stand size (mean/plot size) [ha]	Input data	Model used	Spatial resolution	R^2 adjR^2 (r)	RMSE [unit as estimated variable] (rRMSE [%])
Santoro et al., 2007/[27]	ERS-1/2	C-band VV 23	Russian Fed./Central Siberia/6773	20 (10 pairs)	Stem volume [m^3/ha]	0-470 (156-231)/ (17.2-49.5)	Backscattering coefficient and InSAR coherence	Semi-empirical model (IWCM)	Forest stand	0.5-0.8	45-75 (25-41)
Engdahl et al., 2008/[28]	ERS1/2	C-band VV 23	Finland/ Tuusula/134	28 (14)	Stem volume [m^3/ha]	0-339 (174)/ 1.5-13.8 (3.2)	Backscattering coefficient and InSAR coherence	Semi-empirical model (IHUT)	Forest stand	(0.87)	95 (54)
Askne & Santoro, 2009/[29]	ERS-1/2	C-band VV 23	Sweden/ Kättbäle/42	8 (4 pairs)	Stem volume [m^3/ha]	0-334 (135)/4-21	Backscattering coefficient and InSAR coherence	Semi-empirical model (IWCM)	Forest stand	0.9	24 (18)
Folkesson et al., 2009/[30]	*CARABAS-II*	VHF HH 46-66	Sweden/Tönne rsjöheden/ 37 (~370)	10 4	Stem volume [m^3/ha]	80-700 (193)/ (0.3)	Backscattering amplitude	Semi-empirical model (forward model)	Forest stand	0.45-0.77 0.88-0.91	55-131 (28.5*-68*) 54-64 (28*-33*)
Solberg et al., 2010/[31]	SRTM	X-band VV 55	Norway/ Aurskog-Høland/(241)	DSM	AGB [tons/ha]	20-355 (121)/ (0.02-0.1)	InSAR height	Empirical model (simple regression)	Forest stand	-	(19)
Sandberg et al., 2011/[32]	*E-SAR*	L-band P-band III, HV, VV 28-50	Sweden/ Remningstorp /58	5 6	AGB [tons/ha]	9-287 (129)/ 0.5-9.4 (2.0)	Backscattering coefficient	Empirical model (multiple regression)	Forest stand	0.39-0.61 (LHV) 0.72-0.75 (PHH)	40-48 (31-37) 30-32 (23-25)
Sun et al., 2011/[33]	ALOS PALSAR	L-band Quad-Pol HH & HV 21.5 34.3	USA/ Northern Experiment Forest, Maine/20	4	AGB [tons/ha]	40-280.5/-	Backscattering coefficient Coherence	Empirical model (multiple regression)	0.0225 ha px 15 m	0.63-0.71 (incl. height information)	28.2-32

Reference	Sensor *Airborne* Satellite	Wavelength Polarization Incident or off-nadir angle [°]	Location/ site/No. of stands (No. of plots)	No. of images/ measurements	Estimated variable	Range of estimated variable (mean) /range of stand size (mean/plot size) [ha]	Input data	Model used	Spatial resolution	R^2 adjR^2 (r)	RMSE [unit as estimated variable] (rRMSE [%])
Santoro et al., 2011/[34]	Envisat ASAR	C-band HH, VV 18-45	Sweden/Västerbotten/- Sweden/ Västra/- Russian Fed./Central Siberia/- Canada/Lac Mistassini/-	Hyper-temporal dataset (from two years)	Stem volume [m^3/ha]	0-184 (95)/- 0-386 (173)/- 0-470 (167.2)/- 0-271 (103.2)/-	Backscattering coefficient	Semi-empirical model (WCM)	100 ha px 1 km	(0.34) (0.26) (0.65) (0.33-0.49)	(47.7) (35.7) (34.2) (44.5-48.1)
Andersen et al., 2011/[35]	ALOS PALSAR	L-band HH & HV 34.3	USA/Tanana valley, Alaska/ (79)	Multi-temporal	AGB [tons/ha]	1.1-253.5 (78.1)/ (1/30)	Backscattering coefficient	Empirical model (machine learning, kNN algorithm)	Forest plot	-	(5.1)
Neumann et al., 2012/[36]	*E-SAR*	L-band P-band HH, HV, VV 28-50	Sweden/ Krycklan/27	Multiple acquisitions	AGB [tons/ha]	23-183 (94.3)/ 2.4-26.3	Backscattering coefficient and PolInSAR coherence	Semi-empirical model (RVoG)	0.25 ha px 50 m	(0.49-0.86) (0.23-0.84)	21.3-36.2 (23-38) 22.7-40.7 (24-43)
Cartus et al., 2012/[37]	ALOS PALSAR	L-band HH & HV 34.3	USA/ transitional forests/2007	655	AGB [tons/ha]	-	Backscattering coefficient	Semi-empirical model (WCM)	County	0.86	12.9
Karjalainen et al., 2012/ [38]	TerraSAR-X	X-band HH & VV 35.8-52	Finland/ Southern Finland/(110)	4	Stem volume [m^3/ha]	79.7-503.1 (256.4)/(0.021)	Backscattering coefficient (radargrammetry)	Empirical model (machine learning, random forest)	Forest plot	-	87.9 (34)

Reference	Sensor *Airborne* Satellite	Wavelength Polarization Incident or off-nadir angle [°]	Location/ site/No. of stands (No. of plots)	No. of images/ measurements	Estimated variable	Range of estimated variable (mean) /range of stand size (mean/plot size) [ha]	Input data	Model used	Spatial resolution	R^2 adjR^2 (r)	RMSE [unit as estimated variable] (rRMSE [%])
Antropov et al., 2013/[39]	ALOS PALSAR	L-band HH & HV 34.3	Finland/ Knorrane/123	3	Stem volume [m^3/ha]	0-314 (95)/(3)	Backscattering coefficient	Semi-empirical model (HUT model)	Forest stand	0.65	41.2 (43.4)
			Finland/ Heinävesi/103	3		0-425 (110)/(4.8)				0.71	47.0 (42.8)
Soja et al., 2013/[40]	*E-SAR*	P-band HH, HV, VV 26-35	Sweden/ Remningstorp /50 (10)	9	AGB [tons/ha]	52-267 (181)/ 0.5-9.4	Backscattering coefficient	Empirical model (multiple regression)	Forest stand	0.22-0.64	40-59 (22-33)
			Sweden/ Krycklan/ 29 (97)	7		8-257 (95)/ 1.5-22				0.31-0.64	27-40 (28-42)
Peregon et al., 2013/[11]	ALOS PALSAR	L-band HH & HV 34.3	Russian Fed. /Western Siberia/(430)	5	AGB [tons/ha]	10-190 (73)/(0.01)	Backscattering coefficient	Semi-empirical model (IWCM)	Forest stand	0.35-0.49	46-55 (25-32)
Solberg et al., 2013/[42]	TanDEM-X	X-band HH 36 & 42	Norway/ Lardal/28 (192)	4 (2 pairs)	Stem volume [m^3/ha]	0-596 (216)/ 1-2.9 (0.025)	InSAR height	Empirical model (simple regression)	Forest plot and stand	-	94 (44) plot 44 (20) stand
					AGB [tons/ha]					(0.98)	57 (43) plot 25 (19) stand
Santoro et al., 2013/[43]	ENVISAT ASAR	C-band HH or VV 18-45	Sweden/ country/ 11425	Hyper-temporal dataset	Stem volume [m^3/ha]	(125)	Backscattering coefficient	Semi-empirical model (WCM)	~3080 km^2 px 0.5°	(0.73)	(22)
			Russian Fed./Central Siberia/46487			(180)/(26)				(0.86)	(15)
			Canada/ Québec/731			(63)				(0.93)	(27)

Reference	Sensor *Airborne* Satellite	Wavelength Polarization Incident or off-nadir angle [°]	Location/ site/No. of stands (No. of plots)	No. of images/ measurements	Estimated variable	Range of estimated variable (mean) /range of stand size (mean/plot size) [ha]	Input data	Model used	Spatial resolution	R^2 adjR^2 (r)	RMSE [unit as estimated variable] (rRMSE [%])
Askne et al., 2013/[44]	TanDEM-X	X-band HH 34 & 41	Sweden/ Remningstorp /201	36 (18 pairs)	AGB [tons/ha]	6-267 (150)/>1	InSAR height	Semi-empirical models: IWCM RVoG PD	Forest stand	- - -	(16.7-33) (16.7-39.7) (17.9-33.1)
Persson & Fransson, 2014/[45]	TerraSAR-X	X-band HH, HV, VV 32.3, 40.7, 47.6 40.5, 49.6	Sweden/ Krycklan/751 Sweden/ Remningstorp /531	4 3	AGB [tons/ha]	2-162 (77)/ 0.5-51.2 7-275 (110)/-	Backscattering coefficient (radargrammetry)	Empirical model (multiple regression)	Forest stand	0.48 0.81	24.3 (31.6) 24.9 (22.9)
Vastaranta et al., 2014/ [46]	TerraSAR-X	X-band - -	Finland/Espoo - Kirkkonummi/ 91 (207)	4	AGB [tons/ha]	3.9-347.1 (116.5)/ 0.5-12.2 (4.1)	Backscattering coefficient (radargrammetry)	Empirical model (multiple regression)	Forest stand	-	15.6-16.7 (16.1-16.7)
Chowdhury et al., 2014/ [47]	ALOS PALSAR	L-band Quad-Pol 21.5 & 23.1	Russian Fed./ Shestakovsky/ 304	3	Stem volume [m^3/ha]	0-350 (189)/ 2-60 (22)	PolInSAR coherence	Empirical model (exponential model)	Forest stand	0.61-0.73	33-51 (17*-27*)
Lüttich et al., 2014/[48]	ALOS PALSAR ENVISAT ASAR	L-band HH & HV 34.3 C-band - - (15-45)	Russian Fed./Central Siberia/ 120636	4 PALSAR mosaics 2007-2010 Multiple acquisitions200 9-2011	Stem volume [m^3/ha]	(167.1)/- (17)	Backscattering coefficient	Empirical model (machine learning, random forest.) Semi-empirical model (WCM)	0.0625 ha px 25 m 100 ha px 1km	(0.3-0.55)	58.9-71.3 (35.06-42.44) 47.7-64.9 (28..39-38.63)

Reference	Sensor *Airborne* Satellite	Wavelength Polarization Incident or off-nadir angle [°]	Location/ site/No. of stands (No. of plots)	No. of images/ measurements	Estimated variable	Range of estimated variable (mean) /range of stand size (mean/plot size) [ha]	Input data	Model used	Spatial resolution	R^2 $\overline{adjR^2}$ (r)	RMSE [unit as estimated variable] (rRMSE [%])
Atwood et al., 2014/[49]	ALOS PALSAR	L-band HH & HV 34.3	USA/ Tanana Valley, Alaska/(79)	8	AGB [tons/ha]	(0-250)/(1/30)	Backscattering coefficient	Empirical model (polynomial regression)	Forest plot LiDAR-derived biomass	0.9	34.7 LiDAR 37.3 plot
Wilhelm et al., 2014/[50]	ALOS PALSAR	L-band HV & HH 34.3	Russian Fed./Central Siberia/more than 400	4 PALSAR mosaics 2007-2010	Stem volume [m^3/ha]	(0-320 (165)/ 1.85-485.15	Backscattering coefficient	Empirical model (machine learning, random forest)	(0.0625 ha px 25 m	-	55.2-63.3 (33.4-38.4)*
Rahlf et al., 2014/[51]	TanDEM-X TerraSAR-X	X-band - 36 & 43 X-band - 21-53	Norway/ Lærdal/ 25 (170) 6 (3 pairs)	3	Stem volume [m^3/ha]	(0-596 (186.45)/ 1-3 (0.025) Backscattering coefficient (polargrammetry)	InSAR height	Empirical model (simple regression)	Forest plot and stand	-	77.56 (41.60) plot 33.74 (18.10) stand 82.82 (44.42) plot 43.38 (23.27) stand
Karila et al., 2015/[52]	TanDEM-X	X-band - 31 & 48	Finland/Evo/ (335)	10 (5 pairs) bistatic	Stem volume [m^3/ha]	4.7-653.6 (208.9)/(0.03)	InSAR height	Empirical model (machine learning, random forest)	Forest plot	0.49-0.65	67.2-79.8 (32.2-38.9)
Solberg et al., 2015/[53]	TerraSAR-X	X-band - 21.5-52.8	Norway/ Lærdal/ 21 (140)	6 (3 pairs)	AGB [tons/ha]	(0-338 (131)/ 0.1-29 (0.025)	Backscattering coefficient (radargrammetry)	Empirical model (nonlinear regression)	Forest plot and stand	-	58 (55) plot 23 (18) stand

Reference	Sensor *Airborne* Satellite	Wavelength Polarization Incident or off-nadir angle [°]	Location/ site/No. of stands (No. of plots)	No. of images/ measurements	Estimated variable	Range of estimated variable (mean) /range of stand size (mean/plot size) [ha]	Input data	Model used	Spatial resolution	R^2 $\underline{adjR^2}$ (r)	RMSE [unit as estimated variable] (rRMSE [%])
Soja et al. 2015/[54]	TanDEM-X	X-band VV 41.2-41.7	Sweden/ Remningstorp /(32) Sweden/ Krycklan/31	8 (4 pairs) bistatic-interferometric	AGB [tons/ha]	42-242 (148)/ (0.5) 23-183 (94)/ 2.4-26.3	InSAR height	Semi-empirical model (TBM)	Forest plot Forest stand	0.65-0.89 0.81-0.87	(12-19) (14-16)
Askne et al., 2015/[55]	TanDEM-X	X-band VV -	Sweden/ Remningstorp /202	18 (9 pairs) bistatic	AGB [tons/ha]	6-266 (105)/>1	Backscattering coefficient and InSAR coherence	Semi-empirical model (IWCM)	Forest stand	0.72-0.93	(16-32)
Santoro et al., 2015/[56]	ALOS PALSAR	L-band HH, HV Quad-Pol 34.3, 41.5, 50.8 21.5 & 23.1	Sweden/ Krycklan/1131 Sweden/ Remningstorp /56	96 129	Stem volume [m^3/ha]	0-525 (134) /1-64 (4) 35-617 (295)/ 1-11 (3)	Backscattering coefficient	Semi-empirical model (WCM)	Forest stand	0.46-0.14 0.02-0.37	58.4-105.2 (44-79.2) 121.6-299 (35.1-90.7)
Santoro et al., 2015/[57]	ENVISAT ASAR	C-band VV or HH 20-45	Boreal zone/ Canada (12 ecozones) Alaska (12 counties) Russia (82 regions)	several thousand	Stem volume [m^3/ha]	<–300/	Backscattering coefficient	Semi-empirical model (WCM)	1.23 km^2 px 0.01°	0.65-0.82 0.47-0.53 0.65-0.72	28.9-39.9 (20.4-29.4) 48.2-56.1 (20-27.2) 14.1-19.6 (12.2-17.4)

Reference	Sensor *Airborne* Satellite	Wavelength Polarization Incident or off-nadir angle [°]	Location/ site/No. of stands (No. of plots)	No. of images/ measurements	Estimated variable	Range of estimated variable (mean) /range of stand size (mean/plot size) [ha]	Input data	Model used	Spatial resolution	R^2 adjR^2 (r)	RMSE [unit as estimated variable] (rRMSE [%])
Thiel & Schmullius, 2016/[58]	ALOS PALSAR	L-band HH & HV - (34.3)	Russian Fed./Central Siberia/12243	87	Stem volume [m^3/ha]	0-500/>2	Backscattering coefficient InSAR coherence	Empirical model (exponential model)	Forest stand	0.54 0.79	58 (33) 44 (25)
Stelmaszczuk -Górska et al., 2016/[59]	ALOS PALSAR	L-band HH & HV 34.3	Russian Fed./ Krasnoyarsk Kra/Bolshe Murinsky/ 641	19	AGB [tons/ha]	0-224 (98)/ 0.5-130 (16)	Backscattering coefficient and InSAR coherence	Empirical models (machine learning) MaxEnt Random Forest	0.25 ha px 50 m	- -	35.8 (38.8) 35.0 (36.9)
Askne et al., 2017/[60]	TanDEM-X	X-band VV 41	Sweden/ Krycklan/29 619	14 bistatic	AGB [tons/ha]	<183/ 1.2-23.8 <291/1-57.3	Backscattering coefficient, InSAR height & coherence	Semi-empirical model (IWCM)	Forest stand	0.82-0.88 0.83	(15.8-21.2) (18.3)
Persson & Fransson, 2017/[61]	TanDEM-X	X-band VV 41	Sweden/ Krycklan/ 29 (29) Sweden/ Remningstorp /32 (32)	4 (2 pairs) bistatic	AGB [tons/ha]	23-183 (95)/ 2.4-26.1 (0.03) 55-284 (155)/- (0.03)	InSAR height	Empirical model (simple regression)	Forest plot and stand	0.81 0.85 0.34 0.81	23.8 (26.4) plot 16.2 (17.2) stand 54.9 (28.5) plot 22.6 (14.6) stand
Soja et al., 2017/[62]	TanDEM-X	X-band VV 41 & 44	Sweden/ Krycklan/26	87	AGB [tons/ha]	0-300 (94)/ 1.5-22	Backscattering coefficient, InSAR height & coherence	Semi-empirical model (IWCM)	Forest stand	(0.81-0.93)	(18-32)
Antropov et al., 2017/[63]	ALOS PALSAR	L-band Quad-Pol 24	Finland/ Knortane/124	7	Stem volume [m^3/ha]	0-314 (95)/ 2-6 (3.5)	Backscattering coefficient PolInSAR coherence	Empirical model (machine learning, kNN algorithm)	Forest stand	0.35-0.66 0.46-0.77	39.1-56.4 (41.2-59.1) 34.0-51.6 (35.8-54.3)

Reference	Sensor *Airborne* Satellite	Wavelength Polarization Incident or off-nadir angle [°]	Location/ site/No. of stands (No. of plots)	No. of images/ measurements	Estimated variable	Range of estimated variable (mean) /range of stand size (mean/plot size) [ha]	Input data	Model used	Spatial resolution	R^2 $\underline{adjR^2}$ (r)	RMSE [unit as estimated variable] (rRMSE [%])
Persson et al., 2017/[64]	TanDEM-X	X-band IIII 38-45	Sweden/ (2288)	1036 (518 pairs)	AGB [tons/ha]	0-369 (86) /(0.03)	Backscattering coefficient, InSAR height & coherence	Empirical model (multiple regression)	Forest stand	-	27.4-29.7 (20.8-23.4)
Santoro et al., 2018/[65]	ERS-1	C-band - (VV) - (23)	Finland/ Tuusula/37 Sweden/ Kättböle/42 Sweden/ Bäcksjön/40	31 24 29	Stem volume [m^3/ha]	3-482/1.25-7 8-315/2-14 6-291/4-19	InSAR coherence	Semi-empirical model (IWCM)	Forest stand	-	64.4-250.0 (27.8-107.8) 58.4-136.3 (45.9-106.3) -
Stelmaszczuk -Górska et al., 2018/[66]	ALOS-2 PALSAR-2 RADAR-SAT-2	L-band HH&HV 31.4&36.3 C-band HH&HV 32.2-42.1	Russia/ Central Siberia/Bolshe Murtinsky/ 491	2 5	AGB [tons/ha]	0-211 (94)/ 3-127 (18.5)	Backscattering coefficient	Machine learning (Random Forest)	0.25 ha px 50 m	0.53 0.23	29.4 (31) 39.5 (42)
Rodriguez-Veiga et al., 2019/[67]	ALOS PALSAR	L-band HH&HV - (34.3)	Sweden/ (22548)	Multiple acquisitions	AGB [tons/ha]	0- >180/(0.015)	Backscattering coefficient	Machine learning (kNN algorithm)	0.0625 px 25 m	-	32 (39)
Santoro et al., 2019/[68]	TerraSAR-X Sentinel-1 ALOS-2 PALSAR-2	X-band IIII or VV 19-51 C-band VV&VH 39 L-band HH,HV,VV 28-36	Sweden/ Krycklan/325 Sweden/ Remningstorp /48	21/78/15 62/33/24	Stem volume [m^3/ha]	2-649 (158)/ (0.03) 58-691 (320)/ (0.5)	Backscattering coefficient	Semi-empirical model (WCM)	Forest plot	-	(50.3) (32.8)

Reference	Sensor *Airborne* Satellite	Wavelength Polarization Incident or off-nadir angle [°]	Location/ site/No. of stands (No. of plots)	No. of images/ measurements	Estimated variable	Range of estimated variable (mean) /range of stand size (mean/plot size) [ha]	Input data	Model used	Spatial resolution	R^2 adjR^2 (r)	RMSE [unit as estimated variable] (rRMSE [%])
Askne et al., 2019/[69]	TanDEM-X	X-band VV 41	Sweden/ Krycklan/242	1 bistatic pair	Stem volume [m^3/ha]	/>4	Backscattering coefficient, InSAR height & coherence	Semi-empirical (IWCM)	Forest stand	0.85	(17.1)
			Sweden/ Remningstorp /202 (12)	2 bistatic pairs		/>1 (0.28)				0.92	(16.7)
Cartus et al., 2019/[70]	RADARSAT-2 ERS-2 ALOS PALSAR *SETHI*	C-band Quad-Pol 21-41 C-band VV 23 L-band HH&HV 34 P-band Quad-Pol 24-62	Sweden/ Remningstorp /(214)	25 17 6 1	AGB [tons/ha]	<300/(0.03)	Backscattering coefficient	Semi-empirical model (WCM) Empirical model (multiple regression)	Forest plot LiDAR-derived biomass	-	(52-55) plot (51) LiDAR (58-64) plot (39) LiDAR (42) plot (32) LiDAR

* Calculated by authors using provided mean stem volume or aboveground biomass

Acronyms and symbols:

AGB	Aboveground Biomass
AIRSAR	Airborne Synthetic Aperture Radar
ALOS	Advanced Land Observing Satellite
ALS	Airborne Lidar Scanning
ASAR	Advanced Synthetic Aperture Radar
BOREAS	Boreal Ecosystem Atmosphere Study
CARABAS	Coherent All Radio Band Sensing
DSM	Digital Surface Model
EMISAR	Electromagnetic Institute Synthetic Aperture Radar
ENVISAT	ENVIronmental SATellite
ERS	European Remote Sensing
E-SAR	Experimental airborne Synthetic Aperture Radar
GSV	Growing Stock Volume
HH	Horizontal-Horizontal (polarization)
HUT	Helsinki University of Technology
HUTSCAT	Helsinki University of Technology SCATterometer
HV	Horizontal-Vertical (polarization)
IHUT	Interferometric model of the Helsinki University of Technology
InSAR	Interferometric Synthetic Aperture Radar
IWCM	Interferometric Water Cloud Model
JERS	Japanese Earth Resources Satellite
kNN	k-Nearest Neighbors
LiDAR	Light Detection and Ranging
MaxEnt	Maximum Entropy
PD	Penetration Depth
PALSAR	Phased Array type L-band Synthetic Aperture Radar
px	pixel

RADAR	Radio Detection and Ranging
RVoG	Random Volume over Ground
SAR	Synthetic Aperture Radar
SIR	Shuttle Imaging Radar
SPOT XS	Satellite for observation of Earth multispectral (French: Satellite Pour l'Observation de la Terre)
SRTM	Shuttle Radar Topography Mission
TBM	Two-level Biomass Model
VH	Vertical- Horizontal (polarization)
VHF	Very High Frequency
VV	Vertical-Vertical (polarization)
WCM	Water Cloud Model
$adjR^2$	Adjusted coefficient of determination
r	Pearson's correlation coefficient
R^2	Coefficient of determination
RMSE	Root Mean Square Error
rRMSE	relative RMSE
Quad-Pol	Full polarimetric data (HH+VV+HV+VH)
	Wavelength
X-band	3 cm, 3.2 cm
C-band	6 cm
L-band	23.5 cm, 25 cm
P-band	68 cm
VHF	3-15 m

References:

1. Ranson, K. J.; Sun, G. Mapping biomass of a northern forest using multifrequency SAR data. *IEEE Trans. Geosci. Remote Sens.* **1994**, *32*, 388–396.

2. Rauste, Y.; Häme, T.; Pulliainen, J.; Heiska, K.; Hallikainen, M. Radar-based forest biomass estimation. *Int. J. Remote Sens.* **1994**, *15*, 2797 2808.

3. Rignot, E.; Way, J.; Williams, C.; Viereck, L. Radar estimates of aboveground biomass in boreal forests of interior Alaska. *IEEE Trans. Geosci. Remote Sens.* **1994**, *32*, 1117 1124.

4. Dobson, M. C.; Ulaby, F. T.; Pierce, L. E.; Sharik, T. L.; Bergen, K. M.; Kellndorfer, J.; Kendra, J. R.; Li, E.; Lin, Y. C.; Nashashibi, a.; Sarabandi, K.; Siqueira, P. Estimation of forest biophysical characteristics in Northern Michigan with SIR-C/X-SAR. *IEEE Trans. Geosci. Remote Sens.* 1995, *33*, 877–895.

5. Rignot, E. J.; Zimmermann, R.; Zyl, J. J. Van Spaceborne applications of P-band imaging radars for measuring forest biomass. *IEEE Trans. Geosci. Remote Sens.* **1995**, *33*, 1162–1169.

6. Pulliainen, J. T.; Mikkela, P. J.; Hallikainen, M. T.; Ikonen, J. Seasonal dynamics of C-band backscatter of boreal forests with applications to biomass and soil moisture estimation. *IEEE Trans. Geosci. Remote Sens.* **1996**, *34*, 758–770.

7. Ranson, K. J.; Sun, G.; Lang, R. H.; Chauhan, N. S.; Cacciola, R. J.; Kilic, O. Mapping of boreal forest biomass from spaceborne synthetic aperture radar. *J. Geophys. Res.* **1997**, *102*, 29599–29610.

8. Kurvonen, L.; Pulliainen, J.; Hallikainen, M. Retrieval of biomass in boreal forests from multitemporal ERS-1 and JERS-1 SAR images. *IEEE Trans. Geosci. Remote Sens.* **1999**, *37*, 198–205.

9. Pulliainen, J. T.; Kurvonen, L.; Hallikainen, M. T. Multitemporal behavior of L- and C-band SAR observations of boreal forests. *IEEE Trans. Geosci. Remote Sens.* **1999**, *37*, 927 937.

10. Fransson, J. E. S.; Israelsson, H. Estimation of stem volume in boreal forests using ERS-1 C- and JERS-1 L- band SAR data. *Int. J. Remote Sens.* **1999**, *20*, 123 137.

11. Fransson, J. E. S.; WaLter, F.; Ulander, L. M. H. Estimation of forest parameters using CARABAS-II VHF SAR data. *IEEE Trans. Geosci. Remote Sens.* **2000**, *38*, 720–727.

12. Saatchi, S. S.; Moghaddam, M. Estimation of crown and stem water content and biomass of boreal forest using polarimetric SAR imagery. *IEEE Trans. Geosci. Remote Sens.* **2000**, *38*, 697 709.

13. Ranson, K. J.; Sun, G.; Member, S. Effects of Environmental Conditions on Boreal Forest Classification and Biomass Estimates with SAR. *IEEE Geosci. Remote Sens.* **2000**, *38*, 1242–1252.

14. Hyyppa, H.; Inkinen, M.; Engdahl, M. Accuracy comparison of various remote sensing data sources in the retrieval of forest stand attributes. *For. Ecol. Manage.* **2000**, *128*, 109 120.

15. Koskinen, J. T.; Pulliainen, J. T.; Hyyppä, J. M.; Engdahl, M. E.; Hallikainen, M. T. The seasonal behavior of interferometric coherence in boreal forest. *IEEE Trans. Geosci. Remote Sens.* **2001**, *39*, 820 829.

16. Fransson, J. E. S.; Smith, G.; Askne, J.; Olsson, H. Stem volume estimation in boreal forests using ERS-1/2 coherence and SPOT XS optical data. *Int. J. Remote Sens.* **2001**, *22*, 2777–2791.

17. Balzter, H.; Baker, J. R.; Hallikainen, M.; Tomppo, E. Retrieval of timber volume and snow water equivalent over a Finnish boreal forest from airborne polarimetric Synthetic Aperture Radar. *Int. J. Remote Sens.* **2002**, *23*, 3185 3208.

18. Santoro, M.; Askne, J.; Smith, G.; Fransson, J. E. S. Stem volume retrieval in boreal forests from ERS-1 / 2 interferometry. *Remote Sens. Environ.* **2002**, *81*, 19–35.

19. Sun, G.; Ranson, K. J.; Kharuk, V. I. Radiometric slope correction for forest biomass estimation from SAR data in the Western Sayani Mountains, Siberia. *Remote Sens. Environ.* **2002**, *79*, 279–287.

20. Pulliainen, J.; Engdahl, M.; Hallikainen, M. Feasibility of multi-temporal interferometric SAR data for stand-level estimation of boreal forest stem volume. *Remote Sens. Environ.* **2003**, *85*, 397–409.

21. Askne, J.; Santoro, M.; Smith, G.; Fransson, J. E. S. Multitemporal repeat-rass SAR interferometry of boreal forests. *IEEE Trans. Geosci. Remote Sens.* **2003**, *41*, 1540–1550.

22. Engdahl, M. E.; Pulliainen, J. T.; Hallikainen, M. T. Boreal Forest Coherence-Based Measures of Interferometric Pair Suitability for Operational Stem Volume Retrieval. *IEEE Geosci. Remote Sens. Lett.* **2004**, *1*, 228–231.

23. Askne, J.; Santoro, M. Multitemporal repeat pass SAR interferometry of boreal forests. *IEEE Trans. Geosci. Remote Sens.* **2005**, *43*, 1219–1228.

24. Rauste, Y. Multi-temporal JERS SAR data in boreal forest biomass mapping. *Remote Sens. Environ.* **2005**, *97*, 263 275.

25. Santoro, M.; Eriksson, L.; Askne, J.; Schmullius, C. Assessment of stand-wise stem volume retrieval in boreal forest from JERS-1 L-band SAR backscatter. *Int. J. Remote Sens.* **2006**, *27*, 3425–3454.

26. Askne, J.; Santoro, M. Selection of forest stands for stem volume retrieval from stable ERS tandem InSAR observations. *IEEE Geosci. Remote Sens. Lett.* **2007**, *4*, 46–50.

27. Santoro, M.; Shvidenko, A.; Mccallum, I.; Askne, J.; Schmullius, C. Properties of ERS-1 / 2 coherence in the Siberian boreal forest and implications for stem volume retrieval. *Remote Sens. Environ.* **2007**, *106*, 154–172.

28. Engdahl, M. E.; Pulliainen, J.; Hallikainen, M. Segment-based stem volume retrieval in boreal forests using multitemporal ERS-1/2 InSAR data. *Can. J. Remote Sens.* **2008**, *34*, 46–55.

29. Askne, J. I. H.; Santoro, M. Automatic model-based estimation of boreal forest stem volume from repeat pass C-band InSAR coherence. *IEEE Trans. Geosci. Remote Sens.* **2009**, *47*, 513–516.

30. Folkesson, K.; Smith-jonforsen, G.; Ulander, L. M. H. Model-based compensation of topographic effects for improved stem-volume retrieval from CARABAS-II VHF-band SAR images. *IEEE Trans. Geosci. Remote Sens.* **2009**, *47*, 1045–1055.

31. Solberg, S.; Astrup, R.; Gobakken, T.; Næsset, E.; Weydahl, D. J. Estimating spruce and pine biomass with interferometric X-band SAR. *Remote Sens. Environ.* **2010**, *114*, 2353–2360.

32. Sandberg, G.; Ulander, L. M. H.; Fransson, J. E. S.; Holmgren, J.; Le Toan, T. L- and P-band backscatter intensity for biomass retrieval in hemiboreal forest. *Remote Sens. Environ.* **2011**, *115*, 2874–2886.

33. Sun, G.; Ranson, K. J.; Guo, Z.; Zhang, Z.; Montesano, P.; Kimes, D. Forest biomass mapping from lidar and radar synergies. *Remote Sens. Environ.* **2011**, *115*, 2906–2916.

34. Santoro, M.; Beer, C.; Cartus, O.; Schmullius, C.; Shvidenko, A.; Mccallum, I.; Wegmüller, U.; Wiesmann, A. Retrieval of growing stock volume in boreal forest using hyper-temporal series of Envisat ASAR ScanSAR backscatter measurements. *Remote Sens. Environ.* **2011**, *115*, 490–507.

35. Andersen, H.; Strunk, J.; Temesgen, H.; Atwood, D.; Winterberger, K. Using multilevel remote sensing and ground data to estimate forest bi mass resources in remote regions: a case stu y in the boreal forests of interior Alaska. *Can. J. Remote Sens.* **2011**, *37*, 1–16.

36. Neumann, M.; Saatchi, S. S.; Ulander, L. M. H.; Fransson, J. E. S. Assessing performance of L- and P-Band polarimetric interferometric SAR data in estimating boreal forest above-ground biomass. *IEEE Trans. Geosci. Remote Sens.* **2012**, *50*, 714–726.

37. Cartus, O.; Santoro, M.; Kellndorfer, J. Mapping forest aboveground biomass in the Northeastern United States with ALOS PALSAR dual-

polarization L-band. *Remote Sens. Environ.* **2012**, *124*, 466–478.

38. Karjalainen, M.; Kankare, V.; Vastaranta, M.; Holopainen, M.; Hyyppä, J. Prediction of plot-level forest variables using TerraSAR-X stereo SAR data. *Remote Sens. Environ.* **2012**, *117*, 338–347.

39. Antropov, O.; Rauste, Y.; Ahola, H.; Häme, T. Stand-level stem volume of boreal forests from spaceborne SAR imagery at L-band. *IEEE Trans. Geosci. Remote Sens.* **2013**, *6*, 4776–4779.

40. Soja, M. J.; Sandberg, G.; Ulander, L. M. H.; Member, S. Regression-based retrieval of boreal forest biomass in sloping terrain using P-band SAR backscattor intensity data. *IEEE Trans. Geosci. Remote Sens.* **2013**, *51*, 2646–2665.

41. Peregon, A.; Yamagata, Y. The use of ALOS/PALSAR backscatter to estimate above-ground forest biomass: A case study in Western Siberia. *Remote Sens. Environ.* **2013**, *137*, 139 146.

42. Solberg, S.; Astrup, R.; Breidenbach, J.; Nilsen, B.; Weydahl, D. Monitoring spruce volume and biomass with InSAR data from TanDEM-X. *Remote Sens. Environ.* **2013**, *139*, 60–67.

43. Santoro, M.; Cartus, O.; Fransson, J.; Shvidenko, A.; McCallum, I.; Hall, R.; Beaudoin, A.; Beer, C.; Schmullius, C. Estimates of Forest Growing Stock Volume for Sweden, Central Siberia, and Québec Using Envisat Advanced Synthetic Aperture Radar Backscatter Data. *Remote Sens.* **2013**, *5*, 4503–4532.

44. Askne, J.; Fransson, J.; Santoro, M.; Soja, M.; Ulander, L. Model-based biomass estimation of a hemi-boreal forest from multitemporal TanDEM-X acquisitions. *Remote Sens.* **2013**, *5*, 5574–5597.

45. Persson, H.; Fransson, J. Forest variable estimation using radargrammetric processing of TerraSAR-X images in boreal forests. *Remote Sens.* **2014**, *6*, 2084–2107.

46. Vastaranta, M.; Niemi, M.; Karjalainen, M.; Peuhkurinen, J.; Kankare, V.; Hyyppä, J.; Holopainen, M. Prediction of forest stand attributes using TerraSAR-X stereo imagery. *Remote Sens.* **2014**, *6*, 3227–3246.

47. Chowdhury, T. A.; Thiel, C.; Schmullius, C. Growing stock volume estimation from L-band ALOS PALSAR polarimetric coherence in Siberian forest. *Remote Sens. Environ.* **2014**, *155*, 129–144.

48. Hüttich, C.; Korets, M.; Bartalev, S.; Zharko, V.; Schepaschenko, D.; Shvidenko, A.; Schmullius, C. Exploiting Growing Stock Volume Maps for Large Scale Forest Resource Assessment: Cross-Comparisons of ASAR- and PALSAR-Based GSV Estimates with Forest Inventory in Central Siberia. *Forests* **2014**, *5*, 1753–1776.

49. Atwood, D. K.; Andersen, H. E.; Matthiss, B.; Holecz, F. Impact of topographic correction on estimation of aboveground boreal biomass using multi-temporal, L-band backscatter. *IEEE J. Sel. Top. Appl. Earth Obs. Remote Sens.* **2014**, *7*, 3262–3273.

50. Wilhelm, S.; Hüttich, C.; Korcts, M.; Schmullius, C. Large area mapping of boreal Growing Stock Volume on an annual and multi-temporal level using PALSAR L-band backscatter mosaics. *Forests* **2014**, *5*, 1999–2015.

51. Rahlf, J.; Breidenbach, J.; Solberg, S.; Næsset, E.; Astrup, R. Comparison of four types of 3D data for timber volume estimation. *Remote Sens. Environ.* **2014**, *155*, 325–333.

52. Karila, K.; Vastaranta, M.; Karjalainen, M.; Kaasalainen, S. Tandem-X interferometry in the prediction of forest inventory attributes in managed boreal forests. *Remote Sens. Environ.* **2015**, *159*, 259–268.

53. Solberg, S.; Riegler, G.; Nonin, P. Estimating forest biomass from TerraSAR-X stripmap radargrammetry. *IEEE Trans. Geosci. Remote Sens.* **2015**, *53*, 154–161.

54. Soja, M. J.; Persson, H. J.; Ulander, L. M. H. Estimation of forest biomass from two-level model inversion of single-pass InSAR data. *2015 IEEE Int. Geosci. Remote Sens. Symp.* **2015**, *53*, 3886–3889.

55. Askne, J. I. H.; Santoro, M. On the Estimation of Boreal Forest Biomass From TanDEM-X Data Without Training Samples. *IEEE Geosci. Remote Sens. Lett.* **2015**, *12*, 771–775.

56. Santoro, M.; Eriksson, L.; Fransson, J. Reviewing ALOS PALSAR Backscatter Observations for Stem Volume Retrieval in Swedish Forest. *Remote Sens.* **2015**, *7*, 4290–4317.

57. Santoro, M.; Beaudoin, A.; Beer, C.; Cartus, O.; Fransson, J. E. S.; Hall, R. J.; Pathe, C.; Schmullius, C.; Shepaschenko, D.; Shvidenko, A.; Thurner, M.; Wegmüller, U. Forest growing stock volume of the northern hemisphere: Spatially explicit estimates for 2010 derived from Envisat ASAR. *Remote Sens. Environ.* **2015**, *168*, 316–334.

58. Thiel, C.; Schmullius, C. The potential of ALOS PALSAR backscatter and InSAR coherence for forest growing stock volume estimation in Central Siberia. *Remote Sens. Environ.* **2016**, *173*, 258–273.

59. Stelmaszczuk-Górska, M. A.; Rodriguez-Veiga, P.; Ackermann, N.; Thiel, C.; Balzter, H.; Schmullius, C. Non-Parametric Retrieval of Aboveground Biomass in Siberian Boreal Forests with ALOS PALSAR Interferometric Coherence and Backscatter Intensity. *J. Imaging* **2016**, *2*, 24.

60. Askne, J. I. H.; Soja, M. J.; Ulander, L. M. H. Biomass estimation in a boreal forest from TanDEM-X data, lidar DTM, and the interferometric water cloud model. *Remote Sens. Environ.* **2017**, *196*, 265–278.

61. Persson, H. J.; Fransson, J. E. S. Comparison between TanDEM-X- and ALS-based estimation of aboveground biomass and tree height in boreal forests. *Scand. J. For. Res.* **2017**, *32*, 306–319.

62. Soja, M. J.; Askne, J. I. H.; Ulander, L. M. H. Estimation of Boreal Forest Properties from TanDEM-X Data Using Inversion of the Interferometric Water Cloud Model. *IEEE Geosci. Remote Sens. Lett.* **2017**, *14*, 997–1001.

63. Antropov, O.; Rauste, Y.; Häme, T.; Praks, J. Polarimetric ALOS PALSAR time series in mapping biomass of boreal forests. *Remote Sens.* **2017**, *9*, 1–24.

64. Persson, H.; Olsson, H.; Soja, M.; Ulander, L.; Fransson, J. Experiences from Large-Scale Forest Mapping of Sweden Using TanDEM-X Data. *Remote Sens.* **2017**, *9*, 1253.

65. Santoro, M.; Wegmüller, U.; Askne, J. Forest stem volume estimation using C-band interferometric SAR coherence data of the ERS-1 mission 3-days repeat-interval phase. *Remote Sens. Environ.* **2018**, *216*, 684–696.

66. Stelmaszczuk-Górska, M. A.; Urbazaev, M.; Schmullius, C.; Thiel, C. Estimation of Above-Ground Biomass over Boreal Forests in Siberia using updated in situ, ALOS-2 PALSAR-2, and RADARSAT-2 Data. *Remote Sens.* **2018**, *10*, 1550.

67. Rodríguez-veiga, P.; Quegan, S.; Carreiras, J.; Persson, H. J.; Fransson, J. E. S.; Hoscilo, A.; Zió, D.; Stere, K.; Lohberger, S.; Stängel, M.; Berninger, A.; Siegert, F.; Avitabile, V.; Herold, M.; Mermoz, S.; Bouvet, A.; Le, T.; Carvalhais, N.; Santoro, M.; Cartus, O.; Rauste, Y.; Mathieu, R.; Asner, G. P.; Thiel, C.; Pathe, C.; Schmullius, C.; Martin, F.; Tansey, K.; Balzter, H. Forest biomass retrieval approaches from earth observation in different biomes. *Int. J. Appl. Earth Obs. Geoinf.* **2019**, *77*, 53–68.

68. Santoro, M.; Cartus, O.; Fransson, J. E. S.; Wegmüller, U. Complementarity of X-, C-, and L-band SAR Backscatter Observations to Retrieve Forest Stem Volume in Boreal Forest. *Remote Sens.* **2019**, *11*, 1–25.

69. Askne, J. I. H.; Persson, H. J. On the Sensitivity of TanDEM-X-Observations to Boreal Forest Structure. *Remote Sens.* **2019**, *11*, 1–22.

70. Cartus, O.; Santoro, M.; Wegmüller, U.; Rommen, B. Benchmarking the Retrieval of Biomass in Boreal Forests Using P-Band SAR Backscatter with Multi-Temporal C- and L-band Observations. *Remote Sens.* **2019**, *11*, 20.

Manuscript Overview

Erklärung zu den Eigenanteilen des Promovenden/der Promovendin sowie der weiteren Doktoranden/Doktorandinnen als Koautoren an den Publikationen und Zweitpublikationsrechten bei einer kumulativen Dissertation

Für alle in dieser kumulativen Dissertation verwendeten Manuskripte liegen die notwendigen Genehmigungen der Verlage („Reprint permissions“) für die Zweitpublikation vor.

Die Co-Autoren der in dieser kumulativen Dissertation verwendeten Manuskripte sind sowohl über die Nutzung als auch über die oben angegebenen Eigenanteile informiert und stimmen dem zu.

M. A. Stelmaszczuk-Górska	Jena,	
Name Promovend/-in	Ort, Datum	Unterschrift

Ich bin mit der Abfassung der Dissertation als publikationsbasiert, d.h. kumulativ, einverstanden und bestätige die vorstehenden Angaben.

Prof. Dr. C. Schmullius	Jena,	
Name Erstbetreuer	Ort, Datum	Unterschrift

PD Dr. C. Thiel	Jena,	
Name Zweitbetreuer	Ort, Datum	Unterschrift

Manuscript 1

Hüttich, C., **Stelmaszczuk-Górska, M.**, Eberle, J., Kotzerke, P., & Schmullius, C. C. (2014). Operational forest monitoring in Siberia using multi-source Earth Observation data. *Siberian Journal of Forest Science*, *5*, 38–52.

	Hüttich, C.	**Stelmaszczuk-Górska, M.**	**Eberle, J.**	**Kotzerke, P.**	**Schmullius, C.**
Forschungskonzeption	☒	☒	☒	☒	☒
Untersuchungsplanung	☒	☒	☒	☒	
Datenerhebung und -verarbeitung	☒	☒	☒	☒	
Datenanalyse und -interpretation	☒	☒	☒	☒	
Schreiben des Manusktipts	☒	☒	☒	☒	
Publikationsäquivalent	n/a	**1**	n/a	n/a	n/a

Manuscript 2

Stelmaszczuk-Górska, M. A., Rodriguez-Veiga, P., Ackermann, N., Thiel, C., Balzter, H., & Schmullius, C. (2016). Non-Parametric Retrieval of Aboveground Biomass in Siberian Boreal Forests with ALOS PALSAR Interferometric Coherence and Backscatter Intensity. *Journal of Imaging, 2*(1), 24.

	Stelmaszczuk-Górska, M.	**Rodriguez-Veiga, P.**	**Ackermann, N.**	**Thiel, C.**
Forschungskonzeption	☒	☒	☒	☒
Untersuchungsplanung	☒	☒	☒	
Datenerhebung und -verarbeitung	☒			
Datenanalyse und -interpretation	☒	☒		☒
Schreiben des Manusktipts	☒	☒	☒	☒
Publikationsäquivalent	**1**	n/a	n/a	n/a

	Balzter, H.	**Schmullius, C.**
Forschungskonzeption	☒	☒
Untersuchungsplanung		
Datenerhebung und -verarbeitung		
Datenanalyse und -interpretation		
Schreiben des Manusktipts		
Publikationsäquivalent	n/a	n/a

Manuscript 3

Stelmaszczuk-Górska, M. A., Thiel, C. J., & Schmullius, C. C. (2017). Remote Sensing for Aboveground Biomass Estimation in Boreal Forests. In H. Balzter (Ed.), *Earth Observation for Land and Emergency Monitoring* (1st ed., pp. 33–55). © 2017 John Wiley & Sons Ltd.

	Stelmaszczuk-Górska, M.	**Thiel, C.**	**Schmullius, C.**
Forschungskonzeption	☒	☒	☒
Untersuchungsplanung	☒		
Datenerhebung und -verarbeitung	☒		
Datenanalyse und -interpretation	☒		
Schreiben des Manusktipts	☒	☒	
Publikationsäquivalent	**0,5**	n/a	n/a

Manuscript 4

Stelmaszczuk-Górska, M. A., Urbazaev, M., Schmullius, C., & Thiel, C. (2018). Estimation of Above-Ground Biomass over Boreal Forests in Siberia using updated in situ, ALOS-2 PALSAR-2, and RADARSAT-2 Data. *Remote Sensing*, *10*(10), 1550.

	Stelmaszczuk-Górska, M.	**Urbazaev, M.**	**Schmullius, C.**	**Thiel, C.**
Forschungskonzeption	☒		☒	☒
Untersuchungsplanung	☒			☒
Datenerhebung und -verarbeitung	☒			
Datenanalyse und -interpretation	☒	☒		
Schreiben des Manusktipts	☒	☒		☒
Publikationsäquivalent	**1**	n/a	n/a	n/a

Statement of Authorship

Selbstständigkeitserklärung:

Ich erkläre, dass ich die vorliegende Arbeit selbstständig und unter Verwendung der angegebenen Hilfsmittel, persönlichen Mitteilungen und Quellen angefertigt habe.

Jena, _____ _____

Ort, Datum Martyna Anna Stelmaszczuk-Górska